

N° d'ordre : 40751

ECOLE DES MINES DE DOUAI



UNIVERSITE DE LILLE 1



Habilitation à Diriger des Recherches

présentée à

l'Université de Lille 1

en

Spécialité : Sciences Physiques

par

Alexandre TOMAS

Contribution à l'étude des mécanismes d'oxydation atmosphérique de COV oxygénés. Développement de nouveaux outils.

Soutenue le 6 décembre 2011 devant le jury d'examen :

Présidente et Rapportrice	C. Fittschen, DR CNRS, Université Lille 1
Rapporteur	A. Mellouki, DR CNRS, Orléans
Rapporteur	E. Villenave, Pr., Université Bordeaux 1
Examineur	A. Chakir, MC HDR, Université de Reims
Directeur d'HDR	P. Coddeville, Pr., Ecole des Mines de Douai

Laboratoire d'accueil : Département Chimie et Environnement de l'Ecole des Mines de Douai
Ecole Doctorale SMRE 104 (Lille I, Artois, ULCO, Chimie Lille)

A Anne-Laure

**A Jérémie, Myriam, Anaïs
Domitille et Manon**

REMERCIEMENTS

La préparation d'une Habilitation à Diriger des Recherches représente un travail de synthèse d'activités de recherche couvrant plusieurs années et permet de se projeter dans l'avenir au travers de perspectives.

Les travaux de recherche présentés dans cette synthèse sont le fruit d'un effort collectif qui a impliqué de nombreuses personnes que je désire ici sincèrement remercier :

- mes anciens doctorants : E. Turpin, S. Crunaire, A. Guilloteau, M. Djehiche, E. Szabo et M. Duncianu ;
- l'ensemble du personnel du département Chimie et Environnement, et notamment : V. Riffault, pour notre collaboration sur la thématique de formation des AOS, J.-C. Galloo, ancien chef du département et P. Coddeville, chef du département, qui m'ont encouragé à préparer cette HDR, T. Léonardis, pour son soutien technique et sa disponibilité ;
- des personnels du laboratoire PC2A, et notamment : C. Fittschen, qui m'a guidé, conseillé et aiguillé avec beaucoup de disponibilité et gentillesse tout au long de ces années, dans les bons et les mauvais moments, C. Schoemaeker et A. Parker pour leur grande aide dans le montage CSA-CRDS.

Je remercie également la direction de l'Ecole des Mines de Douai qui m'a donné les moyens de développer pleinement mes activités de recherche.

Un grand merci aux membres du jury : C. Fittschen, A. Mellouki et E. Villenave, qui ont accepté la lourde tâche de rapporter le mémoire, A. Chakir pour sa participation à la soutenance et à l'évaluation de mes travaux et P. Coddeville, garant de mon HDR, en particulier pour ses conseils lors de la finalisation du manuscrit.

Enfin, je remercie mes parents, ma femme et mes enfants, pour leur amour et tout l'encouragement qu'ils ont pu m'apporter dans toutes ces années.

SOMMAIRE

Curriculum Vitae incluant les titres et travaux publiés	11
Document de synthèse	25
Chapitre I. Introduction	27
I.1 Généralités	29
I.1.1 Eléments de contexte atmosphérique	29
I.1.2 Eléments de chimie atmosphérique	31
I.2 Objectifs des travaux de recherche	34
I.3 Activités de recherche	35
I.3.1 Développement de nouveaux outils expérimentaux	35
I.3.2 Cinétiques et mécanismes d'oxydation de COVO	37
I.3.3 Formation des aérosols organiques secondaires	39
Chapitre II. Développement de nouveaux outils expérimentaux	41
II.1 Les chambres de simulation atmosphérique (CSA)	43
II.1.1 Développement d'une CSA souple pour l'étude de la photochimie de COV	43
II.1.1.1 Description du dispositif	43
II.1.1.2 Méthode de production des radicaux OH	44
II.1.1.3 Outils d'analyse du milieu réactionnel	44
II.1.1.4 Validation du dispositif	45
II.1.2 Développement de la spectroscopie cw-CRDS	46
II.1.2.1 Principe de la spectroscopie cw-CRDS	47
II.1.2.2 Couplage cw-CRDS-CSA souple et tests de validation	50
II.1.3 Développement d'une CSA rigide avec spectroscopie cw-CRDS <i>in situ</i>	52

II.1.3.1 Développement expérimental	52
II.1.3.2 Etude des produits de photolyse du nitrite de méthyle	55
II.1.3.2.1 Introduction	
II.1.3.2.2 Approche bibliographique	
II.1.3.2.3 Questionnements scientifiques	
II.1.3.2.4 Résultats obtenus	
II.1.3.3 Etude des cinétiques du radical HO ₂ [•] dans la photolyse de Cl ₂ en présence de CH ₃ OH	58
II.1.3.3.1 Introduction	
II.1.3.3.2 Principaux résultats obtenus	
Publication n°1 : First direct detection of HONO in the reaction of methylnitrite (CH ₃ ONO) with OH radicals, Djehiche M., Tomas A., Fittschen C., Coddeville P., <i>Environmental Science and Technology</i> 45 (2011) 608-614.	65
Publication n°2 : First cavity ring-down spectroscopy HO ₂ measurements in a large photoreactor, Djehiche M., Tomas A., Fittschen C., Coddeville P., <i>Zeitschrift für Physikalische Chemie</i> , 225 (2011) 983-992.	75
II.2 Le réacteur à écoulement pour l'étude des aérosols organiques secondaires	87
II.2.1 Développement instrumental	88
II.2.2 Validation : étude de cinétiques d'ozonolyse	93
Publication n°3 : Development of a new flow-reactor for kinetic studies. Application to the ozonolysis of a series of alkenes, Duncianu M., Olariu R.I., Visez N., Riffault V., Tomas A., Coddeville P., <i>Journal of Physical Chemistry A</i> , soumis (novembre 2011).	95

Chapitre III. Cinétiques et mécanismes d'oxydation de composés organiques volatils oxygénés **135**

III.1 Rôle et importance des composés organiques volatils oxygénés dans la chimie atmosphérique	137
III.1.1 Les sources des composés organiques volatils oxygénés	137
III.1.2 Impacts des composés organiques volatils carbonylés et hydroxylés	139
III.2 La réaction acétone + OH	141
III.2.1 Sources atmosphériques de l'acétone	141
III.2.2 Réactivité de l'acétone dans l'atmosphère	141
III.2.2.1 Réaction avec le radical OH	
III.2.2.2 Photolyse par le rayonnement solaire	
III.2.2.3 Dépôt	

III.2.3 Intérêt de la réaction et présentation de l'histoire des différentes études	144
III.2.4 Travaux réalisés	145
III.2.5 Discussion et conclusion	146
Publication n°4 : Acetone-h ₆ or -d ₆ + OH reaction products: Evidence for heterogeneous formation of acetic acid in a simulation chamber, Turpin E., Tomas A., Fittschen C., Devolder P., Galloo J.-C., <i>Environmental Science and Technology</i> 40 (2006) 5956-5961.	149
III.3 La réaction acide acétique + OH	157
III.3.1 Sources atmosphériques de l'acide acétique	157
III.3.2 Réactivité et impact de l'acide acétique dans l'atmosphère	157
III.3.3 Intérêt de la réaction et présentation de l'histoire des différentes études	159
III.3.4 Travaux réalisés	160
III.3.5 Discussion et conclusion	160
Publication n°5 : Use of cw-CRDS for studying the atmospheric oxidation of acetic acid in a simulation chamber, Crunaire S., Tarmoul J., Fittschen C., Tomas A., Lemoine B., Coddeville P., <i>Applied Physics B</i> 85 (2006) 467-476.	161
Publication n°6 : Kinetics of the OH-radical initiated reactions of acetic acid and its deuterated isotopes, Szabo E., Tarmoul J., Tomas A., Fittschen C., Dobe S., Coddeville P., <i>Reaction Kinetics and Catalysis Letters</i> 96 (2009) 299-309.	173
III.4 Cinétiques et mécanismes d'oxydation de composés multi-oxygénés	187
III.4.1 Sources atmosphériques des composés α-dicétones	188
III.4.2 Réactivité des composés α-dicétones	188
III.4.3 Travaux réalisés	189
Publication n°7 : Atmospheric chemistry of 2,3-pentanedione: Photolysis and reaction with OH radicals, Szabo E., Djehiche M., Riva M., Fittschen C., Coddeville P., Sarzynski D., Tomas A., Dobé S., <i>Journal of Physical Chemistry A</i> 115 (2011) 9160-9168.	191
Chapitre IV. Formation des aérosols organiques secondaires	203
IV.1 Rôle et importance des aérosols organiques secondaires	205
IV.1.1 Les aérosols atmosphériques : caractéristiques et impacts	205
IV.1.2 Les aérosols organiques secondaires	207

IV.2 Ozonolyse des catéchols	210
IV.2.1 Sources et importance atmosphérique des catéchols	210
IV.2.2 Cinétique d'ozonolyse des catéchols	213
IV.2.3 Formation des aérosols organiques secondaires	213
IV.2.3.1 Etude au Centre de Recherche Européen Euphore à Valencia (Espagne)	
IV.2.3.2 Etudes à Cork et Wimereux	
IV.2.3.3 Conclusions et dernières publications dans la littérature	
 Publication n°8 : Kinetics of the reaction of O ₃ with selected benzenediols, Tomas A., Olariu R.I., Barnes I., Becker K.H., <i>International Journal of Chemical Kinetics</i> 35 (2003) 223-230.	217
 Publication n°9 : Atmospheric ozone degradation reaction of 1,2-dihydroxybenzene: Aerosol formation study, Olariu R.I., Tomas A., Barnes I., Wirtz K., The European Photoreactor EUPHORE, 4 th report 2001, 47-63.	227
 Publication n°10 : Aerosol formation yields from the reaction of 1,2-dihydroxybenzene with ozone, Coeur-Tourneur C., Tomas A., Guilloteau A., Henry F., Ledoux F., Visez N., Riffault V., Wenger J., Bedjanian Y., <i>Atmospheric Environment</i> 43 (2009) 2360-2365.	249
 Conclusion et perspectives	257
 Références bibliographiques	263

Curriculum Vitae incluant les titres et travaux publiés

Curriculum vitae, activités d'enseignement, de recherche et d'animation

Alexandre TOMAS

Né le 10/05/1974

Nationalité française

Situation familiale : marié, cinq enfants

Ecole des Mines de Douai

Département Chimie et Environnement

941, rue Charles Bourseul – BP 10838

59508 Douai Cedex

☎ 03 27 71 26 51

E-mail : alexandre.tomas@mines-douai.fr

Fonction : Enseignant-chercheur à l'Ecole des Mines de Douai depuis septembre 2001

FORMATION

1998-2000 : **Doctorat de l'Université Bordeaux I, Spécialité Chimie-Physique**
soutenu le 4 Septembre 2000 à Bordeaux (Mention Très Honorable)
Titre de la thèse : *Stabilité et réactivité de radicaux acyles et acylperoxydes d'intérêt en chimie de l'atmosphère.*

Travail réalisé au Laboratoire de Physico-Chimie Moléculaire (CNRS UMR 5803, Université Bordeaux I, directeur J.C. Rayez)
Directeur de thèse : R. Lesclaux

Devant la commission d'examen formée de :

G. Scacchi, Professeur à l'INPL, Nancy

F. Zabel, Professeur à l'Université de Stuttgart, Allemagne

Rapporteurs

J.C. Rayez, Professeur à l'Université Bordeaux I

F. Caralp, Chargée de recherche au CNRS à Bordeaux

R. Lesclaux, Directeur de recherche au CNRS à Bordeaux

B. Maillard, Directeur de recherche au CNRS à Bordeaux

G. Poulet, Professeur à l'Université d'Orléans

Examineurs

1996-1997: **Diplôme d'Etudes Approfondies de Chimie-Physique**
en troisième année de l'ENSGTI (Mention AB)

1994-1997: **Diplôme d'ingénieur de l'Ecole Nationale Supérieure en Génie des Technologies Industrielles de Pau (ENSGTI)**

1992-1994: Mathématiques Supérieures et Mathématiques Spéciales au **Lycée Champollion de Grenoble**

EXPERIENCE PROFESSIONNELLE

- 2001-: Enseignant-chercheur au *département Chimie et Environnement* de l'Ecole des Mines de Douai
Responsable axe « Réactivité des polluants » depuis fin 2010
- 2000-2001: Stage post-doctoral au *département de Chimie Physique* de l'Université de Wuppertal, Allemagne, sous la direction de I. Barnes
« Investigation of the aerosol formation from the photooxidation of aromatic hydrocarbons: Quantification and speciation. »
Financement : programme de recherche européen EXACT
- 1998-2000: Thèse de doctorat au *Laboratoire de Physico-Chimie Moléculaire* (CNRS UMR 5803, Université Bordeaux I), directeur de thèse : R. Lesclaux
« Stabilité et réactivité de radicaux acyles et acylperoxydes d'intérêt en chimie de l'atmosphère. »
Financement : programme de recherche européen AFCAR
- Juillet - Décembre 1997: Stage de recherche de DEA puis CDD au *Département Finissages* de la société *Sollac* (groupe *Usinor/Arcelor*) à Fos-sur-mer
« Etude du processus de formation des oxydes de fer au four Rüttner : Qualité des oxydes de fer et conditions de fonctionnement. »
- Juillet 1996 - Janvier 1997: Stage ingénieur au Service *Process Energie* de la société *Sollac* à Fos-sur-mer
« Modélisation d'un dispositif de régénération de bains acides usés provenant de lignes de décapage. »

Liste des travaux, ouvrages, articles et réalisations

MEMOIRES (1-3), RAPPORTS DE RECHERCHE (1-10), ARTICLES DANS DES REVUES INTERNATIONALES (1-17), COMMUNICATIONS AVEC ACTES (1-18), COMMUNICATIONS SANS ACTES (1-38)

MEMOIRES

1. Stabilité et réactivité de radicaux acyles et acylperoxydes d'intérêt en chimie de l'atmosphère, A. Tomas, *Thèse de doctorat*, Université Bordeaux I, **2000**.
2. Etude du processus de formation des oxydes de fer au four Rüttnner, A. Tomas, *DEA Chimie-Physique*, Université de Pau et des Pays de l'Adour, **1997**.
3. Le four Rüttnner, A. Tomas, *Mémoire de fin d'études*, ENSGTI, **1997**.

RAPPORTS DE RECHERCHE

1. Kinetics and mechanistic studies of radical reactions important in tropospheric VOC oxidation processes, R. Lesclaux, F. Berho, F. Caralp, M.-T. Rayez, A. Tomas, E. Villenave, *CMD annual report 1998*.
2. Kinetics and mechanistic studies of radical reactions important in tropospheric VOC oxidation processes, R. Lesclaux, F. Caralp, R. Mereau, M.-T. Rayez, A. Tomas, E. Villenave, *CMD annual report 2000*.
3. Étude de l'analyseur de BTX G2000 SERES, A. Tomas et N. Locoge avec la collaboration technique de T. Léonardis, *Rapport d'activités LCSQA n°3, 2002, 68 p.*
4. Mise au point de la mesure en continu de COV toxiques dans les réseaux de surveillance de la qualité de l'air. A. Tomas, F. Troussier et N. Locoge avec la collaboration technique de T. Léonardis, *Rapport d'activités LCSQA n°3, 2003, 46 p.*
5. Atmospheric ozone degradation reaction of 1,2-dihydroxybenzene: Aerosol formation study, R.I. Olariu, A. Tomas, I. Barnes, K. Wirtz, *The European Photoreactor EUPHORE, 4th Report 2001*, Ed. I. Barnes, Institute of Physical Chemistry, Bergische Universität Wuppertal, Novembre **2003**.
6. Mise au point de la mesure en continu de COV toxiques dans les réseaux de surveillance de la qualité de l'air. A. Tomas, F. Troussier et N. Locoge avec la collaboration technique de T. Léonardis, *Rapport d'activités LCSQA n°8, 2004, 74 p.*
7. Mesure des COV chlorés par échantillonnage passif. A. Tomas, N. Locoge et H. Plaisance avec la collaboration technique de T. Léonardis, *Rapport d'activités LCSQA, 2006, 34 p.*
8. Mesure des COV toxiques chlorés par échantillonnage passif. A. Tomas, N. Locoge et H. Plaisance avec la collaboration technique de C. Auzou et T. Léonardis, *Rapport d'activités LCSQA, 2007, 51 p.*
9. Élaboration d'une méthode d'échantillonnage des COV odorants, N. Locoge, E. Turpin et A. Tomas, *Rapport final convention Ademe n°0562C0076, 2008, 101 p.*
10. Mesure des COV, A. Tomas et N. Locoge, *Rapport d'activités LCSQA, 2008, 47 p.*

ARTICLES DANS DES REVUES INTERNATIONALES

1. Kinetics of the $(\text{CH}_3)_2\text{CHCO}$ and $(\text{CH}_3)_3\text{CCO}$ Radical decompositions: Temperature and pressure dependences. A. Tomas, E. Villenave et R. Lesclaux, *Physical Chemistry Chemical Physics*, 2, 1165 – 1174, **2000**.
2. Kinetics of $(\text{CH}_3)_2\text{CHC}(\text{O})\text{O}_2$ and $(\text{CH}_3)_3\text{CC}(\text{O})\text{O}_2$ peroxy radical self reactions between 275 K and 363 K. A. Tomas et R. Lesclaux, *Chemical Physics Letters*, 319, 521 – 528, **2000**.
3. Decomposition of the CF_3CO radical: Pressure and temperature dependences of the rate constant. A. Tomas, F. Caralp et R. Lesclaux, *Zeitschrift für Physikalische Chemie* (Troel's Festschrift, Special Issue), 214, 1349 – 1365, **2000**.
4. Reactions of the HO_2 radical with CH_3CHO and $\text{CH}_3\text{C}(\text{O})\text{O}_2$ in the gas phase. A. Tomas, E. Villenave et R. Lesclaux, *Journal of Physical Chemistry A*, 105, 3505 – 3514, **2001**.
5. Kinetics of the reaction of O_3 with selected benzenediols. A. Tomas, R.I. Olariu, I. Barnes, K.H. Becker, *International Journal of Chemical Kinetics*, 35, 6, 223 – 230, **2003**.

6. Reaction of OH radicals with acetone: determination of the branching ratio for the abstraction pathway at 298K and 1 Torr. E. Turpin, C. Fittschen, A. Tomas, P. Devolder, *Journal of Atmospheric Chemistry*, 46, 1, 1 – 13, **2003**.
7. Acetone-h₆ or -d₆ + OH reaction products: Evidence for a heterogeneous formation of acetic acid in a simulation chamber. E. Turpin, A. Tomas, C. Fittschen, P. Devolder, J.-C. Galloo, *Environmental Science and Technology*, 40, 19, 5956 – 5961, **2006**.
8. Use of cw-CRDS for studying the atmospheric oxidation of acetic acid in a simulation chamber. S. Crunaire, J. Tarmoul, C. Fittschen, A. Tomas, B. Lemoine, P. Coddeville, *Applied Physics B*, 85, 2-3, 467 – 476, **2006**.
9. Secondary organic aerosol formation from the gas phase reaction of hydroxyl radicals with o-, m- and p-cresol. F. Henry, C. Coeur-Tourneur, F. Ledoux, A. Tomas, D. Menu, *Atmospheric Environment*, 42, 13, 3035 – 3045, **2008**.
10. On the direct formation of HO₂ radicals after 248 nm irradiation of benzene C₆H₆ in the presence of O₂. A. Aluculesei, A. Tomas, C. Schoemaeker, C. Fittschen, *Applied Physics B*, 92, 3, 379 – 385, **2008**.
11. Aerosol formation yields from the reaction of 1,2-dihydroxybenzene with ozone. C. Coeur – Tourneur, A. Tomas, A. Guilloteau, F. Henry, F. Ledoux, N. Visez, V. Riffault, J. Wenger and Y. Bedjanian, *Atmospheric Environment*, 43, 14, 2360 – 2365, **2009**.
12. Kinetics of the OH-radical initiated reactions of acetic acid and its deuterated isomers. E. Szabo, J. Tarmoul, A. Tomas, C. Fittschen, S. Dobé, P. Coddeville, *Reaction Kinetics and Catalysis Letters*, 96, 2, 299 – 309, **2009**.
13. Desorption of polycyclic aromatic hydrocarbons from a soot surface: three- to five-ring PAHs. A. Guilloteau, Y. Bedjanian, M. L. Nguyen, A. Tomas, *Journal of Physical Chemistry A*, 114, 942 – 948, **2010**.
14. First direct detection of HONO in the reaction of methylnitrite (CH₃ONO) with OH radicals. M. Djehiche, A. Tomas, C. Fittschen, P. Coddeville, *Environmental Science and Technology*, 45, 2, 608 – 614, **2011**.
15. Atmospheric Chemistry of 2,3-Pentanedione: Photolysis and Reactions with OH Radicals. E. Szabó, M. Djehiche, M. Riva, C. Fittschen, P. Coddeville, D. Sarzyński, A. Tomas, S. Dóbé, *Journal of Physical Chemistry A*, 115, 33, 9160 – 9168, **2011**.
16. First cavity ring-down spectroscopy HO₂ measurements in a large photoreactor. M. Djehiche, C. Fittschen, P. Coddeville, A. Tomas, *Zeitschrift für Physikalische Chemie* (Hippler's Festschrift, Special Issue), 225, 983 – 992, **2011**.
17. Development of a new flow-reactor for kinetic studies. Application to the ozonolysis of a series of alkenes. M. Duncianu, R.I. Olariu, N. Visez, V. Riffault, A. Tomas, P. Coddeville, *Journal of Physical Chemistry A*, soumis (2011)

COMMUNICATIONS AVEC ACTES

1. Flash photolysis study of the decomposition rate of the isopropionyl radical *i*-C₃H₇CO in the temperature range 413 - 523 K. A. Tomas et R. Lesclaux, *Proceedings of the 15th International Symposium on Gas Kinetics*, Bilbao, Espagne, 6 - 12 Septembre **1998**.
2. A reinvestigation of the CH₃C(O)O₂ + HO₂ reaction and a new study of the reaction of HO₂ with acetaldehyde. A. Tomas, E. Villenave, F. Caralp et R. Lesclaux, *Proceedings of the EUROTRAC-2 Symposium 2000*, P.M. Midgley, M. Reuther (Eds.) Margraf Verlag, Weikersheim (Allemagne), Garmisch-Partenkirchen, Allemagne, 27 - 31 Mars **2000**.
3. Theoretical and experimental studies of acyl radical decomposition. R. Méreau, A. Tomas, M.T. Rayez, J.C. Rayez, F. Caralp et R. Lesclaux, *Proceedings of the 16th International Symposium on Gas Kinetics*, Cambridge, UK, 23 - 27 Juillet **2000**.
4. Atmospheric chemistry of benzenediols: Reaction with ozone. A. Tomas, R. Olariu, I. Barnes, I. Bejan, H. Geiger et R. Mocanu, *Proceedings of the EUROTRAC-2 Symposium 2002*, P.M. Midgley, M. Reuther (Eds.) Margraf Verlag, Weikersheim (Allemagne), Garmisch-Partenkirchen, Allemagne, 11 - 15 Mars **2002**.
5. Organic aerosol formation during the atmospheric ozone degradation of 1,2-dihydroxybenzenes. R.I. Olariu, A. Tomas, I. Barnes, I. Bejan, C. Arsene et K. Wirtz, *Proceedings of the EGU 2004 General Assembly*, Nice, France, 25 - 30 avril, Geophysical Research Abstracts, Vol. 6, 07103, **2004**.
6. Gas-phase reactions of the OH radicals with catechol. E. Turpin, A. Tomas, C. Fittschen, N. Locoge, P. Devolder, *Proceedings of the 18th International Symposium on Gas Kinetics*, Bristol, UK, 7 - 12 Août **2004**.

7. Simulation chamber study of the oxidation of acetic acid by OH radicals: detection of reaction products by cw-CRDS in the NIR. S. Crunaire, C. Fittschen, B. Lemoine, A. Tomas, P. Coddeville, *Proceedings of the EGU 2005 General Assembly*, Vienne, Autriche, 24-29 Avril, Geophysical Research Abstracts, Vol. 7, 01145, **2005**.
8. On the KIE in the oxidation of acetic acid by OH radicals. S. Crunaire, J. Tarmoul, A. Tomas, P. Coddeville, C. Fittschen, B. Lemoine, *Proceedings of the 19th International Symposium on Gas Kinetics*, Orléans, France, 22 – 27 juillet **2006**.
9. Simulation chamber study of the oxidation of acetic acid by OH radicals: Detection of reaction products by cw-CRDS in the near-infrared range, S. Crunaire, C. Fittschen, B. Lemoine, A. Tomas, P. Coddeville, *Proceedings of the NATO ARW "Environmental Simulation Chambers – Application to Atmospheric Chemical Processes"*, Zakopane, Pologne, 1-4 October 2004, NATO Science Series, IV. Earth and Environmental Sciences, Kluwer Academic Publishers, Dordrecht, **2006**.
10. IRENI air quality research program: Study of the interactions of oxygenated volatile organic compounds with aerosols in a coastal industrial atmosphere (Dunkerque, France). C. Aghnatiou, L. Aimoz, C. Brémond, M. Choël, P. Coddeville, C. Coeur- Tourneur, S. Crunaire, K. Deboudt, P. Devolder, P. Diévert, G. Falgayrac, C. Fittschen, P. Flament, J. C. Galloo, F. Henry, G. Khomenko, J. Laureyns, B. Lemoine, F. Louis, J. P. Sawerysyn, S. Sobanska, J. Thiébaud, A. Tomas, E. Turpin, *Proceedings of the 15th IUAPPA regional conference*, Lille, France, 5-8 Septembre **2006**.
11. Benzene photolysis at 254 nm: quantum yield and reaction products, E. Szabo, A. Tomas, C. Fittschen, P. Coddeville, R. Nadasdi, S. Dobe, *Proceedings of the 20th International Symposium on Gas Kinetics*, Manchester, UK, 20 – 25 juillet **2008**.
12. On the direct detection of HO₂ radicals after 248nm irradiation of benzene C₆H₆ in the presence of O₂ by laser photolysis / cw-CRDS, C. Fittschen, A. Aluculesei, C. Schoemacker and A. Tomas, *Proceedings of the 20th International Symposium on Gas Kinetics*, Manchester, UK, 20 – 25 juillet **2008**.
13. Photolysis quantum yield and OH reaction rate constant for methyl-ethyl-ketone, R. Nadasdi, G. L. Zügner, I. Szilagyi, S. Dobé, E. Szabo, A. Tomas and C. Fittschen, *Proceedings of the 20th International Symposium on Gas Kinetics*, Manchester, UK, 20 – 25 juillet **2008**.
14. Secondary Organic Aerosol formation from the gas-phase reaction of catechol with ozone, C. Coeur – Tourneur, A. Tomas, A. Guilloteau, F. Henry, F. Ledoux, N. Visez, V. Riffault, J. Wenger, Y. Bedjanian and V. Foulon, *Proceedings of the EGU 2009 General Assembly*, Vienne, Autriche, 19-24 Avril, Geophysical Research Abstracts, Vol. 11, 640-1, **2009**.
15. First in situ detection of HO₂ radical in a smog chamber by cw-CRDS, M. Djehiche, J. Tarmoul, A. Tomas, C. Fittschen, and P. Coddeville, *Proceedings of the EGU 2009 General Assembly*, Vienne, Autriche, 19-24 Avril, Geophysical Research Abstracts, Vol. 11, 604, **2009**.
16. Validation of a new flow-reactor for the study of secondary organic aerosol (SOA) formation, M. Duncianu, V. Riffault, A. Tomas, P. Coddeville, *Chemical Engineering Transactions*, Vol. 22, 161-166, **2010**.
17. Methanol oxidation by Cl atoms: experimental study in an environmental simulation chamber with in-situ cw-CRDS. M. Djehiche, A. Tomas, C. Fittschen, and P. Coddeville, *Proceedings of the 21th International Symposium on Gas Kinetics*, Leuven, Belgique, 18 – 23 juillet **2010**.
18. Kinetic and photochemical study on the atmospheric fate of 2,3-pentanedione. E. Szabo, D. Sarzynski, A. Tomas, C. Fittschen and S. Dobé, *Proceedings of the 21th International Symposium on Gas Kinetics*, Leuven, Belgique, 18 – 23 juillet **2010**.

COMMUNICATIONS SANS ACTES

1. Flash photolysis study of the decomposition rate of the isopropionyl radical *i*-C₃H₇CO in the temperature range 413 - 523 K. A. Tomas, E. Villenave et R. Lesclaux, Second Workshop of the Eurotrac-2 Subproject CMD, Karlsruhe, Allemagne, 23 - 25 Septembre 1998. **Poster**.
2. Stability and reactivity of acyl and acylperoxy radicals. A. Tomas, E. Villenave et R. Lesclaux, EC / Eurotrac-2 Joint Workshop, Aix-la-Chapelle, Allemagne, 20 - 22 Septembre 1999. **Poster**.
3. Etude expérimentale et théorique des constantes de vitesse de décomposition des radicaux *i*-C₃H₇CO et *t*-C₄H₉CO. A. Tomas, E. Villenave, F. Caralp and R. Lesclaux, Journée de Cinétique et Photochimie en Phase Gazeuse, Paris, 9 Juin 1999. **Oral**.
4. Is the acetylperoxy radical CH₃C(O)O₂ a good model for RC(O)O₂ + HO₂ reactions? J-P. Le Crâne, A. Tomas et E. Villenave, EC / EUROTRAC-2 Joint Workshop, Paris, 9-11 Septembre 2002. **Poster**.

5. Détermination du rapport de branchement de la réaction entre l'acétone et les radicaux OH. E. Turpin, C. Fittschen, A. Tomas, P. Devolder. Journées de Cinétique et Photochimie en Phase Gazeuse, Orléans, 2-3 Juin 2003. **Communication orale.**
6. L'analyseur de BTX 2000 G SERES, A. Tomas, Séminaire technique du LCSQA, LNE, Paris, 20 Juin 2003. **Communication orale.**
7. Réaction entre l'acétone et les radicaux OH : détermination du rapport de branchement. E. Turpin, A. Tomas, C. Fittschen et P. Devolder, Journée Interdisciplinaire Qualité de l'Air, Université des Sciences et Technologies de Lille, Villeneuve d'Ascq, 29 janvier 2004. **Poster.**
8. Conception et validation d'un spectromètre cw-CRDS dans le proche infrarouge pour application à la métrologie des polluants. S. Crunaire, C. Fittschen, B. Lemoine, A. Tomas, P. Coddeville, Journée Interdisciplinaire Qualité de l'Air, Université des Sciences et Technologies de Lille, Villeneuve d'Ascq, 29 janvier 2004. **Poster.**
9. Conception d'un spectromètre cw-CRDS dans le proche infra-rouge : application à la détection de polluants en chambre de simulation atmosphérique. S. Crunaire, C. Fittschen, B. Lemoine, A. Tomas, P. Coddeville, Journées de Cinétique et Photochimie en Phase Gazeuse, Bordeaux, 22-23 Juin 2004. **Communication orale.**
10. Réaction en phase gazeuse du catéchol avec les radicaux OH. E. Turpin, A. Tomas, C. Fittschen, N. Locoge, P. Devolder, Journées de Cinétique et Photochimie en Phase Gazeuse, Bordeaux, 22-23 Juin 2004. **Poster.**
11. Simulation chamber study of the oxidation of volatile organic compounds: detection of pollutants by cw-CRDS in the NIR. S. Crunaire, C. Fittschen, B. Lemoine, A. Tomas, P. Coddeville, Cavity Ring-Down User Meeting, Eindhoven, Pays-Bas, 7 – 8 Octobre 2004. **Poster.**
12. Développement d'un spectromètre cw-CRDS dans le proche IR et application à l'étude de mécanismes de réactions en chambre de simulation. S. Crunaire, C. Fittschen, B. Lemoine, P. Coddeville, A. Tomas, Workshop « Interfaces Chimie-Spectroscopie Atmosphériques », Villeneuve d'Ascq, 7-8 Avril 2005. **Communication orale.**
13. Simulation chamber study of the oxidation of acetic acid by oh radicals: detection of reaction products by cw-CRDS in the NIR. S. Crunaire, C. Fittschen, B. Lemoine, A. Tomas, P. Coddeville, 130th Faraday Discussion on Atmospheric Chemistry, Leeds, UK, 11-13 Avril 2005. **Poster.**
14. Etude par cw-CRDS du rapport de branchement de la réaction de l'acide acétique avec OH. S. Crunaire, A. Tomas, P. Coddeville, C. Fittschen et B. Lemoine, Journées de Cinétique et Photochimie en Phase Gazeuse, Rennes, 22-23 Juin 2005. **Poster.**
15. Use of cw-CRDS for solving VOCs degradation problems in atmospheric simulation chamber. S. Crunaire, A. Tomas, P. Coddeville, C. Fittschen, B. Lemoine, Cavity Ring-Down User Meeting, Oxford, UK, 20 – 21 Septembre 2005. **Communication orale.**
16. Mécanisme de dégradation de l'acide acétique et de ses isotopes deutérés. S. Crunaire, J. Tarmoul, A. Tomas, P. Coddeville et C. Fittschen, Journées de Cinétique et Photochimie en Phase Gazeuse et du Groupement Français de Combustion, Nancy, 10-11 Mai 2006. **Poster.**
17. Mesures par cw-CRDS de produits de réaction en chambre de simulation atmosphérique. A. Tomas, J. Tarmoul, S. Crunaire, C. Fittschen, P. Coddeville, Workshop « Interfaces Chimie-Spectroscopie Atmosphériques », Marseille, 5-6 Juin 2007. **Communication orale.**
18. In situ monitoring of HO₂ radicals in a photochemical reactor using a cw cavity ringdown spectrometer. J. Tarmoul, A. Tomas, P. Coddeville, C. Fittschen, Cavity Ring-Down User Meeting, Greifswald, Allemagne, 18 – 19 Septembre 2007. **Poster.**
19. Détection in-situ du radical HO₂ dans une chambre de simulation atmosphérique couplée à un spectromètre cw-CRDS. J. Tarmoul, A. Tomas, P. Coddeville, C. Fittschen, Journées Interdisciplinaires de la Qualité de l'Air, Villeneuve d'Ascq, 7 – 8 Février 2008. **Poster.**
20. Formation d'aérosols organiques secondaires lors de l'oxydation de composés organiques biogéniques. N. Visez, V. Riffault, A. Tomas, Journées Interdisciplinaires de la Qualité de l'Air, Villeneuve d'Ascq, 7 – 8 Février 2008. **Communication orale.**
21. Oxydation de l'acide acétique et de ses isotopes deutérés par le radical OH dans une chambre de simulation atmosphérique. E. Szabo, J. Tarmoul, A. Tomas, C. Fittschen, P. Coddeville, S. Dobé, Journées Interdisciplinaires de la Qualité de l'Air, Villeneuve d'Ascq, 7 – 8 Février 2008. **Poster.**
22. Formation des radicaux HO₂ après 248 nm irradiation d'un mélange de C₆H₆ / O₂ observé par photolyse laser / cw-CRDS. A. Aluculesei, A. Tomas, C. Schoemaeker, C. Fittschen, Journées de Cinétique et Photochimie en Phase Gazeuse, Strasbourg, 9 – 10 Juin 2008. **Poster.**

23. Photolyse du benzène à 254 nm en chambre de simulation atmosphérique. E. Szabo, A. Tomas, C. Fittschen, P. Coddeville, S. Dobe, Journées de Cinétique et Photochimie en Phase Gazeuse, Strasbourg, 9 – 10 Juin 2008. **Communication orale.**
24. Développement d'un nouveau réacteur pour l'étude de la formation des aérosols organiques secondaires lors de l'ozonolyse de composés organiques volatils. N. Visez, A. Renard, V. Riffault, A. Tomas, Journées de Cinétique et Photochimie en Phase Gazeuse, Strasbourg, 9 – 10 Juin 2008. **Poster.**
25. Détection *in-situ* de radicaux HO₂ en chambre de simulation par cw-CRDS. J. Tarmoul, A. Tomas, C. Fittschen, P. Coddeville, Journées de Cinétique et Photochimie en Phase Gazeuse, Créteil, 17 – 18 Juin 2009. **Poster.**
26. Secondary Organic Aerosol formation from the gas-phase reaction of catechol with ozone. C. Coeur – Tourneur, A. Tomas, A. Guilloteau, F. Henry, F. Ledoux, N. Visez, V. Riffault, J. Wenger, Y. Bedjanian and V. Foulon, Journées de Cinétique et Photochimie en Phase Gazeuse, Créteil, 17 – 18 Juin 2009. **Poster.**
27. The application of cw-CRDS in the photolysis of methyl nitrite. M. Djehiche, A. Tomas, C. Fittschen, P. Coddeville, Cavity Enhanced Spectroscopy: recent developments and new challenges, Lorentz Center, Leiden, Pays-Bas, 2 – 6 Novembre 2009. **Poster.**
28. Validation d'un réacteur à écoulement pour l'étude de la formation des aérosols organiques secondaires : réaction d'ozonolyse de l'alpha-pinène. M. Duncianu, V. Riffault, A. Tomas, P. Coddeville, Congrès Français des Aérosols, Paris, 13 – 14 Janvier 2010. **Communication orale.**
29. Etude de la photochimie de quelques COV par cw-CRDS. M. Djehiche, A. Tomas, P. Coddeville, C. Fittschen, Journées Interdisciplinaires de la Qualité de l'Air, Villeneuve d'Ascq, 4 – 5 Février 2010. **Communication orale.**
30. Etude de la formation d'aérosols organiques secondaires (AOS) par ozonolyse de composés organiques volatils (COV). M. Duncianu, V. Riffault, A. Tomas, P. Coddeville, Journées Interdisciplinaires de la Qualité de l'Air, Villeneuve d'Ascq, 4 – 5 Février 2010. **Poster.**
31. Etude cinétique en réacteur à écoulement de l'ozonolyse d'une série d'alcènes. M. Duncianu, V. Riffault, A. Tomas, P. Coddeville, Journées de Cinétique et Photochimie en Phase Gazeuse, Wimereux, 9 – 10 Juin 2010. **Poster.**
32. Etude cinétique de la photolyse de CH₃ONO et de la réaction CH₃OH + Cl par la technique cw-CRDS. M. Djehiche, A. Tomas, C. Fittschen, P. Coddeville, Journées de Cinétique et Photochimie en Phase Gazeuse, Wimereux, 9 – 10 Juin 2010. **Communication orale.**
33. Validation of a new flow reactor for the study of secondary organic aerosol (SOA) formation. M. Duncianu, V. Riffault, A. Tomas, P. Coddeville, Advanced Atmospheric Aerosol Symposium, Florence, Italie, 19 – 22 septembre 2010. **Communication orale.**
34. Réactions de pentènes méthylés et de l'α-pinène avec O₃ : coefficients de vitesse et produits formés. M. Duncianu, V. Riffault, A. Tomas, P. Coddeville, Journées de Cinétique et Photochimie en Phase Gazeuse, Villeneuve d'Ascq, 30 – 31 Mai 2011. **Communication orale.**
35. Etudes expérimentales en chambre de simulation couplée à la cw-CRDS *in-situ*. M. Djehiche, A. Tomas, C. Fittschen, P. Coddeville, Journées de Cinétique et Photochimie en Phase Gazeuse, Villeneuve d'Ascq, 30 – 31 Mai 2011. **Poster.**
36. Réacteur à écoulement pour l'étude de la formation des aérosols organiques secondaires par ozonolyse de composés organiques volatils. M. Duncianu, V. Riffault, A. Tomas, P. Coddeville, Journées Nord-Ouest Européennes des Jeunes Chercheurs, Caen, 14-15 juin 2011. **Poster.**
37. Détection de HONO dans la réaction CH₃ONO + OH. M. Djehiche, A. Tomas, C. Fittschen, P. Coddeville, Premier colloque francophone sur les « Polluants organiques générés par l'agriculture et les transports », Agadir, Maroc, 25 – 27 Octobre 2011. **Poster.**
38. Coefficients de vitesse et produits en phase gazeuse obtenus dans les réactions d'ozonolyse d'une série de pentènes ramifiés. M. Duncianu, V. Riffault, R. Olariu, C. Arsene, A. Tomas, P. Coddeville, Premier colloque francophone sur les « Polluants organiques générés par l'agriculture et les transports », Agadir, Maroc, 25 – 27 Octobre 2011. **Communication orale.**

Activités d'enseignement et d'encadrement

☞ Cours de chimie-physique

- **Cours de Spectroscopie Moléculaire** en 2^{ème} année d'IUT Mesures Physiques (Université Bordeaux I)

contenu: spectres d'absorption UV-Visible, niveaux d'énergie, orbitales moléculaires, résonance magnétique nucléaire, mésomérie.

volume: 2 groupes d'une vingtaine d'étudiants de l'option Matériaux et Contrôles Physico-Chimiques (20h), suivi d'un devoir surveillé (1999-2000)

- **Cours de Cinétique Chimique** en 3^{ème} année d'école d'ingénieurs, option Environnement et Industrie (Ecole des Mines de Douai)

contenu: critères de classification des réactions, méthodes de détermination d'ordre de réaction et de constante de vitesse, calcul de l'énergie d'activation, exercices d'application.

volume: groupe d'une vingtaine d'étudiants de l'option Environnement et Industrie (8h par année scolaire), suivi d'un devoir surveillé (2002-2005)

- **Cours de Cinétique appliquée à la Chimie Atmosphérique** en 3^{ème} année d'école d'ingénieurs, option Environnement et Industrie (Ecole des Mines de Douai)

contenu: rappel des grands problèmes environnementaux liés à l'atmosphère, chimie atmosphérique, techniques d'étude en laboratoire, exemples d'application.

volume: groupe d'une vingtaine d'étudiants de l'option Environnement et Industrie (7h par année scolaire (2006-)

- **Cours sur la Mesure et le Traitement des Odeurs** en 3^{ème} année d'école d'ingénieurs, option Environnement et Industrie (Ecole des Mines de Douai)

contenu: origine des odeurs, seuils olfactifs, méthodes de mesure, procédés de traitement

volume: groupe d'une vingtaine d'étudiants de l'option Environnement et Industrie (2h par année scolaire (2008-)

☞ Travaux dirigés de chimie (TD)

- **TD de Chimie Générale et Organique** en 1^{ère} année d'école d'ingénieurs (Ecole des Mines de Douai)

contenu: nomenclature, bilans matière, spectroscopie, calcul d'incertitudes, oxydo-réduction, ...

volume: 12 séances de 2h (2004-2011)

☞ Travaux pratiques de chimie (TP)

- **TP de Chimie Générale** en 1^{ère} année d'IUT Mesures Physiques (Université Bordeaux I)

contenu: mesure de pH, propriétés des solutions tampons, dosages acide-base par pH-métrie

volume: 5 séances de 4h (1999-2000)

- **TP de Chimie Analytique** en 3^{ème} année d'école d'ingénieurs (Ecole des Mines de Douai). Développement et responsabilité d'un TP GC-IRTF.

contenu: séparation et identification de composés organiques par chromatographie en phase gazeuse couplée à la spectrométrie infrarouge à Transformée de Fourier
volume: 8 séances de 4h par année scolaire (2001-2004)

• **TP de Chimie Générale et Analytique** en 1^{ère} année d'école d'ingénieurs (Ecole des Mines de Douai)

contenu: chromatographie en phase gazeuse, spectroscopies IRTF et UV-visible, spectroscopie d'absorption atomique, calorimétrie, cinétique en phase liquide, oxydo-réduction, diagrammes binaires, analyse thermique différentielle, thermodynamique
volume: 6 séances de 4h par année scolaire (2001-2011)

☞ Autres activités d'enseignement

• **Séminaires sur la mesure et le traitement des odeurs** dans le cadre de la formation continue des DREAL (4 séminaires de 2,5 h par an) (2005-)

• **Ecoles d'été** « Physico-chimie de l'Atmosphère » :

- Université « Al. I. Cuza », Iasi, Roumanie, 3 – 14 juillet 2006 : conférences sur l'utilisation des chambres de simulation atmosphérique, la mesure des odeurs et l'organisation de la surveillance de la qualité de l'air en France (6h).
- Université « Ovidius », Constanta, Roumanie, 10 – 16 juillet 2008 : conférence sur la chimie atmosphérique et l'utilisation des chambres de simulation atmosphérique (2h).

☞ Activités d'encadrement

• **Projet de Découverte de la Recherche** (2008-) en 3^{ème} année d'école d'ingénieurs (Ecole des Mines de Douai). Le travail confié aux étudiants leur permet une première approche (80h) du domaine de la recherche.

sujets de recherche : dosage de composés aromatiques hydroxylés en chambre de simulation, cinétiques d'ozonolyse de composés oléfiniques

volume: 2 à 3 élèves-ingénieurs de l'option Environnement et Industrie ; encadrement technique et scientifique, participation au jury en anglais

• **Etudes bibliographiques** en 1^{ère} année d'école d'ingénieurs (Ecole des Mines de Douai). Il est demandé aux étudiants d'effectuer une recherche bibliographique complète sur un sujet donné (du domaine technique), l'objectif étant de les initier aux difficultés de la recherche bibliographique et du travail de synthèse.

Exemples d'études encadrées :

"Le PAN (peroxyacétylnitrate) : quelle place dans l'atmosphère ?" (2004)

"Les nez électroniques" (2007)

"Les atmosphères extra-planétaires : moyens d'étude et caractéristiques physico-chimiques" (2009)

"Les lasers femto secondes : fonctionnement et applications" (2010)

volume: groupes de 2 élèves-ingénieurs ; suivi du projet et participation aux jurys de soutenance

• **Stagiaires : Licence et Maîtrise de chimie-physique** (Université Bordeaux I), **DEA Structure de la matière** (Université de Lille I / Ecole des Mines de Douai), **IUT Chimie**

(Université de Lille I et Université d'Artois), **Ecole Supérieure de Métrologie** (Ecole des Mines de Douai)

• **Doctorants** encadrés à l'Ecole des Mines de Douai

2001 – *Estelle Turpin* (collaboration avec le laboratoire PC2A de l'Université des Sciences et Technologies de Lille) – Encadrement : 60 % avec C. Fittschen.

« Cinétique et mécanisme de dégradation atmosphérique de trois composés organiques volatils : l'acétone, le phénol et le catéchol ».

Thèse soutenue le 10 décembre 2004

2002 – *Sabine Crunaire* (collaboration avec les laboratoires PhLAM et PC2A de l'Université des Sciences et Technologies de Lille) – Encadrement : 60 % avec B. Lemoine et C. Fittschen.

« Développement d'un spectromètre CRDS dans le proche infrarouge : application à la métrologie des polluants dans une chambre de simulation atmosphérique ».

Thèse soutenue le 6 décembre 2005

2004 – *Angélique Guilloteau* (collaboration avec le laboratoire LCSR du CNRS à Orléans) – Encadrement : 60 % avec Y. Bedjanian.

« Etude multiphasique de polluants organiques aromatiques : répartition des Hydrocarbures Aromatiques Polycycliques dans les suies et formation d'aérosols dans l'ozonolyse du catéchol ».

Thèse soutenue le 18 décembre 2007

2006 – *Emese Szabo* (en co-tutelle entre l'Université de Lille 1 et l'Université de Szeged, Hongrie) – Encadrement : 50 % avec le Prof. S. Dobé.

« Atmospheric kinetics and photochemistry of oxygenated volatile organic compounds ».

Soutenance prévue le 21 novembre 2011.

2008 – *Mokhtar Djehiche* – Encadrement : 100 %.

« Développement d'un couplage cw-CRDS – chambre de simulation pour la mesure in situ du radical HO₂ et d'espèces d'intérêt atmosphérique ».

Soutenance prévue le 21 octobre 2011.

2008 – *Marius Duncianu* – Encadrement : 100 % (avec V. Riffault).

« Réacteur à écoulement pour l'étude de la formation des aérosols organiques secondaires par ozonolyse de composés organiques volatils : développement analytique, validation cinétique et ozonolyse de composés biogéniques ».

Soutenance prévue 1^{er} trimestre 2012.

2011 – *Hichem Bouzidi* – Encadrement : 100 %.

« Etude de la photochimie atmosphérique de composés organiques carbonylés par spectroscopie cw-CRDS en chambre de simulation atmosphérique ».

2011 – *Tristan Braure* – Encadrement : 100 % (avec V. Riffault).

« Cinétique et mécanismes de réactions de composés organiques volatils conduisant à la formation d'aérosols organiques secondaires ».

• **Post-docs** à l'Ecole des Mines de Douai

2005 : E. Turpin : Élaboration d'une méthode d'échantillonnage des COV odorants (1 an)

2007 : J. Thiébaud : Mesure du spectre NIR du radical HO₂ (4 mois)

2008 : N. Visez : Développement d'un réacteur à aérosol pour l'étude des AOS (1 an)

• **Professeurs invités** à l'Ecole des Mines de Douai

2010 : R.I. Olariu (1 mois, financement IRENI) : Cinétiques d'ozonolyse de pentènes en chambre de simulation atmosphérique

2011 : - T. Gierczak (1 mois, financement IRENI) : Photolyse de la 2,3-pentanedione : Détermination des rendements quantiques

- R.I. Olariu (1 mois, financement EMD) : Produits d'ozonolyse de pentènes en réacteur à écoulement

- C. Arsene (1 mois, financement EMD) : Produits d'ozonolyse de pentènes en réacteur à écoulement

☞ **Formation continue suivie**

• **Formation à la pédagogie** (Ecole des Mines de Douai) : Stage théorique de 11 jours animé par des chercheurs de l'IRAP (Institut de Recherche et d'Animation en Pédagogie, Belgique) en 2003

• **Formation à la conduite de projets** (Ecole des Mines de Douai) : initiation à la gestion de projet (2 jours en 2003) pour l'encadrement d'un groupe d'étudiants entreprenant un projet avec un client extérieur à l'Ecole (module de Pédagogie Par Projet)

• **Sauveteur Secouriste du Travail** depuis 2002 (recyclage tous les 2 ans)

• **Formation d'anglais** (Ecole des Mines de Douai) : obtention du TOEIC en 2007 (940)

Activités d'animation et de rayonnement

Mes activités d'animation et autres fonctions collectives peuvent se décliner de la façon suivante :

- participation aux commissions de suivi pédagogique des élèves-ingénieurs de 1^{ère} année et aux conseils des professeurs de 1^{ère} et 3^{ème} année de l'Ecole des Mines de Douai,
- participation aux jurys de concours du recrutement des élèves-ingénieurs de l'Ecole des Mines de Douai, aux jurys de stages et projets de fin d'étude,
- membre titulaire de la commission de spécialistes (sections 31-32-33-40) de l'ULCO (2007-2009),
- membre du Comité Hygiène et Sécurité (CHS) de l'Ecole des Mines de Douai depuis 2009 et animation du comité Hygiène et Sécurité interne au sein du département Chimie – Environnement,
- responsable de l'animation de l'axe « Réactivité des polluants » (5 enseignants-chercheurs) au sein du département Chimie – Environnement,
- réponse à des appels d'offres, montage de projets de recherche (CPER, ANR, LCSQA) et gestion des budgets alloués, expertise de rapports d'activités de projets de recherche (PRIMEQUAL) et d'articles scientifiques (Applied Physics B (1), Atmospheric Environment (1), International Journal of Chemical Kinetics (1) et Reaction Kinetics and Catalysis Letters (1)),
- activités de promotion de l'Ecole des Mines de Douai (participation à des colloques et séminaires, visite du laboratoire, accompagnement des élèves-ingénieurs en visite d'entreprise).

Document de synthèse

Chapitre I. Introduction

I.1 Généralités

I.1.1 Eléments de contexte atmosphérique

L'atmosphère terrestre est une fine couche de gaz entourant la Terre et indispensable au maintien de la vie. Son épaisseur est inférieure à 1% du rayon terrestre et sa densité varie de 1000 hPa au niveau des océans (soit $\sim 2,5 \times 10^{19}$ molécules.cm⁻³), à 10⁻³ hPa ($\sim 2,5 \times 10^{13}$ molécules.cm⁻³) vers 100 km d'altitude, au sommet de la thermosphère. La composition chimique de l'atmosphère terrestre est très particulière et typique de notre planète : elle est caractérisée par la présence dominante de diazote N₂ ($\sim 78\%$ en volume) et de dioxygène O₂ ($\sim 21\%$ en volume) complétée, d'une part, de quelques autres gaz dont la teneur est spatialement constante (gaz rares, H₂, CO₂) et, d'autre part, d'une multitude d'autres espèces gazeuses à l'état de trace (molécules, ions, radicaux) dont la concentration peut être extrêmement variable dans le temps et l'espace et en tout cas inférieure au ppmv (partie par million en volume), comme, par exemple, les composés organiques volatils (COV) et les radicaux peroxy RO₂[•]. La très grande variabilité spatio-temporelle de ces espèces est le résultat de phénomènes physico-chimiques très complexes, comme la réactivité chimique, le transfert de phase et le transport. Pour être complet, il convient de mentionner i) la vapeur d'eau qui tient une place à part étant donné sa très grande variabilité en concentration dans l'espace et le temps et son rôle majeur dans le climat de la Terre ; ii) les particules, très diverses en qualité (minérales, organiques, pollens, etc.), de teneurs très variables et dont l'impact sur le climat est également important mais sujet à de nombreuses incertitudes (1).

On divise habituellement l'atmosphère en « couches » dont les frontières sont délimitées par les zones d'inversion de température. Depuis le haut de l'atmosphère, on trouve successivement la thermosphère et la mésosphère (au-dessus de 50 km d'altitude), puis la stratosphère et, enfin, la troposphère, cette dernière étant la couche la plus basse de l'atmosphère et s'étendant de la surface de la Terre jusqu'à environ 10-15 km d'altitude. Cette partie de l'atmosphère revêt une importance particulière, car c'est là que les êtres vivants et la végétation sont présents : tout changement physique ou chimique dans les propriétés de la troposphère aura un impact potentiel sur les vies animale et végétale telle que nous la connaissons sur la Terre. C'est donc sur le devenir des COV dans cette couche atmosphérique qu'ont porté mes travaux de recherche. La pollution atmosphérique, qui est *“ l'introduction par l'homme directement ou indirectement dans l'atmosphère ou dans les espaces clos de substances ayant des conséquences préjudiciables de nature à mettre en danger la santé humaine, à nuire aux ressources biologiques et aux écosystèmes, à influencer sur les changements climatiques, à détériorer les biens matériels, à provoquer des nuisances olfactives excessives ”* (Loi sur l'Air et l'Utilisation Rationnelle de l'Energie du 30

décembre 1996) constitue justement un de ces changements au sein de l'atmosphère dont les effets sur l'environnement sont aujourd'hui clairement avérés. Aux premiers évènements locaux bien connus de smogs urbains extrêmes des années 1950 (Londres, Los Angeles) se sont succédé d'autres phénomènes beaucoup plus étendus dans leurs impacts : les pluies acides, le trou d'ozone stratosphérique, l'augmentation de la capacité oxydante de l'atmosphère et le changement climatique, finissant de prouver, s'il en était besoin, la sensibilité de l'atmosphère terrestre aux activités humaines. Les recherches menées au cours des dernières décennies ont révélé l'extrême complexité du fonctionnement du compartiment 'atmosphère' de la Terre, celui-ci comportant à la fois des aspects chimiques, dynamiques et physiques et étant également fortement lié aux autres compartiments que sont les océans, les surfaces continentales, la végétation, etc.

La dégradation de la qualité de l'air, initialement dans les zones urbaines puis sur des régions entières (comme le fameux 'Asian Brown Cloud'), est un phénomène qui est apparu avec le développement de l'industrie et des transports motorisés vers la fin du 19^{ème} siècle – début du 20^{ème} siècle. L'impact de cette altération de la qualité de l'air par des espèces traces sur la santé humaine et, plus globalement, sur l'environnement (climat, végétation, bâti, ...) est aujourd'hui pleinement reconnu, avec des conséquences économiques importantes, notamment à cause des coûts liés à la santé et des baisses de rendements agricoles (2, 3).

Les connections entre la pollution de l'air et ses effets sur la santé humaine sont aujourd'hui très largement documentées grâce à de nombreuses études épidémiologiques (4, 5) et l'Organisation Mondiale de la Santé (OMS) a classé la pollution de l'air en zone urbaine comme facteur de risque significatif (**Figure I.1**). La pollution de l'air est caractérisée par la présence de nombreux photo-oxydants, dont l'ozone (O₃) et les oxydes d'azote (NO_x), ainsi que des particules fines ; ces trois polluants ont fait l'objet de recherches sanitaires approfondies ces dernières années (6). L'ozone est un déclencheur du stress oxydant, des crises d'asthme et d'accident vasculaire-cérébral chez les sujets sensibles (7, 8) ; d'autres effets comme la formation de kystes sébacés (athérogenèse) (9) ont été répertoriés. En dépit d'efforts importants pour diminuer ses concentrations atmosphériques, les niveaux d'ozone 'de fond' augmentent de 1 à 2 % par an depuis 40 ans (10-12). Des liens entre les niveaux d'oxydes d'azote et la mortalité ont aussi été démontrés en zone urbaine, quoique moins évidents que l'ozone (13-15). Enfin, les effets des particules sur la santé humaine ont été clairement mis en évidence dans de nombreuses études (6, 16, 17).

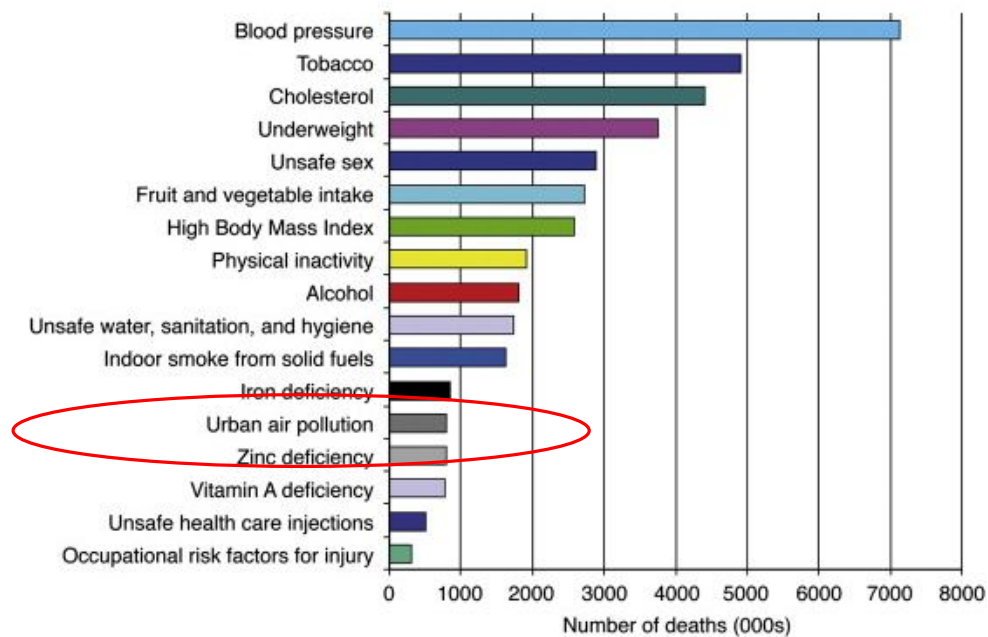


Figure I.1 : Nombre de morts (en milliers au niveau mondial) attribuables aux principaux facteurs de risques répertoriés (18)

Bien que le risque moyen de mortalité ou morbidité lié à la pollution atmosphérique soit plutôt faible comparé à d'autres facteurs bien connus (tabac, ...), l'impact demeure important compte tenu du grand nombre de personnes exposées (19). Par ailleurs, étant donné l'accroissement de l'urbanisation et des très grandes agglomérations (actuellement, 26 ont plus de 10 millions d'habitants) attendu dans les années à venir, le problème de la pollution de l'air en milieu urbain risque de s'accroître à l'avenir. Selon une estimation de l'OMS, les pics de pollution à l'ozone seraient responsables de plus de 20 000 morts prématurées chaque année en Europe (20). Récemment, une étude menée dans 25 grandes villes européennes (projet APHEKOM) a montré que 19 000 vies pourraient être épargnées si les recommandations de l'OMS sur les concentrations de PM2.5 étaient strictement respectées et, corrélativement, que 31,5 milliards d'euros seraient économisés en dépenses de santé, absentéisme, etc. (rapport disponible à <http://www.endseurope.com/docs/110302b.pdf>). Enfin, en Inde, la pollution atmosphérique serait responsable de la mort de 2 millions de personnes chaque année (21).

I.1.2 Eléments de chimie atmosphérique

La pollution de l'air est le résultat d'une chimie très complexe 'alimentée' par les sources d'émission des composés organiques volatils (COV) et des NO_x (NO + NO₂) et initiée essentiellement par le rayonnement solaire incident. L'impact d'un COV émis dans l'atmosphère va être déterminé principalement par son devenir atmosphérique, lequel est conditionné par les

processus de transport, réactivités homogène et hétérogène et dépôts. La chimie atmosphérique consiste à étudier comment une molécule émise est dégradée et comment cette dégradation affecte la composition et les propriétés de l'atmosphère. Les sources de COV sont traditionnellement divisées en sources anthropiques et biogéniques. En France, ces deux types de sources sont sensiblement équivalents (en tonnes d'équivalent C) tandis qu'au niveau global, la source biogénique excède largement la source anthropique (22, 23). La chimie atmosphérique revêt des aspects à la fois homogènes (réactions en phase gazeuse ou liquide) et hétérogènes (transferts gaz – particules, réactions de surfaces, ...). A caractère oxydant, elle conduit à la formation de produits secondaires, dont, en particulier, les COV oxygénés (COVO : composés carbonylés, peroxydes, ...) selon le mécanisme simplifié présenté en **Figure I.2**.

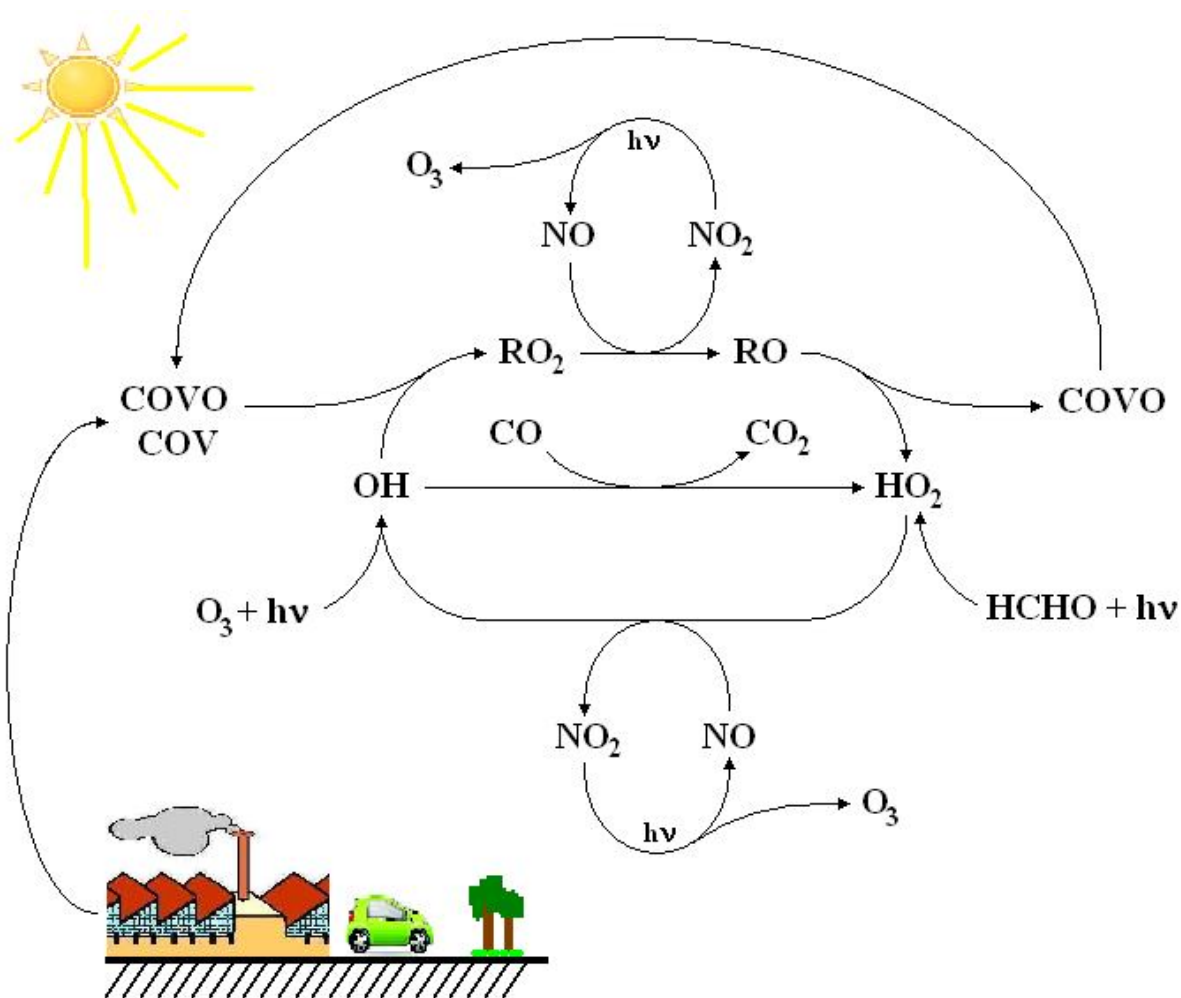


Figure I.2 : Schéma simplifié du cycle d'oxydation d'un COV par le radical OH[•], montrant la double source primaire et secondaire des COVO

Dans cette figure, RH représente un COV, RO_2^\bullet et RO^\bullet des radicaux peroxydes et alkoxydes. On remarque immédiatement la place centrale des radicaux hydroxyles OH^\bullet et hydroperoxydes HO_2^\bullet ainsi que le rôle des oxydes d'azote NO et NO_2 dans la production d'ozone O_3 . Les radicaux OH^\bullet proviennent principalement de la photolyse de l'ozone en présence d'eau et de la réaction $\text{HO}_2^\bullet + \text{NO}$. D'autres sources peuvent être localement importantes, comme la photolyse de l'acide nitreux HONO et les réactions d'ozonolyse des alcènes.

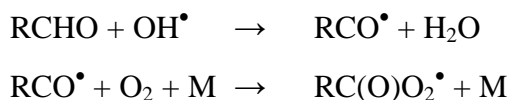
La **Figure I.2** suggère que les COVO possèdent, outre des sources primaires très variées (feux de biomasse, végétation, océans, solvants industries chimiques, etc.), une source secondaire qui peut être très importante selon les composés (par ex. le formaldéhyde, l'acétone) et selon l'environnement (par ex. urbain ou forestier). Les concentrations de COVO dans les atmosphères urbaines peuvent représenter parfois plus de 50 % des COV totaux (24). De plus, la réactivité spécifique des COVO fait qu'ils contribuent de manière très significative à la formation d'ozone troposphérique et des espèces réservoirs (peroxydes, nitrates) (25). Lors de la campagne de mesure MILAGRO dans la région de Mexico, *Apel et al.* (26) ont montré que la réactivité des COVO vis-à-vis du radical OH^\bullet pouvait être aussi importante que celle des hydrocarbures non méthaniques. Une connaissance fine du devenir des composés organiques volatils oxygénés – les réactions d'initiation, les mécanismes d'oxydation en phase gazeuse et la formation éventuelle d'aérosols organiques secondaires (AOS) – est donc nécessaire pour une meilleure compréhension et modélisation de la chimie troposphérique.

Un autre domaine majeur de la chimie atmosphérique, dans lequel les COVO jouent un rôle très actif est la formation des aérosols organiques secondaires (27, 28). Ces aérosols, issus de processus de conversion gaz-particule, viennent renforcer la charge en matière particulaire du milieu atmosphérique, peuvent modifier le bilan radiatif terrestre, et agissent sur la formation des noyaux de condensation (qui sont à la base du processus de formation des nuages). Les composés aromatiques (toluène, xylènes, etc.) et les composés biogéniques (notamment les terpènes) sont les principaux précurseurs d'AOS dans l'atmosphère. Les aérosols organiques (et pas seulement les secondaires) subissent une oxydation lors de leur séjour dans l'atmosphère, ce qui se traduit par une augmentation de la fraction oxygénée et, souvent, de l'hygroscopicité. Les campagnes de terrain ont montré que la fraction oxygénée de la matière carbonée des AOS était souvent très importante, avec une récurrence des fonctions acides et carbonyles. Une bonne connaissance des composés à l'origine des aérosols organiques secondaires et des rendements en aérosols des réactions d'oxydation de ces précurseurs est donc là aussi nécessaire pour représenter fidèlement la partie condensée de l'atmosphère. Par ailleurs, les propriétés physiques (tailles des particules,

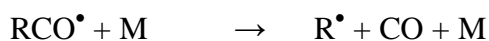
concentrations) et chimiques des AOS étant primordiales d'un point de vue sanitaire et climatique, il convient d'améliorer nos connaissances de la composition des AOS et de leur devenir une fois formés dans l'atmosphère.

I.2 Objectifs des travaux de recherche

De formation initiale en génie des procédés industriels, mon premier contact avec le monde de la recherche s'est réalisé au cours de mon stage de DEA à Sollac-Fos/mer, durant lequel j'ai travaillé sur la compréhension et l'optimisation d'un procédé de traitement d'effluents acides industriels. Mes travaux de recherche en lien avec la qualité de l'air ont véritablement débuté lors de ma thèse de doctorat à l'Université de Bordeaux 1, laquelle portait sur l'étude de cinétiques de réactions radicalaires d'intérêt atmosphérique. Ces premiers travaux de recherche m'ont rapidement plongé au cœur de la chimie atmosphérique. En effet, les réactions radicalaires en phase gazeuse, et notamment celles impliquant les radicaux peroxydes RO_2^\bullet , sont à la base de l'ensemble des processus chimiques atmosphériques. Je me suis intéressé à l'étude des cinétiques de radicaux acyles RCO^\bullet et acylperoxydes RC(O)O_2^\bullet qui sont formés lors de l'oxydation des composés carbonylés par le radical hydroxyle OH^\bullet :



M représente un auxiliaire de collision (N_2 ou O_2 généralement) qui sert à dissiper l'excès d'énergie présent sur RC(O)O_2^\bullet lors de la réaction. La première problématique était de déterminer le devenir du radical acyle en fonction de la structure de R, en particulier l'importance de la voie de décomposition :



par rapport à la voie d'oxydation avec O_2 . La deuxième problématique portait sur l'influence de la structure du groupement alkyle R sur les cinétiques des réactions mutuelles et croisées des radicaux RC(O)O_2^\bullet . Enfin, le troisième questionnement concernait la cinétique de la réaction $\text{CH}_3\text{C(O)O}_2^\bullet + \text{HO}_2^\bullet$, réaction essentielle dans les modèles de chimie atmosphérique. L'étude de cette réaction, pour laquelle il existait une controverse importante (facteur 3 dans la cinétique) ainsi que l'étude de la réaction équilibrée $\text{HO}_2^\bullet + \text{CH}_3\text{CHO}$, a permis de lever cette incertitude majeure.

Les travaux menés ensuite lors de mon post-doctorat à l'Université de Wuppertal (Allemagne) puis dans mon poste actuel à l'Ecole des Mines de Douai concernent essentiellement l'étude de réactions d'oxydation de composés organiques volatils oxygénés dans l'atmosphère. Ces travaux revêtent plusieurs aspects :

- le développement de nouveaux outils expérimentaux : chambres de simulation, spectroscopie cw-CRDS (continuous wave – cavity ring-down spectroscopy), réacteur à écoulement ;
- l'étude des cinétiques et mécanismes réactionnels de composés organiques volatils oxygénés en phase gazeuse ;
- l'étude des phénomènes de formation des aérosols organiques secondaires à partir de l'ozonolyse de composés aromatiques et biogéniques.

Ces trois axes sont brièvement explicités dans le paragraphe suivant puis plus complètement développés dans le deuxième chapitre.

I.3 Activités de recherche

I.3.1 Développement de nouveaux outils expérimentaux

L'étude de ce système complexe qu'est la chimie atmosphérique a débuté par une investigation assez globale des phénomènes homogènes au moyen de chambres à smog (les 'smog chambers' (29, 30)), en lien avec l'observation du smog photochimique de Los Angeles au début des années 1950 et dans le but de comprendre les relations entre les émissions atmosphériques et la formation de ce smog (31, 32). Ces premières études (et d'autres sur le terrain) ont révélé l'importance du cycle O_3 -NO- NO_2 et le rôle des précurseurs du smog, *i.e.* les composés organiques volatils. La nécessité d'aller plus loin dans la compréhension des phénomènes, en particulier en s'intéressant aux cinétiques et mécanismes des processus élémentaires, a encouragé le développement d'autres outils complémentaires, notamment les réacteurs à écoulement (33, 34) et les réacteurs de photolyse (35). Dans le même temps, les chambres à smog ont évolué pour permettre l'étude des mécanismes d'oxydation des composés organiques volatils au travers d'expériences en atmosphères mieux contrôlées et dans des conditions simplifiées par rapport aux conditions réelles de l'atmosphère, d'où l'apparition des chambres de simulation atmosphérique actuelles ('atmospheric simulation chambers' en France (36, 37), aux USA (38, 39), au Japon (40), par exemple).

Les plus récents développements concernant les chambres de simulation ont plutôt trait aux outils d'analyse qui leur sont associés et aux niveaux de contamination très faibles en NO_x et en

composés carbonés. On peut citer en particulier les chambres de simulation en Californie, à Caltech (41) et à l'Université de Riverside (42), en Europe les chambres à irradiation naturelle SAPHIR (43) et EUPHORE (44), et le réacteur de laboratoire HIRAC à Leeds en Angleterre (45).

A mon arrivée à l'École des Mines de Douai en septembre 2001, un enseignant-chercheur avait commencé à construire une enceinte en bois supportant un système d'irradiation et deux extracteurs d'air dans le but de développer une chambre de simulation très simple de type réacteur souple en Téflon. L'achèvement du montage du dispositif et la mise en place d'un outil d'analyse original basé sur un système de thermodésorption, un chromatographe en phase gazeuse couplée à la spectroscopie infrarouge et à un détecteur à ionisation de flamme (GC-IRTF-FID) ont été effectués dans le cadre d'un stage de master que j'ai encadré (46). Ce premier réacteur a permis de répondre à un questionnement scientifique portant sur le mécanisme d'oxydation de l'acétone par le radical OH^\bullet (thèse d'E. Turpin (47)). A ce moment-là, le développement très récent d'une nouvelle technique de spectroscopie ultra-sensible, la « continuous-wave cavity ring-down spectroscopy » cw-CRDS (48) a amené simultanément quelques équipes de la Région Nord-Pas de Calais travaillant dans le domaine de la qualité de l'air à entreprendre le développement de cellules optiques utilisant cette technique. En collaboration avec le PC2A et le PhLAM, et dans le cadre de la thèse de S. Crunaire (49), nous avons, dans un premier temps, développé une cellule cw-CRDS puis, dans un deuxième temps, nous l'avons couplée à la chambre de simulation souple dans l'objectif d'utiliser les capacités de la cw-CRDS, en particulier sa sensibilité et sa sélectivité, pour étudier le mécanisme d'oxydation de l'acide acétique et de ses isotopes deutérés. La principale limitation de cette cellule résidait dans son incapacité à détecter des espèces chimiques instables, typiquement des radicaux, car l'analyse du mélange réactionnel nécessitait un prélèvement vers la cellule cw-CRDS. Ceci nous a naturellement conduits à développer une nouvelle chambre de simulation équipée d'un spectromètre cw-CRDS *in situ*, le réacteur (rigide cette fois) jouant alors à la fois le rôle d'enceinte photochimique et de cellule spectroscopique. Ce dispositif expérimental innovant, développé dans le cadre de la thèse de M. Djehiche (50), a servi à démontrer la formation de HONO dans la réaction $\text{CH}_3\text{ONO} + \text{OH}^\bullet$, le méthyl nitrite CH_3ONO étant très largement utilisé dans les études de cinétiques en laboratoire comme source de radicaux OH^\bullet ((51) : **publication n°1**). Dans un deuxième temps, l'étude d'un système réactionnel relativement simple (photolyse de Cl_2 en présence de CH_3OH et d'air) a permis pour la première fois de détecter et quantifier *in situ* le radical HO_2^\bullet dans une chambre de simulation, sans prélèvement préalable ni conversion chimique. L'étude des cinétiques de disparition des radicaux HO_2^\bullet dans le réacteur a montré que les parois internes du réacteur constituaient un puits assez important pour cette espèce, notamment à basse

pression (< 50 Torr), ce qui serait susceptible de modifier de façon significative les mécanismes réactionnels étudiés dans ce type de réacteur ((52) : **publication n°2**).

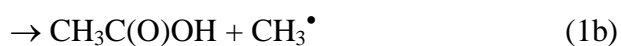
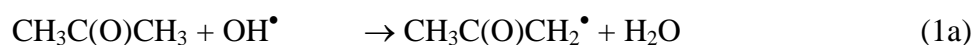
En parallèle à ces développements expérimentaux, mon intérêt pour la problématique de la formation des aérosols organiques secondaires m'a amené à développer un autre dispositif en vue d'étudier les premières étapes de la formation des particules. C'est ainsi qu'un réacteur à écoulement à flux laminaire dédié à l'étude de la formation des aérosols organiques secondaires a été développé, autorisant des temps de séjour de quelques dizaines de secondes jusqu'à quelques minutes, en fonction des conditions de l'écoulement et de la position de l'injecteur central dans le tube. Je tiens à préciser que ce développement s'est réalisé en collaboration avec Dr. V. Riffault, enseignante-chercheuse au département et dans le cadre d'un post-doc (Dr. N. Visez) puis d'un travail de thèse (M. Duncianu) encadrés conjointement par Dr. V. Riffault et moi-même (53). Les premiers travaux ont porté sur la validation cinétique du réacteur au travers de l'étude de réactions d'ozonolyses de composés insaturés ((54) : **publication n°3**), travaux réalisés avec la collaboration des Dr. R.I. Olariu et C. Arsene de l'Université de Iasi (Roumanie).

Pour terminer cette présentation succincte de ce premier aspect de mes activités de recherche, je tiens à souligner que l'ensemble de ces développements expérimentaux n'auraient pas vu le jour sans la précieuse collaboration de nombreuses personnes, notamment des personnels du département Chimie et Environnement, du PC2A et du PhLAM, ainsi que des étudiants en thèse.

I.3.2 Cinétiques et mécanismes d'oxydation de COVO

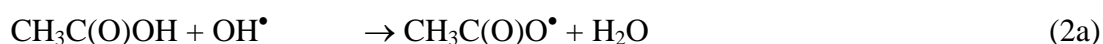
Nous nous sommes tout d'abord intéressés au devenir atmosphérique de deux espèces oxygénées majeures de l'atmosphère : l'acétone ($\text{CH}_3\text{C}(\text{O})\text{CH}_3$) et l'acide acétique ($\text{CH}_3\text{C}(\text{O})\text{OH}$), dans le cadre de leurs réactions avec le radical OH^\bullet . Les résultats obtenus ont permis de contribuer à une meilleure connaissance du mécanisme initial d'attaque du radical hydroxyle sur les molécules étudiées.

Dans le cas de l'acétone, l'objectif de ces travaux a été de déterminer l'importance de la voie d'addition-élimination conduisant à la formation d'acide acétique (voie (1b)) :



Les premières expériences ont été réalisées au PC2A sur le tube à écoulement rapide (55). Nous avons ensuite examiné cette réaction par des expériences en chambre de simulation atmosphérique en utilisant deux sources de radicaux OH[•] et deux réacteurs différents. Puis, dans une approche complémentaire, l'acétone complètement deutéré a été employé : la constante de vitesse de la réaction CD₃C(O)CD₃ + OH[•] a été déterminée ainsi que le rapport de branchement de la voie formant l'acide acétique deutéré. En effet, les cinétiques des réactions de transfert d'un atome d'hydrogène dépendent fortement de la substitution isotopique, notamment à cause de l'abaissement de l'énergie de point zéro (ZPE) avec la substitution qui a pour effet d'augmenter la barrière d'activation (56). Cette deuxième série d'expériences a permis de confirmer la prédominance de la voie d'arrachement dans la réaction CH₃C(O)CH₃ + OH[•] ((57) : **publication n°4**).

Dans le cas de l'acide acétique, l'objectif des travaux était de déterminer la proportion de radicaux OH réagissant sur l'hydrogène de la fonction acide (voie (2a)) :



Deux méthodes ont été principalement utilisées pour investiguer ce mécanisme : la mesure du CO₂ formé dans la voie (2a) après dissociation du radical CH₃C(O)O[•] ((58) : **publication n°5**) et l'étude des cinétiques d'oxydation par OH[•] des isotopes deutérés de l'acide acétique ((59) : **publication n°6**). Les résultats montrent que la voie d'attaque principale du radical OH[•] se fait sur l'hydrogène carboxylique (pour CH₃C(O)OH et CD₃C(O)OH). L'acide glyoxylique HC(O)C(O)OH, issu de l'autre voie d'attaque, a par ailleurs été détecté, ce qui semble indiquer que le radical [•]OCH₂C(O)OH réagit (au moins partiellement) avec O₂, conformément à des résultats de calculs quantiques (60).

Mes travaux de recherche les plus récents portent sur le devenir de composés carbonylés multi-oxygénés. Nous avons souligné au paragraphe I.1.2 la place des COVO dans les cycles d'oxydation des COV et leur importance dans la chimie atmosphérique. Au cours de leur dégradation en phase gazeuse, les COV passent par des intermédiaires radicalaires de type alkoxy RO[•] dont l'oxydation va conduire à des COVO porteurs de fonctions carbonyles et/ou hydroxyles. Ces deux fonctions sont en effet fréquemment retrouvées parmi les produits d'oxydation des COV. Le devenir de ce type de composés multifonctionnels est cependant très peu connu et par conséquent, les modèles de chimie atmosphérique ne peuvent pas les intégrer de façon précise.

Comme beaucoup d'autres COV, la réaction avec le radical OH^\bullet est probablement importante ; toutefois, la présence d'une fonction carbonyle peut rendre le composé aisément photolysable, ce qui tend à alimenter la charge radicalaire de l'atmosphère et augmente sa capacité oxydante. Par ailleurs, la solubilité des COVO peut fortement s'accroître en fonction du type de fonctions présentes dans la molécule, ce qui peut modifier complètement le devenir et l'impact de l'espèce oxygénée dans l'atmosphère. A l'instar d'autres familles de COV comme les alcènes, il ne peut s'agir d'étudier tous les composés possibles, mais de chercher plutôt à dégager des tendances dans leur réactivité en étudiant de façon ciblée quelques composés représentatifs. Dans ce contexte, nous avons orienté nos recherches vers les familles des α -dicarbonylés, ces composés étant issus (outre les sources primaires) de l'oxydation des composés aromatiques et des alcènes (61, 62). Nos travaux ont concerné, dans un premier temps, la réactivité de la 2,3-pentanedione, travaux réalisés dans le cadre d'une collaboration avec le Prof. S. Dobé de l'Académie des Sciences de Budapest ((63) : **publication n°7**).

I.3.3 Formation des aérosols organiques secondaires

Mes travaux sur la formation des aérosols organiques secondaires ont commencé lors de mon séjour post-doctoral à l'Université de Wuppertal (Allemagne), alors que nous nous intéressions à la réactivité des catéchols (1,2-dihydroxybenzènes) avec le radical nitrate NO_3^\bullet . Les catéchols sont fortement présents dans les produits de combustion de biomasse et peuvent également être formés dans l'oxydation du benzène et du toluène par le radical OH^\bullet . Dans les conditions expérimentales utilisées, le radical NO_3^\bullet était généré *in situ* par réaction entre O_3 et NO_2 . Or, les premières expériences impliquant le composé organique et l'ozone uniquement ont rapidement montré une réactivité importante des catéchols avec l'ozone ainsi que la formation de nanoparticules lors d'épisodes de nucléation homogène.

Ceci nous a conduits à déterminer les cinétiques d'ozonolyse du 1,2-dihydroxybenzène et de ses deux dérivés méthylés (3-méthyl et 4-méthyl), confirmant le caractère inhabituel de la réactivité avec O_3 pour des composés aromatiques ((64) : **publication n°8**). Les rendements de formation en aérosols organiques secondaires ont ensuite été déterminés ((65, 66) : **publication n°9 et 10**) et se trouvent être relativement élevés (jusqu'à 86%). Ces derniers travaux ont été réalisés dans trois chambres de simulation différentes, en collaboration avec Dr. C. Cœur (LPCA Dunkerque) et Dr. J. Wenger (UCC Cork, Irlande) dans le cadre d'un financement INTROP.

Chapitre II. Développement de nouveaux outils expérimentaux

II.1 Les chambres de simulation atmosphérique

Les chambres de simulation atmosphérique (CSA) sont l'un des outils les plus répandus pour l'étude de la réactivité des composés organiques volatils. Ces réacteurs sont construits en matière souple (Téflon) ou rigide (verre, acier ou plexiglas) et développent un volume très variable (quelques centaines de mL pour les plus petites jusqu'à 250 m³). Les réactions étudiées sont initiées par un rayonnement artificiel (tubes fluorescents) ou par le rayonnement naturel (lumière solaire) et le mélange réactionnel est sondé par des techniques analytiques très diverses, allant de la chromatographie en phase gazeuse à la spectrométrie IRTF *in-situ*. A l'inverse du milieu atmosphérique, les conditions expérimentales dans les CSA sont parfaitement contrôlées et le milieu fortement simplifié : quelques polluants seulement sont introduits initialement dans le réacteur. Ceci permet (et a permis) de déterminer des données cinétiques et mécanistiques avec une bonne fiabilité.

II.1.1 Développement d'une CSA souple pour l'étude de la photochimie de COV

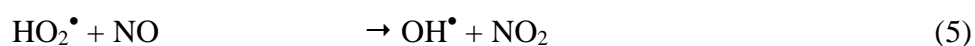
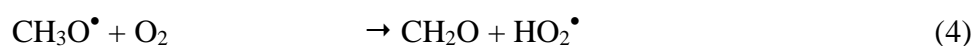
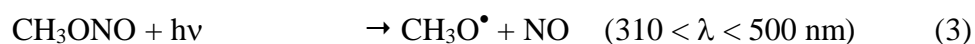
II.1.1.1 Description du dispositif

Le premier dispositif développé au département Chimie et Environnement (CE) est une CSA en Téflon d'un volume d'environ 300 L associée à la technique d'analyse par chromatographie en phase gazeuse couplée à la détection par spectrométrie IRTF. A mon arrivée en septembre 2001, seule l'enceinte en bois (~ 1 m³) supportant les tubes fluorescents et munie de deux extracteurs d'air (régulation de la température interne) était en place, suite au stage d'un étudiant en DEA (ex Master 2). Deux types de rayonnement étaient disponibles : des tubes à vapeur de mercure basse pression pour une émission monochromatique à 253.7 nm (6 tubes, Philips™ TMX 204 LS, 30 W) et des tubes fluorescents émettant sous forme d'un continuum entre 310 et 500 nm (8 tubes, Philips™ TMX 200 LS, 18 W). L'intérieur de l'enceinte en bois était recouvert de feuilles d'aluminium afin d'homogénéiser la répartition du rayonnement.

Après une première phase de validation du protocole de fabrication des chambres en Téflon par thermosoudage de deux rectangles de film (Téflon FEP, 50 µm d'épaisseur) de 1,2 × 1,2 m, des lignes d'introduction et de prélèvement en Téflon ¼ " ont été reliées au réacteur via des connections standard de type Swagelock™ (Supelco). Une rampe à vide en verre chauffée (température ajustable entre 40°C et 150°C environ) a ensuite été installée sur la ligne d'entrée des gaz pour l'introduction des réactifs (souvent sous forme liquide à température ambiante) dans la CSA.

II.1.1.2 Méthode de production des radicaux OH•

Les radicaux OH• utilisés dans les différentes études réalisées sont produits par photolyse de nitrite de méthyle CH₃ONO (synthétisé au laboratoire d'après *Taylor et al. (67)*) en présence de NO sous rayonnement UV proche :



Le composé synthétisé, de couleur jaune pale, est soit conservé au congélateur (-20°C environ) dans un piège en verre muni d'un septum (méthode utilisée dans les premières années), soit transféré dans un canister (initialement sous vide), lequel est ensuite pressurisé à l'azote à 4 bars. Dans ce dernier cas, on ne garde que 80% du méthyl nitrite synthétisé, les ~10% (en volume) initiaux et ~10% finaux étant éliminés.

II.1.1.3 Outils d'analyse du milieu réactionnel

Il a été nécessaire d'adapter le dispositif analytique existant (TD-GC-IRTF-FID) à l'analyse des gaz. Afin de remédier au faible niveau de sensibilité du dispositif analytique, une méthode de prélèvement par boucle à gaz grand volume, piégeage cryogénique à l'azote liquide et thermodésorption flash a été mise au point, permettant d'atteindre des limites de détection satisfaisantes pour des études de cinétiques et mécanismes d'oxydation de COV.

Ce dispositif de thermodésorption s'appuie sur un préconcentrateur – injecteur TCT-Chrompack (Thermodesorption and Cold Trap) constitué de deux compartiments successifs :

- un four de thermodésorption de cartouches d'adsorbants, contenant dans notre cas une cartouche vide ;
- un piège froid constitué d'un morceau de colonne capillaire désactivée (environ 30 cm de long) remplie de billes de verre.

En amont de ce dispositif se trouve une boucle à gaz (Silcosteel ¼ de pouce, 20 mL), initialement non thermostatée, puis installée (en 2006) dans le four du GC, et servant à échantillonner le mélange réactionnel. L'ensemble « boucle à gaz – TCT » fonctionne selon trois étapes successives :

1. balayage de la boucle à gaz pendant 3 min à $\sim 100 \text{ mL min}^{-1}$ avec le mélange réactionnel et refroidissement du piège cryogénique par de l'azote liquide à -190°C ; ces conditions permettent d'assurer un échantillonnage représentatif de la chambre de simulation ;
2. basculement de la vanne en position injection et transfert de l'échantillon vers le piège froid du TCT ; durant cette étape, le four contenant la cartouche vide est chauffé à 100°C de manière à éviter une rétention des composés les moins volatils ;
3. chauffage très rapide ($\sim 60^\circ\text{C/s}$) du piège froid de -190°C à 250°C (température ajustable) et injection flash de l'ensemble des composés dans la colonne du GC.

Un analyseur d'oxydes d'azote (TEI 42C) et un analyseur d'ozone (TEI 49C) viennent compléter le GC-IRTF-FID. Ces deux analyseurs bénéficient de l'expertise du laboratoire LMPA (Laboratoire de Métrologie des Polluants Atmosphériques : accréditation COFRAC pour NO_x et O_3) au sein du département CE pour leur étalonnage régulier via des matériels standard certifiés. Des analyses par GC-MS sont également possibles mais nécessitent un prélèvement sur cartouche d'adsorbants.

II.1.1.4 Validation du dispositif

La validation de l'ensemble de l'appareillage (CSA et GC-IRTF) a été réalisée par l'étude de la cinétique de la réaction toluène + OH^\bullet . La constante de vitesse de la réaction $\text{C}_7\text{H}_8 + \text{OH}^\bullet$ à température ambiante a été déterminée par la méthode de cinétique relative en utilisant deux composés de référence : le n-heptane et le cyclohexane (**Figure II.1**). La valeur moyenne obtenue ($k_{\text{toluène}+\text{OH}} = 5,3 \times 10^{-12} \text{ cm}^3 \cdot \text{molécule}^{-1} \cdot \text{s}^{-1}$) est très proche de celle de la littérature ($k = 5,63 \times 10^{-12} \text{ cm}^3 \cdot \text{molécule}^{-1} \cdot \text{s}^{-1}$ (68)) et permet de valider le système développé pour l'étude de la réactivité des COV.

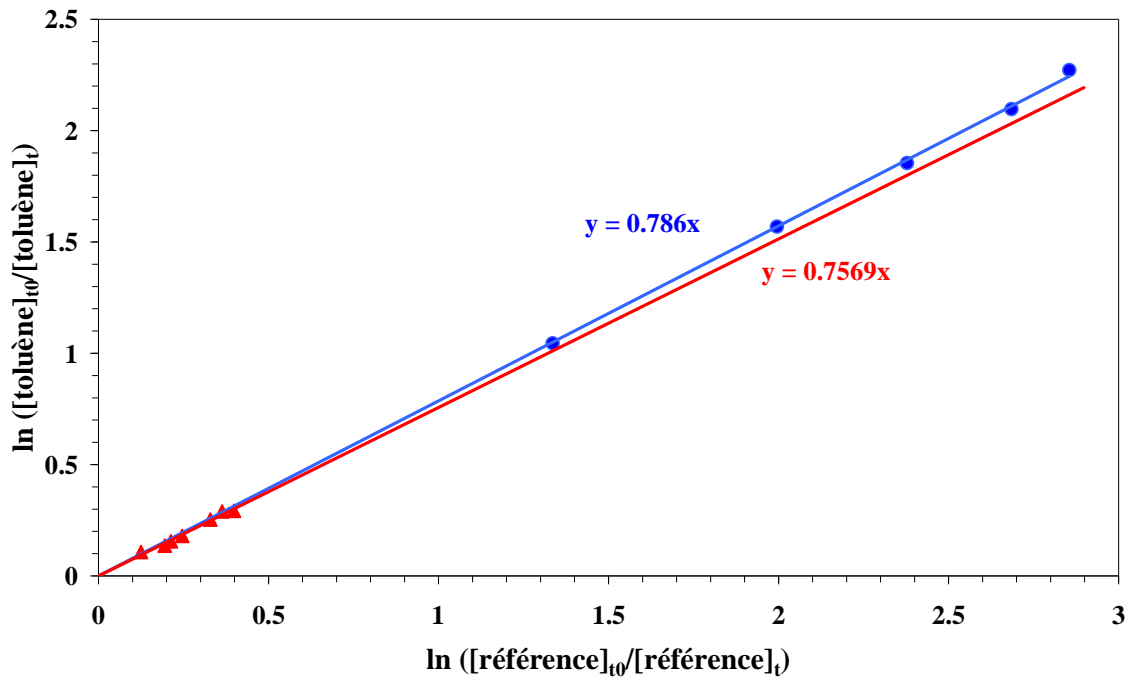


Figure II.1 : Droites de cinétiques relatives obtenues dans l'étude de la réaction toluène + OH[•]. Composés de référence : n-heptane (en bleu) et cyclohexane (en rouge).

Cette première étape de développement de la CSA a aussi permis de soulever quelques limitations du système : 1) sensibilité du détecteur IRTF limitée, entraînant des difficultés pour la mise en évidence de produits minoritaires de réaction : cette contrainte pourra être tempérée par la possibilité de réaliser des spectres de masse des composés par GC-MS ; 2) échantillonnage par boucle à gaz risqué dans le cas de composés 'collants' (type aromatiques oxygénés) : la méthode de prélèvement sur cartouche de charbon actif sera développée dans ce cas-là.

L'ensemble de ce travail a été réalisé dans le cadre d'un stage de DEA 'Structure et Dynamique des Systèmes Réactifs' (46).

II.1.2 Développement de la spectroscopie cw-CRDS

L'équipement d'analyse associé aux chambres de simulation atmosphérique permet généralement d'avoir accès aux concentrations des espèces stables, notamment des composés organiques volatils et des oxydes d'azote. Suite aux premières études des années 70 – 80, le besoin s'est alors fait sentir de pouvoir aussi sonder les espèces radicalaires peroxyées, essentielles en chimie atmosphérique. Au cours des années 90 ont été développées différentes techniques plus ou moins complexes : on peut citer la mesure des radicaux peroxyés par MIESR (Matrix Isolation

Electron Spin Resonance : 1^{ère} mesure directe du HO₂[•] dans l'atmosphère en 1978), par amplification chimique (PERCA : PEROxy Radical detection by Chemical Amplification) et la technique FAGE (Fluorescence Assay by Gas Expansion) pour les radicaux OH[•] et HO₂[•] (69, 70). Très récemment est apparue la technique PeRCIMS (Peroxy Radical Chemical Ionization Mass Spectrometry) qui combine la conversion chimique et la spectrométrie de masse à ionisation chimique et permet de différencier et mesurer les radicaux HO₂[•] et RO₂[•] (71). Ces méthodes demandent toutefois une haute technicité et sont coûteuses à mettre en place.

La faisabilité de la spectroscopie cw-CRDS a fait l'objet d'un premier article par *Romanini et al.* en 1997 (48). Les avantages indéniables de cette technique – rapidité de la mesure, résolution spectrale, sensibilité, faible coût – ont rapidement entraîné son développement dans de très nombreux domaines de la physique et de la chimie. Ses potentialités en termes de détection de radicaux nous ont amené à envisager son développement au laboratoire, son couplage à la chambre de simulation atmosphérique souple dans un premier temps, puis son intégration dans une nouvelle chambre de simulation rigide. Dans les paragraphes suivants, nous présentons le principe de la spectroscopie cw-CRDS, le développement du premier couplage puis la construction de la nouvelle chambre de simulation avec cw-CRDS *in situ*.

II.1.2.1 Principe de la spectroscopie cw-CRDS

Le principe de la spectroscopie cw-CRDS a été expliqué et développé dans de nombreux articles et ouvrages ((72, 73)) et je ne rappellerai que les éléments essentiels dans les paragraphes suivants.

Cavité résonnante

L'acronyme anglo-saxon cw-CRDS pourrait être traduit en français par « spectroscopie en cavité résonnante avec source d'émission continue ». Dans le domaine du proche IR, on utilise généralement des lasers de type diodes DFB (distributed feedback) issues de l'industrie des télécommunications et assez bon marché. Ces diodes émettent une lumière monochromatique (largeur de la raie de quelques MHz soit $\Delta\nu < 0.001 \text{ cm}^{-1}$) de faible puissance (quelques mW) qu'on cherche à coupler à un résonateur de Fabry-Pérot. Ce dernier consiste en deux miroirs plans parallèles possédant un coefficient de réflectivité R proche de 1. L'étude de la fonction de transmission du résonateur montre que la cavité ne laisse passer quasiment aucune lumière (car R est proche de 1) sauf pour les fréquences ν_i telles que $L = n/2\nu_i$ où L est la distance séparant les 2 miroirs et n un nombre entier. En effet, dans ce dernier cas, des interférences constructives se mettent en place à l'intérieur de la cavité qui devient quasi transparente à l'émission laser. Si l'on

stoppe alors l'injection de lumière dans la cavité, l'intensité de la lumière piégée dans la cavité formée des 2 miroirs hautement réfléchissants va décroître de façon exponentielle à une vitesse $k = (1 - R)c/L$ où c est la vitesse de la lumière. L'inverse de k est appelé temps de déclin $\tau = 1/k$ (ring-down time) et représente le temps moyen passé par un photon dans la cavité. C'est la mesure de ce temps de déclin qui va permettre la détermination de la concentration d'une espèce absorbante présente dans la cellule.

Mesure de la concentration d'une espèce absorbante

En l'absence d'espèce absorbante entre les 2 miroirs, on peut montrer que le temps de déclin, noté alors τ_0 , ne dépend que du coefficient R (74) :

$$\tau_0 = \frac{L}{c(1 - R)} \quad (\text{Eq. I})$$

En présence d'une espèce absorbante A , on démontre que le temps de déclin s'écrit (74) :

$$\tau = \frac{L}{c(1 - R + \alpha_\lambda d)} \quad (\text{Eq. II})$$

où α_λ est le coefficient d'absorption de A à la longueur d'onde λ et d la longueur d'absorption. La combinaison de ces deux dernières équations donne accès au coefficient α_λ :

$$\alpha_\lambda = \frac{R_L}{c} \left(\frac{1}{\tau} - \frac{1}{\tau_0} \right) \quad (\text{Eq. III})$$

où R_L est le rapport entre la distance entre les 2 miroirs (L) et la longueur d'absorption (d).

En pratique, le temps de déclin 'cavité vide' τ_0 est pris au pied de la raie d'absorption et est supposé ne pas varier de façon significative sur la largeur de la raie (72). La concentration de l'espèce $[A]$ est déduite de cette dernière relation si l'on connaît la section efficace d'absorption σ de l'espèce à la fréquence de résonance :

$$[A] = \frac{\alpha_\lambda}{\sigma_\lambda} \quad (\text{Eq. IV})$$

La détermination de la concentration d'une espèce absorbante repose donc sur la mesure d'un temps de déclin et non d'une intensité comme en spectroscopie d'absorption classique. On peut noter aussi que la mesure de α_λ permet de déterminer σ_λ si l'on connaît la concentration de l'espèce absorbante [A].

Limite de détection

La limite de détection d'un composé est calculée à partir de l'absorption minimum α_{\min} détectable dans une région spectrale donnée, lorsque τ tend vers τ_0 (75) :

$$\alpha_{\min} = \frac{\Delta\tau_{\min}}{c \tau_0^2} \quad (\text{Eq. V})$$

$\Delta\tau_{\min}$ représente le plus petit changement détectable dans le temps de déclin. La valeur obtenue α_{\min} est aisément convertie en limite de détection LD_A en divisant par la section efficace d'absorption σ du composé A :

$$LD_A = \frac{\alpha_{\min}}{\sigma} = \frac{\Delta\tau_{\min}}{\sigma c \tau_0^2} \quad (\text{Eq. VI})$$

Pour améliorer la limite de détection, 3 leviers d'action sont disponibles : i) augmenter la valeur de τ_0 en augmentant la distance L entre les deux miroirs ou en augmentant le coefficient de réflectivité R des miroirs ; ii) améliorer le $\Delta\tau_{\min}$ en supprimant au maximum les modes transverses (qui engendrent des décroissances multi-exponentielles (76)), en stabilisant mécaniquement la cavité et en augmentant le nombre de ring-down moyennés ; iii) choisir une raie d'absorption plus intense pour augmenter la valeur de σ .

Largeur des raies

Dans le domaine du proche IR et à basse pression (< 100 Torr) où l'effet Doppler est dominant, la largeur d'une raie à mi-hauteur est donnée par l'équation suivante (77) :

$$\Delta\nu_D = \nu_0 \sqrt{\frac{2kT \ln 2}{m c^2}} \quad (\text{Eq. VII})$$

où ν_0 est la fréquence d'absorption de la raie considérée, k la constante de Boltzmann ($1,38 \times 10^{-23}$ J.K⁻¹), T la température, m la masse de composé considéré ($m = M/N_A$ où M est la masse molaire et

N_A le nombre d'Avogadro) et c la vitesse de la lumière. Cet élargissement conduit à un profil de raie gaussien. Dans le cas du formaldéhyde à température ambiante et pour une raie d'absorption vers $1,5 \mu\text{m}$, $\Delta\nu_D = 220 \text{ MHz}$.

L'élargissement dû à la pression provient des collisions entre molécules. La théorie des collisions permet de montrer que cet élargissement (en termes de largeur à mi-hauteur) est de la forme (77, 78) :

$$\Delta\nu_p = \frac{1}{2\pi t} = C d^2 \sqrt{\frac{2kT}{\pi\mu}} \quad (\text{Eq. VIII})$$

où t est la durée moyenne entre deux collisions, C la concentration du gaz principal (généralement $\text{N}_2 + \text{O}_2$), d le diamètre moyen des molécules du gaz principal et μ la masse réduite. A 20 Torr de pression d'air, l'élargissement est de 20 MHz environ. On constate ainsi que l'effet Doppler est dominant dans l'élargissement des raies dans les conditions expérimentales présentes et que les raies auront un profil plutôt gaussien.

II.1.2.2 Couplage cw-CRDS – CSA souple

Le développement du couplage cw-CRDS – CSA souple et les tests de validation ont été effectués dans le cadre de la thèse de S. Crunaire (49). Sans vouloir reprendre point par point tous les choix effectués et les caractéristiques finales de ce couplage qui sont détaillés dans cette thèse, nous en rappellerons les grandes lignes.

La cellule cw-CRDS développée (**Figure II.2**) est un tube en Pyrex de 70 cm de long et 1,5 cm de diamètre auquel sont soudés deux tubes de 5 cm de long pour l'entrée et la sortie des gaz. Ces deux tubes sont munis de connections standard de type KF qui permettent d'assurer une bonne étanchéité. La cellule est reliée à la CSA souple au moyen d'une ligne en Téflon $\frac{1}{4}$ " côté entrée et à un RDM $100 \text{ mL}\cdot\text{min}^{-1}$ et une pompe type Drycal™ côté sortie. Aux deux extrémités de la cellule sont fixés des éléments en aluminium pouvant recevoir les supports de miroirs cw-CRDS.

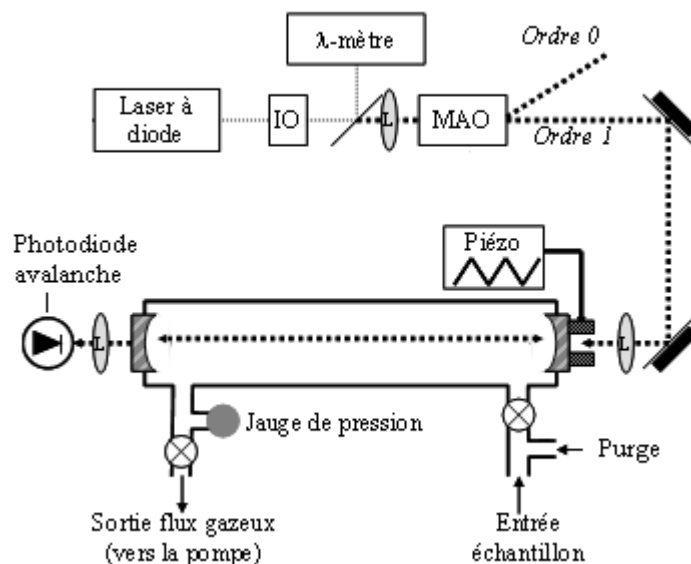


Figure II.2 : cellule cw-CRDS (adaptée de (49))

Le montage optique comprend, côté entrée :

- une diode laser (habituellement une DFB fibrée ; nous avons également utilisé ponctuellement une diode à cavité externe) ;
- un modulateur acousto-optique (MAO) fibré, qui permet d'interrompre l'injection de lumière dans la cavité afin d'observer le ring-down ;
- une lentille ($f = 30$ cm) pour réaliser l'accord de mode.

Côté sortie, il comprend :

- une photodiode avalanche de type InGaAs pour la détection ;
- une lentille ($f = 5$ cm) pour la focalisation sur la fenêtre active de la photodiode.

La position des différents éléments d'optique par rapport aux miroirs de la cavité est calculée au moyen d'un programme développé dans l'équipe de D. Romanini. Il y a en effet une contrainte forte sur la position de ces éléments, pour que l'enveloppe du faisceau incident recouvre parfaitement l'enveloppe du faisceau réfléchi.

La détermination du temps de déclin τ se fait par moyennage d'un certain nombre de décroissances exponentielles (généralement une trentaine) puis extraction de τ en utilisant la méthode d'ajustement de Levenberg-Marquardt, qui offre les meilleures performances en terme de précision (75). L'acquisition d'une raie d'absorption se fait par balayage en fréquence de la diode

laser. La concentration de l'espèce gazeuse observée est déterminée par la mesure du coefficient d'absorption α_λ (voir Eq. III).

L'application de ce développement expérimental a concerné le branchement de la réaction $\text{CH}_3\text{C}(\text{O})\text{OH} + \text{OH}^\bullet$ dont l'étude est décrite dans le chapitre III, paragraphe III.3.

II.1.3 Développement et validation d'une CSA rigide avec spectroscopie cw-CRDS *in situ*

Le développement du couplage cw-CRDS – CSA rigide et les tests de validation ont été effectués dans le cadre de la thèse de M. Djehiche (50).

II.1.3.1 Développement expérimental

L'objectif qui sous-tendait le développement d'une nouvelle chambre de simulation avec spectroscopie cw-CRDS *in situ* était de pouvoir détecter des espèces réactives à courte durée de vie, typiquement les radicaux HO_2^\bullet , ces derniers étant des intermédiaires majeurs dans les mécanismes chimiques atmosphériques. L'objectif à terme est d'étudier les processus de photolyse de composés carbonylés, dont les produits de réactions les plus fréquemment observés sont le CO, le CO_2 , le formaldéhyde et le radical HO_2^\bullet comme intermédiaire de réaction. Or, ces espèces sont aisément mesurées par cw-CRDS dans le proche IR. Deux aspects essentiels peuvent être rappelés ici concernant le rôle des radicaux HO_2^\bullet : (i) ils conditionnent la formation du radical OH^\bullet *via* la réaction $\text{HO}_2^\bullet + \text{NO}$; (ii) ils interviennent dans les réactions de terminaison des cycles photochimiques *via* les réactions du type $\text{HO}_2^\bullet + \text{RO}_2^\bullet$. Le précédent développement expérimental n'offrant pas cette possibilité et ayant gagné une certaine expérience en spectroscopie cw-CRDS, nous avons décidé de construire un nouveau réacteur rigide. Le quartz a été choisi pour sa très bonne transmission de la lumière UV, ce qui autoriserait des expériences de photolyse à 254 nm. Les dimensions du réacteur étaient nécessairement limitées, pour des raisons de coût et d'encombrement. Le cylindre en quartz (80 cm de long, 44 cm de diamètre interne) est enfermé dans une enceinte en bois supportant des lampes de photolyse (254 nm et 365 nm, jusqu'à 19 lampes au total). Les côtés du cylindre sont fermés par des flancs en acier inoxydable munis chacun d'une ouverture pour l'alignement et de raccords standards de type KF pour la connexion des arrivées et sorties des gaz et le raccordement des supports des miroirs cw-CRDS. De part et d'autre du cylindre-réacteur sont installées deux tables optiques sur plots en caoutchouc sur lesquelles sont positionnés les différents éléments d'optique classiques d'un montage cw-CRDS. Le dispositif étant très proche du premier présenté plus haut, nous ne reviendrons pas sur les détails du montage. Les deux tables optiques ont été surélevées par rapport au réacteur afin d'éviter l'usage de pieds optiques trop grands, ce qui nuit à la stabilité et engendre du bruit.

Le schéma final de la nouvelle chambre de simulation est présenté sur la **Figure II.3** et une photographie d'une vue d'ensemble sur la **Figure II.4**.

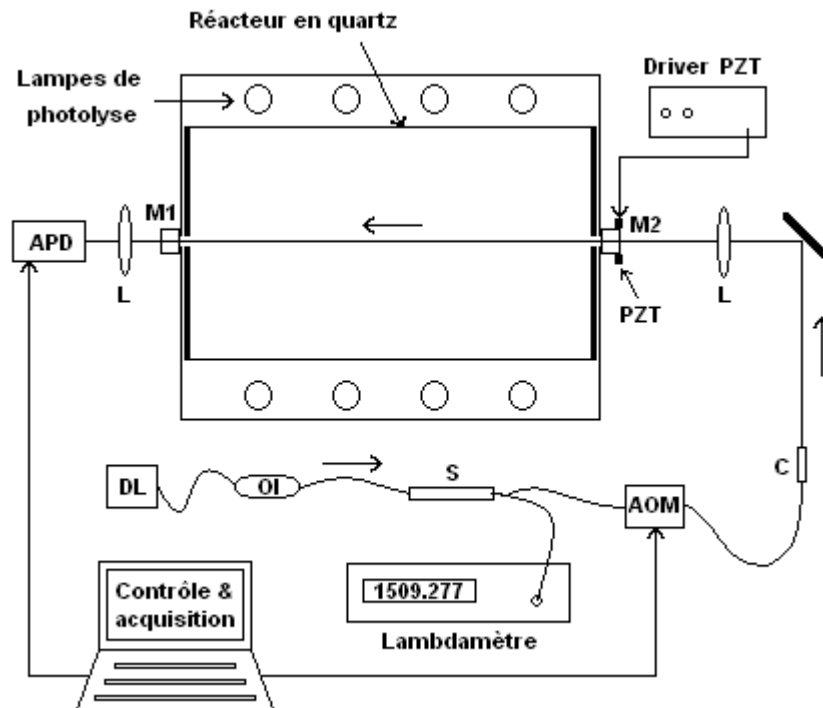


Figure II.3 : schéma du montage : M1 et M2 : miroirs cw-CRDS ; PZT : quartz piézoélectrique ; L : lentille ; C : collimateur ; AOM : modulateur acousto-optique ; S : splitter ; OI : isolateur optique ; DL : diode laser DFB ; APD : photodiode avalanche.

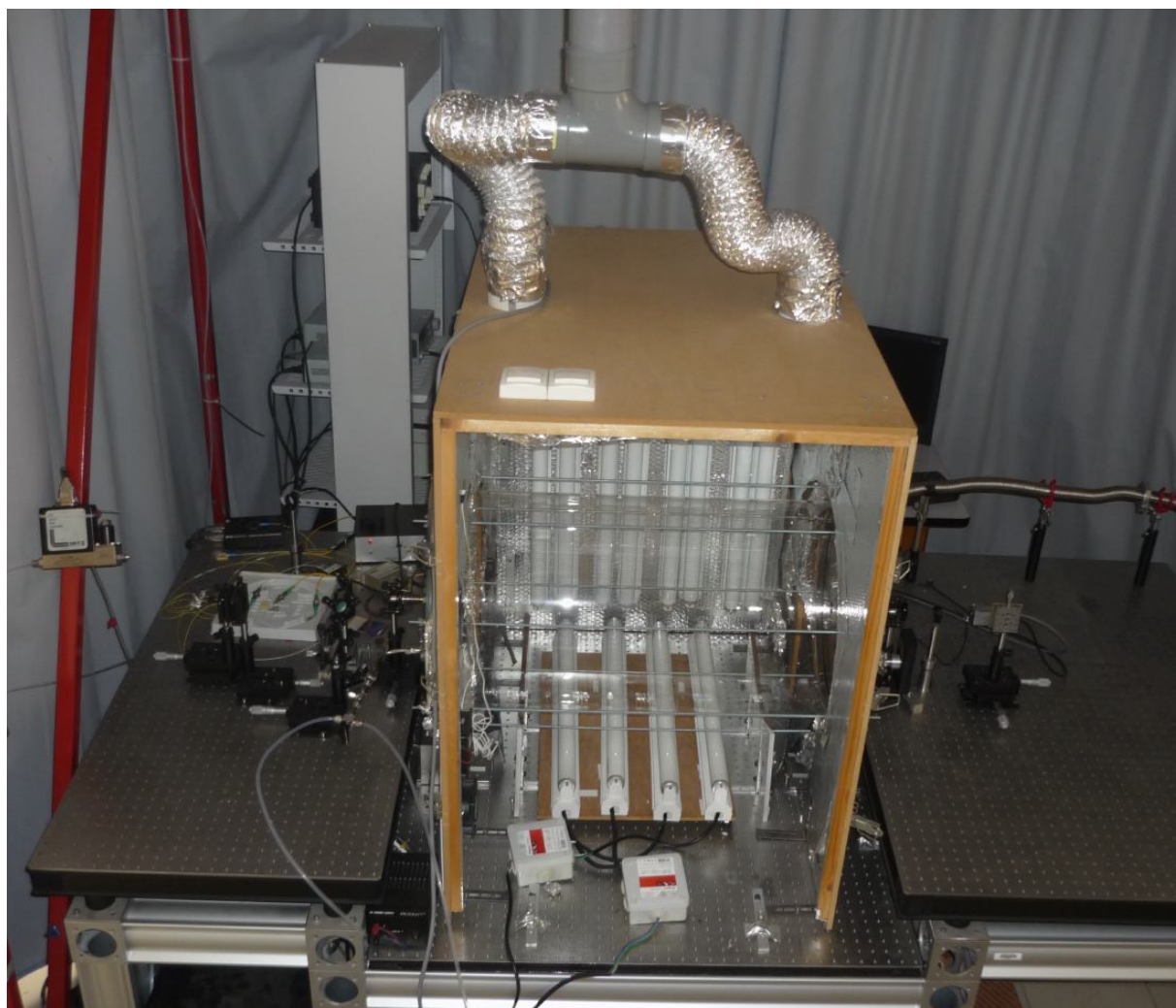


Figure II.4 : photographie d'une vue d'ensemble du dispositif : au centre l'enceinte de protection (ouverte) abritant la chambre en quartz cylindrique, à gauche la table optique supportant tous les éléments optiques depuis la diode laser jusqu'au premier miroir cw-CRDS, à droite la partie détection du signal (lentille de focalisation et photodiode avalanche). On remarque sur le haut de l'enceinte deux conduits souples reliés à des ventilateurs permettant la régulation de la température du réacteur.

Les deux premiers systèmes chimiques étudiés sont relativement bien connus, afin de pouvoir valider le dispositif et de caractériser ses performances : la photolyse du nitrite de méthyle (CH_3ONO) et l'oxydation du méthanol initiée par les atomes de chlore.

II.1.3.2 Etude des produits de photolyse du nitrite de méthyle

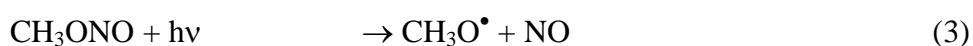
II.1.3.2.1 Introduction

Dans cette première étude, nous avons souhaité approcher un système chimique bien connu et d'intérêt en chimie atmosphérique. Par ailleurs, les produits de réaction devaient pouvoir être détectés par cw-CRDS vers 1,5 μm . Nous avons donc opté pour la photolyse du nitrite de méthyle, procédé couramment utilisé dans les expériences en chambre de simulation atmosphérique pour étudier les cinétiques et mécanismes des réactions d'oxydation des COV par les radicaux OH^\bullet . Les produits de photolyse, parmi lesquels CH_2O , NO_2 et HO_2^\bullet , étaient susceptibles d'être observés dans la région du proche IR.

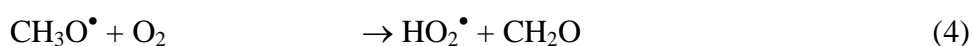
II.1.3.2.2 Approche bibliographique

Dans les années 1980, le groupe de R. Atkinson a proposé une nouvelle méthode pour générer des concentrations élevées de radicaux hydroxyles OH^\bullet dans les chambres de simulation atmosphérique (79). Cette méthode, qui mettait en œuvre la photolyse de nitrite de méthyle CH_3ONO dans le proche UV, s'est rapidement imposée dans la communauté des utilisateurs de chambres de simulation et a permis le développement d'une base de données importante sur les cinétiques et mécanismes d'oxydation des COV par les radicaux OH^\bullet (80, 81).

Les premières étapes réactionnelles dans la photolyse du nitrite de méthyle dans le proche UV (300 – 450 nm) sont bien connues. L'absorption d'un photon rompt la liaison O-NO et donne le radical methoxy $\text{CH}_3\text{O}^\bullet$ et le monoxyde d'azote NO :

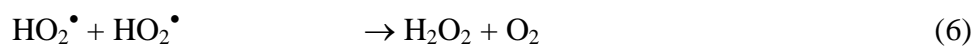


Wiebe et al. (82) ont obtenu un rendement quantique primaire de 0,76 à 366 nm. Des études plus récentes sur le nitrite de méthyle et l'isopropyl nitrite semblent toutefois indiquer que ce rendement quantique est voisin de 1 pour une irradiation entre 300 et 450 nm (83, 84). En présence de l'oxygène de l'air, le radical methoxy réagit principalement avec O_2 pour donner le radical hydroperoxyde HO_2^\bullet et un premier produit stable : le formaldéhyde CH_2O :

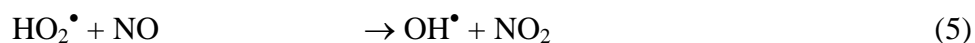


$$k_4 = 1,9 \times 10^{-15} \text{ cm}^3 \cdot \text{molécule}^{-1} \cdot \text{s}^{-1} \text{ à } 296 \text{ K} \quad (85)$$

Le radical HO_2^\bullet réagit soit avec un autre radical HO_2^\bullet soit avec le NO formé dans la réaction (3) :



$$k_6 = 1,7 \times 10^{-12} \text{ cm}^3 \cdot \text{molécule}^{-1} \cdot \text{s}^{-1} \text{ à } 296 \text{ K (86)}$$

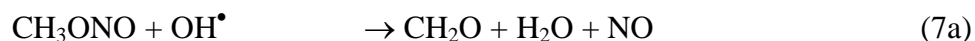


$$k_5 = 8,8 \times 10^{-12} \text{ cm}^3 \cdot \text{molécule}^{-1} \cdot \text{s}^{-1} \text{ à } 296 \text{ K (86)}.$$

Cette dernière réaction conduit au radical hydroxyl OH^\bullet et on peut obtenir assez aisément des concentrations photostationnaires de radicaux OH^\bullet de l'ordre de quelques $10^8 \text{ molécules} \cdot \text{cm}^{-3}$ par cette méthode.

II.1.3.2.3 Questionnements scientifiques

Les étapes suivantes du mécanisme de photolyse sont bien moins connues, et notamment la réaction entre les radicaux OH^\bullet et le nitrite de méthyle qui est supposée avoir lieu selon deux chemins (83) :



La constante de vitesse de la réaction (7) est assez faible : $k_7 = k_{7a} + k_{7b} = 2,8 \times 10^{-13} \text{ cm}^3 \cdot \text{molécule}^{-1} \cdot \text{s}^{-1}$ à température ambiante (87). Alors que la voie (7a) est une voie de terminaison, la voie (7b) est une voie de propagation radicalaire et produit le radical methoxy $\text{CH}_3\text{O}^\bullet$ et l'acide nitreux HONO qui est facilement photolysé dans l'UV proche et alimente ainsi la réactivité du mélange réactionnel. L'acide nitreux n'a toutefois jamais été détecté. Le rapport de branchement $k_{7a}/(k_{7a} + k_{7b}) = 0,55$ proposé dans la littérature est basé sur le résultat de simulations numériques des profils de NO (83). HONO présentant une absorption sous forme de raies dans la région de $1,5 \mu\text{m}$ (88), nous avons donc cherché à l'observer pour améliorer notre connaissance du mécanisme de la réaction (5).

Par ailleurs, une étude des produits de photolyse du nitrite de méthyle par ICOS (Integrated Cavity Output Spectroscopy, qui est une variante de la CRDS) à $1,5 \mu\text{m}$, a récemment reporté l'évolution temporelle des produits de photolyse NO_2 et CH_2O (89). Le comportement du dioxyde d'azote observé par les auteurs est toutefois assez surprenant avec une disparition rapide en période « lampes off », attribué à la réaction hétérogène $\text{NO}_2 + \text{CH}_3\text{OH}$.

II.1.3.2.4 Résultats obtenus

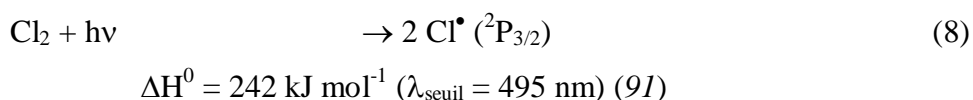
Les résultats obtenus dans notre travail ont démontré pour la première fois la formation du HONO dans la réaction $\text{OH}^\bullet + \text{CH}_3\text{ONO}$. La présence d'un spectre de raies dense de *cis*-HONO a été observée vers 6620 cm^{-1} , confirmant les premières observations de *Guilmot et al.* (88). La section efficace d'absorption du *cis*-HONO a été estimée à $6625,69 \text{ cm}^{-1}$ à $3,8 \times 10^{-21} \text{ cm}^2$, en très bon accord avec la récente détermination de *Jain et al.* (90) ; ceci confirme la cohérence de la valeur du rapport de branchement suggérée par *Cox et al.* (83) pour la voie formant HONO dans $\text{OH}^\bullet + \text{MN}$. Le NO_2 n'a pu être détecté dans cette région du spectre au cours de la photolyse du MN, en contraste avec les résultats de *Zhao et al.* (89). Le spectre du dioxyde d'azote a été déterminé dans la gamme spectrale $6612 - 6645 \text{ cm}^{-1}$, ainsi que sa section efficace à $6625,67 \text{ cm}^{-1}$: $\sigma = 5,3 \times 10^{-25} \text{ cm}^2$. Cette valeur de σ est trop faible pour pouvoir détecter le NO_2 dans la photolyse de MN dans nos conditions expérimentales. Le radical HO_2^\bullet n'a pas non plus été détecté, probablement à cause de ses concentrations photostationnaires trop faibles dues aux concentrations élevées de NO. Ceci indique une limitation du réacteur développé à l'étude du radical HO_2^\bullet dans des systèmes pauvres en NO_x .

L'ensemble des résultats a été publié dans *Environmental Science and Technology* (**publication n°1, (51)**).

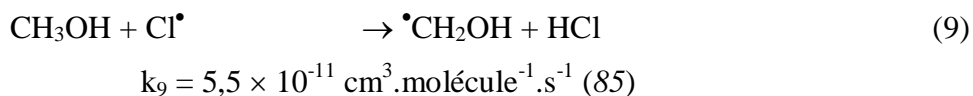
II.1.3.3 Etude des cinétiques du radical HO₂[•] dans la photolyse de Cl₂ en présence de CH₃OH

II.1.3.3.1 Introduction

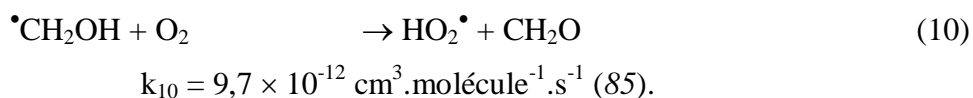
L'un des principaux objectifs dans le développement de ce nouveau dispositif expérimental était de pouvoir observer *in situ* et quantifier les radicaux hydroperoxydes HO₂[•] présents dans l'essentiel des mécanismes réactionnels de la chimie atmosphérique. Ne l'ayant pas détecté dans la photolyse du nitrite de méthyle (concentrations photostationnaires trop faibles < 10¹⁰ molécule.cm⁻³), nous nous sommes tournés vers un autre système chimique bien connu et plus simple : l'oxydation du méthanol initiée par les atomes de chlore. A l'instar du nitrite de méthyle, ce système chimique est également très utilisé par la communauté scientifique des chimistes de l'atmosphère pour générer de façon simple les radicaux HO₂[•], selon les réactions suivantes :



Le dichlore Cl₂ absorbe dans l'UV proche sous la forme d'une large bande entre 260 et 470 nm centrée à 330 nm (91). Les atomes de chlore formés arrachent un hydrogène méthylique de la molécule de méthanol (85) :



La présence d'oxygène en quantité importante (expériences réalisées dans l'air) conduit finalement à la formation du radical HO₂[•] et du formaldéhyde :



Notons en passant que le méthanol est un des composés organiques oxygénés les plus abondants dans l'atmosphère (92) et que son oxydation par Cl[•] peut être significative dans les zones côtières (93) et urbaines (94).

II.1.3.3.2 Principaux résultats obtenus

Pour la première fois, à notre connaissance, les concentrations photostationnaires des radicaux HO_2^\bullet ont été mesurées *in situ* et de manière directe dans une chambre de simulation atmosphérique. Ces concentrations, ainsi que celles de formaldéhyde, ont été mesurées au cours du temps dans des conditions expérimentales variées (concentrations initiales, flux actinique et pression totale).

Cinétiques de disparition du radical HO_2^\bullet

Les premiers résultats tirent parti de l'observation des cinétiques de disparition du radical HO_2^\bullet après extinction des lampes ; ils mettent en évidence la concomitance de deux phénomènes cinétiques attendus : la réaction mutuelle $\text{HO}_2^\bullet + \text{HO}_2^\bullet$ (réaction (6)) et la diffusion aux parois, ce qui se traduit par l'équation de vitesse suivante :

$$-\frac{d[\text{HO}_2^\bullet]}{dt} = 2 \times k_6 \times [\text{HO}_2^\bullet]^2 + k_w \times [\text{HO}_2^\bullet] \quad (\text{Eq. IX})$$

où k_w représente la constante de premier ordre de perte aux parois du HO_2^\bullet . La résolution de cette équation donne une expression de $[\text{HO}_2^\bullet]$ en fonction du temps :

$$\frac{1}{[\text{HO}_2^\bullet]} = \left(\frac{1}{[\text{HO}_2^\bullet]_0} + \frac{2 \times k_6}{k_w} \right) \times \exp(k_w \times t) - \frac{2 \times k_6}{k_w} \quad (\text{Eq. X})$$

Les cinétiques enregistrées à 5 Torr, 19 Torr et 90 Torr ont été reproduites de façon satisfaisante en utilisant des coefficients de diffusion de la littérature et en ajustant la constante de vitesse k_6 . Les résultats obtenus pour k_6 sont en bon accord avec la recommandation de la littérature, ce qui confirme notamment la valeur de la section efficace de la raie à $6638,20 \text{ cm}^{-1}$ déterminée par (95). La limite de détection du HO_2^\bullet est d'environ $1 \times 10^{10} \text{ molécule.cm}^{-3}$ pour la raie à $6638,20 \text{ cm}^{-1}$. Ces travaux sont développés dans la **publication n°2**, (52) parue dans *Zeitschrift für Physikalische Chemie*.

Profils temporels des concentrations de HO_2^\bullet et de CH_2O

La deuxième partie de ce travail s'est focalisée sur les concentrations photostationnaires de HO_2^\bullet au cours de l'oxydation du méthanol par Cl^\bullet . On observe tout d'abord (**Figure II.5**) que les concentrations photostationnaires initiales de HO_2^\bullet augmentent de 30% entre 5 Torr et 70 Torr pour

des conditions expérimentales identiques (concentrations initiales, nombre de lampes allumées), ce qui est à attribuer à la diffusion du radical HO_2^\bullet vers les parois, beaucoup plus importante à 5 Torr qu'à 70 Torr.

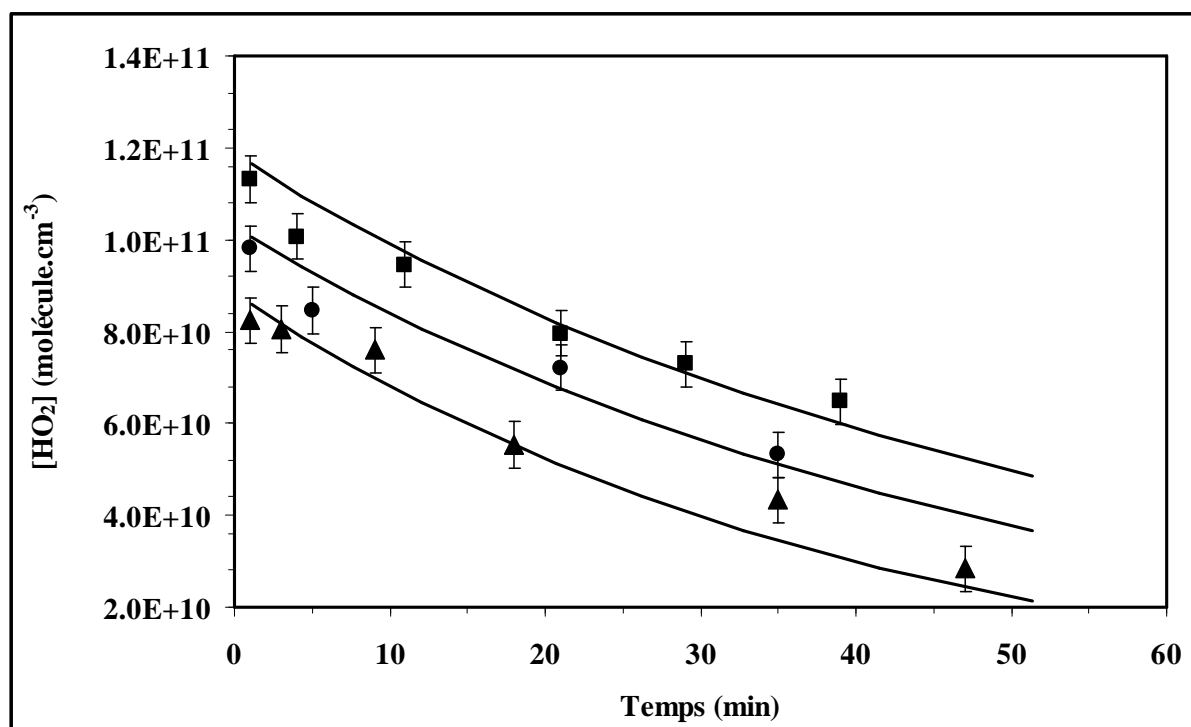


Figure II.5 : Profils temporels du radical HO_2^\bullet en fonction de la pression totale dans le réacteur. ■ : 70 Torr, ● : 18 Torr, ▲ : 5 Torr. $[\text{CH}_3\text{OH}]_0 = 6,8 \times 10^{14} \text{ molécule.cm}^{-3}$, $[\text{Cl}_2]_0 = 9,3 \times 10^{13} \text{ molécule.cm}^{-3}$, 8 lampes allumées. Les courbes correspondent aux simulations numériques basées sur le mécanisme réactionnel du Tableau II.1.

Ce phénomène est susceptible de modifier les mécanismes des réactions étudiées dans ce type de réacteur et, par conséquent, les rendements de produits formés. Par exemple, lorsque le milieu est pauvre en NO_x , les radicaux HO_2^\bullet réagissent préférentiellement avec d'autres radicaux peroxydes $\text{RC}(\text{O})\text{O}_2^\bullet$ et RO_2^\bullet . Ces dernières réactions (qui sont pour la plupart des réactions de terminaison) conduisent à la formation d'espèces stables du type acides et peracides organiques $\text{RC}(\text{O})\text{OH}$ et $\text{RC}(\text{O})\text{OOH}$, ozone, hydroperoxydes ROOH qui jouent un rôle très important dans l'atmosphère, notamment dans la formation des aérosols organiques secondaires. Si les concentrations de HO_2^\bullet dans le réacteur sont plus faibles que prévues, la formation de ces espèces sera fortement réduite et les réactions $\text{RO}_2^\bullet + \text{RC}(\text{O})\text{O}_2^\bullet$, $\text{RO}_2^\bullet + \text{R}'\text{O}_2^\bullet$ ou $\text{RO}_2^\bullet + \text{NO}_x$ (qui sont des réactions de propagation) seront favorisées. Ce phénomène a été observé par exemple dans une étude sur l'effet de l'inhibiteur de radicaux OH^\bullet dans l'ozonolyse de l' α -pinène (96).

Dans un deuxième temps ont été comparés les niveaux photostationnaires de HO_2^\bullet mesurés et simulés au cours du temps, en s'appuyant sur les concentrations mesurées de formaldéhyde. Les simulations prennent en compte l'ensemble des réactions reportées dans le **Tableau II.1**.

Les concentrations photostationnaires de HO_2^\bullet observées sont en très bon accord avec les concentrations simulées (exemple en **Figure II.6**) pour 4, 8 et 12 lampes allumées et des expériences à trois pressions différentes (5, 19 et 70 Torr). Ceci démontre d'une part la bonne connaissance du mécanisme réactionnel d'oxydation du méthanol par Cl^\bullet , d'autre part que les concentrations en formaldéhyde et radical hydroperoxyde sont correctement mesurées. Cependant, les concentrations observées en formaldéhyde apparaissent significativement plus faibles que les valeurs attendues en considérant les concentrations initiales en réactifs. De nouvelles expériences seront nécessaires pour comprendre ce désaccord.

Ces derniers résultats, présentés en détail dans la thèse de M. Djehiche (50), seront soumis à publication prochainement.

Tableau II.1 : Mécanisme réactionnel utilisé dans les simulations de [HO₂•] et [CH₂O]

	Réaction	Constante de vitesse (20 Torr, 296 K) (cm ³ .molécule ⁻¹ .s ⁻¹)	Référence
(8)	Cl ₂ + hv → 2 Cl•	variable	Ce travail
(9)	CH ₃ OH + Cl• → •CH ₂ OH + HCl	5,5 × 10 ⁻¹¹	(97)
(10)	•CH ₂ OH + O ₂ → CH ₂ O + HO ₂ •	9,1 × 10 ⁻¹²	
(6)	HO ₂ • + HO ₂ • (+ M) → H ₂ O ₂ + O ₂ (+ M)	1,75 × 10 ⁻¹²	Ce travail
	HO ₂ • + diffusion →	0,075 ^a	(98)
(11)	HO ₂ • + CH ₂ O → •OHCH ₂ O ₂	5,0 × 10 ⁻¹⁴	(97)
(12)	•OHCH ₂ O ₂ → HO ₂ • + CH ₂ O	150 ^a	
(13)	CH ₂ O + Cl• → CHO• + HCl	7,3 × 10 ⁻¹¹	
(14)	CHO• + O ₂ → CO + HO ₂ •	5,2 × 10 ⁻¹²	
(15a)	HO ₂ • + •OHCH ₂ O ₂ → HCOOH + H ₂ O + O ₂	4,8 × 10 ⁻¹²	(99)
(15b)	HO ₂ • + •OHCH ₂ O ₂ → OHCH ₂ OOH + O ₂	7,2 × 10 ⁻¹²	
(16)	HCOOH + Cl• (+ O ₂) → HCl + CO ₂ + HO ₂ •	2,0 × 10 ⁻¹³	(97)

a : en s⁻¹

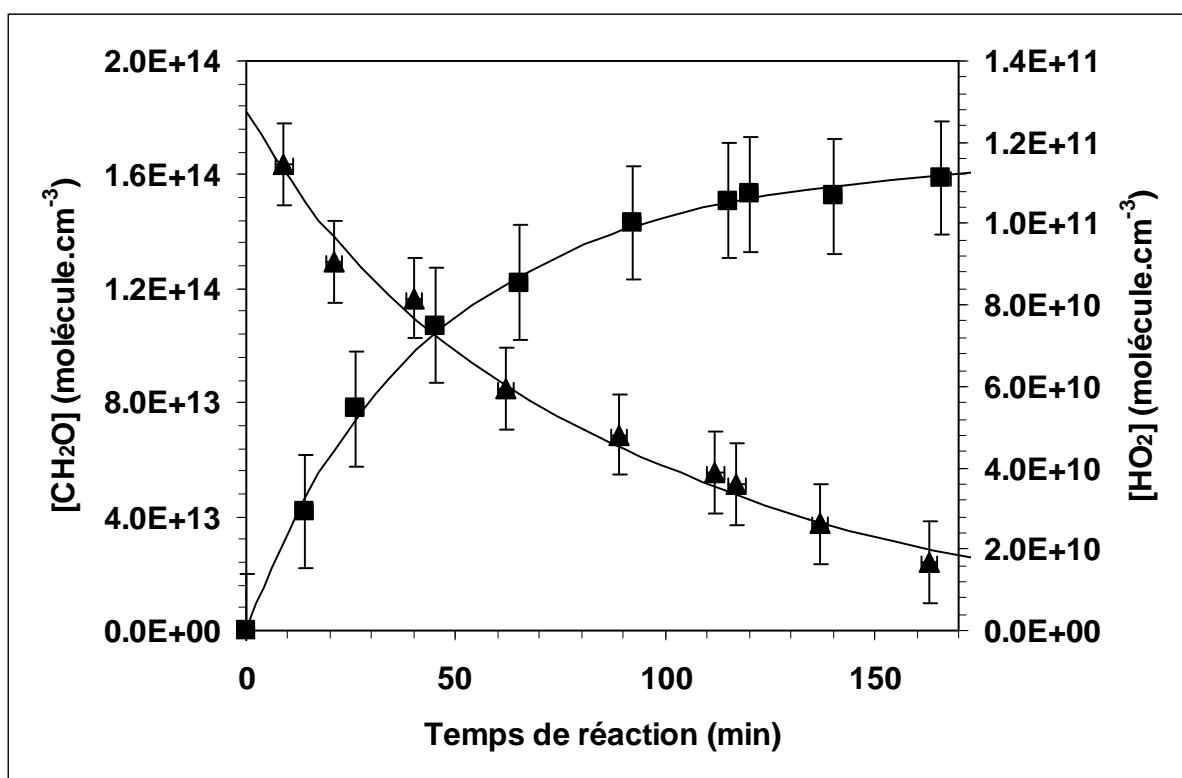


Figure II.6 : Evolution temporelle des concentrations expérimentales en HO_2^\bullet (\blacktriangle) et en CH_2O (\blacksquare). $[\text{CH}_3\text{OH}]_0 = 1,35 \times 10^{15}$ molécule. cm^{-3} , $[\text{Cl}_2]_0 = 2,8 \times 10^{14}$ molécule. cm^{-3} , $P = 19$ Torr, 4 lampes allumées. Les courbes correspondent aux simulations numériques basées sur le mécanisme réactionnel du Tableau II.1.

Publication n°1

(parue dans la revue *Environmental Science and Technology* en 2011)

First Direct Detection of HONO in the Reaction of Methylnitrite (CH₃ONO) with OH Radicals

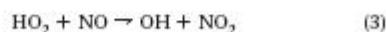
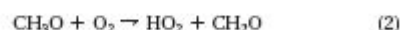
M. DJEHICHE,^{†,‡} A. TOMAS,^{*,†,‡} C. FITTSCHEN,^{†,§} AND P. CODDEVILLE^{†,‡}
Université Lille Nord de France, F-59500 Lille, France, École des Mines de Douai, Département Chimie-Environnement, F-59508 Douai, France, and Laboratoire de Physico-Chimie des Processus de Combustion et de l'Atmosphère - CNRS UMR 8522, Université des Sciences et Technologies de Lille, F-59655 Villeneuve d'Ascq, France

Received September 8, 2010. Revised manuscript received November 16, 2010. Accepted November 17, 2010.

We report on the development of a new environmental simulation chamber coupled with an in situ continuous wave cavity ring-down spectrometer operating in the near IR (~1.5 μm). The first application reported in this paper dealt with the chemical mechanism of UV photolysis of methyl nitrite (CH₃ONO) in air. HONO has been detected for the first time and shown to be formed in the OH + CH₃ONO reaction. A dense spectrum of *cis*-HONO absorption lines has been observed near 1.5 μm, in agreement with a previous study (Guilmot et al.). CH₂O has been measured as primary product with good sensitivity and time resolution. In contrast to Zhao et al., we did not detect any NO₂ absorption features in this wavelength range. Calibration experiments provided very low NO₂ absorption cross sections in this region (~10⁻²³ cm²), leading to conclude that NO₂ cannot be observed in this wavelength range in the presence of equal amounts of CH₂O.

Introduction

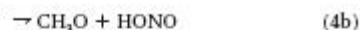
Methyl nitrite (CH₃ONO), hereafter noted MN, is an organic compound largely used in environmental simulation chamber experiments to investigate the OH reaction kinetics of atmospheric interest. It is well known that the OH radical controls the removal of organics from the troposphere. Because of strong absorption features of CH₃ONO in the UV region and especially in the near-UV (300–450 nm) range (1), methyl nitrite photodissociates easily giving rise to OH radicals following the well-known reaction chain (2):



This process has allowed the study of many OH reaction kinetics of atmospheric interest in the past 30 years (2–4). The photolysis of methyl nitrite in the near-UV range has also been used as a convenient source of methoxy radicals

CH₃O, one of the most important intermediates in atmospheric chemistry (5, 6).

Although the first steps in the photolysis of methyl nitrite are quite well known, this is not the case for the subsequent chemistry. The reaction of the OH radicals, produced in reaction (3), with CH₃ONO is assumed to be governed through two channels:



with a fairly low rate constant of $k_4 = 2.8 \times 10^{-13}$ cm³ molecule⁻¹ s⁻¹ at ambient temperature (7).

Channel (4a) corresponds to the direct H-abstraction by OH from the methyl group, whereas channel (4b) is thought to proceed via OH addition forming the CH₃ON(OH)O adduct followed by decomposition yielding CH₃O and HONO (8). A branching ratio $k_{4a}/k_{4b} = 1.25$ has been suggested based on the NO time profiles in the initial stages of the photolysis reaction, yet without detecting HONO formation (8). In a more recent study, Zhao et al. (9) investigated the photolysis of CH₃ONO using an experimental set up, similar to the one presented in this work: an atmospheric simulation chamber coupled to integrated cavity output spectroscopy near 1.5 μm. They interpreted the observed time-resolved absorption features as the formation of NO₂ and CH₂O. However, no quantification of the observed absorption signals was presented. Also, they observed a rapid decay of NO₂ concentration after turning off the lamps, while the CH₂O concentration was stable. Such a time evolution of the two products is difficult to reconcile.

Experimental Section

Cavity ring-down spectroscopy with continuous wave light (cw-CRDS) is a fairly new technique. It has been implemented by many groups in various research fields and the reader is invited to refer to good reviews (10–12) for more details on the fundamentals of the technique.

The experimental setup is schematically reproduced on Figure 1. The photoreactor consists of a quartz cylindrical cell of 110 L (90 cm length, 44 cm internal diameter) closed by two stainless steel flanges. The quartz material was chosen because of its high transparency level allowing photolysis experiments up to the UV-C range to be done. The reactor is placed inside a wooden box equipped with an irradiation system and a temperature regulation device, the latter consisting of fans fixed at the bottom of the box and flushing air-conditioned laboratory air through it. The internal walls of the box are covered with aluminum sheets to homogenize direct and reflected light emitted by the 8 fluorescent tubes (Philips TL-K 40W/05). The emission of the lamps covers the range 300–460 nm with a maximum at 365 nm. Standard vacuum KF connections have been welded on the flanges to allow easy handling of gases and to ensure that a good vacuum can be maintained inside the reaction chamber (~40 Torr with leak rate <0.5 Torr per hour). The reactor was designed to serve as spectroscopic cell for the CRDS apparatus in order to measure in situ the target species. From this point of view, the high reflectivity mirrors (Los Gatos Research, 1 m radius of curvature, ~0.9998 reflectivity) were inserted into home-made stainless steel supports fixed in the middle of the flanges through KF connections, thus forming the CRDS cavity (101 cm). The alignment of the CRDS spectrometer is carried out at atmospheric pressure; the reactor is then slowly pumped down to about 40 Torr with a frequently slight realignment.

* Corresponding author phone: 00.33.3.27.71.26.51; fax: 00.33.3.27.71.29.14; e-mail: alexandre.tomas@mines-douai.fr.

† Université Lille Nord de France.

‡ École des Mines de Douai.

§ Université des Sciences et Technologies de Lille.

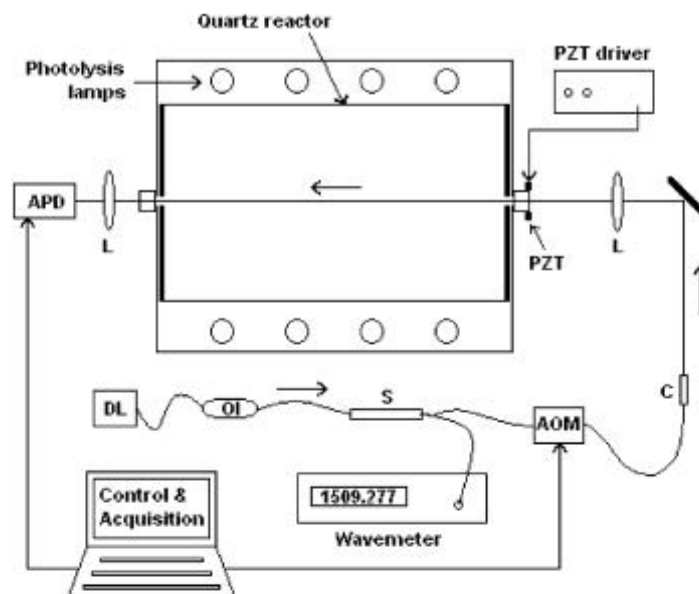


FIGURE 1. Scheme of the experimental setup: DL, distributed feedback diode laser; OI, optical isolator; S, splitter 90/10; AOM, acousto-optic modulator; C, collimator; L, lens; PZT, piezoelectric transducer; APD, avalanche photodiode.

The reactor remains for weeks at low pressure and the alignment should (normally) not be lost.

Two fiber distributed feed-back (DFB) diode lasers emitting at around $1.5 \mu\text{m}$ (Fitel, 20 mW) have been used as the continuous-wave light source. The laser diodes are tunable over a large range ($6610 - 6645 \text{ cm}^{-1}$) using temperature- and current-controllers (ILX-Lightwave LDT-5412 and LDX-3525, respectively). A fiber optical isolator (Newport ISC-1550) is connected to the output of the laser to diminish the feedback of the light into the laser. A fiber 90%/10% beam splitter (AC Photonics) directs 10% part of the light into a wavemeter (Burleigh WA-1100, accuracy of 0.01 cm^{-1}) allowing thus the monitoring of the emission laser wavelength. A key point in cw-CRD spectroscopy is the active frequency matching between the laser wavelength and a cavity mode: this has been achieved by mounting one of the mirrors on a ring-shaped piezoelectric transducer fed with a triangular voltage and modulating the length of the cavity over a free spectral range (13). Once the cavity output exceeds a predetermined threshold on the avalanche photodiode (PerkinElmer C30662E), the light input into the cavity is interrupted by deviation of the laser beam using a fiber acousto-optic modulator (Gooch & Housego MO40-8J-F25) and the ring-down time τ is recorded. The acquisition of an absorption spectrum is automatically managed by a *Labview* 7.1 program through a fast National Instruments acquisition card (PCI-6111E, 12 bits, 5 MS/s).

All of the obtained individual exponential decays were fitted by a Levenberg-Marquardt procedure included in the *Labview* software. For obtaining a spectrum, 10 individual ring-down events have typically been averaged before incrementing the laser wavelength for 0.002 cm^{-1} . The characteristic decay time τ can be readily shown to be related to the number density N (molecule cm^{-3}) of the gaseous absorbing species in the cavity through the following equation (10):

$$N = \frac{1}{\sigma_{\lambda} \times c} \left(\frac{1}{\tau} - \frac{1}{\tau_0} \right) \quad (1)$$

where c is the speed of light (cm s^{-1}), σ_{λ} the absorption cross section of the absorbent ($\text{cm}^2 \text{ molecule}^{-1}$) at the wavelength

λ and τ_0 the ring-down time (s) in the absence of the absorbent. Knowing the absorption cross sections of the target species enables the determination of the related number density. Conversely, knowing the concentration of the species allows the calculation of the absorption cross sections. The time necessary for one point concentration determination lies between 1 and 5 min, depending on the alignment of the cavity.

Formaldehyde was detected at a wavenumber of 6625.74 cm^{-1} . Staak et al. (14) recorded the CH_2O spectrum using pure formaldehyde samples and determined CH_2O absorption cross sections at 1.52 Torr. As the broadening coefficients are not known, we have determined CH_2O absorption cross sections at 40 Torr in air using calibrated formaldehyde standard cylinders and obtained a cross section value of $2.7 \times 10^{-23} \text{ cm}^2$ for the line at 6625.74 cm^{-1} . Using a minimum detectable absorption coefficient $\alpha_{\text{min}} = N_{\text{min}} \times \sigma_{\lambda} = 1 \times 10^{-8} \text{ cm}^{-1}$ representative of our setup allows us to determine a CH_2O detection limit of about $4 \times 10^{13} \text{ molecules cm}^{-3}$ in the spectral range used.

Methyl nitrite was synthesized as needed following the procedure of Taylor et al. (1) and the whole quantity (a few mL) was transferred into a 6 L canister. The canister was then filled with air up to about 3.5 bar and further used as reservoir to introduce the reactant into the reaction chamber. Known amounts of methyl nitrite were put in the reactor and diluted with synthetic air leading to estimated concentrations of $(0.3 - 4.0) \times 10^{16} \text{ molecules cm}^{-3}$ in the photoreactor. Before turning on the lamps, the methyl nitrite was allowed to stabilize for about 1 h. The experiments have been performed at low pressure (generally around 40 Torr) to avoid spectral line enlarging and at $(300 \pm 2) \text{ K}$.

Results and Discussion

Detection of CH_3ONO Photolysis Primary Products. The continuous photolysis of methyl nitrite CH_3ONO in synthetic air generates NO, CH_2O , and NO_2 as primary molecular products according to steps (1) to (3). Parts a and b of Figure 2 present two distinct regions (around 6625 cm^{-1} and around 6636 cm^{-1}) of the spectrum, the black curves have been recorded after 30 min of irradiation of $\sim 3 \times 10^{15} \text{ molecules}$

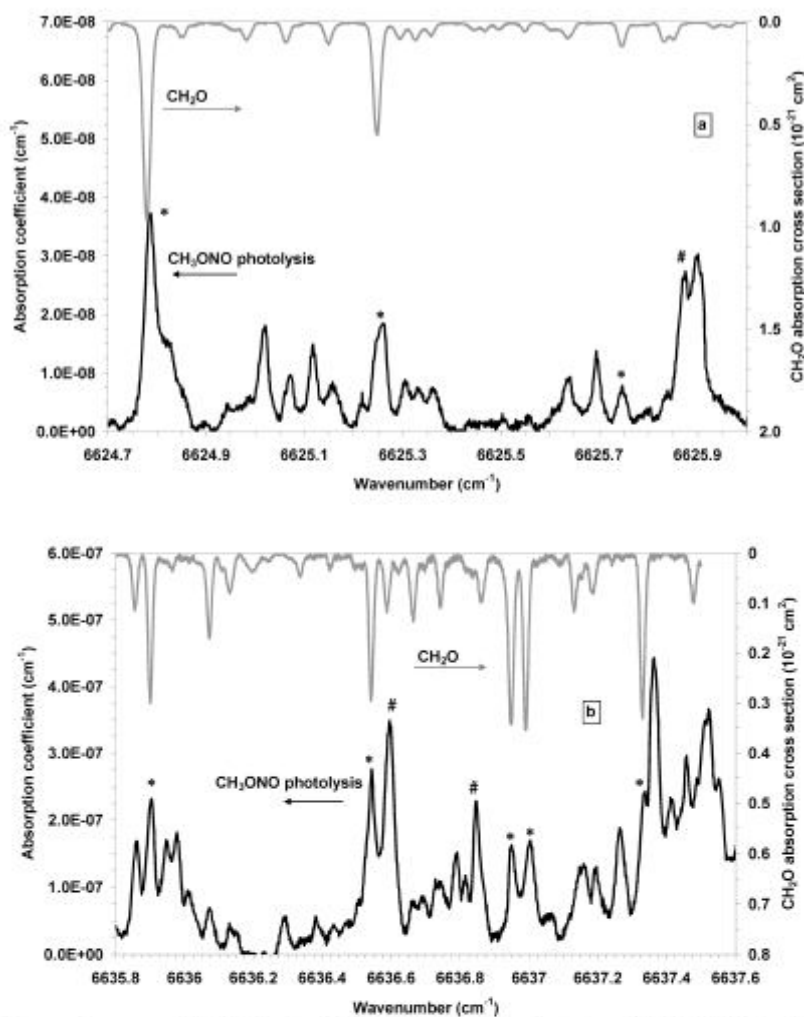


FIGURE 2. Absorption spectrum recorded after 30 min photolysis of $\sim 3 \times 10^{15}$ molecules cm^{-3} CH_3ONO (black, left scale). The CH_2O absorption spectrum (gray, right scale (14)) is given for comparison. The stars * indicate formaldehyde lines appearing on the CH_3ONO photolysis spectrum. The symbol # indicates water lines (15) a) 6624.7 – 6626.0 cm^{-1} , b) 6635.8 – 6637.6 cm^{-1} .

cm^{-3} CH_3ONO . The absorption coefficient (y -axis) is $N \times \sigma_\lambda = (1/c) \times [(1/\tau) - (1/\tau_0)]$ (eq 1). The near IR rovibrational spectrum published by Staak et al. (14) is shown in the same Figures as gray lines, and formaldehyde was readily identified particularly due to its absorption lines at 6624.78 and 6625.25 cm^{-1} (part a of Figure 2) and 6635.90, 6636.54, and 6636.95 cm^{-1} (part b of Figure 2). Three H_2O lines at 6625.87, 6636.59, and 6636.85 cm^{-1} can also be noticed (15). The shape and position of the lines are slightly different since Staak et al. recorded the CH_2O spectrum at 2 mbar and in pure formaldehyde (14).

As for nitrogen dioxide NO_2 produced in reaction (3), Zhao et al. recently claimed to have observed its formation in the photolysis of CH_3ONO in air, especially at 6625.69 cm^{-1} where we also observed a well-defined line not belonging to CH_2O (9). Yet, very weak absorption cross sections of $\sim 1 \times 10^{-24}$ cm^2 are expected in this region (16). We thus decided to record the nitrogen dioxide absorption spectrum near 6625 cm^{-1} and to determine absorption intensities. Pure gaseous NO_2 aliquots were injected into the reactor at low pressure followed by addition of air to increase the total pressure to 40 Torr, leading to NO_2 concentrations of the order of a few 10^{17} molecules cm^{-3} . In these conditions, the dinitrogen tetroxide N_2O_4 arising from the $\text{NO}_2 + \text{NO}_2$ equilibrated

reaction is calculated to represent less than 1% of NO_2 (17). The spectrum obtained for $[\text{NO}_2] = 4.2 \times 10^{17}$ molecules cm^{-3} at 40 Torr air is presented in Figure 3. Please note that the aforementioned absorption line at 6625.69 cm^{-1} is actually at 6625.67 cm^{-1} . Estimation of the absorption cross section at 6625.67 cm^{-1} led to a value of $(4.8 \pm 1.0) \times 10^{-25}$ cm^2 at a total pressure of 40 Torr. The uncertainty is mainly due to the relatively weak absorption and the precision on the NO_2 concentration. This value confirms the low absorption of NO_2 in this region (16). Using a minimum detectable absorption coefficient $\alpha_{\text{min}} = 1 \times 10^{-8}$ cm^{-1} allows to determine a NO_2 detection limit of about 2×10^{16} molecules cm^{-3} . Comparing the NO_2 absorption cross section with those of CH_2O in this region, e.g. 5.5×10^{-22} cm^2 at 6625.25 cm^{-1} (14) displays a ratio of nearly 3 orders of magnitude clearly pointing out the impossibility to detect NO_2 in the presence of equal concentrations of CH_2O , as will be the case in the photolysis of CH_3ONO . In addition, comparison with the line positions mentioned by Zhao et al. indicates that the compound observed in their experiments may not be NO_2 (9).

As for nitrogen oxide NO , the HITRAN database provides extremely weak absorption lines in this region (15) and thus,

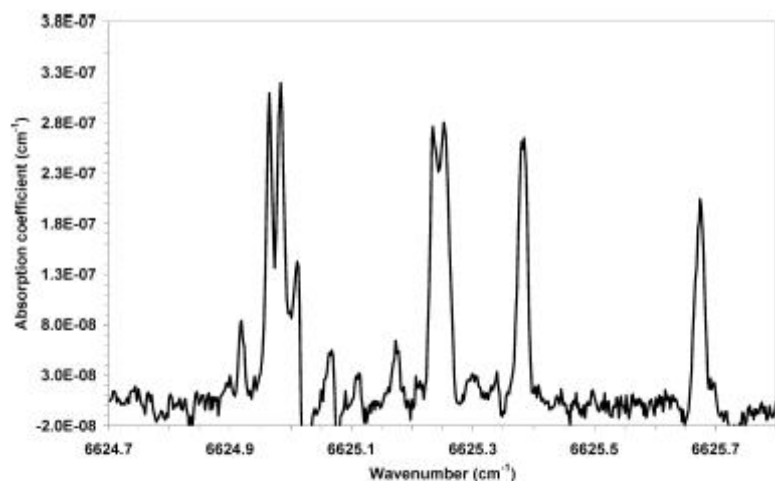


FIGURE 3. NO_2 absorption spectrum. $[\text{NO}_2] = 42 \times 10^{17}$ molecules cm^{-3} in N_2 and total pressure: 40 Torr.

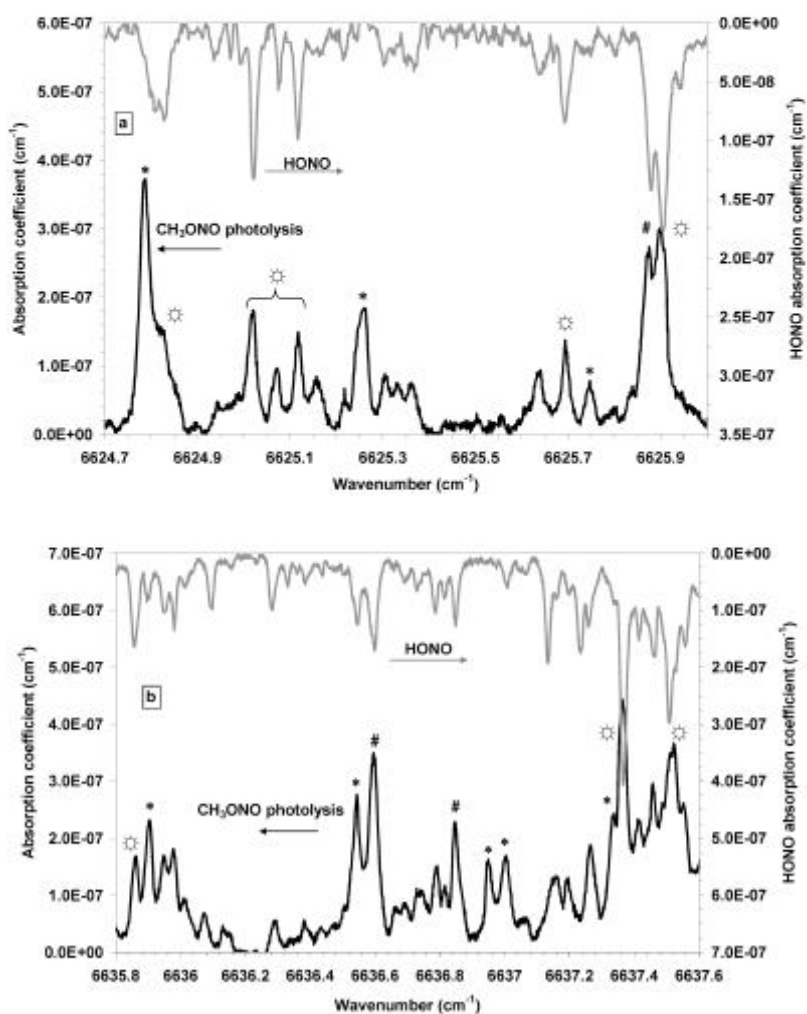


FIGURE 4. Absorption spectrum recorded after 30 min photolysis of $\sim 3 \times 10^{15}$ molecules cm^{-3} CH_2ONO (black, left scale) and absorption spectrum of *cis*-HONO (gray, right scale). The symbol \square indicates nitrous acid lines. The symbol # indicates water lines (15) and the stars CH_2O lines (14): a) 6624.7–6626.0 cm^{-1} , b) 6635.8–6637.6 cm^{-1} .

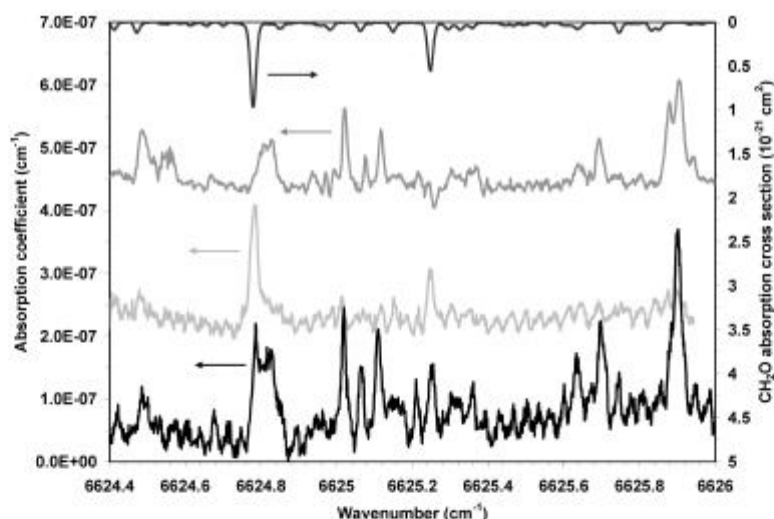


FIGURE 5. From top to bottom, absorption spectra of: CH_2O from Staak et al. (14) (dark gray, right scale); HONO (intermediate gray, left scale, shifted by $4.3 \times 10^{-7} \text{ cm}^{-1}$ for clarity); 30 min photolysis of $4 \times 10^{15} \text{ molecule cm}^{-3} \text{ CH}_3\text{ONO}$ with $6 \times 10^{14} \text{ molecules cm}^{-3}$ TMP (bright gray, left scale, shifted by $2 \times 10^{-7} \text{ cm}^{-1}$ for clarity); 30 min photolysis of $4 \times 10^{15} \text{ molecules cm}^{-3} \text{ CH}_3\text{ONO}$ (black, full line, left scale). Note that all of the absorption features from HONO have disappeared from the bright gray spectrum.

NO could not be detected in our experiments. The HO_2 radical produced in reaction (2) has been recently shown to be detectable near $1.5 \mu\text{m}$ in our group (18, 19): the absorption cross section of a strong absorption line at 6638.2 cm^{-1} has been determined to be $2.72 \times 10^{-19} \text{ cm}^2$ in 50 Torr Helium (20). Using a broadening coefficient of $0.12 \text{ cm}^{-1}/\text{atm}$ (21), an absorption cross section of $2.20 \times 10^{-19} \text{ cm}^2$ under our experimental conditions can be estimated. Using a detection limit of $\alpha_{\text{min}} = 1 \times 10^{-8} \text{ cm}^{-1}$, we can calculate a detection limit for HO_2 radicals of $5 \times 10^{10} \text{ molecules cm}^{-3}$. However, we were not able to detect any HO_2 in the photolysis of CH_3ONO , probably because of the low HO_2 photostationary concentrations.

After exclusion of possible byproduct, some absorption features still remained unresolved and we decided to further investigate toward the possibility of observing nitrous acid HONO.

Detection of HONO. One of the main goals of the present study was to investigate the suggested formation of HONO through the reaction of OH radicals with CH_3ONO (3). To identify HONO, we relied on the work of Guilmot et al. who recorded a spectrum of *cis*-HONO and attributed the absorption features observed around 6660 cm^{-1} to the $2\nu_1$ band (22). The relatively poor resolution of the spectrum presented by Guilmot et al. (22) prevented us to clearly identify HONO line positions from the Figure 6 in their publication.

A qualitative HONO spectrum was recorded in two spectral regions: $6624.7\text{--}6626 \text{ cm}^{-1}$ and $6635.8\text{--}6637.6 \text{ cm}^{-1}$. HONO was synthesized using a similar procedure as for CH_3ONO but replacing methanol by water (23). The synthesized compound was immediately injected in the reaction chamber under dark conditions. The resulting spectrum is reported on parts a and b of Figure 4 and shows a dense line pattern in both regions. The purity of the synthesized HONO was not checked and it is probable that trace amounts of impurities like NO_2 could be found (23). In addition, water could not be completely removed and a few water lines can be observed. Thus, the obtained spectrum should not be considered as a strict reference spectrum for *cis*-HONO. Comparison with the absorption spectrum of the CH_3ONO photolysis (parts a and b of Figure 4) shows similar absorption lines, in particular the three lines between 6625.0 and 6625.15

cm^{-1} , those at 6625.69 and 6625.90 cm^{-1} (part a of Figure 4), and those at 6635.86 , 6637.36 , and 6637.51 cm^{-1} (part b of Figure 4). It should be emphasized that the most intense lines on the recorded HONO spectrum appear also on the spectrum obtained after CH_3ONO photolysis, giving a strong indication that the unresolved absorption features observed in the photolysis of methyl nitrite belong to nitrous acid *cis*-HONO. Not all of the less intense absorption lines in the HONO spectrum can be observed in the photolysis product spectrum: this can be due either to interferences with other absorption features (e.g., from CH_2O) or to impurities in the synthesized HONO.

To confirm the origin of HONO from the $\text{OH} + \text{CH}_3\text{ONO}$ reaction, additional experiments with 2,4,4-trimethyl-2-pentene (TMP) added to the reaction mixture were carried out. A rate constant of $\sim 10^{-10} \text{ cm}^3 \text{ molecule}^{-1} \text{ s}^{-1}$ for the reaction of OH with TMP was assumed taking into account literature data on similar olefin reactions (4). A TMP concentration of $6 \times 10^{14} \text{ molecules cm}^{-3}$ was injected in the photoreactor to scavenge $>98\%$ OH radicals. As a result, and by comparison with the analogous experiment carried out without TMP, no absorption lines attributed to HONO appears after 30 min of irradiation (Figure 5), thereby supporting the implication of OH radicals in the formation of HONO. Another source of HONO could be the reaction $\text{OH} + \text{NO}$. Cox et al. noted that during CH_3ONO photolysis NO is present at a very low stationary level during the reaction time (8) and our own calculations confirmed that under our conditions NO concentrations remained $<10^{14} \text{ molecules cm}^{-3}$. These considerations suggest that the $\text{OH} + \text{NO}$ reaction should be negligible in the formation of HONO and that the principal route for HONO is through reaction between OH and CH_3ONO .

Simulation of CH_2O and HONO Time Profiles. As mentioned previously, the cross section for one CH_2O absorption line was determined in our experimental conditions in order to enable us to calculate absolute CH_2O concentration time profiles. The line at 6625.74 cm^{-1} was chosen because of its proximity from a relatively strong, well-defined HONO band at 6625.69 cm^{-1} , facilitating the simultaneous recording of CH_2O and HONO profiles. The CH_2O concentrations were determined using eq 1 using the

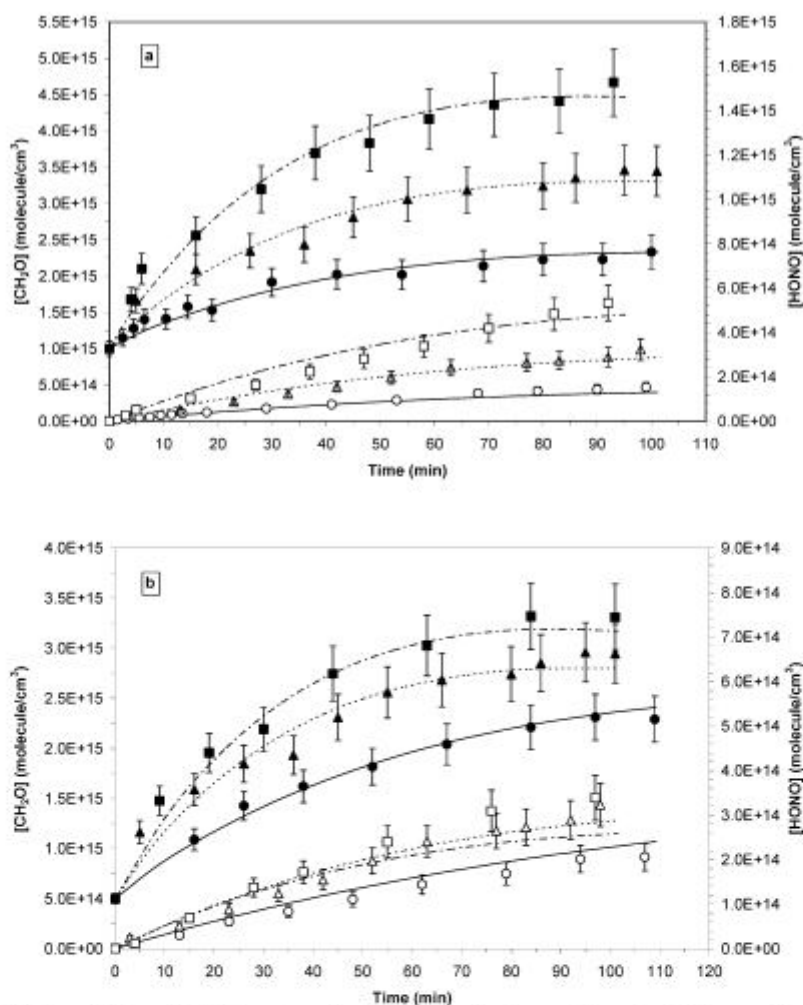


FIGURE 6. CH₂O (filled symbols) and HONO (empty symbols) concentration time profiles; a) with three different CH₃ONO initial concentrations (in 10¹⁶ molecules cm⁻³): 1.2 (circles), 2.4 (triangles), and 3.9 (squares); the CH₂O concentrations have been shifted by 1 × 10¹⁵ molecules cm⁻³ for clarity; b) with different photolysis lamps switched on: 2 (circles), 4 (triangles), and 6 (squares); the CH₂O concentrations have been shifted by 5 × 10¹⁴ molecules cm⁻³ for clarity.

absorption cross section determined in the present work at 40 Torr, $\sigma(6625.74 \text{ cm}^{-1}) = 2.7 \times 10^{-23} \text{ cm}^2$.

Three experiments were performed with varying CH₃ONO initial concentrations (part a of Figure 6) and three others with varying the number of photolysis lamps switched on using the same initial CH₃ONO concentration (part b of Figure 6). A continuous production of CH₂O was observed during the irradiation period, the rate of formation slightly decreasing with time. This decrease is mainly due to two reasons: (a) the decrease of CH₃ONO concentration with advancing reaction time and hence a decrease of the reaction rate and (b) the increasing consumption of CH₂O due to reaction with OH radicals, a side effect of the decreasing CH₃ONO concentration. The formation of formaldehyde and HONO was simulated using a simple homemade box model taking into account the reactions reported in Table S1 of the Supporting Information. All of the reaction rate constants were taken from the evaluations of Atkinson et al. (24) and Sander et al. (17). HONO and NO₂ photolysis rate coefficients were determined by independent experiments, yielding values between 2 and 6 × 10⁻⁵ s⁻¹ and 1 and 3 × 10⁻⁴ s⁻¹, respectively. Secondary reactions like OH + CO, CH₂O, and O₃ photolysis

were neglected in the model due to the low rate coefficients known from the literature (17, 24, 25) and/or from independent experiments. Only two parameters were adjusted to fit the experimental data: the CH₃ONO photolysis rate j_1 and the OH radical photostationary concentration. The CH₃ONO photolysis rate is essentially determined by the initial CH₂O formation rate, whereas the photostationary OH radical concentration rather influences the curvature of the CH₂O formation. Best fits were obtained with OH radical concentrations between 2 and 3 × 10⁷ molecules cm⁻³. Absolute absorption cross section for HONO are not known, we have therefore set the branching ratio of reaction (4) at the value proposed by Cox et al. (8): $k_{4a}/k_{4b} = 1.25$. This way, the simulations provided HONO concentration time profiles, which were used to estimate the *cis*-HONO absorption cross section at 6625.69 cm⁻¹; assuming that the *cis*-HONO is roughly two times less abundant than the *trans*-HONO (26), a value of $\sigma_{\text{HONO}}(6625.69 \text{ cm}^{-1}) = 4.2 \times 10^{-21} \text{ cm}^2$ at 40 Torr was obtained, yielding a detection limit of about 2 × 10¹² molecules cm⁻³. As shown in Figure 6, the concentration time profiles are quite well reproduced with the simple reaction mechanism from Table S1 of the Supporting

Information. The CH₃ONO photolysis rate constant arising from the fits of part b of Figure 6 shows a fairly good correlation with the number of lamps turned on: $k_1 = 5 \times 10^{-5} \text{ s}^{-1}$ (2 lamps), $1 \times 10^{-4} \text{ s}^{-1}$ (4 lamps), and $1.3 \times 10^{-4} \text{ s}^{-1}$ (6 lamps), keeping in mind that all of the lamps are not equivalent in terms of efficiency. The fraction of MN reacting with OH radicals is determined to be smaller than 10%. HONO formation during the photolysis of methyl nitrite is thus estimated to be of 5% of the total MN consumption at the most in the present experimental conditions.

Acknowledgments

This work is jointly supported by the Nord-Pas de Calais region in the frame of the IRENI research program, by the French Research Ministry and by the European funds for Regional Economic Development (FEDER). Mokhtar Djehiche gratefully acknowledges the financial support from the Ecole des Mines de Douai.

Supporting Information Available

Reaction mechanism used for the numerical simulations (including the rate constants). This material is available free of charge via the Internet at <http://pubs.acs.org>.

Literature Cited

- (1) Taylor, W. D.; Allston, T. D.; Moscato, M. J.; Fazekas, G. B.; Kozlowski, R.; Takacs, G. A. Atmospheric photodissociation lifetimes for nitromethane, methyl nitrite, and methyl nitrate. *Int. J. Chem. Kin.* 1980, 12, 231–240.
- (2) Atkinson, R.; Carter, W. P. L.; Winer, A. M.; Pitts, J. N., Jr. An experimental protocol for the determination of OH radical rate constants with organics using methyl nitrite photolysis as an OH radical source. *J. Air Poll. Control Assoc.* 1981, 31, 1090–1092.
- (3) Mellouki, A.; Le Bras, G.; Sidebottom, H. Kinetics and mechanisms of the oxidation of oxygenated organic compounds in the gas phase. *Chem. Rev.* 2003, 103 (12), 5077–5096.
- (4) Atkinson, R.; Arey, J. Atmospheric degradation of volatile organic compounds. *Chem. Rev.* 2003, 103 (12), 4605–4638.
- (5) Caralp, F.; Rayez, M.-T.; Forst, W.; Gomez, N.; Delcroix, B.; Flittschen, C.; Devolder, P. Kinetic and mechanistic study of the pressure and temperature dependence of the reaction CH₂O + NO. *J. Chem. Soc., Faraday Trans.* 1998, 94, 3321–3330.
- (6) Flittschen, C.; Delcroix, B.; Gomez, N.; Devolder, P. Rate constants for the reactions of CH₂O with CH₂O, CH₃CHO and *i*-C₄H₁₀. *J. Chem. Phys.* 1998, 95 (10), 2129–2142.
- (7) Nielsen, O. J.; Sidebottom, H.; Donlon, M.; Treacy, J. Rate constants for the gas-phase reactions of OH radicals and Cl atoms with *n*-alkyl nitrites at atmospheric pressure and 298 K. *Int. J. Chem. Kin.* 1991, 23, 1095–1109.
- (8) Cox, R. A.; Derwent, R. G.; Kearsley, S. V.; Batt, L.; Patrick, K. G. Photolysis of methyl nitrite: Kinetics of the reaction of the methoxy radical with O₂. *J. Photochem.* 1980, 13, 149–163.
- (9) Zhao, W.; Gao, X.; Hao, L.; Huang, M.; Huang, T.; Wu, T.; Zhang, W.; Chen, W. Use of integrated cavity output spectroscopy for studying gas phase chemistry in a smog chamber: Characterizing

the photolysis of methyl nitrite (CH₃ONO). *Vib. Spectrosc.* 2007, 44, 388–393.

- (10) Berden, G.; Peeters, R.; Meijer, G. Cavity ring-down spectroscopy: Experimental schemes and applications. *Int. Rev. Phys. Chem.* 2000, 19 (4), 565–607.
- (11) Brown, S. S. Absorption spectroscopy in high-finesse cavities for atmospheric studies. *Chem. Rev.* 2003, 103 (12), 5219–5238.
- (12) Mazurenka, M.; Orr-Ewing, A. J.; Peverall, R.; Ritchie, G. A. D. Cavity ring-down and cavity enhanced spectroscopy using diode lasers. *Annu. Rep. Prog. Chem., Sect. C* 2005, 101, 100–142.
- (13) Romanini, D.; Kachanov, A. A.; Sadeghi, N.; Stoekel, F. CW cavity ring down spectroscopy. *Chem. Phys. Lett.* 1997, 264, 316–322.
- (14) Staak, M.; Gash, E. W.; Venables, D. S.; Ruth, A. A. The rotationally-resolved absorption spectrum of formaldehyde from 6547 to 6804 cm⁻¹. *J. Mol. Spectrosc.* 2005, 229, 115–121.
- (15) HITRAN, <http://www.hitran.com>; 2004.
- (16) Yamano, D.; Yabushita, A.; Kawasaki, M.; Perrin, A. Absorption spectrum of nitrous acid for the $\nu_1+2\nu_2$ band studied with continuous-wave cavity ring-down spectroscopy and theoretical calculations. *J. Quant. Spectrosc. Radiat. Transfer* 2010, 111, 45–51.
- (17) Sander, S. P.; Finlayson-Pitts, B. J.; Friedl, R. R.; Golden, D. M.; Huie, R. E.; Keller-Rudek, H.; Kolb, C. E.; Kurylo, M. J.; Molina, M. J.; Moortgat, G. K.; Orkin, V. L.; Ravishankara, A. R.; Wine, P. H. Chemical kinetics and photochemical data for use in atmospheric studies, Evaluation number 15. Jet Propulsion Laboratory: Pasadena, 2006.
- (18) Thiébaud, J.; Flittschen, C. Near infrared cw-CRDS coupled to laser photolysis: spectroscopy and kinetics of the HO₂ radical. *Appl. Phys. B: Laser Opt.* 2006, 85 (2–3), 383–389.
- (19) Djehiche, M.; Tomas, A.; Flittschen, C.; Coddeville, P. First in situ measurement of HO₂ radicals by cw-CRDS in a simulation chamber. 2010, to be submitted.
- (20) Thiébaud, J.; Crunale, S.; Flittschen, C. Measurements of line strengths in the 2 ν_1 band of the HO₂ radical using laser photolysis/continuous wave cavity ring-down spectroscopy (cw-CRDS). *J. Phys. Chem. A* 2007, 111, 6959–6966.
- (21) Ibrahim, N.; Thiébaud, J.; Orphal, J.; Flittschen, C. Air-broadening coefficients of the HO₂ radical in the 2 ν_1 band measured using cw-CRDS. *J. Mol. Spectrosc.* 2007, 242, 64–69.
- (22) Guilmo, J.-M.; Mélen, F.; Herman, M. Rovibrational parameters for *cis*-nitrous acid. *J. Mol. Spectrosc.* 1993, 160, 401–410.
- (23) Ten Brink, H. M.; Spoelstra, H. The dark decay of HONO in environmental (smog) chambers. *Atmos. Environ.* 1998, 32 (2), 247–251.
- (24) Atkinson, R.; Baulch, D. L.; Cox, R. A.; Crowley, J. N.; Hampson, R. F.; Hynes, R. G.; Jenkin, M. E.; Rossi, M. J.; Troe, J. Evaluated kinetic and photochemical data for atmospheric chemistry: Volume II. Gas phase reactions of organic species. *Atmos. Chem. Phys.* 2006, 6, 3625–4055.
- (25) Atkinson, R.; Baulch, D. L.; Cox, R. A.; Crowley, J. N.; Hampson, R. F.; Hynes, R. G.; Jenkin, M. E.; Rossi, M. J.; Troe, J. Evaluated kinetic and photochemical data for atmospheric chemistry: Volume I—gas phase reactions of O₂, HO₂, NO₂, and SO₂ species. *Atmos. Chem. Phys.* 2004, 4, 1461–1738.
- (26) Varma, R.; Curl, R. F. Study of the N₂O₂-H₂O-HNO₂ equilibrium by intensity measurements in microwave spectroscopy. *J. Phys. Chem.* 1976, 80, 402–409.

ES103076E

Publication n°2
(parue dans la revue *Zeitschrift für Physikalische Chemie* en 2011)

First Cavity Ring-Down Spectroscopy HO₂ Measurements in a Large Photoreactor

By Mokthar Djehiche^{1,2}, Alexandre Tomas^{1,2,*}, Christa Fittschen^{1,3}, and Patrice Coddeville^{1,2}

¹ Univ. Lille Nord de France, 59500 Lille, France

² EMDouai, CE, 941 rue Bourseul, 59500 Douai, France

³ USTL, PC2A, UMR CNRS 8522, 59650 Villeneuve d'Ascq, France

Dedicated to Prof. Horst Hippler on the occasion of his 65th birthday

(Received July 4, 2011; accepted in revised form September 16, 2011)

HO₂ Radical / CRDS / Kinetics / Atmospheric Simulation Chamber

The HO₂ radical is one of the most important intermediate species in atmospheric chemistry. We report on the development of a new photoreactor with first *in-situ* measurement of HO₂ radical photostationary concentrations using continuous wave cavity ring-down spectrometry (cw-CRDS). Characterization of the actinic photon flux was carried out by NO₂ actinometry. Photolysis of Cl₂/methanol mixtures in air under UV light allowed the measurement of HO₂ photostationary concentrations of a few 10¹⁰ molecules cm⁻³ with an HO₂ detection limit of 1.5 × 10¹⁰ molecules cm⁻³ at 6638.207 cm⁻¹. The feasibility of HO₂ direct measurement in a reaction chamber is demonstrated through the measurement of the HO₂ overall loss at different pressures showing the importance of HO₂ diffusion and wall loss in such low pressure quartz reactor. The rate coefficient for the HO₂ + HO₂ reaction has been measured at 6.6, 24 and 118 mbar and found to be in good agreement with the recommended value.

1. Introduction

For a long time, the hydroperoxy radical HO₂ has been recognized to play a central role in the chemistry of the atmosphere. In particular, the RO_x + NO reactions, where RO_x represents peroxy radicals (HO₂ and RO₂), are thought to explain the photochemical formation of ozone in the troposphere [1]. In addition, though fairly low HO₂ concentrations are detected in the lower troposphere (around 10⁸ molecules cm⁻³) [1–3], the HO₂ radical strongly influences the oxidizing capacity of the atmosphere acting as chain propagating radical and regenerating the OH radical through the NO + HO₂ reaction.

Environmental simulation chambers have been developed to investigate the kinetics of atmospheric-relevant reactions as well as the chemical mechanisms involved in the atmospheric chemistry of organic species. Chromatographic techniques have been

* Corresponding author. E-mail: alexandre.tomas@mines-douai.fr

currently used as off-line methods to measure stable organic compounds inside the photoreactor. Direct spectroscopic techniques have also been deployed combined with long optical paths to reach satisfactory detection limits (see for example [4,5]). In the past two decades, efforts have been undertaken to develop techniques with very high sensitivity able to detect and quantify intermediate species directly inside the reactor, especially OH and HO₂ radicals [6]. The possibility to measure radical concentration levels during photooxidation experiments is highly desirable, since it could be largely profitable in the understanding of chemical processes and in the assessment of the performance of detailed degradation mechanisms [7,8]. In addition, many studies have pointed out discrepancies in the HO_x budgets between models and observations [9–11]; moreover, the mechanisms of peroxy radical reactions involving HO₂ radicals, such as the CH₃C(O)O₂ + HO₂ reaction, are still the object of disagreement in terms of the OH yield [12,13]. Thus, the possibility to measure radicals should be very useful for investigating the unknown radical sinks and sources and for understanding reaction mechanisms [14,15].

The techniques currently used to measure peroxy radicals are (1) the peroxy radical chemical amplifier, (2) the laser induced fluorescence (LIF) technique through the conversion of RO_x into OH radicals by adding excess NO, (3) the peroxy radical chemical ionization mass spectrometry, and (4) the matrix isolation electron spin resonance spectroscopy. While the first three techniques include a RO_x conversion step, the last technique is the only direct technique. The limits of detection of these techniques are of the order of 10⁶–10⁷ molecule cm⁻³, which is sufficient for atmospheric measurement [3]. The major disadvantage is that they all require a calibration step. In addition, measurements of HO₂ by LIF have been shown very recently to be subject of significant bias when carried out in the presence of high organic peroxy radical concentrations [16]. To our knowledge, the measurement of peroxy radical photostationary concentrations in large photoreactors during photooxidation experiments is rather scarce. Pinceloup *et al.* used the chemical amplifier technique to measure HO₂ concentrations in a 1 m³ environmental chamber and determined the thermal decomposition rate constant of the HO₂-CH₂O adduct [17]. Qi *et al.* determined the peroxy radical yields in the ozonolysis of ethene in a 6 m³ environmental chamber by using also the chemical amplifier technique [18]. More recently, Wyche *et al.* measured hydroxy- and organic- peroxy radicals in 1,3,5-trimethylbenzene photoexperiments by chemical amplification too and pointed out the role of self and cross peroxy radical reactions in the formation of secondary organic aerosols [19]. In addition to the calibration step, another drawback of this technique for the measurement of HO₂ concentrations is the interference from the other peroxy radicals [3].

The cavity ring-down spectroscopy (CRDS) technique has been developed and applied in the field of atmospheric chemistry in the past ten years and a few radicals of atmospheric interest have been measured using this technique, like NO₃ [20–22], peroxy radicals RO₂ [23,24] and the hydroperoxy radical HO₂ [25,26]. Contrary to the above mentioned peroxy radical chemical amplifier technique, the CRDS technique does not require any calibration stage and is practically free from interferences [25]. A few very recent studies have shown the interest to combine CRDS and photoreactors, measuring small stable molecules like CO₂, HONO and CH₂O as well as the NO₃ radical [27–30]. We present here the first *in-situ* detection of HO₂ radicals by cw-CRDS

in an atmospheric simulation chamber in the photolysis of Cl₂/CH₃OH/air mixtures. This reaction system was chosen because it has a very simple, well-known chemical mechanism and it is often used as a straightforward source of HO₂ radicals through its photolysis in the near-UV region. The main purpose of this study is to show the applicability of the new reaction chamber facility to measure the HO₂ radicals with good time resolution and high sensitivity and demonstrate the interest of monitoring radical concentrations in an atmospheric reaction chamber. The experiments were designed to characterize the new photoreactor in terms of HO₂ losses.

2. Material and methods

Cavity ring-down spectroscopy (CRDS) is a spectroscopic technique based on the specific feature of the Fabry–Pérot interferometer to hugely increase the optical absorption path lengths and, consequently, to significantly decrease the detection limits. The possibility of using continuous wave light source (cw-CRDS) has been demonstrated by Romanini and co-workers about ten years ago [31] and the principle of this technique has been extensively reviewed [32–34]. The details of our experimental setup have been described in a previous publication [30] and only the main technical and experimental aspects will be reminded in the next paragraphs.

The photoreactor consists of a quartz cylindrical cell of 110 L (surface to volume ratio of 11.8 m⁻¹) surrounded by 19 near-UV, vertically-disposed fluorescent tubes (Philips TL-K 40W/05), the emission of which is centred at 370 nm (see emission spectrum in Fig. 1). The reactor was also designed to serve as spectroscopic cell for the CRDS apparatus in order to measure HO₂ radicals directly inside the reactor. From this point of view, the high reflectivity mirrors (ATFilms, 2 m radius of curvature, ~0.99993 reflectivity at 1510 nm) forming the CRDS cavity were inserted into home-made stainless-steel supports fixed in the centre of the flanges, resulting in a cavity of 101 cm length. A DFB diode laser at 1506 nm (Nel 10 mW NLK1S5EAAA) has been used as continuous light source to detect HO₂. The signal is recorded by a National Instruments data acquisition card (PCI-6111E, 12 bits) with 200 ns time resolution and the ring down time is extracted through an exponential fit, automatically managed by a Labview 7.1 program.

The characteristic decay time can be readily shown to be related to the number density [N] (molecules cm⁻³) of the gaseous absorbing species in the cavity through the following equation [31]:

$$[N] = \frac{R_L}{c \times \sigma_\lambda} \left(\frac{1}{\tau_t} - \frac{1}{\tau_0} \right) \quad (1)$$

where c is the speed of light (cm s⁻¹), σ_λ the absorption cross section of the molecule (cm² molecule⁻¹) at the wavelength λ , R_L is the ratio between the cavity length L (101 cm), *i.e.* the distance between the two cavity mirrors, to the length L_A over which the absorber is present (80 cm) and τ_0 and τ the ring-down times (s) in the absence and in the presence of the absorbing species, respectively. By measuring τ and τ_0 and knowing the absorption cross section of the target species enables the determination of the concentration.

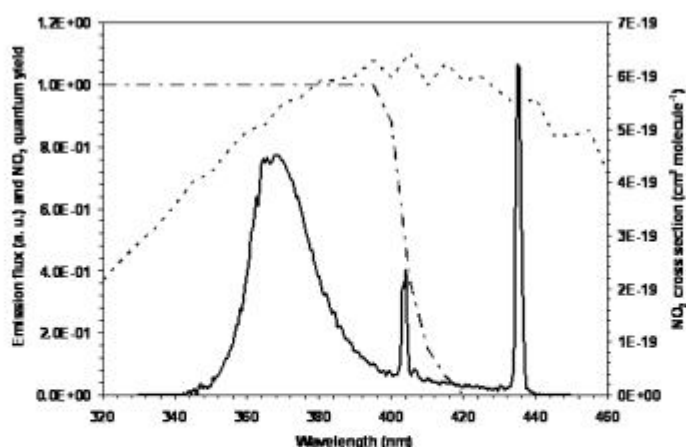
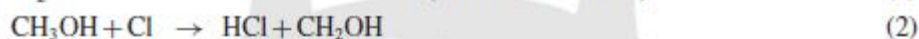


Fig. 1. Solid line: Emission spectrum of the photolysis lamps recorded by using a Sola Check spectroradiometer (0.5 nm resolution). Dotted line: NO_2 absorption spectrum [41]. Dash-dot line: NO_2 photolysis quantum yield [41].

HO_2 radicals have been produced in a usual way by the continuous photolysis of chlorine Cl_2 in the presence of methanol CH_3OH and molecular oxygen O_2 following the accepted, simple reaction mechanism:



In a typical experiment, aliquots of gaseous Cl_2 (5% in N_2 , Air Products) and liquid CH_3OH (98% Sigma-Aldrich) are introduced in the reactor at low pressure (~ 1 mbar) via a septum port under a gentle stream of air. The reactor is filled with air up to a few tens of mbar, in any case < 150 mbar to limit spectral line broadening. Homogenization of the reactants is allowed for about 30 min before turning on the irradiation lamps. Initial concentrations of Cl_2 and CH_3OH had values in the range $(0.05\text{--}8.4) \times 10^{15}$ and $(0.06\text{--}1.9) \times 10^{15}$ molecules cm^{-3} , respectively. Under these rather low methanol concentrations formation of the $\text{HO}_2\text{-CH}_3\text{OH}$ complex is negligible, as can be estimated from Christensen *et al.* [35]. All experiments have been conducted at a temperature of (296 ± 2) K.

HO_2 concentrations were quantified by cw-CRDS at 6638.207 cm^{-1} : this is by far the strongest absorption line in this spectral region [36]. Absorption cross sections of $\sigma_{6638.207 \text{ cm}^{-1}} = 3.95, 3.22$ and $1.54 \times 10^{-19} \text{ cm}^2 \text{ molecule}^{-1}$ have been used for 6.6, 24 and 118 mbar, respectively. These values are based on the absorption cross sections published by Tang *et al.* [37]. They have published pressure dependent absorption cross section for the line at 6638.207 cm^{-1} , which translates into a line strength of $S_{6638.207 \text{ cm}^{-1}} = 6.47 \times 10^{-21} \text{ cm}^{-1}$ and a broadening coefficient of $\gamma_{\text{N}_2} = 0.093 \text{ cm}^{-1} \text{ atm}^{-1}$, assuming a Voigt profile. In order to estimate the accuracy of these absorption cross sections, the data can be compared to other liter-

ature values: Thiébaud *et al.* [33] have measured the absorption cross section for the quoted line in 66 mbar He only: from their average He-broadening coefficient ($\gamma_{\text{He}} = 0.057 \text{ cm}^{-1} \text{ atm}^{-1}$) a line strength of $S_{6638.207 \text{ cm}^{-1}} = 6.35 \times 10^{-21} \text{ cm}^{-1}$ is obtained, in excellent agreement with Tang *et al.* [32]. While the N₂-broadening coefficient for the specific HO₂ line at 6638.207 cm⁻¹ has never been measured before, several works on other lines have recently been published: Ibrahim *et al.* found quantum number dependent broadening coefficients between $\gamma_{\text{N}_2} = 0.09\text{--}0.14 \text{ cm}^{-1} \text{ atm}^{-1}$ for 34 absorption lines between 6631 and 6671 cm⁻¹ [38]. Kanno *et al.* obtained $\gamma_{\text{N}_2} = 0.101 \text{ cm}^{-1} \text{ atm}^{-1}$ for one line at 7020.766 cm⁻¹ [39]. In a very recent work of Miyano and Tonokura, the N₂-broadening coefficients for 4 lines around 1065 cm⁻¹ have been determined in the range $\gamma_{\text{N}_2} = 0.09\text{--}0.118 \text{ cm}^{-1} \text{ atm}^{-1}$ [40]. The broadening coefficient obtained by Tang *et al.* [32] is at the lower end of all determinations; however an error in the broadening coefficient has only limited impact on the absorption cross section: an increase of 20% of γ_{N_2} would lead to a decrease in the absorption cross section of only 12% for the worst case, 118 mbar. Together with an uncertainty in the line strength, we therefore estimate the total uncertainty of the measured HO₂ concentration to about 25%.

The detection limit for HO₂ was evaluated taking into account the signal to noise ratio (SNR). The SNR varied from one experiment to the other, especially depending on the alignment of the whole optical system. In the best conditions, taking into account a minimum detectable absorption $\alpha_{\text{min}} = 5 \times 10^{-9} \text{ cm}^{-1}$, we estimated a limit of quantification of $1.5 \times 10^{10} \text{ molecules cm}^{-3}$ at 6638.207 cm⁻¹ with a line scan time of $\sim 2 \text{ min}$. This detection limit can be decreased to below $1 \times 10^{10} \text{ molecules cm}^{-3}$ by performing experiments at fixed wavelengths such as shown in Fig. 3.

3. Results and discussion

3.1 NO₂ actinometry

Nitrogen dioxide actinometry in N₂ was used to characterize the photolysis flux of the irradiation system, as NO₂ photodissociates easily in the near-UV (Fig. 1). Aliquots of a few ml of pure gaseous NO₂ were injected in the reaction chamber in the dark resulting in concentrations of about $1 \times 10^{16} \text{ molecule cm}^{-3}$. Under these conditions, the formation of N₂O₄ is expected to be very limited ($< 2\%$) [41]. Actinometry was carried out by switching on the lamps and monitoring the NO₂ decay at 6639.53 cm⁻¹, as it has been shown that NO₂ absorbs weakly in this wavelength domain [30]. The NO₂ data were analysed following the procedure described by Holmes *et al.* [42] assuming null initial NO and O₂ concentrations. An average photolysis frequency of $(0.24 \pm 0.02) \text{ min}^{-1}$ was obtained for total pressures between 13 and 65 mbar with all the lamps switched on, corresponding to a photolysis flux of $8.5 \times 10^{15} \text{ photons cm}^{-2} \text{ s}^{-1}$. Using the known Cl₂ absorption spectrum [41] enables to determine a Cl₂ photolysis frequency of $(0.036 \pm 0.003) \text{ min}^{-1}$.

3.2 Detection of HO₂

The HO₂ radical is readily observed at 6638.207 cm⁻¹ in the form of a sharp absorption line (Fig. 2), in agreement with the HO₂ line position and line width quoted by

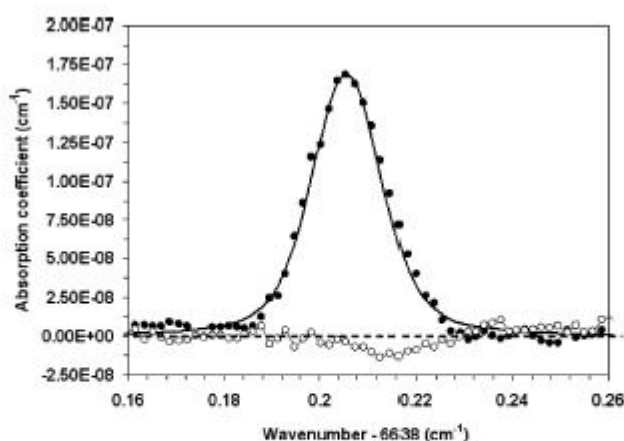


Fig. 2. HO₂ absorption line at 6638.207 cm⁻¹ ([HO₂] ≈ 4.7 × 10¹¹ molecule cm⁻³); open circles for lamps off; solid circles for lamps on. Total pressure was 24 mbar. The line corresponds to a Voigt fit.

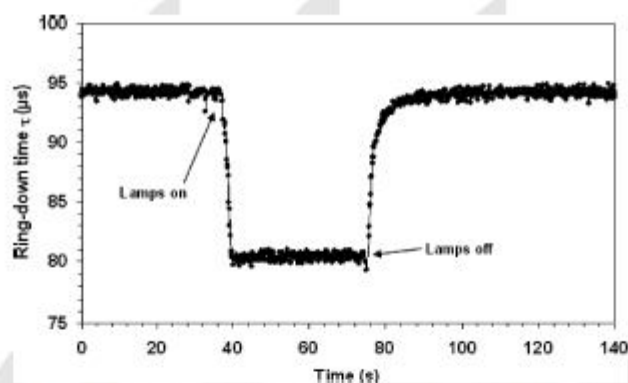


Fig. 3. Ring-down times measured at 6638.207 cm⁻¹ (no averaging) as a function of time at 24 mbar: the decrease of the signal when the photolysis lamps were turned on indicates an additional absorption due to the formation of HO₂ radicals; the increase of the signal when the lamps were turned off is due to the HO₂ + HO₂ recombination reaction and HO₂ radical diffusion leading to the complete removal of HO₂ radicals.

Thiébaud *et al.* [36] and Tang *et al.* [37]. The HO₂ line was not observed if one of the reactants (CH₃OH or Cl₂) was missing, indicating that the HO₂ radical arises from the Cl + CH₃OH initiation reaction. It should be stressed that the HO₂ radical formation is observed immediately after starting the irradiation of the reaction mixture. Thus, recording the signal at the centre of the line at 6638.207 cm⁻¹ and switching alternatively on and off the lamps exhibited a fast formation and consumption (within a few seconds) of a transient species, clearly confirming the presence of this radical in the photoreactor (Fig. 3). A steady-state concentration is reached after a few seconds, indicating that radical production rate (*i.e.* Cl₂ photolysis) is equal to radical consumption. To our knowledge, this is the first direct detection of HO₂ radicals by cw-CRDS in a large photoreactor designed for atmospheric studies.

The measured HO₂ steady state concentrations can be used to calculate a theoretical Cl₂ photolysis frequency. Assuming the steady state approximation for HO₂ radicals and Cl atoms yields:

$$j_1 = \frac{2 \times k_4 \times [\text{HO}_2] + k_5[\text{HO}_2]}{2 \times [\text{Cl}_2]_0} \quad (\text{II})$$

where j_1 is the Cl₂ photolysis frequency, k_4 is the HO₂ self reaction rate constant, [HO₂] is the measured HO₂ steady state concentration, k_5 is the HO₂ wall loss rate coefficient and [Cl₂]₀ is the initial Cl₂ concentration. The value of k_5 is from the literature [43] whereas the kinetic constant k_4 is taken from the present work (see next section). Using an average HO₂ steady state concentration of 2.2×10^{11} molecule cm⁻³ with all the lamps on, a theoretical Cl₂ photolysis frequency of (0.041 ± 0.004) min⁻¹ is obtained, in very good agreement with the experimental value determined in the previous section.

3.3 HO₂ kinetics

Modelling the time resolved HO₂ increase is not very precise, because the fluorescence lamps need a few seconds to reach their stable state when switched on and this influences markedly the time resolution. The rapid decrease of the HO₂ absorbance is easier to observe, as turning off the lamps is instantaneous. The absorbance was converted into absolute HO₂ concentrations using equation (I). The decay is expected to be mainly linked to the self recombination reaction (Eq. 4) as well as loss through heterogeneous wall reaction, expressed as a HO₂ radial diffusion to the wall (Eq. 5):



The HO₂ kinetic equation is thus

$$-\frac{d[\text{HO}_2]}{dt} = 2 \times k_4 \times [\text{HO}_2]^2 + k_5 \times [\text{HO}_2] \quad (\text{III})$$

which integrates into

$$\frac{1}{[\text{HO}_2]} = \left(\frac{1}{[\text{HO}_2]_0} + \frac{2 \times k_4}{k_5} \right) \exp(k_5 \times t) - \frac{2 \times k_4}{k_5} \quad (\text{IV})$$

In Fig. 4 are shown the time-resolved HO₂ experimental signals at 6.6, 24 and 118 mbar after turning off the lamps, plotted as 1/[HO₂] as a function of time t . HO₂ diffusion coefficients of 110, 30 and 7 cm² s⁻¹ at 6.6, 24 and 118 mbar, respectively, were used, based on the expression of Marrero and Mason [43]. The second-order rate coefficients k_4 obtained from the average of all the measurements are $(1.65 \pm 0.2) \times 10^{-12}$, $(1.75 \pm 0.3) \times 10^{-12}$ and $(1.9 \pm 0.3) \times 10^{-12}$ cm³ molecules⁻¹ s⁻¹ at 6.6, 24 and 118 mbar, respectively, in good agreement with the recommendation from Atkinson *et al.* of 1.7×10^{-12} cm³ molecules⁻¹ s⁻¹ at 24 mbar and 296 K [44].

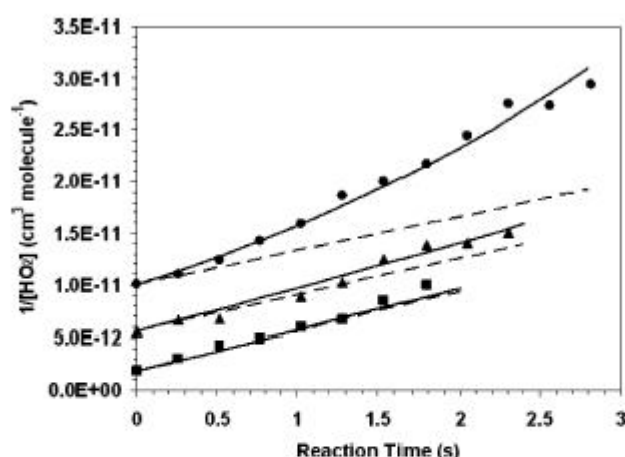


Fig. 4. Typical kinetic plots of $1/[\text{HO}_2]$ vs. time as a function of the pressure inside the reactor: Circles: 6.6 mbar, triangles: 24 mbar and squares: 118 mbar. The solid lines represent the analytical solution of the HO_2 kinetic equation (equation (III)). The dotted lines represent the plots assuming HO_2 loss through self-reaction only. The y-axis data at 6.6 mbar (circles) as well as the corresponding simulation curves have been shifted by 4×10^{-12} for clarity. The y-axis data at 118 mbar (squares) as well as the corresponding simulation curves have been shifted by -2×10^{-12} for clarity.

Note that the recommended $\text{HO}_2 + \text{HO}_2$ rate coefficient is slightly increasing from 1.65×10^{-12} (at 6.6 mbar) to $1.8 \times 10^{-12} \text{ cm}^{-3} \text{ molecules}^{-1} \text{ s}^{-1}$ (at 118 mbar), which trend is reflected by the present measurements. The reported error limits (2σ) take into account the statistical uncertainty in the HO_2 concentration ($\sim 15\%$). The accuracy of the HO_2 absorption cross section is estimated at $\sim 25\%$, which could be an additional source of systematic error of the same magnitude on k_4 . Spatial heterogeneities in the HO_2 concentrations along the main axis of the reactor are also possible, especially near the flanges: Cl-atoms are known to recombine efficiently on stainless steel surfaces (sticking coefficient $\gamma \approx 0.85$) [45]. This would lead to a lower HO_2 concentration near the flanges and hence to a higher concentration in the centre of the cell which would lead in turn to an overestimation of the HO_2 second-order self reaction rate constant. However, the associated uncertainty, of the order of a few percent, is probably less than other statistical or systematic errors [46]. The total uncertainty in k_4 (2σ) can be estimated to about 30%.

The simulated fits taking into account the HO_2 self-recombination only (dotted lines) are plotted for comparison. As expected, the pressure effect on the HO_2 kinetics is more important at lower pressure and almost negligible at 118 mbar. This suggests that HO_2 radicals are lost on the walls of the reaction chamber and shows that the HO_2 diffusion may play a significant role on the HO_2 kinetics in the photoreactor. Note that the uncertainty on the HO_2 diffusion coefficient is of the order of 50% with a larger impact on the low- than on the high-pressure kinetics. The diffusion process and recombination on surfaces of the hydroperoxy radical has been suggested for a long time [47,48] and in a very recent publication [49], the efficient recombination of HO_2 radicals on glass surfaces has even been employed for a selective denuding of HO_2 radicals. Reactivity of peroxy radicals on aerosol surfaces has also been proposed [50,51] and could be import-

ant for high aerosol content [2]. The present work suggests that the HO₂ loss on a quartz surface could be significant, especially at pressures less than ~60 mbar. It should be stressed that wall losses of HO₂ radicals in similar reactors are generally not known, as HO₂ radicals are often not measured in such reactors.

3.4 Conclusions

The present work demonstrates the feasibility of measuring HO₂ radical concentrations in a large photoreactor by direct cw-CRDS spectroscopy and underlines the interest of measuring peroxy radicals like HO₂ in low pressure reactors, since large losses of radicals can significantly affect the reaction mechanism and the resulting final product distribution. Future work will focus on the understanding of chemical mechanisms by combining simultaneous HO₂ radical and stable species (like CH₂O [30]) measurements by cw-CRDS.

Acknowledgement

This work is jointly supported by the Nord-Pas de Calais region in the frame of the IRENI research program, by the French Research Ministry and by the European funds for Regional Economic Development (FEDER). M. D. gratefully acknowledges the financial support from the Ecole des Mines de Douai.

References

1. M. E. Jenkin and K. C. Clemitshaw, *Atmos. Environ.* **34** (2000) 2499.
2. D. R. Crosley, *J. Atmos. Sci.* **52** (1995) 3299.
3. D. Heard and M. J. Pilling, *Chem. Rev.* **103** (2003) 5163.
4. K. H. Becker, *The European Photoreactor EUPHORE*, BUGH-Wuppertal (Germany), 1996.
5. J.-F. Doussin, D. Ritz, R. Durand-Jolibois, A. Monod, and P. Carlier, *Analisis (Paris)* **25** (1997) 236.
6. H. Fuchs, T. Brauers, H.-P. Dorn, H. Harder, R. Häseler, A. Hofzumahaus, F. Holland, Y. Kanaya, Y. Kajii, D. Kubistin, S. Lou, M. Martinez, K. Miyamoto, S. Nishida, M. Rudolf, E. Schlosser, A. Wahner, A. Yoshino, and U. Schurath, *Atm. Chem. Phys.* **10** (2010) 12233.
7. D. Mihelcic, M. Heitlinger, D. Kley, P. Mütgen, and A. Volz-Thomas, *Chem. Phys. Lett.* **301** (1999) 559.
8. G. K. Moortgat, *Evaluation of radical sources in atmospheric chemistry through chamber and laboratory studies*, RADICAL final report, JRC Ispra (Italy), 2002.
9. J. Lelieveld, T. M. Butler, J. N. Crowley, T. J. Dillon, H. Fischer, L. Ganzeveld, H. Harder, M. G. Lawrence, M. Martinez, D. Taraborrelli, and J. Williams, *Nature* **452** (2008) 737.
10. C. Bloss, V. Wagner, M. E. Jenkin, R. Volkamer, W. J. Bloss, J. D. Lee, D. E. Heard, K. Wirtz, M. Martin-Reviejo, G. Rea, J. C. Wenger, and M. J. Pilling, *Atmos. Chem. Phys.* **5** (2005) 641.
11. A. Hofzumahaus, F. Rohrer, K. Lu, B. Bohn, T. Brauers, C.-C. Chang, H. Fuchs, F. Holland, K. Kita, Y. Kondo, X. Li, S. Lou, M. Shao, L. Zeng, A. Wahner, and Y. Zhang, *Science* **324** (2009) 1702.
12. A. Tomas, E. Villenave, and R. Lesclaux, *J. Phys. Chem. A* **105** (2001) 3505.
13. M. E. Jenkin, M. D. Hurley, and T. J. Wallington, *Phys. Chem. Chem. Phys.* **9** (2007) 3149.
14. D. R. Glowacki, A. Goddard, K. Hemavibool, T. L. Malkin, R. Commane, F. Anderson, W. J. Bloss, D. E. Heard, T. Ingham, M. J. Pilling, and P. W. Seakins, *Atmos. Chem. Phys.* **7** (2007) 5371.
15. M. S. Alam, M. Camredon, A. R. Rickard, T. Carr, K. P. Wyche, K. E. Hornsby, P. S. Monks, and W. J. Bloss, *Phys. Chem. Chem. Phys.* **13** (2011) 11002.

16. H. Fuchs, B. Bohn, A. Hofzumahaus, F. Holland, K. D. Lu, S. Nehr, F. Rohrer, and A. Wahner, *Atmos. Meas. Tech.* **4** (2011) 1209.
17. S. Pinceloup, G. Laverdet, F. Maguin, J. F. Doussin, P. Carlier, and G. Le Bras, *J. Photochem. Photobiol. A* **157** (2003) 275.
18. B. Qi, K. Sato, T. Imamura, A. Takami, S. Hatakeyama, and Y. Ma, *Chem. Phys. Lett.* **427** (2006) 461.
19. K. P. Wyche, P. Monks, A. M. Ellis, R. L. Cordell, A. E. Parker, C. Whyte, A. Metzger, J. Dommen, J. Duplissy, A. S. H. Prévot, U. Baltensperger, A. R. Rickard, and F. Wulfert, *Atmos. Chem. Phys.* **9** (2009) 635.
20. M. D. King, E. M. Dick, and W. R. Simpson, *Atmos. Environ.* **34** (2000) 685.
21. S. M. Ball, I. M. Povey, E. G. Norton, and R. L. Jones, *Chem. Phys. Lett.* **342** (2001) 113.
22. S. S. Brown, H. Stark, and A. R. Ravishankara, *Appl. Phys. B* **75** (2002) 173.
23. D. B. Atkinson and J. L. Spillman, *J. Phys. Chem. A* **106** (2002) 8891.
24. P. Rupper, E. N. Sharp, G. Tarczay, and T. A. Miller, *J. Phys. Chem.* **111** (2007) 832.
25. J. Thiébaud and C. Fittschen, *Appl. Phys. B* **85** (2006) 383.
26. A. Aluculesei, A. Tomas, C. Schoemaeker, and C. Fittschen, *Appl. Phys. B* **92** (2008) 379.
27. S. Crunaire, J. Tarmoul, C. Fittschen, A. Tomas, B. Lemoine, and P. Coddeville, *Appl. Phys. B* **85** (2006) 467.
28. W. Zhao, X. Gao, L. Hao, M. Huang, T. Huang, T. Wu, W. Zhang, and W. Chen, *Vib. Spectrosc.* **44** (2007) 388.
29. D. S. Venables, T. Gherman, J. Orphal, J. C. Wenger, and A. A. Ruth, *Environ. Sci. Technol.* **40** (2006) 6758.
30. M. Djehiche, A. Tomas, C. Fittschen, and P. Coddeville, *Environ. Sci. Technol.* **45** (2011) 608.
31. D. Romanini, A. A. Kachanov, N. Sadeghi, and F. Stoeckel, *Chem. Phys. Lett.* **264** (1997) 316.
32. M. D. Wheeler, S. M. Newman, A. J. Orr-Ewing, and M. N. R. Ashfold, *J. Chem. Soc., Faraday Trans.* **94** (1998) 337.
33. J. J. Scherer, J. B. Paul, A. O'Keefe, and R. J. Saykally, *Chem. Rev.* **97** (1997) 25.
34. B. A. Paldus and A. A. Kachanov, *Can. J. Phys.* **83** (2005) 975.
35. L. E. Christensen, M. Okumura, J. C. Hansen, S. P. Sander, and J. S. Francisco, *J. Phys. Chem. A* **110** (2006) 6948.
36. J. Thiébaud, S. Crunaire, and C. Fittschen, *J. Phys. Chem. A* **111** (2007) 6959.
37. Y. Tang, G. S. Tyndall, and J. J. Orlando, *J. Phys. Chem. A* **114** (2010) 369.
38. N. Ibrahim, J. Thiébaud, J. Orphal, and C. Fittschen, *J. Mol. Spectrosc.* **242** (2007) 64.
39. N. Kanno, K. Tonokura, A. Tezaki, and M. Koshi, *J. Mol. Spectrosc.* **229** (2005) 193.
40. S. Miyano and K. Tonokura, *J. Mol. Spectrosc.* **265** (2011) 47.
41. S. P. Sander, B. J. Finlayson-Pitts, R. R. Friedl, D. M. Golden, R. E. Huie, H. Keller-Rudek, C. E. Kolb, M. J. Kurylo, M. J. Molina, G. K. Moortgat, V. L. Orkin, A. R. Ravishankara, and P. H. Wine, *Chemical kinetics and photochemical data for use in atmospheric studies*, Evaluation number 15, Jet Propulsion Laboratory, Pasadena (California), 2006.
42. J. R. Holmes, R. J. O'Brien, J. H. Crabtree, T. A. Hecht, and J. H. Seinfeld, *Environ. Sci. Technol.* **7** (1973) 519.
43. T. R. Marrero and E. A. Mason, *J. Phys. Chem. Ref. Data* **1** (1972) 3.
44. R. Atkinson, D. L. Baulch, R. A. Cox, J. N. Crowley, R. F. Hampson, R. G. Hynes, M. E. Jenkin, M. J. Rossi, and J. Troe, *Atmos. Chem. Phys.* **4** (2004) 1461.
45. G. P. Kota, J. W. Coburn, and D. B. Graves, *J. Vac. Sci. Technol. A* **16** (1998) 270.
46. A. Fahr and A. H. Laufer, *Int. J. Chem. Kin.* **25** (1993) 1029.
47. C. A. Cantrell, D. H. Stedman, and G. J. Wendel, *Anal. Chem.* **56** (1984) 1496.
48. C. M. Mihele, M. Mozurkewich, and D. R. Hastie, *Int. J. Chem. Kin.* **31** (1999) 145.
49. K. Miyazaki, A. E. Parker, C. Fittschen, P. S. Monks, and Y. Kajii, *Atmos. Measur. Tech.* **3** (2010) 1547.
50. D. J. Jacob, *Atmos. Environ.* **34** (2000) 2131.
51. C. A. Cantrell, R. E. Shetter, T. M. Gilpin, J. G. Calvert, F. L. Eisele, and D. J. Tanner, *J. Geophys. Res.* **101** (1996) 14653.

II.2 Le réacteur à écoulement pour l'étude des aérosols organiques secondaires

Mon deuxième axe de recherche porte sur l'étude de la formation et du vieillissement des aérosols organiques secondaires (AOS). Parmi les grands questionnements actuels en chimie atmosphérique, deux thèmes sont particulièrement sensibles : (i) le mécanisme de formation des particules ultrafines ; (ii) le devenir atmosphérique de ces particules. En effet, comme rappelé en introduction, si les particules submicroniques représentent une part négligeable de la charge massique en aérosols atmosphériques, leur impact sanitaire et environnemental (effet de serre, chimie atmosphérique) est considérable. Une connaissance approfondie des processus physico-chimiques auxquels ces particules sont soumises est donc indispensable.

Les campagnes de mesures en atmosphère réelle et les études en chambres de simulation sont les deux outils classiquement utilisés pour aborder les AOS. Les campagnes de mesures donnent des informations importantes, notamment en termes de sources, granulométrie, composition chimique et vitesse d'accroissement de la taille des particules. Elles sont toutefois limitées du fait du nombre de paramètres non contrôlés et non mesurés et de la complexité de la composition chimique du milieu (partie gazeuse et particulaire). Les études en laboratoire sont, pour la plupart, réalisées dans des grandes chambres de simulation atmosphériques en atmosphère contrôlées et s'affranchissent ainsi des inconvénients des campagnes de terrain. Malgré tout, les concentrations en réactifs utilisés sont souvent beaucoup plus élevées que dans l'environnement et elles peuvent être sujettes à artéfacts dus à de possibles réactions hétérogènes sur les parois. Par ailleurs, les CSA ne permettent souvent pas l'étude des premières étapes de formation des particules, fournissant au contraire des rendements globaux de formation des AOS.

Nous avons donc choisi de développer un dispositif basé sur un réacteur à écoulement laminaire où le temps de réaction est variable mais limité à quelques minutes et nous avons couplé le réacteur à diverses techniques d'analyse des phases organiques gazeuse et particulaire. Les avantages de ce type de réacteur sont (i) des temps de réaction faibles, ce qui permet d'étudier les premières étapes de formation des AOS (ii) un écoulement laminaire qui limite les effets de paroi (iii) la possibilité d'échantillonner des volumes importants (vu que l'écoulement est stationnaire), ce qui implique de pouvoir travailler à des concentrations en réactifs faibles. On peut noter que ce type de réacteur avec une application 'AOS' est assez peu courant en chimie atmosphérique et le nombre d'articles publiés est également limité. Signalons le développement récent d'un réacteur à but similaire (mais de dimensions beaucoup plus imposantes) dans le groupe de B.J. Finlayson-Pitts à l'Université de Californie (100).

Les objectifs à l'origine de ce projet étaient de deux ordres :

1. dans un premier temps, caractériser les espèces chimiques à l'origine de la formation des AOS dans des réactions d'ozonolyse de terpènes et déterminer l'influence des conditions expérimentales sur la formation des AOS.
2. dans un deuxième temps, observer l'évolution de l'AOS formé dans le réacteur au cours du temps en le soumettant à un vieillissement accéléré en chambre de simulation atmosphérique.

Les terpènes ont été choisis car ils contribuent de façon importante à la charge globale en AOS dans l'atmosphère ; ils sont également présents dans de nombreux produits ménagers (ex. : limonène) et donc en atmosphère intérieure. La formation d'aérosols organiques secondaires à partir de terpènes est connue depuis de nombreuses années (101). La plupart des études ont été réalisées en chambres de simulation atmosphérique et ont permis de déterminer les rendements en aérosols et de comprendre globalement les mécanismes chimiques d'oxydation de ces espèces (102-104). Les premières étapes de formation des nanoparticules sont toutefois difficiles à appréhender avec ce type de réacteur, car l'avancement de la réaction augmente en continu. C'est pourquoi nous avons envisagé de développer un réacteur à écoulement permettant de travailler à des avancements de réaction faibles et d'étudier ainsi les premières phases de formation des particules.

II.2.1 Développement expérimental

Le développement du réacteur à écoulement et les tests de validation ont été effectués dans le cadre du post-doctorat de N. Visez (2007-2008) et de la thèse de M. Duncianu (2008-2011) (53). Les principales étapes sont rappelées dans cette section, ainsi que les résultats obtenus.

Dans le cadre de ce projet, les principales contraintes ont porté sur :

- le temps de réaction, qui devait être variable de quelques secondes à quelques minutes ;
- l'écoulement des gaz, laminaire pour limiter les artéfacts avec les parois et assurer un régime stationnaire ;
- l'encombrement, nécessairement limité, notamment pour un réacteur en position verticale ;
- les outils d'analyse, adaptés aux objectifs scientifiques proposés.

Par ailleurs, la thématique scientifique envisagée touchait aux mécanismes de formation des AOS par des composés terpéniques, mécanismes principalement représentés par les réactions d'ozonolyse (105). C'est pourquoi, lors de la conception du réacteur, nous avons volontairement restreint (au moins dans un premier temps) les possibilités d'application du dispositif aux réactions d'ozonolyse.

Sur la base de ce cahier des charges, le réacteur à écoulement a été développé et comporte les caractéristiques techniques suivantes :

- un tube en Pyrex de 1 m de long et 10 cm de diamètre (tube calibré) maintenu verticalement dans une enceinte en bois ; compte tenu des débits totaux envisagés ($0,5$ à 5 L min^{-1}), un nombre de Reynolds < 70 peut être calculé, ce qui indique des conditions d'écoulement laminaire ;
- une tête d'injection mobile dans laquelle les réactifs sont mélangés ; elle est remplie de billes de verre afin de diminuer le temps de mélange et coulisse à l'intérieur du réacteur, ce qui permet de modifier le volume – et donc le temps – de réaction de $1,5 \text{ L}$ à $7,1 \text{ L}$;
- une zone de prélèvement en bout de réacteur, comportant un tube central ($\frac{1}{4}$ ' de diamètre) pour l'échantillonnage des particules et un tube latéral pour un échantillonnage complémentaire des gaz et des particules et l'évacuation du flux total.

Deux parties complètent le réacteur : la génération des flux de réactifs et les outils d'échantillonnage et d'analyse des phases gazeuses et particulaires (**Figure II.7**).

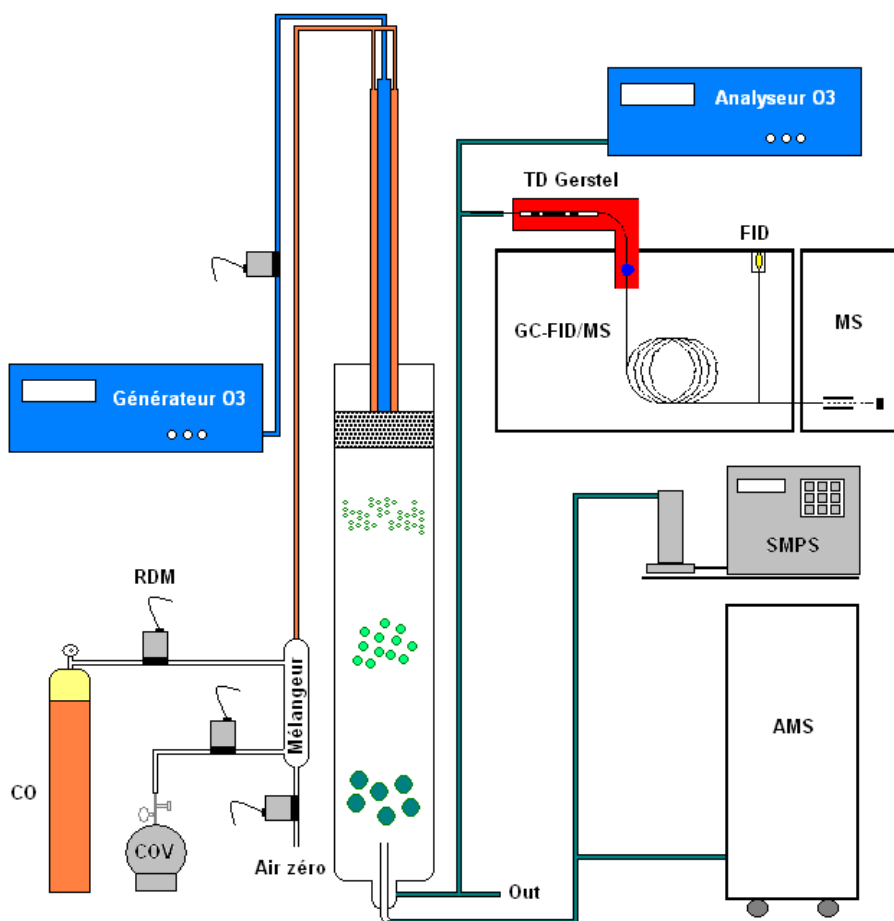


Figure II.7 : schéma du réacteur à écoulement (au centre) avec zone d'injection (à gauche) et zone d'analyse (à droite)

Génération des flux de réactifs

L'ozone est produit par un générateur d'ozone commercial (Thermo Scientific™ Model 146i) à partir de la photolyse de l'oxygène dans l'UV. Le débit massique d'ozone est ajustable par variation de l'intensité de la lampe de photolyse et peut atteindre 0,2 mg.h⁻¹. Le débit volumique variable (entre 0 et 3 L.min⁻¹) permet également d'ajuster la concentration en sortie du générateur.

La source de réactif organique consiste en un canister (6 L) dans lequel est vaporisé une certaine quantité du réactif et complété à l'air zéro jusqu'à 3-4 bars de pression. Les débits étant de l'ordre de la dizaine de mL.min⁻¹, ce dispositif permet de générer un flux de concentration constante de réactif pendant plusieurs heures. Le flux est envoyé vers une chambre de dilution à l'air zéro où la concentration du composé organique est abaissée à la valeur souhaitée.

Les flux d'ozone et de réactif organique dilué arrivent *via* des lignes distinctes jusqu'à la tête d'injection du réacteur.

L'air zéro issu d'un générateur (Claind™ AZ 2020) est utilisé comme gaz vecteur principal. Le taux d'humidité dans l'air zéro est faible et reste inférieur à 5%. Le débit total est variable de 0,5 à 5 L.min⁻¹, ce qui implique des temps de réaction d'environ 10 s à 16 min.

Outils d'échantillonnage et d'analyse des phases gazeuses et particulaires

Les outils d'analyse des phases gazeuses et particulaires mis en place dans un premier temps sont au nombre de quatre :

- La chromatographie en phase gazeuse couplée à une double détection par ionisation de flamme (FID) et spectrométrie de masse (MS) (Agilent™ 6890 – MSD 5973). Le chromatographe est couplé en amont à un thermodésorbeur (TDS Gerstel™) qui permet soit d'analyser des cartouches d'adsorbants préalablement échantillonnées, soit d'échantillonner directement le milieu réactionnel du réacteur. Notons que les deux composantes gazeuses et particulaires sont prélevées et analysées en même temps avec ce système.
- Un analyseur d'ozone (TEI 49C) par spectroscopie d'absorption UV. L'analyseur prélève à un débit de 1,4 L.min⁻¹. La limite de détection, d'environ 1 ppbv et la résolution temporelle, de l'ordre de 20 s, sont suffisantes pour notre application. L'analyseur est calibré au laboratoire grâce à un étalon raccordé au Laboratoire National d'Essai (LNE).
- Un granulomètre laser SMPS (Scanning Mobility Particle Sizer, Grimm™ 5403) comprenant deux colonnes de classification interchangeables (gammes 5 – 350 nm et 10 – 1100 nm) et un compteur de particules (concentration max. 10⁷ particules.cm⁻³). Le débit de prélèvement est de 0,3 L.min⁻¹.
- Un spectromètre de masse à aérosol haute résolution (Aerodyne™ HR-ToF-AMS) permettant d'acquérir la distribution en taille (par le temps de vol, dans la gamme 30 – 600 nm) et, après

impaction et vaporisation des particules, leur composition chimique. La résolution en masse ($m/\Delta m$) est de 1000 en mode V et 3000 en mode W¹. Le débit de prélèvement est de $\sim 80 \text{ mL}\cdot\text{min}^{-1}$.

D'autres outils complémentaires devraient être intégrés dans les prochaines années, notamment pour l'analyse fine de la composition chimique des particules (par exemple, prélèvement sur filtre, dérivatisation, PTR-MS couplé à un thermodésorbeur).

Une photographie montrant une vue d'ensemble du dispositif est présentée sur la **Figure II.8**.

¹ Les modes V et W font référence à la forme de la trajectoire effectuée par les ions dans le spectromètre de masse. En mode W, le chemin parcouru est plus important (et par conséquent le temps de vol également), ce qui a pour effet d'augmenter la résolution.



Figure II.8 : photographie d'une vue d'ensemble du dispositif

II.2.2 Validation : étude de cinétiques d'ozonolyse

La validation cinétique du réacteur à écoulement a été réalisée en étudiant quelques réactions du type pentènes + ozone ainsi que la réaction α -pinène + ozone, réactions dont les cinétiques sont documentées dans la littérature (au moins une publication existante par réaction étudiée). L'importance de l'ozonolyse des alcènes dans l'atmosphère est connue depuis longtemps. Une des caractéristiques majeures de ces réactions est la formation de radicaux OH^\bullet dans le mécanisme réactionnel. Cette formation est loin d'être anodine dans la chimie atmosphérique, puisqu'elle peut représenter l'essentiel de la source de radicaux OH^\bullet dans l'atmosphère l'hiver en zone urbaine (106). Pendant la canicule de 2003 en Europe, Lee *et al.* ont montré que l'ozonolyse des alcènes représentait une source de radicaux RO_2^\bullet plus importante que la photolyse du formaldéhyde (107). Le choix de l' α -pinène se justifie dans la mesure où il forme des AOS lors de son ozonolyse et qu'il représente ainsi une étape vers l'étude de la formation des aérosols organiques secondaires.

Les cinétiques d'ozonolyse du 4-méthyl-1-pentène, du 2-méthyl-2-pentène, du 2,4,4-triméthyl-1-pentène, du 2,4,4-triméthyl-2-pentène et de l' α -pinène ont été déterminées à température ambiante en conditions de pseudo-premier ordre, la concentration initiale du composé insaturé (alcène ou α -pinène) étant en excès par rapport à celle de l'ozone. Les résultats obtenus sont en très bon accord avec la littérature. Des expériences complémentaires réalisées dans la chambre de simulation en Téflon dans des conditions expérimentales proches ont permis d'obtenir les constantes de vitesse d'ozonolyse par une technique différente et en très bon accord avec les résultats en tube à écoulement. Enfin, l'application d'une relation structure-activité de la littérature sur l'ozonolyse des alcènes (108) a montré une très bonne corrélation entre les valeurs mesurées et les valeurs prédites, ce qui a conforté les résultats et la validation du réacteur à écoulement.

L'ensemble des résultats a été soumis au *Journal of Physical Chemistry A* en novembre 2011 (**publication n°3**, (54)).

L'étude des produits des réactions d'ozonolyse des mêmes pentènes a été réalisée dans un deuxième temps et a permis de mettre en évidence pour la première fois la formation d'un composé non oxydé de type propène, probablement suite à un réarrangement de l'intermédiaire de Criegee (**Figure II.9**). L'observation d'un tel composé démontre tout l'intérêt du dispositif développé pour étudier les mécanismes réactionnels d'oxydation des COV. Ces résultats, obtenus très récemment, sont en cours d'analyse et seront publiés prochainement. Ces travaux sont actuellement poursuivis sur d'autres alcènes méthylés (hexène et heptène) afin de confirmer les hypothèses de mécanismes.

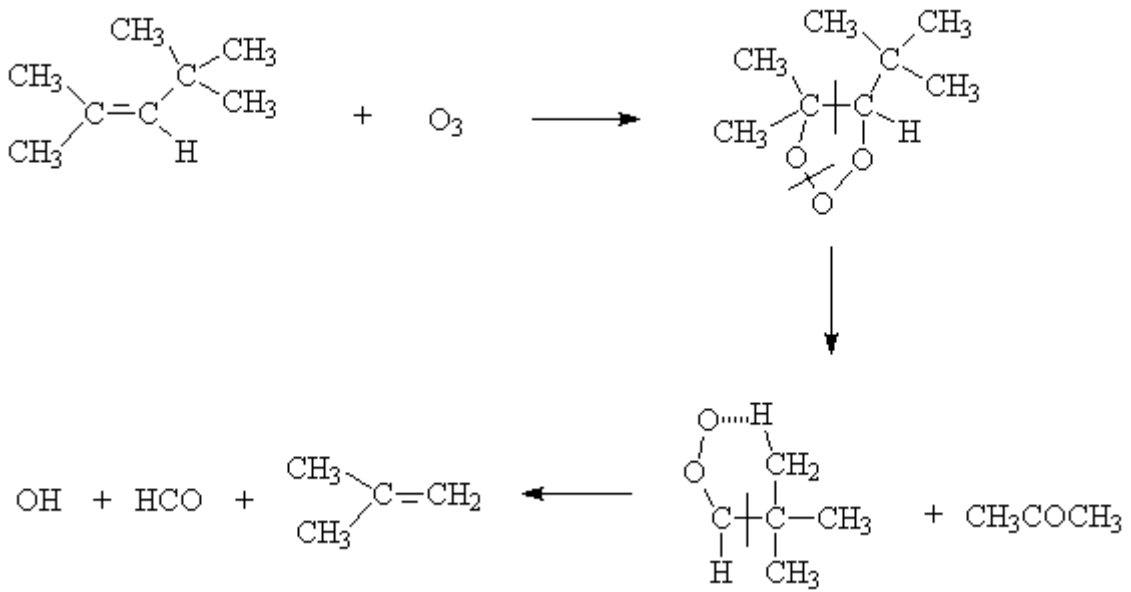


Figure II.9 : Mécanisme hypothétique conduisant à la formation d'un produit non oxydé (2-méthyl-propène) dans l'ozonolyse du 2,4,4-triméthyl-2-pentène

Publication n°3

(soumise dans la revue *Journal of Physical Chemistry A* en novembre 2011)

**Development of a new flow-reactor for kinetic studies.
Application to the ozonolysis of a series of alkenes**

Journal:	<i>The Journal of Physical Chemistry</i>
Manuscript ID:	Draft
Manuscript Type:	Special Issue Article
Date Submitted by the Author:	n/a
Complete List of Authors:	Duncanu, Marius; Univ. Lille Nord de France; EMDouai, CE Olariu, Romeo; "Al. I. Cuza" University of Iasi, Faculty of Chemistry Riffault, Veronique; Univ. Lille Nord de France; EMDouai, CE Visez, Nicolas; Univ. Lille Nord de France Tomas, Alexandre; Univ. Lille Nord de France; EMDouai, CE Coddeville, Patrice; Univ. Lille Nord de France; EMDouai, CE

SCHOLARONE™
Manuscripts

18 Abstract

19 A new flow reactor has been developed to study ozonolysis reactions at ambient pressure and
20 room temperature (297 ± 2 K). The reaction kinetics of O_3 with 4-methyl-1-pentene (4M1P),
21 2-methyl-2-pentene (2M2P), 2,4,4-trimethyl-1-pentene (tM1P), 2,4,4-trimethyl-2-pentene
22 (tM2P) and α -pinene have been investigated under pseudo first order conditions. Absolute
23 measurements of the rate coefficients have been carried out by recording O_3 consumption in
24 excess of organic compound. Alkene concentrations have been determined by sampling
25 adsorbent cartridges which were thermodesorbed and analyzed by gas-chromatography
26 coupled to flame ionization detection. Complementary experimental data have been obtained
27 using a 250 L Teflon smog chamber. The following ozonolysis rate coefficients can be
28 proposed (in $\text{cm}^3 \text{ molecule}^{-1} \text{ s}^{-1}$): $k_{4M1P} = (8.23 \pm 0.50) \times 10^{-18}$, $k_{2M2P} = (4.54 \pm 0.96) \times 10^{-16}$,
29 $k_{tM1P} = (1.48 \pm 0.11) \times 10^{-17}$, $k_{tM2P} = (1.25 \pm 0.10) \times 10^{-16}$ and $k_{\alpha\text{-pinene}} = (1.29 \pm 0.16) \times 10^{-16}$,
30 in very good agreement with literature values. The products of tM2P ozonolysis have been
31 investigated and branching ratios of $(21.4 \pm 2.8)\%$ and $(73.9 \pm 7.3)\%$ have been determined
32 for acetone and 2,2-dimethyl-propanal, respectively. Additionally a new non-oxidized
33 intermediate – 2-methyl-1-propene – has been identified and quantified. A topological SAR
34 analysis was also performed to strengthen the consistency of the kinetic data obtained with
35 this new flow reactor.

36

37 Keywords

38 rate coefficients, structure-activity relationship (SAR), pentene, α -pinene,

39 Introduction

40 A significant part of the total primary volatile organic carbon (VOC) emissions to the
41 atmosphere is formed by alkenes, and their ozonolysis continues to receive attention, due to
42 its important role in atmospheric chemistry. The alkene ozonolysis rate coefficients are useful
43 as input data for comprehensive atmospheric chemical models describing air quality at urban
44 or regional scales, where ozonolysis may be the most important sink for alkenes.

45 Under atmospheric conditions the reactions of ozone with alkenes provide free radicals and
46 reactive intermediates. Gas-phase ozonolysis reactions involving alkenes can be a significant
47 source of hydroxyl radicals in the atmosphere¹⁻³ and precursors of carbonyls or carboxylic
48 acids^{4,6}.

49 In this work, we have studied the ozonolysis kinetics of four methylated pentenes, i.e. 4-
50 methyl-1-pentene (4M1P), 2-methyl-2-pentene (2M2P), 2,4,4-trimethyl-1-pentene (tM1P),
51 2,4,4-trimethyl-2-pentene (tM2P), and α -pinene in a flow reactor newly developed in our
52 laboratory and aiming at investigating the primary particle formation steps. The literature
53 describes a limited number of flow reactors used in the study of the formation, evolution or
54 aging of aerosols⁷⁻¹⁶, and the present study confirms their versatility and the capacity of using
55 them also in kinetic studies.

56 Some of the alkenes investigated in this work (2-methyl-2-pentene and 4-methyl-1-pentene)
57 have been identified in common processes such as tailpipe emissions of volatile hydrocarbons
58 from gasoline-powered motor vehicles¹⁷, residential fireplace combustion of wood¹⁸ or in
59 natural fires of foliage, litter, and herbaceous matter¹⁹. α -pinene is a well-known biogenic
60 compound which forms secondary organic aerosols (SOA) in the atmosphere following
61 oxidation processes.

62 It should be pointed out that the four pentenes have been selected for the validation step
63 because their O₃ reaction rate coefficients are already known in the literature; and yet, while

64 O₃ + alkene reaction kinetics and mechanisms are generally investigated in environmental
65 simulation chambers with large reaction times, the present work on the pentenes is to the best
66 of our knowledge the first one carried out at much shorter reaction times.

67 Moreover, current uncertainties on such alkene oxidation mechanisms result from the
68 incomplete description of the excited Criegee intermediate decay channels, which determine
69 the extent to which each of these channels generate radicals²⁰. α -pinene ozonolysis was also
70 studied, since the reaction system is more complex and involves heterogeneous processes due
71 to the formation of SOA^{21,22}. Beside the main homogeneous process, the presence of
72 particulate matter could induce supplemental reactions in the particulate phase or adsorptive
73 processes.

74 To add more confidence to the data obtained with the flow tube, similar kinetic studies have
75 been performed on the pentenes using a Teflon bag smog chamber. Finally, a Structure
76 Activity Relationship (SAR) analysis has been applied to prove the consistency of the
77 obtained results.

78 **1. Experimental methods**

79 **1.1 Flow reactor setup for kinetic measurements**

80 The new aerosol flow tube is schematically represented in Figure 1. The cylindrical reactor
81 (Pyrex tube with 1 m length and 10 cm i.d.) has been designed to work with total flows of
82 about 1.5 to 5 L min⁻¹, corresponding to reaction times ranging between 30 s and ~ 5 min. Its
83 vertical position assures a gravitational equilibrium of the flow, and a sliding injector ending
84 with a mixing chamber is used to introduce the reagents on two different lines and to ensure
85 homogeneity before their entrance into the reaction volume. The passage of the fluid into the
86 reactor is assured by a sintered glass wall welded to the mixing chamber filled with glass
87 beads (diameter: 2 mm), thus providing optimal conditions to rapidly achieve a laminar flow

88 regime. The injection head has been designed to allow good mixing of the reactive gases at
89 transit times of seconds (1 to 2.5 s) and to support the formation of a laminar flow (Reynolds
90 number, $Re \sim 20$ to 50) in the reactor. The laminar flow in the reactor ensures a stationary
91 mode as a function of the reaction volume, at atmospheric pressure and room temperature
92 ($T = 297 \pm 2$ K). At the bottom of the reactor two exhaust lines consisting of a 1/4-inch glass
93 tubes are used to collect samples. The central one reaches the laminar flow region roughly 15
94 cm above the bottom of the reactor. The reactor height is defined by the distance between the
95 injector head and the central sampling point. The volume difference between the central
96 sampling line and the lateral one was taken into account to correct the reaction time for each
97 reactor height.

98 Additional flow criteria were used to characterize the flow. For all experiments the Péclet
99 number is inferior to 50, indicating non plug flows²³, and the Gaussian distributions of the
100 velocity profile in the laminar flow may be seen in Figure 2a.

101 A pulse tracer study similar to previous approaches²⁴ was performed using either O_3 or CO to
102 validate the calculation of the contact time into the reactor. The concentration profiles of the
103 tracer analytes were monitored with 1s time resolution measurements using spectroscopic
104 analyzers (Models 48C and 49C, Thermo Environmental Instruments) for various heights of
105 the reactor and several characteristic flows. The example given in Figure 2a shows the ozone
106 time profiles and their first derivatives ($\Delta[O_3]/\Delta t$) for a 3150 mL min^{-1} flow. The average bulk
107 velocity was corrected using the ratio between the calculated residence time, $t_{R \text{ calc}}$, as derived
108 from the laminar flow theory and the measured residence time, $t_{R \text{ meas}}$, from the tracer study.
109 The ratio was close to unity for the most part of the flow range (described by Re) whatever
110 the reactor heights (h_R), as seen in Figure 2b. The gray area represents the Re/h_R range of all
111 the kinetic measurements. The response time of the tracer analyzer and the diffusion
112 coefficient of the analyte due to the concentration gradient were taken into account to correct

113 the estimation of the measured residence time. The diffusion correction was under 5% for
114 most experiments and never exceeded 10%.

115 For alkene ozonolysis, a continuous gas flow of the selected VOC is achieved using a
116 pressurized canister, few mL min⁻¹ being released through a mass flow controller (MFC) in a
117 pre-mixing chamber. Purified air is used as a carrier gas and ensures the dilution of the VOC
118 at the requested level of concentration. On the other hand, an ozone generator (Model 146i,
119 Thermo Scientific) provides a controlled flow of oxidant which reaches the injection head via
120 a separate line. The controlled flows of ozone and volatile organic compound enable pre-
121 defined and stable concentrations at the top of the reactor to be obtained.

122 The volume of the flow reactor can be modified by moving up and down the sliding injection
123 head, thus allowing to monitor the evolution of the reagents and products at various reaction
124 times and to estimate kinetic and mechanistic parameters. Different reaction times may also
125 be achieved by changing the total flow rate for a given distance between the movable
126 injection head and the sampling outlet.

127 The side line was used to sample adsorption cartridges, to determine the ozone concentration
128 and evacuate the main flow, while the central one will be used in further studies for aerosol
129 sampling in isokinetic conditions. The cartridges filled with three different adsorbents
130 (Carbopack C, Carbopack B and Carbosieve SIII in 1:2:1 packing ratio from Supelco) were
131 sampled at 50 mL min⁻¹ before injecting ozone to determine the initial concentration of the
132 VOC in excess. A cartridge by-pass was installed to continuously purge the Teflon line with
133 the exhaust air of the reactor before and after sampling. The reactant concentration was
134 estimated using calibration curves obtained with cartridges doped with known concentrations
135 of analytes. Six cartridges were sampled in absence of ozone at different heights in the reactor
136 to check for the concentration of the organic reactant, the potential wall losses (found
137 negligible for all compounds) as well as the reproducibility and accuracy of the sampling. It

138 should be underlined that in presence of ozone, a KI-coated copper tube upstream the
139 sampling cartridge was used as a denuder to avoid the loss of the alkenes through O₃ reaction
140 on the adsorbent²⁵.

141 For the kinetic experiments in the flow reactor, sampled cartridges were then thermally
142 desorbed (within 24-h) in a two-stage thermodesorber (Markes Unity2) and analyzed by
143 GC/FID (Agilent 7890A). A Varian capillary column (CP-Sil 5 CB 50 m, 0.32 mm, 1.2 μm)
144 was used with the following temperature program: 35°C, 15 min isothermal, 4°C min⁻¹ to
145 125°C then 20°C min⁻¹ to 250°C and hold for 6 min. Helium was used as carrier gas with a
146 column flow of ~ 3 mL min⁻¹.

147 Initial concentrations in the flow reactor were: (0.81-8.1) ppm, for the organic compound (1
148 ppm_v = 2.46 × 10¹³ molecule cm⁻³ at 298 K and 1 atm) and (61-374) ppb_v for ozone.

149 The outlet analytical chain includes an online O₃ analyzer (Model 49C, Thermo
150 Environmental Instruments) based on UV absorption spectroscopy. The absence of
151 interferences coming from the alkenes investigated in the present study were checked by
152 considering their UV absorption spectra, as well as by measurement tests in the absence of
153 ozone. As for possible interferences from the ozonolysis products, alkene concentrations were
154 increased progressively until total consumption of ozone in the reactor was reached, while the
155 O₃ analyzer presented a background value similar with the background value of purified air.

156

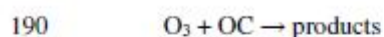
157 **1.2 Smog chamber setup**

158 In order to get additional confirmation of the kinetic parameters obtained with the aerosol
159 flow reactor, complementary experiments were performed on the 4 pentenes in a smog
160 chamber that has been described previously²⁶. Only the aspects specific to the current
161 experiments are presented below.

162 The reaction chamber consists of a Teflon bag with a volume of about 250 L working at
163 atmospheric pressure, (297 ± 2) K and in the dark. Teflon tubes are used for the introduction
164 of the reactants and the sampling by the analytical instruments. Ozone was produced by
165 flowing purified air through a UV lamp ozonizer (Model 165, Thermo Environmental
166 Instrument) which was directly injected in the Teflon chamber at a flow rate of about
167 2.8 L min^{-1} . The ozone concentration was determined as a function of reaction time by using
168 an online ozone analyzer (Model 41M, Environnement S.A.) with a time resolution of about
169 20 s. The analyzer sampling flow rate and precision were 0.90 L min^{-1} and 5 ppb,
170 respectively. Initial O_3 concentrations in the reaction chamber were in the range 70-300 ppb.
171 All the investigated alkenes being liquid reagents, they were injected with microliter syringes
172 into a small heated glass cell placed on a secondary input line of clean air in order to ensure a
173 complete and rapid evaporation. Initial alkene concentrations – calculated by taking into
174 account the injected volume of alkene and the total volume of the bag – were in the range 1.1-
175 3.4 ppm_v. Additional control experiments were carried out to check the stability of the
176 reactants in the Teflon bag, showing that all the selected olefins and O_3 do not suffer any
177 significant wall losses while in the chamber.
178 In a typical experiment, ozone was first added into the Teflon bag. At time zero, the pentene
179 was injected in the reactor using a high flow of purified air ($\sim 15 \text{ L min}^{-1}$), thus ensuring a
180 rapid dilution of the organic reactant in the ozone-containing Teflon chamber. For each
181 investigated compound, one experiment was performed using cyclohexane as an OH
182 scavenger, and no significant difference was observed in the ozone decay and, therefore, in
183 the ozonolysis rate coefficient.
184

185 **1.3 Absolute rate measurements. Kinetic determination formalism**

186 Rate coefficients for the investigated ozone reactions were determined in both reactors by
187 monitoring the O₃ decay rates in the presence of excess and known concentrations of the
188 organic compound (OC). As the ozone loss caused by wall deposition was shown to be
189 negligible, the temporal profile of O₃ is governed by a unique process:



191 leading to the following rate equation:

192
$$-\text{dln}[\text{O}_3]/\text{dt} = k_{\text{OC}} \times [\text{O}_3]_t \times [\text{OC}]_t \quad (\text{eq. 1})$$

193 where [OC]_t and [O₃]_t are the concentrations in organic compound and ozone at time t and k_{OC}
194 is the ozonolysis rate coefficient.

195 The initial organic compound concentration [OC]₀ being in excess by at least a factor of 10
196 over the initial ozone concentration, the OC concentration remains essentially constant
197 throughout the reaction time. This approximation is only valid if there are no other additional
198 processes, as competitive reaction, wall loss or/and OH radical reactions that could contribute
199 to the alkene decay except the ozonolysis.

200 Based on literature data, it is well known that the reaction of ozone with unsaturated species
201 can produce OH radicals^{2,27-33} which may further react with the organic reactant, resulting in a
202 significant change in the OC concentration. Complementary experiments were thus performed
203 with cyclohexane (in smog chamber and flow tube experiments) or CO (in flow tube
204 experiments) added as OH scavenger. CO was preferred because it is an effective scavenger
205 of OH^{34,35} without causing interference in the product study. After data evaluation for
206 experiments with and without OH scavenger, no significant difference was observed in the
207 rate coefficients given the uncertainties. It should also be noted that the reactions were
208 generally carried out in a large excess of the organic reactant, so that the possible additional
209 loss of the OC by reaction with OH would have a limited effect on the OC concentration.

210 Based on the above observations, the pseudo-first order rate coefficient, k'_{OC} , may be
211 introduced as:

$$212 \quad k'_{OC} = k_{OC} \times [OC]_0 \quad (\text{eq. II})$$

213 Eq. I becomes:

$$214 \quad -d\ln[O_3]/dt = k'_{OC} \times [O_3]_t \quad (\text{eq. III})$$

215 Integrating the rate law yields:

$$216 \quad \ln([O_3]_t/[O_3]_i) = k'_{OC} \times t \quad (\text{eq. IV})$$

217 According to the last relation, the slope of the linear fitting of $\ln([O_3]_t/[O_3]_i)$ vs. t gives the
218 pseudo-first order rate coefficient k'_{OC} whose value can be divided by the initial alkene
219 concentration to retrieve the ozonolysis rate coefficient k_{OC} through eq. II.

220 Additional experiments were performed, in the case of α -pinene, in reversed conditions, i.e. in
221 excess of O_3 and monitoring the decay rates of α -pinene. Though giving complimentary
222 results, this strategy was not pursued since the approach was more time consuming and
223 generated higher uncertainties in the α -pinene concentrations (and thus in the k' values) as
224 compared with the general case described above.

225

226 **1.4 Product study in the flow reactor**

227 Because of its higher rate coefficient and the fact that the double bond is not located on a
228 terminal carbon, which facilitates product identification with the available analytical
229 techniques, tM2P was chosen to validate the flow reactor from a mechanistic point of view.

230 The alkene ($[tM2P]_0 = (3.9-4.3) \times 10^{12}$ molecule cm^{-3}) and ozone ($[O_3]_0 = 5.1 \times 10^{12}$ molecule
231 cm^{-3}) were introduced into the flow reactor in the presence of carbon monoxide ($[CO]_0 = 3 \times$
232 10^{16} molecule cm^{-3}) as the OH radical scavenger. A total flow of 900 mL min^{-1} was chosen in
233 order to obtain greater reaction times, required to ensure the conversion of a sufficient amount
234 of reagents at the sampling time.

235 Since the sampling rate of the ozone analyzer (1300 mL min^{-1}) is higher than the total flow
236 rate, an additional amount of dry air was added in the reactor flow during ozone level
237 measurements, and its concentration was corrected for dilution.

238 Gaseous samples were collected on-line (Thermo Desorption System, Gerstel) on adsorbent
239 tubes kept at $0 \text{ }^\circ\text{C}$, trapping the volatile organic compounds at a rate of 50 mL min^{-1} for a total
240 volume of 500 mL. Once collected the analytes are thermodesorbed and transferred towards a
241 cryogenic trapping (Cooled Injection System, CIS) capillary tube of small diameter (2 mm)
242 filled with a few mg of adsorbent (Carbopack B, $\sim 8 \text{ mg}$) to focus analytes before entering the
243 chromatographic column. The chromatographic and spectrometric analysis is further
244 performed by a GC/FID-MS (Agilent 6890N/5975B) instrument equipped with a DB-5ms.
245 (123-5563, $60 \text{ m} \times 0.32 \text{ mm}$, $1 \text{ }\mu\text{m}$) column. The separation was carried out at a 4 mL min^{-1} ,
246 22.1 psi , He carrier flow. The temperature program is starting in cryogenic conditions at 0°C
247 hold for 5 min, followed by a 3°C min^{-1} ramp until 90°C and a steep ramp of $20^\circ\text{C min}^{-1}$ up to
248 250°C (5 min hold).

249 Reproducibility and breakthrough volume tests were equally performed in absence of ozone
250 and in ozonolysis conditions for different sampling volumes. The results showed an excellent
251 correlation between the sampling volume and the quantity of analyte as measured by the FID
252 ($r^2 > 0.998$) with a slope value greater by more than one order of magnitude than the value of
253 the intercept, suggesting the absence of breakthrough and adsorbent rinsing effects.

254

255 1.5 Reagents

256 Chemicals were all commercially available and used as received without further purification.
257 α -pinene ($> 98\%$), 4-methyl-1-pentene (4M1P, 98%) 2,2-dimethyl-propanal (96%), acetone
258 ($> 99.8\%$) and cyclohexane (99.5%) were purchased from Sigma-Aldrich. 2-methyl-1-
259 propene (10 ppm in N_2) was purchased from Messer-Griesheim. 2,4,4-trimethyl-2-pentene

260 (tM2P, > 98%), 2,4,4-trimethyl-1-pentene (tM1P, 99%), 2-methyl-2-pentene (2M2P, > 99%)
261 were from Janssen Chimica.

262 Purified air is produced by an air purifier (AZ 2020, Claind) and is characterized by a relative
263 humidity of less than 5% and an organic carbon content of max. 0.1 ppb_v.

264

265 2. Results and discussion

266 2.1 Pentenes: ozonolysis rate coefficients

267 The alkene compounds investigated in the present study were chosen in order to fill a wide
268 range of rate coefficient values as a certification of the versatility of the flow reactor. In
269 addition, literature data were available for these alkenes (at least one study). Experimental
270 conditions and results for both reactors are presented in Table 1. Plots of $\ln([O_3]_t/[O_3]_0)$ vs.
271 time obtained with the flow reactor are displayed in Figure 3 for each of the four pentenes
272 investigated at different initial concentrations. The uncertainties (1σ) quoted in the graphs of
273 Figure 3 represent the sum of the variation coefficients ($V \equiv s_x/\bar{x}$, where s_x is the standard
274 deviation of a set of samples x_i and \bar{x} its mean) of the recorded series of values for $[O_3]_0$ and
275 $[O_3]_t$ as derived from the equation:

$$276 \quad \sigma \left\{ \ln \left(\frac{[O_3]_0}{[O_3]_t} \right) \right\} = \sqrt{\left(\frac{\sigma[O_3]_0}{[O_3]_0} \right)^2 + \left(\frac{\sigma[O_3]_t}{[O_3]_t} \right)^2 + 2 \times \frac{\sigma[O_3]_0}{[O_3]_0} \times \frac{\sigma[O_3]_t}{[O_3]_t}} \quad (\text{eq. V})$$

277 Non-weighted linear least-squares fits of the data yielded high correlation coefficients and
278 near-zero intercepts and the slopes led to the pseudo-first-order rate coefficients k'_{OC} where
279 quoted uncertainties correspond to the 1σ precision of the fit.

280 Plotting k'_{OC} vs. $[OC]_0$ for the flow reactor (open marks) and the Teflon chamber (full marks)
281 data (Figure 4) gives the ozonolysis rate coefficients, k_{OC} , for all the target compounds,

282 according to eq. II. The uncertainties in Figure 4 represent one standard deviation (1σ) for
283 both axes where the errors on concentrations correspond to 1σ (repeatability) for flow reactor
284 data, and was calculated using the following equation for smog chamber data:

$$285 \quad \sigma_{OC} = \sqrt{\left(\frac{\rho_{OC}}{M_{OC}} N_A\right)^2 \left(\frac{\sigma_{V_i}^2}{V_{total}^2} + \frac{V_i^2}{V_{total}^4} \sigma_{V_{total}}^2\right)} \quad (\text{eq. VI})$$

286 with ρ_{OC} and M_{OC} the density and molar mass of the compound, respectively, N_A the
287 Avogadro number, V_i the injected volume of the compound and V_{total} the total volume of the
288 smog chamber, σ_{V_i} the precision of the microsyringe and $\sigma_{V_{total}}$ obtained by propagating
289 uncertainties considering flows and times for filling up the Teflon bag.

290 Fitting was made taking into account the weighting of the standard deviation on k'_{OC} values.
291 Table 1 shows the k_{OC} values obtained together with the 95% confidence interval (also
292 represented in dashed lines in Figure 4). This error was combined with the one estimated for
293 each compound concentration given the repeatability of the measurements (2M2P: 21%;
294 4M1P: 6%; tM1P: 7%; tM2P: 8%) to give an overall uncertainty reported in Table 2 for each
295 rate coefficient.

296

297 A very good agreement between the kinetic data obtained from two very different systems
298 (flow tube and smog chamber) and for a very wide range of reaction times can be observed
299 for all compounds, as well as a good comparison with literature data.

300 2M2P appears the most reactive compound toward ozone among those investigated, which
301 can be explained by the alkyl substituents increasing the activity of the unsaturated bond
302 together with a minimal inhibiting steric effect due to the lack of massive substituents. The
303 rate coefficient derived from the flow tube and the smog chamber experiments ($k_{2M2P} = 4.50 \times$
304 $10^{-16} \text{ cm}^3 \text{ molecule}^{-1} \text{ s}^{-1}$) and the value from McGillen et al. (2008) ($k_{2M2P} = 4.06 \times 10^{-16} \text{ cm}^3$
305 $\text{molecule}^{-1} \text{ s}^{-1}$) present an excellent agreement. On the opposite, the 4M1P kinetics is the

306 slowest in the studied series ($k_{4M1P} = 8.23 \times 10^{-18} \text{ cm}^3 \text{ molecule}^{-1} \text{ s}^{-1}$), confirming previous
307 studies^{36,37}.

308 While the compounds with substituted methyl groups at the double bond (2M2P, tM2P)
309 present larger rate coefficients, the compounds with terminal double bond (4M1P, tM1P) are
310 clearly less reactive toward ozonolysis. Thus, the present data support very well the increase
311 of the reactivity of the ozone electrophilic addition at the unsaturated carbon-carbon with the
312 degree of substitution, as stated in the literature^{5,6,38,39}. Furthermore, the presence of methyl
313 groups at the vicinal carbon of the double bond reduces the ozonolysis rate coefficient as
314 observed in the comparison between 2M2P and tM2P or tM1P and 2,3,3-trimethyl-1-butene
315 (see Table 4), probably due to the contribution of steric effects³⁶. Finally, as also observed in
316 the literature, this reactivity is not strongly influenced by the size of the substituent
317 (comparison between 4M1P and tM1P).

318

319 2.2 α -Pinene: ozonolysis rate coefficient

320 The ozonolysis of α -pinene is an important source of oxidized species in the atmosphere,
321 which contribute significantly to the atmospheric formation of SOA. The O_3 reaction rate
322 coefficient has been determined by many previous studies and has been reviewed by Atkinson
323 et al. (2006)⁴⁰. The ozonolysis of α -pinene was carried out only in the flow reactor.

324 Data were analyzed using the same procedure as described previously for the methylated
325 pentenes. Graphs of $\ln([\text{O}_3]_t/[\text{O}_3]_0)$ vs. time are presented in Figure 5a for different initial
326 concentrations of α -pinene in excess. Two experiments were also performed in excess of
327 ozone ($[\text{O}_3]_0 = 1.4$ and 2.6 ppm_v). The corresponding slopes have been plotted vs. $[\alpha\text{-pinene}]_0$
328 or $[\text{O}_3]_0$ in Figure 5b. A value of $k_{\alpha\text{-pinene}} = (1.29 \pm 0.16) \times 10^{-16} \text{ cm}^3 \text{ molecule}^{-1} \text{ s}^{-1}$ has been
329 obtained for the slope of the weighted linear least-squares fit forced through zero. Figure 5b
330 also shows the IUPAC recommended value from Atkinson et al. (2006)⁴⁰. A repeatability of

331 12% for α -pinene concentrations is taken into account into the estimation of the overall
332 uncertainty reported in Table 2. Very good agreement could be observed between the results
333 obtained in excess of α -pinene and those obtained in excess of ozone. The larger error bars in
334 $k'_{\alpha\text{-pinene}}$ may be related to the high concentrations of O_3 used which limits the efficiency of
335 the KI scrubbers used upstream of the sampled cartridge, and thus the repeatability of the
336 measurements.

337

338 In the case of α -pinene, the rate coefficient obtained in the present work is in very good
339 agreement with the recommended value⁴⁰. A recent kinetic study⁴¹ involving the use of a
340 similar flow reactor also reports a $k_{\alpha\text{-pinene}}$ value at the upper limit of the IUPAC
341 recommendation ($1.1 \pm 0.1 \times 10^{-16} \text{ cm}^3 \text{ molecule}^{-1} \text{ s}^{-1}$), consistent with our study.

342

343 2.3 tM2P: product study

344 Cartridges were sampled at several reaction times in order to follow the formation of the
345 reaction products and the consumption of reagents. As expected, the two main stable
346 oxidation products were identified by comparison with NIST mass spectra as acetone and 2,2-
347 dimethyl-propanal, and their temporal distribution profiles are presented in Figure 6. A 30%
348 consumption of tM2P was observed at the maximum reaction time, and the molecular balance
349 is stoichiometricly equilibrated by the identified and quantified primary products (Table 3).
350 For all reaction times, there is a close to unity yield balance, with reported yields of ($21.4 \pm$
351 2.8%) and ($73.9 \pm 7.3\%$) for acetone and 2,2-dimethyl-propanal, respectively, for a total of
352 ($95.3 \pm 5.2\%$) of products. A previous FEP Teflon chamber study at ambient temperature and
353 atmospheric pressure⁴², reported formation yields of ($19 \pm 1\%$) and ($84 \pm 4\%$) for acetone and
354 2,2-dimethyl-propanal, respectively, in excellent agreement with our work.

355

356 The experimental results are supportive of the general Criegee mechanism for alkene
357 ozonolysis, in agreement with the literature⁴²⁻⁴⁵, which consists in the concomitant formation
358 of primary carbonyl compounds (2,2-dimethyl-propanal and acetone in the case of tM2P
359 ozonolysis), and other stable oxidized reaction products from the Criegee intermediates such
360 as hydroxy-acetone, methyl glyoxal and formaldehyde. The dual-energy-rich Criegee radicals
361 can follow collision-stabilization processes or unimolecular decomposition processes^{42,43,46} to
362 become low energy chemical entities. When the bi-radical involves a t-butyl substituent,
363 intramolecular migration of a hydrogen atom leading to the formation of a hydroperoxide is
364 not possible, thus implying the absence of hydroxy-carbonyl and α -dicarbonyl products⁶.

365 In addition to the primary reaction products, the study identified and quantified a non-
366 oxidized product, 2-methyl-1-propene, with an average contribution of $(11.9 \pm 2.4)\%$, and
367 profiles reported in Table 3 and Figure 6 for different reaction rates. A new reaction
368 mechanism is proposed involving electron rearrangement in the Criegee intermediate
369 containing the t-butyl substituent, with the formation of OH and HCO radicals and a non-
370 oxidized alkene: 2-methyl-1-propene. Its formation yields present a lowering tendency with
371 reaction time, suggesting competitive reactions of ozone with either the formed alkene or
372 tM2P and they remain invariably below the formation yields of acetone, which is the
373 molecule formed simultaneously in the suggested Criegee reaction mechanism. The two
374 expected stable products from the ozonolysis reaction of 2-methyl-1-propene are acetone and
375 formaldehyde.

376

377 2.4 Structure-activity relationship analysis

378 A structure activity relationship (SAR) analysis based on the data from the present study
379 (Table 2) and literature data (Table 4) was applied to check the consistency of the obtained

380 rate coefficients. Different approaches are presented in the literature regarding the SAR
381 analysis for alkene ozonolysis, involving quantum molecular orbital calculations⁴⁷ or
382 topological SAR method⁴⁸. The second method was chosen as it seems to present a robust
383 molecular approach for the estimation of the alkene ozonolysis kinetics, and the most accurate
384 in the prediction of the rate coefficients.

385 The topological SAR methodology used is based on the influence of the structure of the
386 molecule over the alkene reactivity in the ozonolysis process and is described in detail
387 elsewhere⁴⁸. The calculation of the ozonolysis rate coefficient is based on the estimation of
388 the inductive (I) and steric (S) effects around the unsaturated bond for each molecule and is
389 characterized by the index x calculated as:

$$390 \quad x = (yS) + I \quad (\text{eq. VII})$$

391 y is an empirical constant and is equal to -4.04. Based on the analysis of a series of $C_2 - C_{10}$
392 alkenes, McGillen et al. (2008) derived the following correlation between the logarithm of the
393 room temperature rate coefficient $\log k_{OC}$ and the SAR index x : $\log k_{OC} = (1.28 \pm 0.05)x -$
394 (18.14 ± 0.07) .

395 A series of alkenes and dialkenes ranging from C_2 to C_{14} for which room temperature
396 ozonolysis rate coefficients are available in the literature⁴⁹ were selected (Table 4). The
397 alkenes included in the analysis were chosen on the ground of similarity with the molecules
398 used for the validation of the flow reactor, presenting an internal or a terminal double bond,
399 various degrees of branching and a wide range of ozonolysis rate coefficient values, spanning
400 the range 10^{-15} to 10^{-18} $\text{cm}^3 \text{ molecule}^{-1} \text{ s}^{-1}$. Applying the correlation from McGillen et al.
401 (2008) to the selected alkenes allowed calculating predicted O_3 rate coefficients which, as
402 reported in Table 4, present a general good agreement (within a factor spanning from 0.46 to
403 2.98) to the measured rate coefficients, including those determined in the present work.

404 Within the obtained dataset of the 59 considered compounds, there are three statistical outliers
405 presented in Figure 6 (crosses) but not taken into account into the estimation of the SAR
406 correlation (open squares). It is worth to notice that all estimated rates of ozonolysis of the
407 outliers (1,6-octadiene, 3,7-dimethyl; 2-hexene, 3,4-diethyl and 2,4-hexadiene, 2,5-dimethyl)
408 are measured only once⁴⁹ and various consistency problems for these data are observed⁴⁸.
409 Besides, using the literature data listed in Table 4 and our own values of rate coefficients, a
410 new linear regression, using a larger set of data, of $\log k_{OC}$ as a function of x could be
411 obtained (Figure 6):

$$412 \quad \log k_{OC} = (1.26 \pm 0.10)x - (18.10 \pm 0.14) \quad (\text{eq. VIII})$$

413 where the errors on the slope and the intercept are calculated for a 95% confidence interval
414 and a value of $R^2 \sim 0.93$ has been obtained for the linear regression. This correlation (eq. VIII)
415 is in excellent agreement with the one quoted by McGillen et al. (2008) who took into account
416 a smaller database.

417

418 Conclusion

419 The rate coefficients of the reactions of ozonolysis of four methylated pentenes and α -pinene
420 have been determined using a new flow tube reactor and a Teflon smog chamber. The results
421 obtained have shown very good agreement with literature data, indicating that we may rely on
422 the reactor to perform further kinetic studies on new systems.

423 The present measurements confirmed the strong increase of the ozonolysis rate coefficients
424 with alkyl substitution at the double bond, probably due to the lowering of the ionization
425 potential of the olefin, while substitution with a bulky substituent (like *t*-butyl in tM2P)
426 slightly reduces the reactivity through steric effects. The topological SAR analysis performed
427 using the model of McGillen et al. (2008) provided an excellent correlation with existing data
428 and confirms the consistency of the measured kinetic data.

429 The product yields determined in the tM2P ozonolysis study carried out in the flow reactor at
430 short reaction times were in excellent agreement with the literature data and also allowed the
431 identification of a new unoxidized product (2-methyl-1-propene), probably derived from the
432 electronic rearrangement of one Criegee intermediate. This strongly confirms the flow reactor
433 suitability to carry out further similar studies and its potential to quantify reaction
434 intermediates which are difficult to identify by smog chamber reactors because of their high
435 reactivity, involving competitive formation and consumption.

436 In further studies we will use readily available state-of-the-art instrumentation to characterize
437 SOA by coupling a scanning mobility particle sizer (SMPS) to measure the number and size
438 distribution of particles formed and a High-Resolution Time-of-Flight Aerosol Mass
439 Spectrometer (HR-ToF-AMS) to determine their chemical average composition. The gas
440 phase will be monitored both by online TD/GC/FID-MS and a Proton-Transfer-Reaction
441 Time-of-Flight Mass Spectrometer (PTR-ToF-MS) to try to identify more reactive
442 intermediates.

443

444

445 **Acknowledgements**

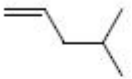
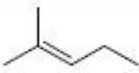
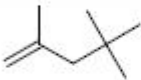
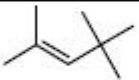
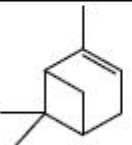
446 Our laboratory participates in the Institut de Recherche en ENvironnement Industriel (IRENI),
447 which is financed by the Communauté Urbaine de Dunkerque, the Nord-Pas de Calais
448 Regional Council, the French Ministry of Higher Education and Research, the CNRS and the
449 European Regional Development Fund (ERDF). R.I. Olariu acknowledges the EMD and the
450 IRENI for a 1-month Invited Professor Fellowship. M. Duncianu is grateful for a PhD
451 scholarship from the Nord-Pas de Calais Regional Council and Armines.

452

- 454 (1) Siese, M.; Becker, K. H.; Brockmann, K. J.; Geiger, H.; Hofzumahaus, A.; Holland, F.;
455 Mihelcic, D.; Wirtz, K. *Environ. Sci. Technol.* **2001**, *35*, 4660.
- 456 (2) Atkinson, R.; Aschmann, S. M. *Environ. Sci. Technol.* **1993**, *27*, 1357.
- 457 (3) Aschmann, S. M.; Arey, J.; Atkinson, R. *Atmospheric Environment* **2002**, *36*, 4347.
- 458 (4) Grosjean, E.; Grosjean, D. *Environ. Sci. Technol.* **1996**, *30*, 2038.
- 459 (5) Grosjean, E.; Grosjean, D. *Atmos. Environ.* **1996**, *30*, 4107.
- 460 (6) Grosjean, E.; Grosjean, D. *Atmos. Environ.* **1998**, *32*, 3393.
- 461 (7) Hearn, J. D.; Smith, G. D. *J. Phys. Chem. A* **2004**, *108*, 10019.
- 462 (8) Stenby, C.; Pöschl, U.; von Hessberg, P.; Bilde, M.; Nielsen, O. J.; Moortgat, G. K. *Atmos.*
463 *Chem. Phys. Discuss.* **2006**, *6*, 10275.
- 464 (9) Bonn, B.; Schuster, G.; Moortgat, G. K. *J. Phys. Chem. A* **2002**, *106*, 2869.
- 465 (10) Jang, M.; Lee, S.; Kamens, R. M. *Atmos. Environ.* **2003**, *37*, 2125.
- 466 (11) Czoschke, N. M.; Jang, M.; Kamens, R. M. *Atmos. Environ.* **2003**, *37*, 4287.
- 467 (12) Morris, J. W.; Davidovits, P.; Jayne, J. T.; Jimenez, J. L.; Shi, Q.; Kolb, C. E.; Worsnop, D. R.;
468 Barney, W. S.; Cass, G. *Geophys. Res. Lett.* **2002**, *29*.
- 469 (13) Ezell, M. J.; Johnson, S. N.; Yu, Y.; Perraud, V.; Bruns, E. A.; Alexander, M. L.; Zelenyuk,
470 A.; Dabdub, D.; Finlayson-Pitts, B. J. *Aerosol Sci. Technol.* **2010**, *44*, 329.
- 471 (14) Lee, S.; Kamens, R. M. *Atmos. Environ.* **2005**, *39*, 6822.
- 472 (15) Bilde, M.; Pandis, S. N. *Environ. Sci. Technol.* **2001**, *35*, 3344.
- 473 (16) Tolocka, M. P.; Heaton, K. J.; Dreyfus, M. A.; Wang, S.; Zordan, C. A.; Saul, T. D.; Johnston,
474 M. V. *Environ. Sci. Technol.* **2006**, *40*, 1843.
- 475 (17) Schauer, J. J.; Kleeman, M. J.; Cass, G. R.; Simoneit, B. R. T. *Environ. Sci. Technol.* **1999**,
476 *33*, 1578.
- 477 (18) Schauer, J. J.; Kleeman, M. J.; Cass, G. R.; Simoneit, B. R. T. *Environ. Sci. Technol.* **2001**, *35*,
478 1716.
- 479 (19) Hays, M. D.; Geron, C. D.; Linna, K. J.; Smith, N. D.; Schauer, J. J. *Environ. Sci. Technol.*
480 **2002**, *36*, 2281.
- 481 (20) Pinho, P. G.; Pio, C. A.; Carter, W. P. L.; Jenkin, M. E. *J. Atmos. Chem.* **2006**, *55*, 55.
- 482 (21) Kroll, J. H.; Seinfeld, J. H. *Environ. Sci. Technol.* **2005**, *39*, 4159.
- 483 (22) Kroll, J. H.; Seinfeld, J. H. *Atmos. Environ.* **2008**, *42*, 3593.
- 484 (23) Bennadji, H.; Glaude, P. A.; Coniglio, L.; Billaud, F. *Fuel* **2011**, *90*, 3237.
- 485 (24) Seeley, J. V.; Jayne, J. T.; Molina, M. J. *Int. J. Chem. Kin.* **1993**, *25*, 571.
- 486 (25) Helmig, D. *Atmos. Environ.* **1997**, *31*, 3635.
- 487 (26) Turpin, E.; Tomas, A.; Fittschen, C.; Devolder, P.; Galloo, J.-C. *Env. Sci. Technol.* **2006**, *40*,
488 5956.
- 489 (27) Malkin, T. L.; Goddard, A.; Heard, D. E.; Seakins, P. W. *Atmos. Chem. Phys.* **2010**, *10*, 1441.
- 490 (28) Kroll, J. H.; Clarke, J. S.; Donahue, N. M.; Anderson, J. G.; Demerjian, K. L. *J. Phys. Chem. A*
491 **2001**, *105*, 1554.
- 492 (29) Kroll, J. H.; Donahue, N. M.; Cee, V. J.; Demerjian, K. L.; Anderson, J. G. *J. Am. Chem. Soc.*
493 **2002**, *124*, 8518.
- 494 (30) Tuazon, E. C.; Aschmann, S. M.; Arey, J.; Atkinson, R. *Environ. Sci. Technol.* **1997**, *31*, 3004.
- 495 (31) Hasson, A. S.; Chung, M. Y.; Kuwata, K. T.; Converse, A. D.; Krohn, D.; Paulson, S. E. *J.*
496 *Phys. Chem. A* **2003**, *107*, 6176.
- 497 (32) Rickard, A. R.; Johnson, D.; McGill, C. D.; Marston, G. J. *Phys. Chem. A* **1999**, *103*, 7656.
- 498 (33) Presto, A. A.; Donahue, N. M. *J. Phys. Chem. A* **2004**, *108*, 9096.
- 499 (34) Guthrod, R.; Meyer, S.; Rahman, M. M.; Schindler, R. N. *Int. J. Chem. Kin.* **1997**, *29*, 717.
- 500 (35) Horie, O.; Moortgat, G. K. *Chem. Phys. Lett.* **1998**, *288*, 464.
- 501 (36) Grosjean, E.; Grosjean, D. *Int. J. Chem. Kin.* **1995**, *27*, 1045.
- 502 (37) Leather, K. E.; McGillen, M. R.; Percival, C. J. *Phys. Chem. Chem. Phys.* **2010**, *12*, 2935.
- 503 (38) Atkinson, R.; Carter, W. P. L. *Chem. Rev.* **1984**, *84*, 437.
- 504 (39) Grosjean, E.; Grosjean, D. *Int. J. Chem. Kin.* **1996**, *28*, 911.
- 505 (40) Atkinson, R.; Baulch, D. L.; Cox, R. A.; Crowley, J. N.; Hampson, R. F.; Haynes, R. G.;
506 Jenkin, M. E.; Rossi, M. J.; Troe, J. *Atmos. Chem. Phys.* **2006**, *6*, 3625.
- 507 (41) Bernard, F.; Fedioun, I.; Peyroux, F.; Quilgars, A.; Daële, V.; Mellouki, A. *J. Aerosol Sci.*
508 **2012**, *43*, 14.
- 509 (42) Grosjean, E.; Grosjean, D. *Environ. Sci. Technol.* **1997**, *31*, 2421.
- 510 (43) Finlayson-Pitts, B. J.; Pitts, J. N. *J. Chemistry and Physics of the Upper and Lower*
511 *Atmosphere*; Wiley, 1999.

- 512 (44) Neeb, P.; Moortgat, G. K. *J. Phys. Chem. A* **1999**, *103*, 9003.
513 (45) Seinfeld, J. H.; Pandis, S. N. *Atmospheric Chemistry and Physics: From Air Pollution to*
514 *Climate Change*; Wiley, 1998; Vol. 2nd Edition.
515 (46) Horie, O.; Moortgat, G. K. *Accounts of Chemical Research* **1998**, *31*, 387.
516 (47) King, M. D.; Canosa-Mas, C. E.; Wayne, R. P. *Phys. Chem. Chem. Phys.* **1999**, *1*, 2231.
517 (48) McGillen, M. R.; Carey, T. J.; Archibald, A. T.; Wenger, J. C.; Shallcross, D. E.; Percival, C.
518 *J. Phys. Chem. Chem. Phys.* **2008**, *10*, 1757.
519 (49) NIST. Chemical Kinetics Database on the Web. In *Standard Reference Database 17, Version*
520 *7.0 (Web Version)*, Release 1.6.0; 7.0 ed., 2011.
521 (50) Cox, R. A.; Penkett, S. A. *J. Chem. Soc., Faraday Trans. 1* **1972**, *68*, 1735.
522
523

524 Table 1. Experimental conditions and results obtained for the ozonolysis reactions in excess of alkenes at ambient temperature and pressure

Alkene		T (K)	Reactor type ^a	no. of decays	[OC] ₀ ($\times 10^{13}$ molecule cm ⁻³)	[O ₃] ₀ ($\times 10^{12}$ molecule cm ⁻³)	k' _{oc} ($\times 10^{-3}$ s ⁻¹)	k _{oc} ^d ($\times 10^{-17}$ cm ³ molecule ⁻¹ s ⁻¹)
Name (Abbreviation)	Structure							
4-methyl-1-pentene (4M1P)		297	FR	3	4.0 – 18.5	2.9 – 3.0	0.64 – 1.92	0.823 ± 0.010
			SC	7	3.6 – 10.0	1.9 – 5.0	0.35 – 0.89	
2-methyl-2-pentene (2M2P)		297	FR	5	1.1 – 13.4	1.3 – 9.2	5.0 – 50.4	45.4 ± 1.2
			SC	8	1.9 – 8.4	2.0 – 4.9	10.3 – 34.0	
2,4,4-trimethyl-1-pentene (tM1P)		297	FR	3	4.2 – 11.3	1.5 – 3.4	0.91 – 1.63	1.481 ± 0.012
			SC	7	2.7 – 6.5	2.5 – 4.4	0.34 – 0.99	
2,4,4-trimethyl-2-pentene (tM2P)		297	FR	4	2.1 – 8.8	1.4 – 3.5	3.0 – 10.8	12.50 ± 0.21
			SC	6	1.5 – 6.5	1.9 – 5.1	2.1 – 8.0	
α -pinene		298	FR	9 ^b	1.4 – 10.1	2.0 – 6.2	1.9 – 12.2	12.94 ± 0.35
				2 ^c	0.02 – 0.04	33.7 – 64.5	3.7 – 7.1	

525 ^a SC: Smog chamber; FR: Flow reactor526 ^b experiments in excess of alkene527 ^c experiments in excess of ozone

528 ^d slope of the weighted linear least-squares fit forced through zero for flow reactor and smog chamber data; the uncertainty was calculated at the 95% confidence level and
529 only represents statistical uncertainty.

530 Table 2. Summary of results and comparison with literature data

Alkene	T (K)	$k_{oc} \times 10^{17}$ ($\text{cm}^3 \text{ molecule}^{-1} \text{ s}^{-1}$)	Experimental setup ^a	Reference
4M1P	296	1.06	SC; O ₃ excess, GC/FID	Cox and Penkett (1972) ³⁰
	287	0.73 ± 0.14	SC; VOC excess; OA	Grosjean and Grosjean (1995) ³⁶
	292	0.79 ± 0.03	SC; VOC excess; OA	Leather et al. (2010) ³⁷
	297	0.92 ^b	-	Leather et al. (2010) ³⁷
	297	0.823 ± 0.050 ^c	FR and SC; VOC excess; OA	this work
2M2P	295	40.6 ± 4.9	SC; VOC excess; OA	McGillen et al. (2008) ⁴⁸
	297	45.4 ± 9.6 ^c	FR and SC; VOC excess; OA	this work
tM1P	290	0.97 ± 0.22	SC; VOC excess; OA	Leather et al. (2010) ³⁷
	297	1.47 ^b	-	Leather et al. (2010) ³⁷
	297	1.48 ± 0.11 ^c	FR and SC; VOC excess; OA	this work
tM2P	297	13.9 ± 3.4	SC; VOC excess; OA	Grosjean and Grosjean (1996) ³⁹
	297	12.5 ± 1.0 ^c	FR and SC; VOC excess; OA	this work
α -pinene	298	9.0	IUPAC data	Atkinson et al. (2006) ⁴⁰
	298	12.9 ± 1.6 ^c	FR; VOC excess; OA	this work

531 ^a SC: Smog chamber; FR: Flow reactor; OA: Ozone analyzer; GC/FID: Gas chromatography/Flame Ionization
532 Detection.

533 ^b values calculated using the proposed Arrhenius equations at 297 K

534 ^c overall uncertainty taking into account the 95% confidence interval on the slope of the weighted linear least-
535 squares fit and the uncertainty on the concentration of the compound in excess using the propagation of
536 uncertainty approach

537 Table 3. tM2P ozonolysis reaction: alkene consumption and product formation yields for different reaction times

Reaction time (s)	$\Delta[tM2P]$ (10^{11} molecule cm^{-3})	Acetone yield (%)	2,2-dimethyl-propanal yield (%)	Σ products (%)	2-methyl-1-propene yield (%)
152	5.28	23.6	67.1	90.7	14.1
204	6.37	25.1	66.8	91.9	14.5
309	8.49	19.8	75.3	95.1	11.8
414	10.6	18.9	75.9	94.8	9.7
518	11.7	19.4	84.5	103.9	9.2
Average yield (%)		21.4 \pm 2.8	73.9 \pm 7.3	95.3 \pm 5.2	11.9 \pm 2.4
Grosjean and Grosjean (1997) ⁴²		19 \pm 1	84 \pm 4	103 \pm 4	-

538

539 Table 4. Ozonolysis rate coefficients predicted by the topological SAR algorithm⁴⁸ taking into
 540 account inductive (I) and steric (S) effects in the estimation of the SAR index (x) and
 541 available in the literature⁴⁹ by averaging values at 297 ± 3 K, unless stated otherwise.

Alkene	$k_{\text{literature}}$	$k_{\text{predicted}}$	I	S	x
	($\times 10^{-18} \text{ cm}^3 \text{ molecule}^{-1} \text{ s}^{-1}$)	($\times 10^{-18} \text{ cm}^3 \text{ molecule}^{-1} \text{ s}^{-1}$)			
Ethene	1.65	0.72	0	0.000	0.000
Propene	10.7	13.8	1	0.000	1.000
Propene, 2-methyl	12.5	25.5	2	0.196	1.208
1-Butene	10.4	9.34	1	0.033	0.867
1-Butene, 2-methyl	13.9	17.3	2	0.229	1.076
1-Butene, 3-methyl	9.51	6.32	1	0.066	0.735
1-Butene, 2,3-dimethyl	10.0 ^b	11.7	2	0.262	0.943
1-Butene, 3,3-dimethyl	3.90 ^b	4.27	1	0.098	0.602
1-Butene, 2,3,3-trimethyl	7.75	7.90	2	0.294	0.811
1-Butene, 2-ethyl	10.9	11.7	2	0.262	0.943
1-Butene, 3-methyl-2-(1-methylethyl)	3.02	5.34	2	0.327	0.678
2-Butene, (Z)-	140	263	2	0.000	2.000
2-Butene, (E)-	223	263	2	0.000	2.000
2-Butene, 2-methyl	486	486	3	0.196	2.208
2-Butene, 2,3-dimethyl	1200	899	4	0.392	2.417
1-Pentene	9.57	7.37	1	0.053	0.787
1-Pentene, 2-methyl	13.1	13.6	2	0.249	0.996
1-Pentene, 3-methyl	3.80 ^b	4.99	1	0.086	0.655
1-Pentene, 4-methyl	8.70 ^a	5.82	1	0.073	0.707
1-Pentene, 2,3-dimethyl	5.12	9.22	2	0.281	0.863
1-Pentene, 2,4,4-trimethyl	14.8 ^a	8.49	2	0.288	0.835
2-Pentene, (Z)-	168	178	2	0.033	1.867
2-Pentene, (E)-	237	178	2	0.033	1.867

2-Pentene, 2-methyl	430 ^a	329	3	0.229	2.076
2-Pentene, 3-methyl, (Z)-	465	329	3	0.229	2.076
2-Pentene, 3-methyl, (E)-	563	329	3	0.229	2.076
2-Pentene, 2,4,4-trimethyl	132 ^a	151	3	0.294	1.811
1-Hexene	10.9	7.37	1	0.053	0.787
2-Hexene, (Z)-	104	140	2	0.053	1.787
2-Hexene, (E)-	182	140	2	0.053	1.787
2-Hexene, 3,4-diethyl, (Z)-	3.99	93.8	3	0.334	1.650
3-Hexene, (Z)-	144	120	2	0.066	1.735
3-Hexene, (E)-	157	120	2	0.066	1.735
3-Hexene, 2,5-dimethyl, (E)-	38.4	55.1	2	0.131	1.470
3-Hexene, 2,2-dimethyl, (E)-	40.4	55.1	2	0.131	1.470
1-Heptene	11.4	7.37	1	0.053	0.787
1-Octene	12.5 ^b	7.37	1	0.053	0.787
4-Octene, (Z)-	89.8	75.0	2	0.105	1.574
4-Octene, (E)-	131 ^c	75.0	2	0.105	1.574
1-Decene	8.00 ^b	7.37	1	0.053	0.787
5-Decene, (Z)-	114	75.0	2	0.105	1.574
1-Tetradecene	22.0	7.37	1	0.053	0.787
1,3-Butadiene	6.57	13.8	2	0.000	1.000
Isoprene	12.6	18.8	3	0.196	1.104
1,3-Butadiene, 2,3-dimethyl	25.6	25.5	4	0.392	1.208
1,3-Pentadiene, (Z)-	27.8	60.3	3	0.000	1.500
1,3-Pentadiene, (E)-	43.2	60.3	3	0.000	1.500
1,3-Pentadiene, 2-methyl	80.0	81.9	4	0.196	1.604
2,4-Hexadiene, (Z,E)-	314	263	4	0.000	2.000
2,4-Hexadiene, (E,E)-	374	263	4	0.000	2.000
1,4-Pentadiene	14.5	13.8	2	0.000	1.000
1,4-Pentadiene, 2-methyl	13.2	18.8	3	0.196	1.104
1,5-Hexadiene, 2-methyl	20.7	10.0	3	0.301	0.891

1,5-Hexadiene, 2,5-dimethyl	14.2	25.5	4	0.392	1.208
2,4-Hexadiene, 2,5-dimethyl	3060	486	6	0.392	2.208
1,3-Hexadiene, 5-methyl	23.9	40.8	3	0.066	1.367
1,3-Hexadiene, 5,5-dimethyl	25.3	33.5	3	0.098	1.301
1,6-Octadiene, 3,7-dimethyl	691	36.0	4	0.334	1.325
α -pinene	90.0	46.1	3	0.394	1.409

542 ^a averaged value between the literature data and the current study

543 ^b values at 288 K

544 ^c values at 290 K

Figure captions

- Figure 1 Schematic of the experimental setup and instrumentation (MFC: mass flow controller).
- Figure 2 (a) Concentration profiles of ozone used as a tracer analyte to characterize the reactor flow for three reactor heights. (b) Correction factor between the calculated average residence time ($t_{R,calc}$) and the measured residence time ($t_{R,meas}$) for several heights of the reactor (h_R) and several characteristic bulk flows in the reactor in laminar flow conditions. The broad line is the exponential regression fit of all the data while the dotted lines represent the 95% confidence interval.
- Figure 3 Plots of ozone consumption vs. time for (a) 4M1P, (b) 2M2P, (c) tM1P and (d) tM2P in the flow reactor experiments.
- Figure 4 Plots of the pseudo-first order rate coefficient k'_{OC} vs. alkene concentration for (a) 4M1P, (b) 2M2P, (c) tM1P and (d) tM2P. Open squares: flow reactor experiments; filled circles: smog chamber experiments. Straight lines are linear regression fits of all the data and curved lines are the 95% confidence intervals.
- Figure 5 Kinetics of α -pinene ozonolysis. (a) Plots of ozone consumption vs. time (excess of α -pinene) (b) Plot of the pseudo-first order rate coefficient k'_{OC} vs. alkene concentration (excess of α -pinene, open circles) or vs. ozone concentration (excess of ozone, filled circles) and comparison with the IUPAC recommendation⁴⁰ (dotted line). The straight line is the linear regression fit and the gray area represents the 95% confidence interval. The broken lines represent the uncertainty limits given by the IUPAC (*i.e.* 5.7 and

$14.3 \times 10^{-17} \text{ cm}^3 \text{ molecule}^{-1} \text{ s}^{-1}$)

Figure 6 Time profiles of the tM2P ozonolysis products in the gas phase in presence of an OH scavenger. Lines in the figure are drawn to guide the eye and do not represent a model fit.

Figure 7 Ozonolysis rate coefficient (log scale) as a function of the SAR index x for the selected alkenes in Table 4 and the corresponding 95% confidence interval (dotted line). Filled circles: this work; open squares: literature data; crosses: outliers of literature data.

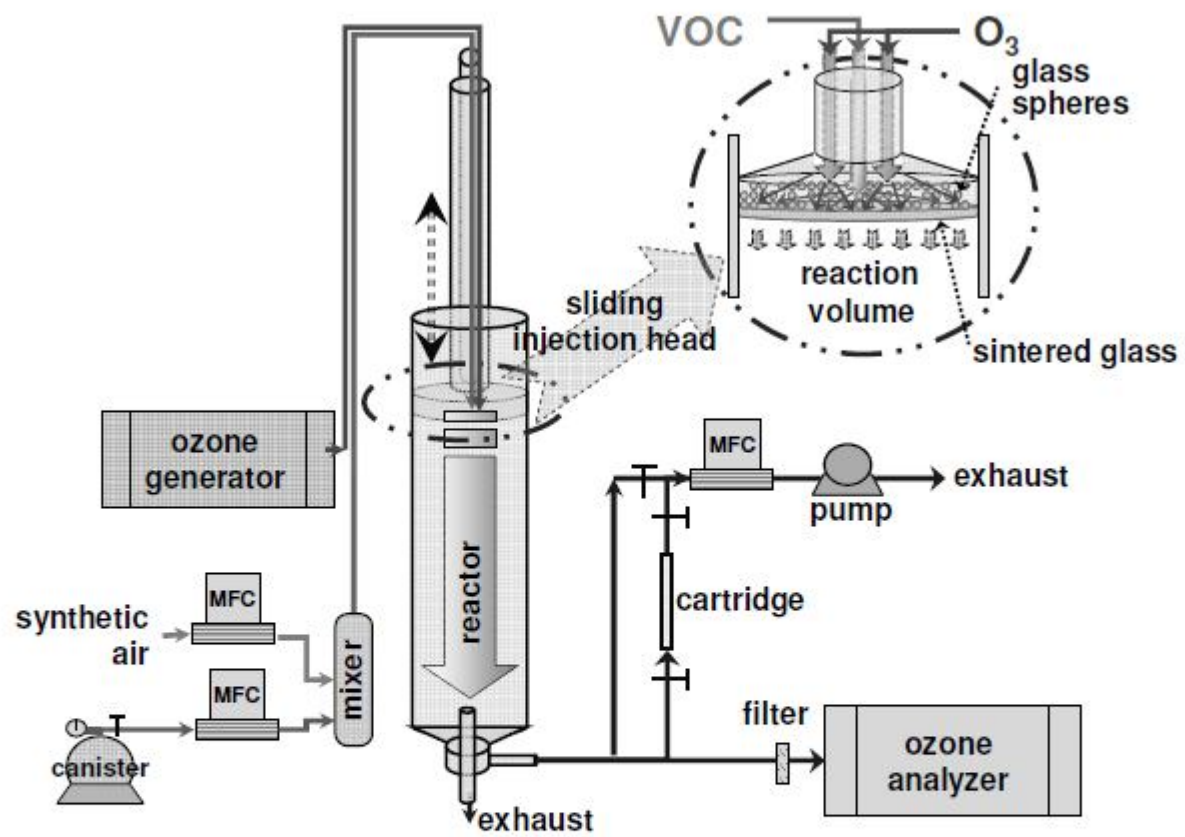


Figure 1

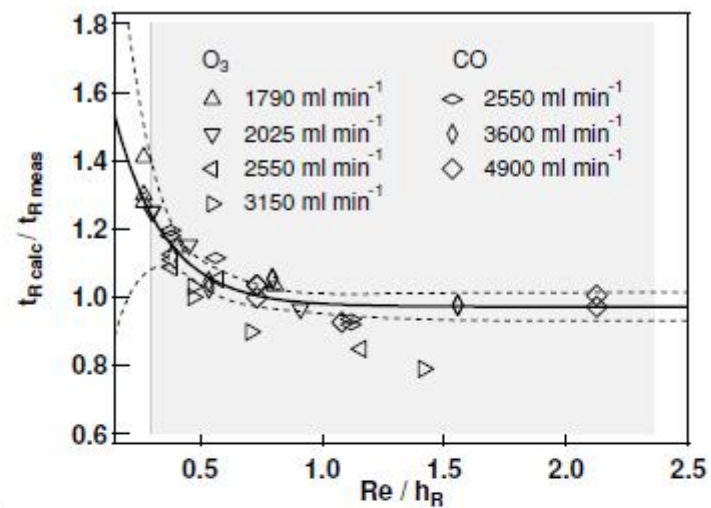
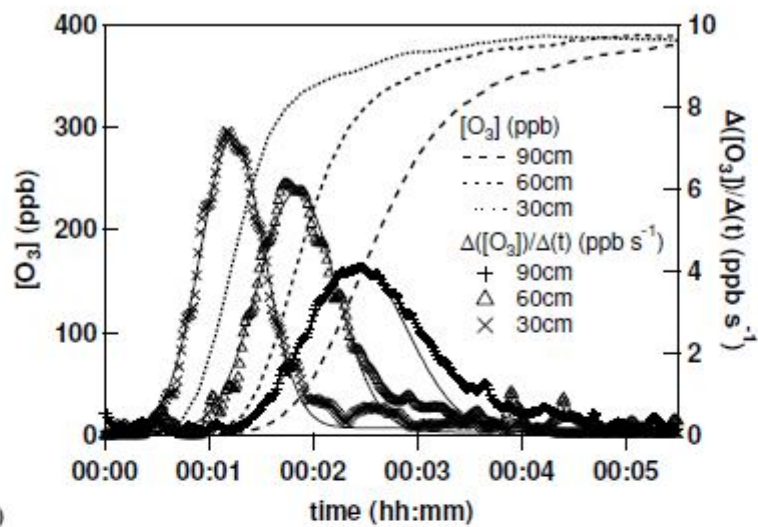
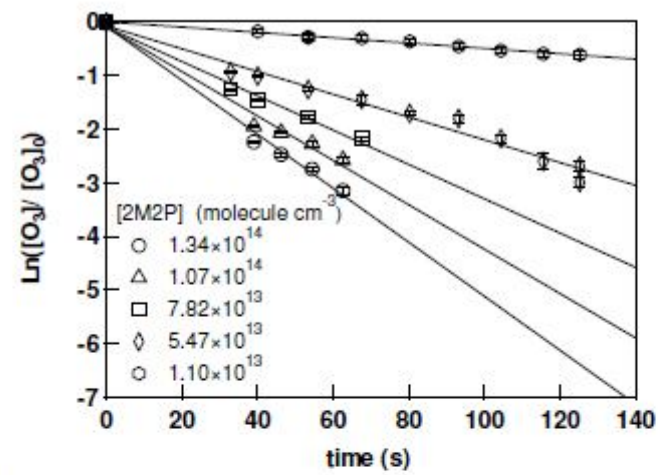
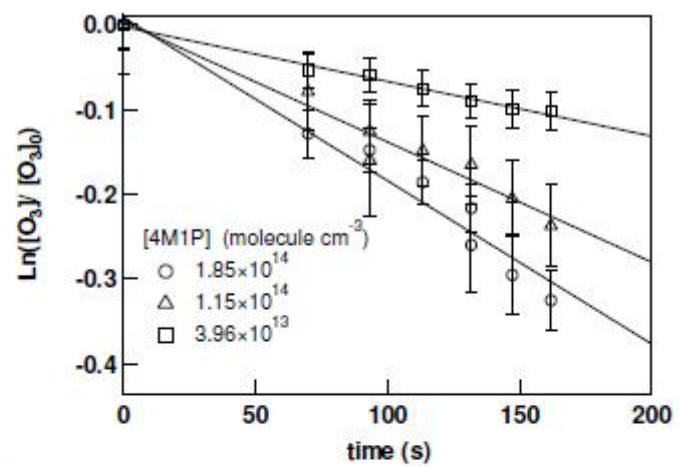
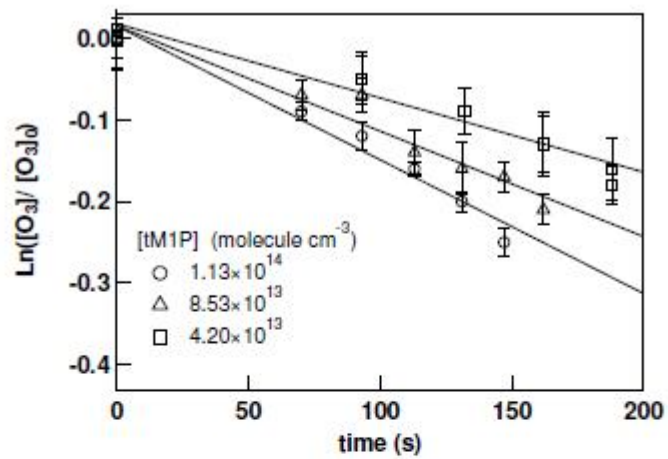
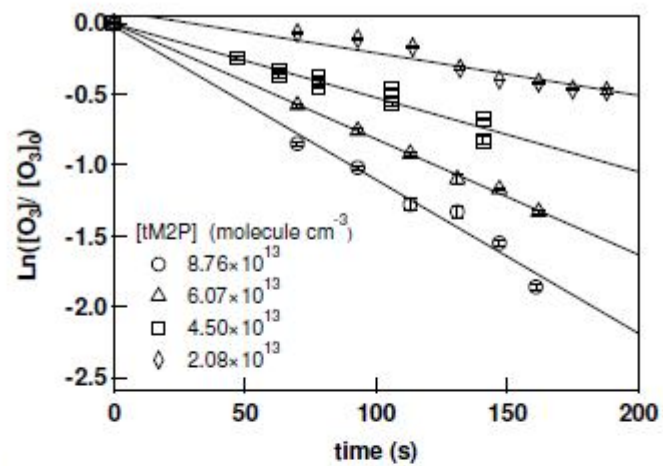


Figure 2



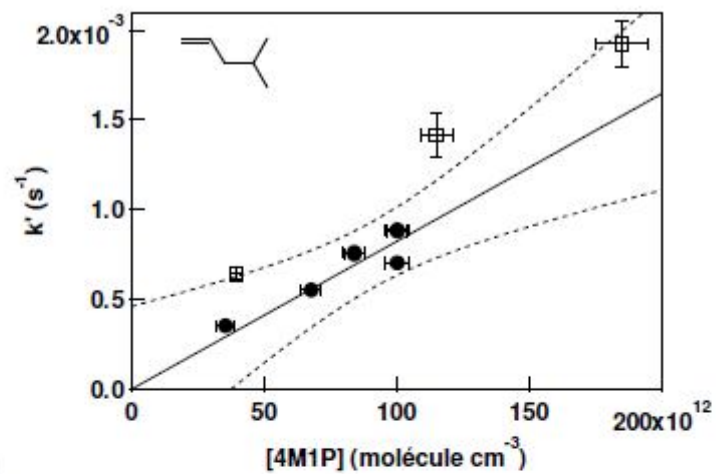


(c)

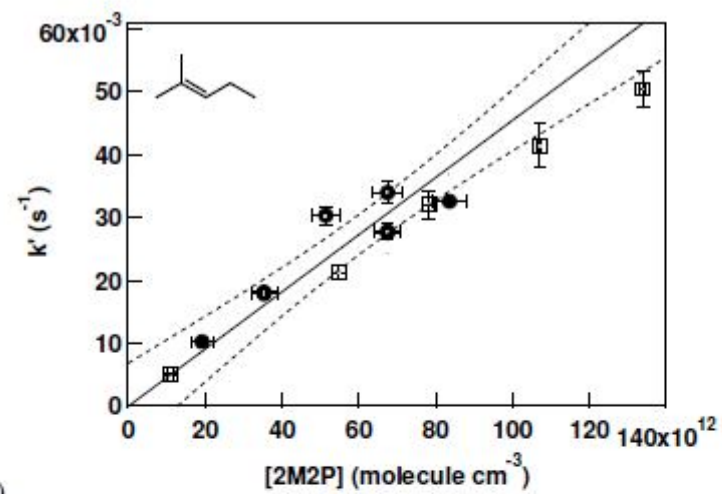


(d)

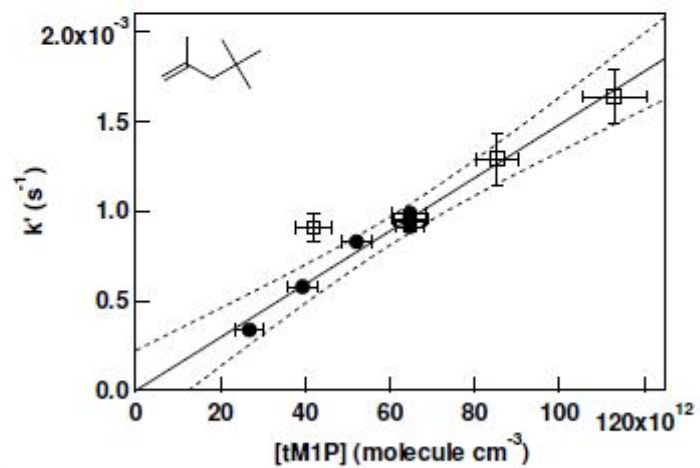
Figure 3



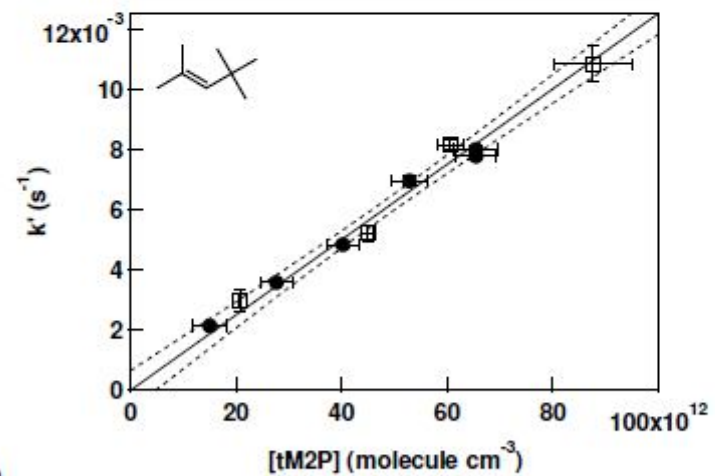
(a)



(b)



(c)



(d)

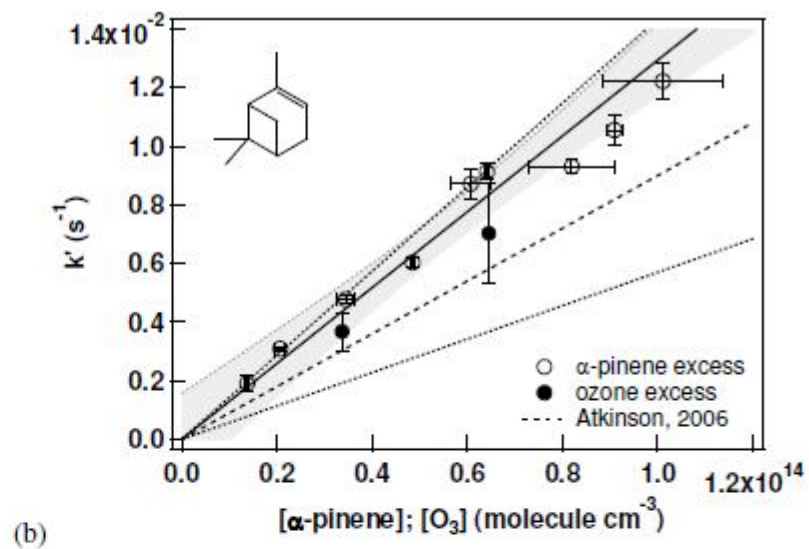
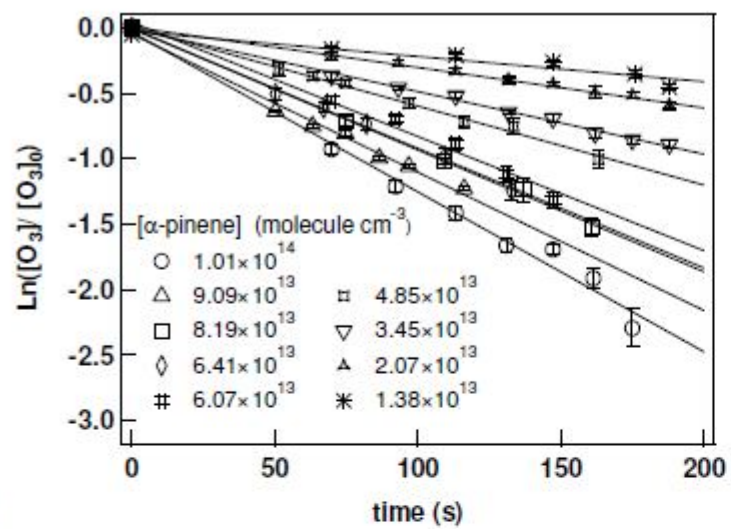


Figure 5

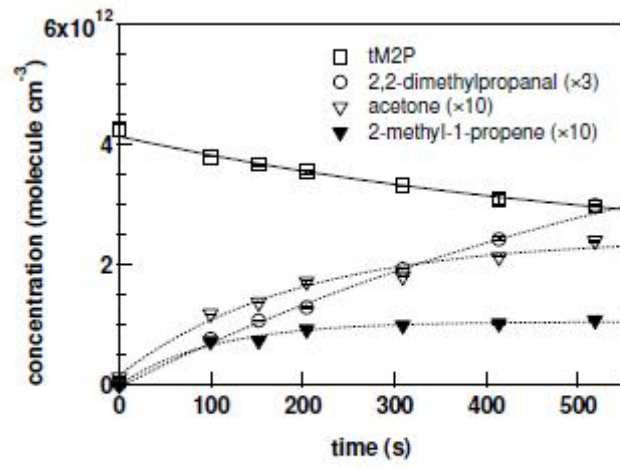
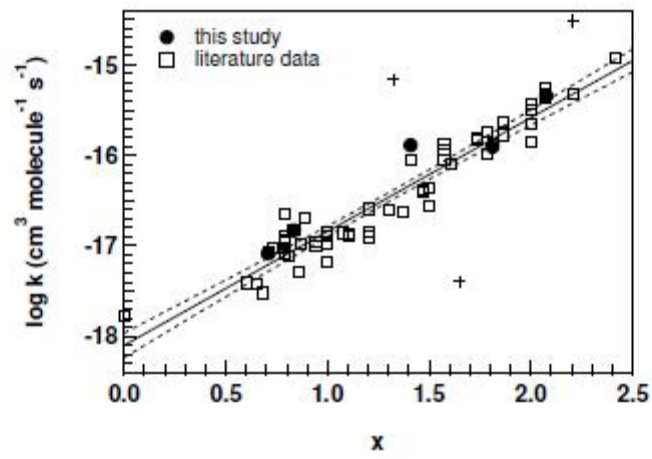


Figure 6



Figure

7

Chapitre III. Cinétiques et mécanismes d'oxydation de composés organiques volatils oxygénés

III.1 Rôle et importance des composés organiques volatils oxygénés dans la chimie atmosphérique

III.1.1 Les sources des composés organiques volatils oxygénés

Les composés organiques volatils oxygénés (COVO) constituent une classe très importante des espèces traces de la troposphère. Dans les dix dernières années, plusieurs campagnes de mesures d'envergure ont montré le rôle majeur joué par les COVO dans les cycles impliquant les NO_x (NO et NO_2), les HO_x^\bullet (OH^\bullet et HO_2^\bullet) et l'ozone. Lors de campagnes de mesure aéroportées dans le Pacifique sud, Singh et coll. ont relevé des concentrations de COVO de deux à cinq fois plus grandes que celles des composés hydrocarbonés (109, 110) et ont calculé une réactivité totale des COVO avec le radical OH^\bullet excédant largement celle des hydrocarbonés (110).

Les sources d'émission de ces COVO sont très diverses et encore mal connues (110). Les sources primaires sont représentées typiquement par (111) :

- des émissions biogéniques, dont les principales sources sont la biosphère terrestre (112), les océans et les feux de biomasse (113, 114) ;
- des sources anthropiques, plus diversifiées : le transport routier (115-117), la production et l'usage de solvants, l'agriculture et les installations de traitement des déchets (118).

Ces sources ne sont toutefois pas encore bien caractérisées, qualitativement et quantitativement, notamment à cause des difficultés analytiques inhérentes au prélèvement et à l'analyse de ces composés oxygénés. Le développement de nouvelles techniques comme la chromatographie 2-D devrait permettre d'améliorer notre connaissance de cette classe de COV très diversifiée (119).

Les émissions secondaires, provenant de l'oxydation atmosphérique des composés hydrocarbonés – alcanes, alcènes, ... – par des espèces comme le radical OH^\bullet et l'ozone, constituent une source essentielle dans le cas de certains COVO. Dans le cas des composés carbonylés et hydroxylés et des acides organiques, la source secondaire peut même largement dépasser la source primaire (120). En effet, la chimie de l'atmosphère est une chimie oxydante : toutes les espèces organiques qui y sont introduites (souvent hydrocarbonées ou partiellement oxydées) vont subir une oxydation plus ou moins importante, en fonction du temps qu'elles vont y passer, et former des composés porteurs d'une fonction carbonylée (121, 122). Le méthane, par exemple, va s'oxyder *in fine* en dioxyde de carbone et eau qui sont les formes moléculaires les plus oxydées du carbone et de l'hydrogène dans l'atmosphère, en passant par le formaldéhyde et le monoxyde de carbone. Dans le cas de molécules hydrocarbonées de poids moléculaire plus important, le nombre d'intermédiaires oxygénés peut augmenter considérablement : pour le

propane, en présence de quelques dizaines de ppt de NO, pas moins de 5 composés organiques oxygénés distincts interviennent dans son mécanisme de dégradation initié par le radical OH (80). Or, comme représenté sur la **Figure III.1**, les produits de dégradation possèdent très souvent un ou plusieurs groupes fonctionnels du type $-C=O$ (carbonyl), $-COOH$ (carboxy) et $-OH$ (hydroxy) suite à la dégradation des radicaux peroxyles RO_2 et alkoxyles RO (80, 123, 124). En lien avec cette source secondaire, plusieurs études ont récemment suggéré que l'oxydation de la matière organique particulière pourrait représenter une nouvelle source atmosphérique de COVO via leur volatilisation (125, 126).

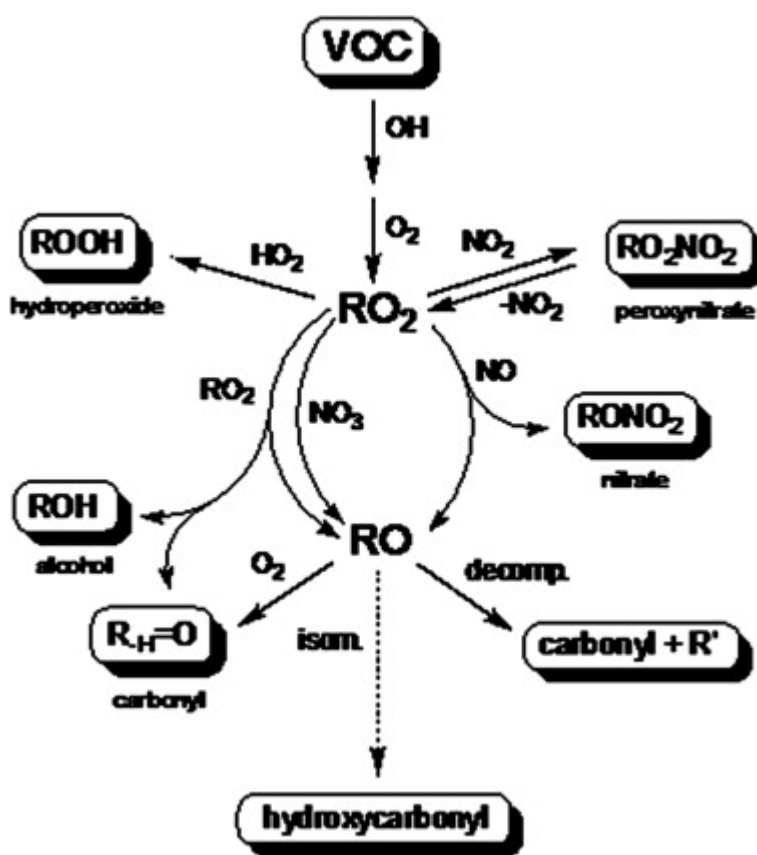


Figure III.1 : Schéma simplifié de l'oxydation atmosphérique d'un COV présentant la formation de divers produits de réaction oxygénés (127)

Les COVO sont aussi présents dans l'air intérieur, issus de sources primaires ou secondaires. La réactivité des COV en air intérieur est surtout due à la présence d'ozone, dont on a pu relever des concentrations jusqu'à quelques dizaines de ppb (128). Cet ozone peut réagir avec des composés insaturés émis par les matériaux, les plantes, les activités ménagères ... et avec des composés

adsorbés sur les surfaces et on a pu observer notamment la formation de nombreux composés carbonylés (128, 129).

III.1.2 Impacts des composés organiques volatils carbonylés et hydroxylés

Les hydrocarbures oxygénés sont des composés clés dans la compréhension des processus atmosphériques. Leurs impacts sur l'environnement revêtent plusieurs aspects :

- Plusieurs équipes de recherche (D. Derwent (130-132), J.H. Seinfeld (133) et W.P.L. Carter (134)) se sont attachées à évaluer l'impact de différents composés organiques sur la formation de **l'ozone** troposphérique. Les différentes méthodes de calcul utilisées montrent de façon cohérente que les composés oxygénés, et notamment les carbonylés et hydroxylés, possèdent des valeurs de potentiels de formation d'ozone parmi les plus élevées (133) et jouent un rôle majeur dans le cycle de l'ozone (135).
- Les composés oxygénés porteurs d'une fonction carbonyle présentent souvent une réactivité accrue, ce qui diminue les distances parcourues par ces composés depuis leur point d'émission et influence la pollution locale (136). La contribution des COVO dans la production diurne de radicaux dans l'atmosphère de Mexico représente 33%, loin devant la photolyse de HCHO et O₃ pris ensemble (20%) (137).
- Les composés oxygénés porteurs d'une fonction hydroxylée ou acide sont souvent plus solubles dans l'eau ; leur disparition dans les hydrométéores devra être prise en compte pour apprécier leur impact global. Ainsi, *Monod et al.* ont montré que les gouttes d'eau pouvaient être de très bons réacteurs pour l'oxydation des COVO (138).
- Ils peuvent transporter de **l'azote** réactif ; *Singh et al.* ont mesuré des concentrations très élevées d'acétone et de méthanol au-dessus de l'océan Pacifique et ont calculé un impact significatif de l'acétone (jusqu'à 50% de contribution) dans la séquestration des NO_x (139). Une production importante de PAN a été clairement associée à la présence de fortes concentrations de méthyl glyoxal et d'hydroxyacétone (140).
- Plusieurs d'entre eux, notamment les carbonylés, sont sensibles à la lumière et peuvent former des **radicaux peroxy** par photolyse (141), jusqu'à devenir le processus majoritaire dans certains cas (106, 142).
- Ils constituent une composante essentielle – jusqu'à 95% (143) – de **l'aérosol organique**, en particulier les acides organiques et les composés dicarbonylés (144, 145). La partie oxygénée de l'aérosol organique est souvent fortement corrélée à l'aérosol organique secondaire (122, 143, 146) et sa proportion augmente lors du transport des masses d'air (147).

- Ils peuvent avoir un impact sur la **santé**, soit directement (toxicité propre) soit indirectement (formation de composés secondaires plus toxiques ou de particules par exemple). Les composés carbonylés sont ainsi suspectés d'induire ou d'exacerber les problèmes d'asthmes (148).

Il apparait clairement que des études de la photochimie des COVO sont nécessaires afin de prévoir d'une façon plus fiable leur rôle dans la chimie troposphérique (111). Nous avons commencé par l'étude mécanistique de deux COVO majeurs, l'acétone et l'acide acétique. Puis, plus récemment, nous avons focalisé notre attention sur les composés multi-oxygénés carbonylés et hydroxylés, qui jouent un rôle spécifique dans la chimie atmosphérique.

III.2 La réaction acétone + OH•

III.2.1 Sources atmosphériques de l'acétone

L'acétone est un COV oxygéné qui a été détecté et mesuré partout dans la troposphère, près du sol comme vers la tropopause, et à des niveaux de concentration proches du ppbv (149, 150). Ses émissions totales sont estimées à environ 95 Tg/an, ce qui fait de l'acétone l'un des COV oxygénés les plus répandus dans l'atmosphère. Ses principales sources sont les émissions directes à partir de la végétation (92, 151, 152) et des océans (153) et la production photochimique secondaire comme par exemple la conversion d'isoalcanes par le radical OH• (154) ou l'oxydation du méthylbuténol (155), qui est estimée représenter au niveau global environ 30% de la source totale (149). L'importance relative de ces différentes sources varie en fonction du type d'environnement considéré. Par exemple, lors d'une campagne de mesures dans la Sierra Nevada (USA), *Goldstein et Schade* (2000) ont montré que plus de 40 % de l'acétone mesuré provenait de la source secondaire (156). Il existe d'autres sources globalement de moindre importance, mais qui peuvent être localement significatives, comme l'oxydation des monoterpènes (157-159) et la combustion du biodiesel (117).

III.2.2 Réactivité de l'acétone dans l'atmosphère

Il existe trois voies de dégradation de l'acétone dans l'atmosphère : la réaction avec le radical OH•, la photolyse par le rayonnement solaire et le phénomène de dépôt sec et humide. *Hermans et al.* ont récemment suggéré l'occurrence d'une quatrième voie par réaction équilibrée entre l'acétone et le radical HO₂• conduisant à l'acide acétique (160). Cette réaction jouerait un rôle important pour des températures de l'atmosphère inférieures à 210 K, *i.e.* dans la région de la tropopause. *Reiner et al.* ont mesuré l'acétone et l'acide acétique lors de vols dans la haute troposphère et ont constaté une bonne corrélation entre ces deux composés ($r^2 = 0,46$) et une concentration maximum d'acide acétique dans cette même région (161). Cette quatrième voie nécessite toutefois d'être confirmée.

L'importance relative de ces différentes voies varie notamment en fonction de la température, de la pression et du type de rayonnement, et par conséquent en fonction de l'altitude. Pour évaluer correctement le devenir de l'acétone dans l'atmosphère, il est nécessaire de renseigner en détail ces voies de disparition.

III.2.2.1 Réaction avec le radical OH[•]



La cinétique de cette réaction ne suit pas une loi d'Arrhenius (**Figure III.2**), car si la constante de vitesse diminue de façon classique avec la température dans la gamme 240 – 400 K, elle se stabilise en dessous de 240 K (- 33 °C).

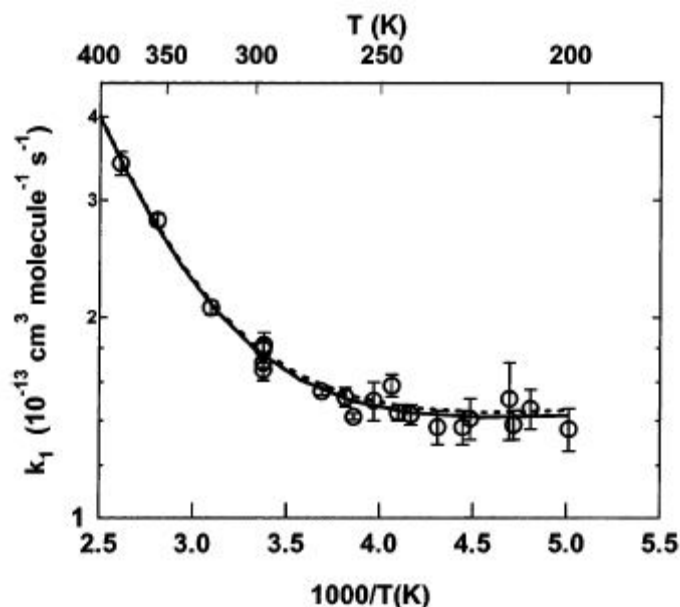


Figure III.2 : Variation de la constante de vitesse k_1 avec la température (162). On observe une stabilisation de k en dessous de 240 K.

Ce comportement a été modélisé par l'expression suivante de la constante de vitesse (97) :

$$k_1 = 1,33 \times 10^{-13} + 3,82 \times 10^{-11} \exp(-2000/T)$$

ce qui donne, à 298 K, une valeur de $1,79 \times 10^{-13} \text{ cm}^3 \cdot \text{molécule}^{-1} \cdot \text{s}^{-1}$.

La découverte de cette stabilisation de la constante de vitesse à des températures rencontrées dans la haute troposphère et la basse stratosphère (UTLS pour Upper Troposphere Lower Stratosphere) revêt une importance considérable, car elle renforce le rôle de la réaction acétone + OH[•] dans cette région de l'atmosphère par rapport au processus de photolyse. Or, ces deux voies ne conduisent pas

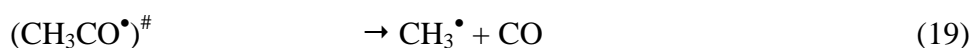
aux mêmes produits de réaction, et la production de radicaux HO_x[•] (OH[•] + HO₂[•]) est plus importante pour la photolyse que pour la réaction avec OH[•] ; l'impact sur la chimie de l'atmosphère sera donc différent. Nous reviendrons sur le mécanisme et les produits de cette réaction dans le paragraphe II.2.3.

III.2.2.2 Photolyse par le rayonnement solaire

L'acétone possède une bande d'absorption dans l'UV centrée à 274 nm avec un étalement entre 200 nm et 330 nm (97). L'étude de la photolyse de l'acétone à des longueurs d'onde typiques de la troposphère et de la stratosphère a fait l'objet de nombreuses publications (160, 163-168). Il en ressort que les produits primaires de photolyse de l'acétone sont les radicaux acétyl et méthyle selon la réaction



où (CH₃CO[•])[#] représente un radical acétyl excité. En fonction de l'énergie absorbée et de la pression, le radical acétyl excité (CH₃CO[•])[#] peut soit se stabiliser par collision soit se dissocier rapidement en CH₃[•] et CO :



Dans la troposphère où λ > 300 nm, la paramétrisation de *Blitz et al.* permet de déterminer un rendement de CO d'environ 5 % à pression atmosphérique, ce qui indique que la voie de photolyse génère essentiellement les radicaux CH₃CO[•] et CH₃[•] (165).

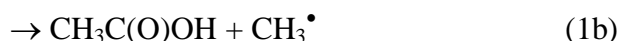
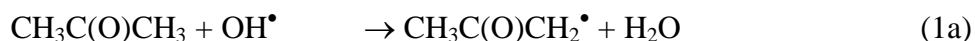
Dans la basse troposphère, la photolyse est minoritaire et représente seulement 30 % de la dégradation de l'acétone ; à l'inverse, dans la région de la haute troposphère / basse stratosphère (UTLS), les basses températures (220 – 250 K) associées à un rayonnement UV plus énergétique rendent la voie de photolyse prépondérante (> 90 %) (163). Ceci est d'un intérêt considérable, car la photolyse d'un composé organique constitue une source directe de radicaux dans l'atmosphère, impactant ainsi sur la quantité d'ozone formée. Les concentrations élevées de OH[•] et HO₂[•] mesurées dans l'UTLS ont été attribuées pour une grande partie (jusqu'à 50% de la formation de OH[•] et HO₂[•]) à la photolyse de composés carbonylés et notamment l'acétone (169, 170).

III.2.2.3 Dépôt

A l'instar de nombreux autres composés organiques, l'acétone peut interagir avec les différentes surfaces solides ou liquides présentes dans l'atmosphère : gouttes d'eau, particules solides, matériaux de construction, végétation, etc. Bien que l'acétone soit soluble dans l'eau, le coefficient de partition gaz – liquide faible (constante de Henry $H(\text{acétone}) = 32 \text{ M atm}^{-1}$ à 298 K) indique une présence en phase gazeuse largement favorisée (171). L'adsorption de l'acétone sur la glace est quant à elle complètement réversible (172). La voie de dépôt semble donc être minoritaire dans l'atmosphère. Toutefois, des mesures aéroportées lors de la campagne AMMA suggèrent que l'océan pourrait être un puits significatif pour l'acétone (173). Enfin, grâce à la mesure des coefficients de capture sur des particules minérales de type SiO_2 , TiO_2 et CaO , l'équipe de V. Grassian a montré que la perte d'acétone par adsorption sur ce type de surfaces dans la haute troposphère pourrait être comparable à celle due à la photolyse et à la réaction avec le radical OH^\bullet (174).

III.2.3 Intérêt de la réaction et présentation de l'historique des différentes études

Deux articles, parus en 2000 et 2001 (175, 176), portant sur la cinétique et le mécanisme de la réaction $\text{CH}_3\text{C}(\text{O})\text{CH}_3 + \text{OH}^\bullet$ ont suggéré la présence d'une deuxième voie de réaction conduisant à l'acide acétique, en plus de celle formant le radical acétonyle $\text{CH}_3\text{C}(\text{O})\text{CH}_2^\bullet$:



La formation d'acide acétique aurait lieu via l'addition électrophile du radical OH^\bullet sur le carbone central de la molécule d'acétone conduisant au complexe $(\text{CH}_3)_2\text{C}(\text{O}^\bullet)\text{OH}$. D'après les auteurs de ces publications, cette deuxième voie serait à l'origine du comportement non-Arrhenius de la constante de vitesse observé sur la **Figure III.2** (la réaction d'addition est favorisée à basse température). Le rapport de branchement R_1 de la voie formant l'acide acétique (voie (1b)), défini par $R_1 = k_{1b}/(k_{1a} + k_{1b})$, était estimé à 0,50 à température ambiante dans ces deux études. La présence d'une seconde voie aussi significative pour cette réaction majeure de l'atmosphère nécessitait des études complémentaires approfondies pour confirmer ou non son existence.

Plusieurs études expérimentales et théoriques ont été publiées à la suite de ces deux études. *Vandenberk et al.* ont obtenu expérimentalement un rapport de branchement maximum de 0,05

confirmé par des calculs de barrière d'énergie des voies (1a) et (1b) (177). *Tyndall et al.* confirmèrent ces résultats avec un rapport de branchement maximum de 0,10 pour la voie (1b) (178). Dans ces deux études expérimentales, il convient de mentionner que l'acide acétique n'a pas été observé, d'où les valeurs maximum indiquées pour R_1 . Dans leur étude théorique, *Masgrau et al.* ont montré que la voie d'addition – élimination (1b) est négligeable (0,02 au plus) quelle que soit la température (179). Dans le cadre de la thèse d'E. Turpin débutée en 2001 (47), nous avons parallèlement réalisé des expériences au laboratoire PC2A dans le tube à écoulement rapide avec détection du radical acétonyle $\text{CH}_3\text{C}(\text{O})\text{CH}_2^\bullet$ par fluorescence induite par laser. Un rapport de branchement pour la voie (1a) ($= 1 - R_1$) de 0,9 a été obtenu, en bon accord avec les dernières études (55). Une question restait cependant en suspens : l'acide acétique est-il effectivement formé dans la réaction $\text{CH}_3\text{C}(\text{O})\text{CH}_3 + \text{OH}^\bullet$ et si oui, dans quelle proportion ? Par ailleurs, il convient de signaler que la réaction acétone + OH^\bullet en phase aqueuse produit de l'acide acétique (180), au même titre que l'oxydation photocatalytique de l'acétone sur TiO_2 (181) et Cu (182).

III.2.4 Travaux réalisés

Les travaux de recherche menés au laboratoire ont porté sur la quantification du rapport de branchement de la voie de formation de l'acide acétique à partir dans la réaction $\text{CH}_3\text{C}(\text{O})\text{CH}_3 + \text{OH}^\bullet$ au travers d'expériences en chambre de simulation atmosphérique. Nous nous sommes attachés, en particulier, à déterminer si l'acide acétique était réellement formé, aucune des études ne l'ayant directement observé. La réaction $\text{CD}_3\text{C}(\text{O})\text{CD}_3 + \text{OH}^\bullet$ a également été étudiée, car les cinétiques des réactions d'addition-élimination, dont était supposée faire partie la réaction (1b), sont connues pour ne pas dépendre d'une substitution isotopique. Les résultats sont présentés dans la **publication n°4** (57).

III.2.5 Discussion et conclusion

A la suite de nos travaux, plusieurs études expérimentales ont été publiées, dont un récapitulatif se trouve dans le **Tableau III.1**. Toutes les études récentes montrent que la voie d'arrachement direct (1a) est majoritaire avec un rapport de branchement supérieur à 0,90. L'absence d'effet de pression sur la cinétique de la réaction confirme par ailleurs que la réaction a lieu par arrachement d'hydrogène et non par addition d' OH^\bullet sur la molécule. En effet, les réactions d'addition (et de décomposition unimoléculaire) sont sensibles à la pression, car l'excès d'énergie sur le produit de réaction est dissipé par collision. L'augmentation de la pression favorise l'élimination de cette énergie et stabilise ainsi le produit. Le fort effet isotopique primaire observé est cohérent avec la formation d'un complexe à une ou deux liaisons hydrogène, et s'explique d'une part par un effet tunnel plus important pour un atome d'hydrogène que pour un atome de deutérium (la probabilité qu'une particule expérimente un effet tunnel dépend exponentiellement de sa masse), d'autre part par la différence des énergies de point zéro dans les réactifs (183).

Le comportement non-Arrhenius de la réaction (1) est expliqué et modélisé par la formation d'un complexe pré-réactif $\text{OH}\bullet\text{CH}_3\text{C}(\text{O})\text{CH}_3$ excité (**Figure III.3**) qui est stabilisé à basse température. Cette hypothèse semble être confirmée par un récent article sur des mesures de la constante de vitesse à très basse température (~ 100 K), où les auteurs ont constaté une augmentation très importante de k_1 ($k_1(86\text{K})/k_1(295\text{K}) = 334$) qu'ils expliquent aussi par la formation d'un complexe à liaison hydrogène (184).

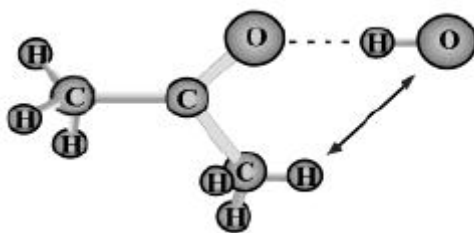


Figure III.3 : Complexe $\text{OH}\bullet\text{CH}_3\text{C}(\text{O})\text{CH}_3$ à six membres et à liaisons hydrogène (185)

Par ailleurs, *Caralp et al.* ont montré que l'effet tunnel² est important dans la réaction acétone + OH^\bullet , effet qui devient majoritaire à très basse température, ce qui explique que la

² L'effet tunnel est la possibilité, pour une molécule, de franchir une barrière d'activation de largeur finie même si l'énergie de cette molécule est plus faible que l'énergie de la barrière de potentiel.

constante de vitesse devienne quasi invariable pour des températures < 250 K (voir **Figure III.2**) (56).

En conclusion de ces travaux, il semble tout à fait clair aujourd'hui que la formation d'acide acétique dans la réaction acétone + OH^\bullet en phase gazeuse homogène n'a pas lieu. Cette conclusion a des répercussions importantes quant à l'impact de l'acétone dans l'atmosphère. En effet, les acides organiques sont connus pour être impliqués, de façon générale, dans la formation des aérosols organiques secondaires, via leur aptitude à créer des noyaux de condensation (186). Cette absence signifie donc que l'acétone ne va pas contribuer, via l'hypothétique chemin réactionnel (1b), à la charge en aérosol de l'atmosphère, notamment dans la basse atmosphère où la réaction avec OH^\bullet est dominante. Par ailleurs, l'acide acétique, à l'image de tous les acides organiques, est beaucoup plus facilement piégé dans les hydrométéores que l'acétone. L'absence de ce chemin réactionnel implique une participation plus grande de l'acétone dans le cycle atmosphérique gazeux des HO_x^\bullet (OH^\bullet et HO_2^\bullet) et un effet moindre sur l'acidification des pluies.

Tableau III.1 : Résumé des études expérimentales sur la réaction $\text{CH}_3\text{C}(\text{O})\text{CH}_3 + \text{OH}^\bullet$ et $\text{CD}_3\text{C}(\text{O})\text{CD}_3 + \text{OH}^\bullet$. Conditions expérimentales et rapport de branchement pour la voie d'arrachement d'un atome H ou D.

$\text{CH}_3\text{C}(\text{O})\text{CH}_3 + \text{OH}^\bullet$						
Référence	Type de réacteur	Source OH^\bullet	Détection^a	[acétone]₀ (molécule.cm⁻³)	Pression (Torr)	R (298 K)
<i>Wollenhaupt et Crowley (175)</i>	Photolyse laser	photolyse HONO	LIF	$(3,4 - 9,7) \times 10^{15}$	10 – 200 (Ar)	0,50
<i>Vasvari et al. (176)</i>	Réacteur à écoulement	radiolyse F ₂	LIF	$(5,8 - 9,6) \times 10^{14}$	2,25 (He)	0,50
<i>Vandenberk et al. (177)</i>	Réacteur à écoulement	radiolyse H ₂	MS	$8,3 \times 10^{15}$	2 (He)	0,95
<i>Tyndall et al. (178)</i>	Photoréacteur Pyrex ou acier inox	photolyse CH ₃ ONO	FTIR	$6,5 \times 10^{15}$	700 (air)	> 0,90
<i>Talukdar et al. (185)</i>	Réacteur à écoulement	radiolyse H ₂	CIMS	$(0,8 - 1,85) \times 10^{15}$	0,5 (He)	> 0,99
<i>Turpin et al. (55)</i>	Réacteur à écoulement	radiolyse CF ₄	LIF	$(0,05 - 5,0) \times 10^{15}$	0,92 (He)	0,8 – 1
<i>Raff et al. (187)</i>	Réacteur Quartz	photolyse O ₃	MS	$(8,0 - 25,1) \times 10^{15}$	735 – 750 (He/O ₂)	0,95 – 0,97
<i>Turpin et al. (57)</i>	Photoréacteur Téflon Photoréacteur Pyrex	photolyse CH ₃ ONO	GC-FTIR	$(3,2 - 7,9) \times 10^{15}$	760 (air)	0,86 > 0,95
$\text{CD}_3\text{C}(\text{O})\text{CD}_3 + \text{OH}^\bullet$						
<i>Raff et al. (187)</i>	réacteur Quartz	photolyse O ₃	MS	$(8,0 - 25,1) \times 10^{15}$	735 – 750 (He/O ₂)	0,813
<i>Turpin et al. (57)</i>	photoréacteur Pyrex	photolyse CH ₃ ONO	GC-FTIR	$(1,2 - 2,5) \times 10^{15}$	760 (air)	0,80

a: LIF: laser induced fluorescence; MS: mass spectrometry; CIMS: chemical ionization mass spectrometry.

Publication n°4

(parue dans la revue *Environmental Science and Technology* en 2006)

Acetone- h_6 or - d_6 + OH Reaction Products: Evidence for Heterogeneous Formation of Acetic Acid in a Simulation Chamber

ESTELLE TURPIN,[†]
ALEXANDRE TOMAS,^{*,†}
CHRISTA FITTSCHEN,[‡]
PASCAL DEVOLDER,[‡] AND
JEAN-CLAUDE GALLOO[†]

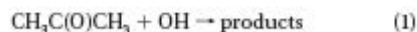
Département Chimie et Environnement, Ecole des Mines de Douai, 941 rue Charles Bourseul, B.P. 10838, F-59508 Douai, Cedex, France, and Physico-Chimie des Processus de Combustion et de l'Atmosphère (PC2A), UMR CNRS 8522, Université des Sciences et Technologies de Lille, F-59655 Villeneuve d'Ascq, Cedex, France

Simulation chamber experiments have been carried out at room temperature to investigate the products of the acetone + OH and acetone- d_6 + OH reactions using two photoreactors made of Teflon or Pyrex and coupled to GC-FTIR-FID analytical techniques. In the Pyrex chamber, the results demonstrated that the channel forming acetic acid is a minor oxidation route in the atmospheric acetone- h_6 + OH reaction (yield < 5%), whereas a higher yield of about 20% was obtained in the case of the acetone- d_6 + OH reaction, in good agreement with previous studies. Existence of a heterogeneous way of formation of acetic acid has also been identified in the Teflon photoreactor.

Introduction

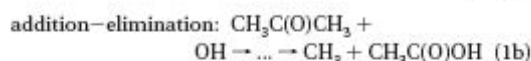
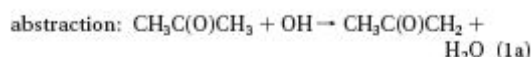
Acetone is one of the most widespread oxygenated volatile organic compounds (VOC) in the atmosphere. Primary emission sources of acetone are biogenic (e.g., from the vegetation) and anthropogenic (e.g., from solvent use), while secondary sources result from the oxidation of other VOC-like isoalkanes in the atmosphere and are estimated to represent about 30% of the total emission rate (1–3). The atmospheric oxidation of acetone is mainly due to either its photolysis by solar UV radiation in the upper troposphere/lower stratosphere (4, 5) or its oxidation by OH radicals in the lower troposphere. Recently, the reaction with HO₂ radicals has also been proposed as an efficient sink at low temperature (220 K) (6). The photooxidation of acetone is recognized to strongly participate in the formation of photooxidants like peroxy radicals or ozone in the free troposphere (7).

The rate constant of the gas-phase reaction between OH radicals and acetone



has been the subject of many studies (8–12) and is now well established with a recommended value of $k_1 = 1.7 \times 10^{-13} \text{ cm}^3 \text{ molecule}^{-1} \text{ s}^{-1}$ at 298 K (13). Identification and yield of

the reaction products have been the subject of many experimental and theoretical studies in the past 5 years. Wollenhaupt et al. (10) investigated the rate constant k_1 as a function of temperature and observed a non-Arrhenius behavior of the rate constant. They assumed that two reaction pathways exist, an abstraction pathway leading to the methylvinyl radical (MV) and an addition–elimination one leading to the acetic acid molecule and the methyl radical, the latter pathway becoming more important as the temperature decreases:



Additional experimental results seemed to confirm this hypothesis, as Wollenhaupt and Crowley (14) and Vasvari et al. (15) determined a branching ratio $R = k_{1a}/(k_{1a} + k_{1b}) \approx 0.50$ at 298 K, independent of pressure.

Further experimental studies did not confirm the occurrence of the addition channel (11, 16–20). In particular, acetic acid formation was never observed, neither in flow tube experiments (16) nor in simulation chamber experiments (17). On the contrary, a recent study (21) using a small quartz reactor coupled to a detection by mass spectrometry seems to contradict the lack of acetic acid since the latter has been clearly detected in yields of 0.09 at 298 K, decreasing to 0.05 with increasing temperature at 353 K. Thanks to numerical simulations involving chemical species in the gas phase, these authors (21) were able to quantify the contribution of secondary processes to their observed yield of acetic acid. These processes account for 50–70% in the system OH + acetone but only for 10% in the system OH + acetone- d_6 . Furthermore, they measured an increase of the acetic acid yield with decreasing temperature, in line with the usual opposite behavior of addition and abstraction reactions with temperature. Particularly noticeable is the significant value of (0.20 ± 0.04) for the yield of $\text{CD}_3\text{C}(\text{O})\text{OH}$ in the reaction $\text{OH} + \text{CD}_3\text{C}(\text{O})\text{CD}_3$ at 283 K. A compilation of all the experimental studies available on acetone- h_6 + OH and acetone- d_6 + OH reaction products is given in Table 1. However, quantum chemical computation aiming at investigating the potential energy surface of reaction 1 pointed out that the energy barrier is much larger for the addition–elimination channel than for abstraction, and thus, the abstraction pathway should be by far the major (if not unique) channel for the $\text{OH} + \text{CH}_3\text{C}(\text{O})\text{CH}_3$ reaction at room temperature and below (15, 16, 22–24).

In the first part of our work (19), we investigated the abstraction pathway (1a) using a fast flow tube by detecting the MV radical excited at 342.6 nm with laser induced fluorescence. The branching ratio R of the path (1a) was determined to be in the range $0.8 \leq R \leq 1$, in good agreement with the more recent findings. As only one study investigated the products of the $\text{OH} + \text{CH}_3\text{C}(\text{O})\text{CH}_3$ reaction in a standard simulation chamber (17) and considering the controversy about acetic acid formation, it appears interesting to further explore this reactive system for this purpose by using two different simulation chambers and detect the acetic acid possibly formed. Since our preliminary results indicated that acetic acid was indeed always present, we decided to carry on more detailed and systematic experiments to elucidate this unexpected formation. Additional experiments were also performed with acetone- d_6 . We report herein the results of

* Corresponding author phone: ++ 33 3 27 71 26 51; fax: ++ 33 3 27 71 29 14; e-mail: tomas@ensm-douai.fr.

[†] Ecole des Mines de Douai.

[‡] Université des Sciences et Technologies de Lille.

TABLE 1. Summary of the Experimental Studies on Acetone- h_2 + OH and Acetone- d_6 + OH Reactions: Experimental Conditions and Branching Ratio for the - H or - D Abstraction Channel

reference	type of reactor	OH source	detection ^a	[acetone] ₀ (molecule cm ⁻³)	pressure (Torr)	<i>R</i> (298 K)
Acetone-h_2 + OH						
14	laser photolysis	HONO photolysis	LIF	(3.4–9.7) × 10 ¹⁵	10–200 (Ar)	0.5
15	discharge flow	a	LIF	(5.8–9.6) × 10 ¹⁴	2.25 (He)	0.5
16	discharge flow	H ₂ radiolysis	MS	8.3 × 10 ¹⁵	2 (He)	0.95
17	Pyrex or stainless steel photoreactors	CH ₃ ONO photolysis	FTIR	6.5 × 10 ¹⁵	760 (air)	> 0.90
18	flow tube	H ₂ radiolysis	CIMS	(0.8–1.85) × 10 ¹⁵	0.5 (He)	> 0.99
19	discharge flow	CF ₄ radiolysis	LIF	(0.05–5.0) × 10 ¹⁵	0.92 (He)	0.8–1
21	quartz reactor	O ₃ photolysis	MS	(8.0–25.1) × 10 ¹⁵	735–750 (He/O ₂)	0.95–0.97
this work	Teflon photoreactor Pyrex photoreactor	CH ₃ ONO photolysis	GC-FTIR	(3.2–7.9) × 10 ¹⁵	760 (air)	0.86 > 0.95
Acetone-d_6 + OH						
21	quartz reactor	O ₃ photolysis	MS	(8.0–25.1) × 10 ¹⁵	735–750 (He/O ₂)	0.813
this work	Pyrex photoreactor	CH ₃ ONO photolysis	GC-FTIR	(1.2–2.5) × 10 ¹⁵	760 (air)	0.8

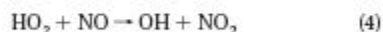
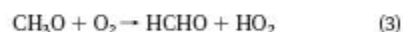
^a Not clear from the text. ^b LIF: laser induced fluorescence; MS: mass spectrometry; CIMS: chemical ionization mass spectrometry.

our experimental study focused on the acetic acid formation in the reaction of acetone with OH radical under various conditions.

Experimental Section

Environmental Chambers. Two different environmental chambers have been used: (i) a collapsible Teflon chamber (FEP 50 μ m thickness) with a volume of about 300 L and (ii) a 35 L cylindrical Pyrex chamber. Both setups operate at room temperature and atmospheric pressure. The chambers are placed inside a wooden box equipped with an irradiation system and a temperature regulation device, the latter consisting of two fans fixed at the top of the box and flushing laboratory air through it. The internal walls of the box are covered with aluminum sheets to homogenize direct and reflected light emitted by the fluorescent tubes. Six fluorescent lamps Philips TMX 200 LS emitting in the range 300–460 nm ($\lambda_{\text{max}} = 365$ nm), disposed on two parallel faces of the box, are used to irradiate the chambers.

The OH radicals were generally produced by photolysis of methyl nitrite (CH₃ONO) in the presence of NO:



Acetone was introduced in the Teflon chamber using a gently heated vacuum line. In the case of the Pyrex photoreactor, acetone was directly injected with a syringe into the chamber evacuated to a pressure of 100 mbar. Initial acetone concentrations were in the range of 130–320 ppm (298 K, 1 atm). The chamber was filled with purified air, and a few tenths cm³ of gaseous CH₃ONO and NO were finally introduced in the chamber. Initial CH₃ONO and NO concentrations were around 60 and 2 ppmv, respectively. Excess NO was added to the reaction mixture to ensure the conversion of HO₂ to OH radicals through reaction 4. The gaseous mixture was left in the dark for 1 h to achieve a good homogeneity of the reactants.

Methylnitrite was synthesized separately by slowly adding diluted H₂SO₄ to a mixture of NaNO₂ and methanol using the method described by Taylor et al. (25). Acetone, acetic acid, acetone- d_6 and acetic acid- d_3 (Acros Organics with purity higher than 99%) were used without further purification. NO (5% in N₂, Air Liquide) was used directly from the cylinder; purified air was produced by a zero air generator (Air Generator Claind 2301 HG).

Sampling and Analysis Method. Products were analyzed by gas chromatography coupled to two different inline techniques: Fourier transform infrared spectroscopy (FTIR), particularly suited for the detection of acetic acid, followed by flame ionization detection (FID), particularly suited for the detection of acetone. A 20 cm³ gas sample loop connected to a six-port Valco valve was used to sample sequences of 40 cm³ gas aliquots from the simulation chamber; preconcentration of the sample was obtained using a TCT thermodesorption device (Chrompack). This allowed a subsequent flash injection of the organic compounds into the chromatographic system (Varian 3300).

IR spectra were collected every 1.2 s with a resolution of 16 cm⁻¹ by a Nicolet 550 spectrometer and integrated by the OMNIC software between 600 and 4000 cm⁻¹. The obtained so-called Gram-Schmidt chromatograms can further be treated to construct the chromatogram resulting from the spectral integration over the 1600–1900 cm⁻¹ band presenting characteristic features of acetic acid. This method allows more precise measurements of acetic acid concentrations.

Several samplings of the reaction mixture were carried out after filling the chamber in order to determine precisely the initial acetone concentration. Then the photoreactor was irradiated up to 4 h with successive samplings performed at regular intervals (about 30 min). At the end of each experiment, the chamber was evacuated, then flushed several times with zero air, and finally cleaned using irradiation over night.

Test experiments were conducted to check for the stability of pure acetone and acetic acid/air mixtures in our simulation chambers, as these compounds could be either photolyzed or adsorbed on the walls during the experiment. For acetone, the variation was below 1% over 5 h. For acetic acid, pseudo-first-order decay rates of 5 × 10⁻⁶ s⁻¹ and 3 × 10⁻⁶ s⁻¹ were observed in the Teflon chamber and in the Pyrex chamber, respectively. On the basis of these results, losses of acetone and acetic acid to the walls were considered to be negligible within the time scale of the experiments.

Calibration Curves and Acetic Acid Detection Limit. Quantification of acetone- h_2 (respectively acetone- d_6) and acetic acid (respectively acetic acid- d_3) concentrations in the gas phase was performed by frequent calibration of the IR and FID detectors. Standard solutions of acetone in n-octane and acetic acid in ethanol were gravimetrically prepared in the range 0.7–15 mg cm⁻³ and 0.05–0.6 mg cm⁻³, respectively. About 1 μ L of these solutions was injected via the split/splitless injector of the gas chromatograph set in the splitless mode. The chromatographic peak area is then plotted versus the mass of the target compound in the injected sample. A good linearity has been obtained for both deuterated

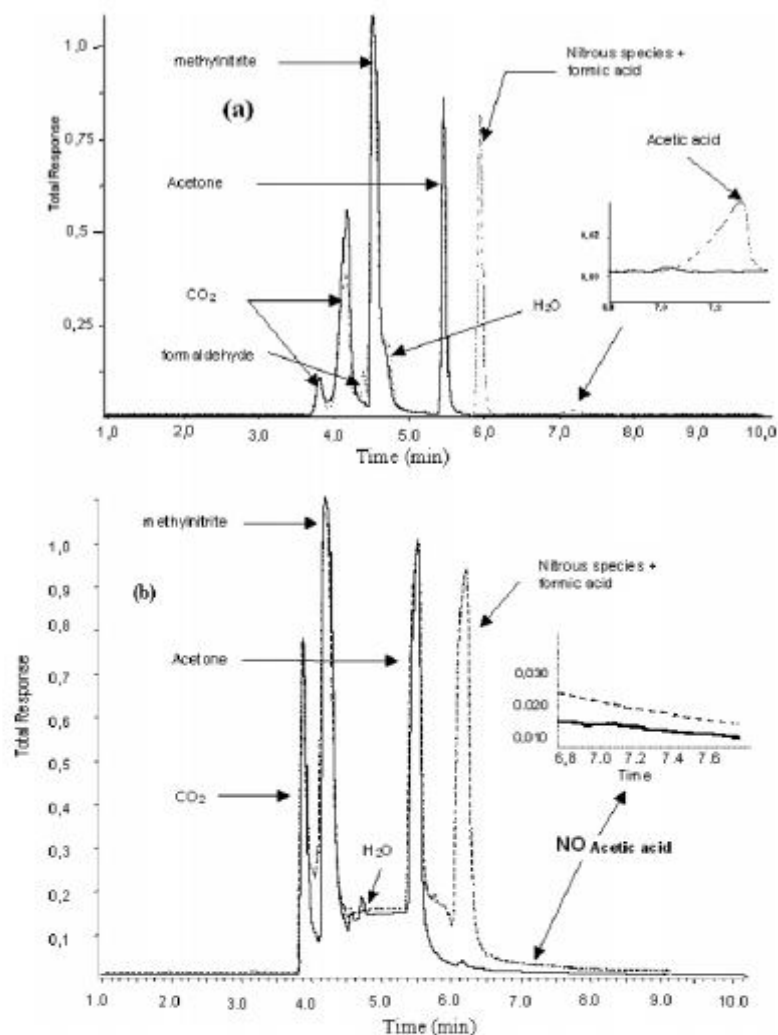


FIGURE 1. Chromatograms resulting from the analysis of two gas aliquots sampled at $t = 0$ (full line) and $t = 60$ min (dotted line) for the reaction acetone + OH investigated in either (a) the Teflon photoreactor or in (b) the Pyrex photoreactor (note the lack of acetic acid).

and nondeuterated compounds. Additional gas injections via the sample loop and the TCT injection system were carried out by sampling from the Teflon chamber filled with known amounts of either acetone or acetic acid. The measured peak areas were consistent with the expected mass of acetone or acetic acid as calculated from the concentration of the compound in the simulation chamber. From the good agreement between the liquid and gas injections, it could be concluded that adsorption of acetone and acetic acid on the surface of the simulation chamber and along the Silcosteel sample line was negligible, confirming previous test experiments. Uncertainties in the quantification of acetone and acetic acid, estimated from repeated sampling from the simulation chamber, were about 6 and 8% (1σ), respectively.

The detection limit (DL) of acetic acid was determined by calculating the standard deviation (σ) of 7 successive liquid injections of a solution at $110 \mu\text{g cm}^{-3}$ using the Student relation: $\text{DL} = t \times \sigma$ with t the Student coefficient (for 7 injections and 95% confidence interval $t = 2.45$). The detection limit was 27 ng, which corresponds to about 270 ppbv

of gaseous acetic acid diluted in a gas sample of 40 cm^3 sampled from the simulation chamber.

Results and Discussion

1. Experiments in Teflon Bags. Acetic Acid Formation Yield.

A series of 7 experiments was carried out in Teflon bags. A typical chromatogram obtained before and after a 60-min irradiation period is shown in Figure 1a. Acetic acid was clearly identified by its retention time (7.2 min) and its IR spectrum. Additional GC analysis with mass spectrometric detection confirmed the formation of acetic acid. It should be noted that test experiments without acetone (i.e., methylnitrite in zero air with UV light) or without UV light irradiation (i.e., acetone with methylnitrite in air in the dark) did not reveal any formation of acetic acid. Therefore it appears that both OH and acetone are required for this formation. In addition, the high NO_x ($\text{NO} + \text{NO}_2$) concentrations in the reaction system preclude any acetic acid formation from peroxy radical reactions like $\text{CH}_3\text{C(O)O}_2 + \text{HO}_2$, since all peroxy radicals are scavenged by their fast reactions with NO (26). Apart from

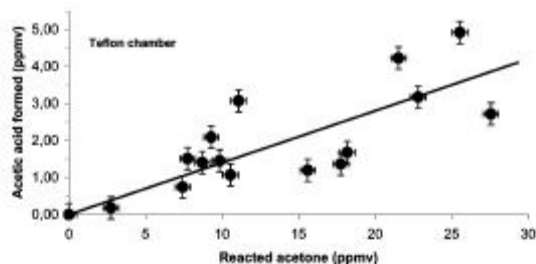


FIGURE 2. Plot of acetic acid formed as a function of acetone- h_3 reacted in the Teflon chamber; the linear regression leads to a yield for acetic acid of (0.14 ± 0.03) (see text).

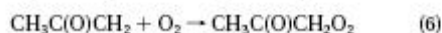
the initial reactants (acetone and methyl nitrite), chromatograms exhibit the presence of formaldehyde, methyl nitrite, and formic acid, usual end products of the OH source.

The quantification of the reacted acetone and the produced acetic acid was based on the calibration curves. In general, 10% of the initial acetone concentration has reacted at the end of the experiment. In typical concentration-time profiles, acetic acid concentrations usually reached a maximum after 60 or 90 min. The subsequent decrease of acetic acid (while acetone is still consumed) cannot be explained by the gas-phase reaction $\text{CH}_3\text{C}(\text{O})\text{OH} + \text{OH}$, since the corresponding pseudo-first-order rate of about 100 s^{-1} (for a maximum acetic acid concentration of 5 ppmv and a rate constant $k_{\text{CH}_3\text{C}(\text{O})\text{OH}+\text{OH}} = 8 \times 10^{-13} \text{ cm}^3 \text{ molecule}^{-1} \text{ s}^{-1}$ at 298 K (27)) is 5 times lower than the $\text{CH}_3\text{C}(\text{O})\text{CH}_3 + \text{OH}$ one under our typical conditions. We suspect that other unknown reactions in the gas phase or on the Teflon walls result in consumption of gaseous acetic acid.

To derive the yield of acetic acid, we have thus only taken into account the data of the first two or three samplings, i.e., before 60 or 90 min of reaction time: $\alpha = [\text{acetic acid}]_{\text{formed}} / [\text{acetone}]_{\text{consumed}} = 1 - R$. The results of all experiments are reported in Figure 2. The rather large scatter of the data is due to a poor reproducibility between the experiments. A linear regression on these data leads to an acetic acid yield of $(14 \pm 4)\%$, corresponding to a branching ratio of $(86 \pm 4)\%$ for the abstraction channel. The quoted uncertainty corresponds only to the 2σ statistical errors from the linear regression analysis at 95% confidence interval.

However, our result was not entirely satisfying, as acetic acid had never been detected except in the last reaction chamber study (21). It should be stressed that the earlier simulation chamber study used Pyrex or stainless steel wall photoreactors (17), while the recent study (21) used a quartz reactor. Thus, we decided to further investigate the acetone + OH reaction in two ways: first by changing the OH radical source and second by repeating the above experiments in a Pyrex chamber.

Further Tests with Another OH Source. Since the presence of acetic acid is still clearly controversial, we have performed supplementary experiments using a quite different OH source. In this set of experiments, OH radicals were produced via UV irradiation of $\text{CH}_3\text{C}(\text{O})\text{CH}_3/\text{Cl}_2/\text{NO}/\text{air}$ mixtures in the Teflon chamber. The Cl-initiated oxidation of acetone is known to lead stoichiometrically ($\sim 99\%$) to the MV peroxy radical $\text{CH}_3\text{C}(\text{O})\text{CH}_2\text{O}_2$ (28):



OH radicals are formed in subsequent very fast reactions implying HO_2 and NO. NO was added in order to avoid the formation of acetic acid through the $\text{CH}_3\text{C}(\text{O})\text{O}_2 + \text{HO}_2$

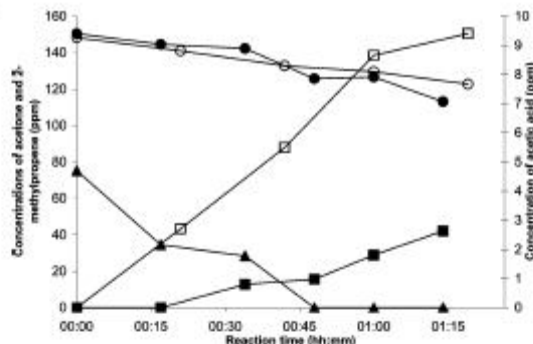


FIGURE 3. Concentration-time profiles of acetone- h_3 (circles), 2-methylpropene (triangles), and acetic acid (squares) in the Teflon chamber. Filled symbols correspond to the reaction acetone- $h_3 + \text{OH}$ in the presence of 2-methylpropene and open symbols to the reaction without 2-methylpropene. 2-Methylpropene values were multiplied by a factor of 10 for clarity.

reaction (26). The OH radicals were then allowed to react with the acetone in excess.

In some experiments, 2-methylpropene $\text{CH}_3\text{C}(\text{CH}_3)=\text{CH}_2$ was added to the reaction mixture to act as scavenger of OH radicals. By comparing the ratios $k_{\text{CH}_3\text{C}(\text{O})\text{CH}_3+\text{Cl}}/k_{\text{CH}_3\text{C}(\text{O})\text{CH}_3+\text{OH}}$ (≈ 14.1 (13, 28)) and $k_{\text{CH}_3\text{C}(\text{CH}_3)=\text{CH}_2+\text{Cl}}/k_{\text{CH}_3\text{C}(\text{CH}_3)=\text{CH}_2+\text{OH}}$ (≈ 5.9 (13, 29, 30)), it proves possible to choose appropriate acetone and 2-methylpropene concentrations (about 200 and 10 ppmv, respectively) so that OH radicals react mostly with 2-methylpropene. As a consequence, this ensured that no OH radicals will react with acetone.

A typical experiment is shown in Figure 3: in experiments without 2-methylpropene, acetic acid is detected immediately. Conversely, when 2-methylpropene was initially added, no acetic acid is formed as long as the 2-methylpropene concentration is sufficiently high to effectively scavenge OH radicals. These experiments demonstrate that OH radicals are essential in the formation of acetic acid and confirm our experiments using methyl nitrite as OH radical source.

2. Experiments in the Pyrex Chamber. Three experiments were carried out in the Pyrex chamber. The experimental conditions (reactant concentrations, pressure, temperature) were similar to those in the Teflon chamber experiments.

Two chromatograms are presented in Figure 1b; the first (full line) corresponds to a sampling carried out before turning on the lamps, and the second (dotted line) corresponds to a sampling carried out 60 min after, i.e., when about 10% of the initial acetone has reacted. In contrast to the experiments in the Teflon simulation chamber, no acetic acid was detected. Taking into account our detection limit, we estimate an upper limit of 5% for the channel (1b).

These results are very consistent with the investigations of Tyndall et al. (17) achieved in Pyrex or stainless steel simulation chambers, where no acetic acid was observed and an upper limit to acetic acid production of 10% was claimed. Furthermore, they agree much better with recent measurements (16, 18), where acetic acid was searched for but not detected, and with theoretical studies of Hénon et al. (23), Canneaux et al. (24), and the very recent work of Caralp et al. (31). The recent chamber study of Raff et al. (21) where acetic acid formation was observed, concludes to a branching ratio of approximately 3% at room temperature, consistent with our detection limit.

3. Experiments with Acetone- d_6 . Complementary experiments have been performed using the fully-deuterated acetone compound $\text{CD}_3\text{C}(\text{O})\text{CD}_3$ with the aim at confirming the present results and providing a better insight into the chemical mechanism.

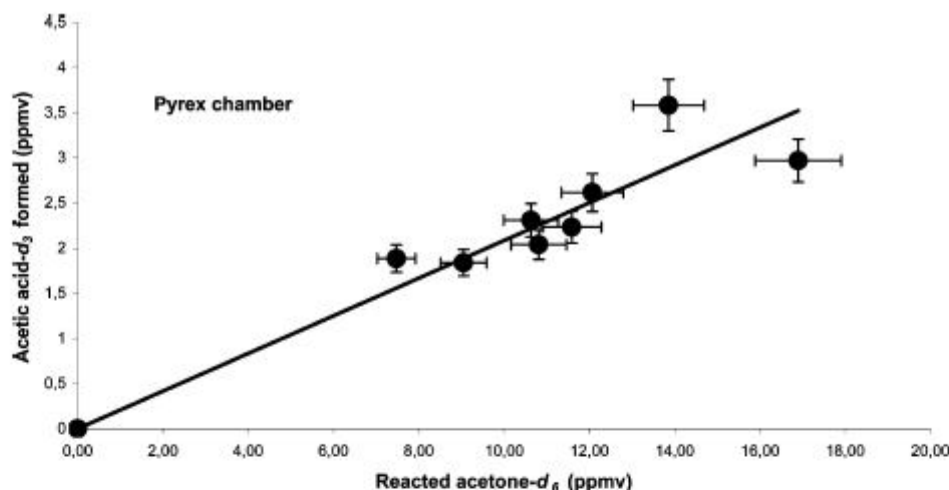
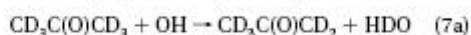


FIGURE 4. Plot of acetic acid- d_3 formed as a function of acetone- d_6 reacted in the Pyrex chamber; the linear regression leads to a yield for acetic acid- d_3 of (0.20 ± 0.06) (see text).



Experiments were carried out either in the Teflon chamber or in the Pyrex one. Experimental conditions and analysis procedures matched those employed previously for acetone- h_6 , with acetone- d_6 concentrations between 50 and 100 ppmv.

As a first goal, relative rate experiments in the Teflon chamber using methyl formate as the reference compound ($k_{\text{ref}}(\text{HC}(\text{O})\text{OCH}_3 + \text{OH}) = 1.87 \times 10^{-13} \text{ cm}^3 \text{ molecule}^{-1} \text{ s}^{-1}$ at 298 K (32)) allowed us to determine the rate constant k_7 . The rate constant ratio of $k_7/k_{\text{ref}} = 0.184$ translates into the following value $k_7 = 3.45 \times 10^{-14} \text{ cm}^3 \text{ molecule}^{-1} \text{ s}^{-1}$ for the $\text{CD}_3\text{C}(\text{O})\text{CD}_3 + \text{OH}$ rate constant, in good agreement with the literature (11, 12, 21, 33, 34).

As a second goal, we tried to detect reaction products in the photolysis of $\text{CD}_3\text{C}(\text{O})\text{CD}_3/\text{CH}_3\text{ONO}/\text{air}$ mixtures. Teflon chamber experiments clearly show the presence of acetic acid- d_3 (identified by its IR spectrum), yet with very poor reproducibility between the experiments, as observed previously with $\text{CH}_3\text{C}(\text{O})\text{CH}_3$; no consistent acetic acid- d_3 yield has been obtained from this set of experiments. Conversely, experiments in the Pyrex photoreactor gave much more reproducible results; acetic acid- d_3 was clearly identified by its IR spectrum; a linear regression of acetic acid- d_3 versus acetone- d_6 reacted (see Figure 4) leads to an acetic acid- d_3 yield of $(20 \pm 6)\%$, corresponding to a branching ratio of $(80 \pm 6)\%$ for the abstraction channel (channel (7a)). This result is not surprising since the barrier for D-abstraction is usually higher than that for H-abstraction (33–36). In addition, the measured acetic acid- d_3 yield compares very well with the only (to our knowledge) investigation of the products of the $\text{CD}_3\text{C}(\text{O})\text{CD}_3 + \text{OH}$ reaction from Raff et al. (21), who determined an acetic acid- d_3 yield of 18.7% at 298 K. Comparing the rate coefficient $k_{7b} = 0.2 \times 3.45 \times 10^{-14} \approx 7 \times 10^{-15} \text{ cm}^3 \text{ molecule}^{-1} \text{ s}^{-1}$ for the formation of acetic acid- d_3 to the upper limit of the formation of acetic acid, $k_{7a} = 0.05 \times 1.7 \times 10^{-13} \approx 8.5 \times 10^{-15} \text{ cm}^3 \text{ molecule}^{-1} \text{ s}^{-1}$, it is noteworthy that both values match fairly well. This would indicate the absence of any isotope effect, which is consistent with an addition-elimination channel.

The reason why acetic acid is observed in the Teflon bag experiments is presently not clear. The set of experiments performed using chlorine photolysis confirms that the pres-

ence of OH radicals is absolutely necessary to observe acetic acid formation. Second, no acetic acid was observed in the Pyrex simulation chamber experiments, in contrast to those performed in the Teflon one. We tentatively suggest that this formation could be attributed to specific heterogeneous reactions of OH radicals with acetone adsorbed on the wall of the Teflon reactor. The rather large scatter of the data (see Figure 2) is consistent with such an uncontrolled heterogeneous process. It should be stressed that such catalytic effects of Teflon films have already been observed in previous smog chamber studies (37–39). In addition, the transformation of acetone into acetic acid was also shown to occur under photocatalytic oxidation conditions implying a chemisorbed propylene oxide (40, 41). Additional experiments carried out in much larger Teflon simulation chambers would have been very useful to confirm this assumption.

These experiments are an example of wall-effects in Teflon simulation chambers. Our results also raise the question whether the acetic acid formation observed by Raff et al. (21) might be assigned to such heterogeneous reactions in their small quartz reactor. The increase of the yield with decreasing temperature observed by these authors (21) might also be related to the well-known increase of the efficiency of wall reactions at low temperatures, especially in the presence of polar molecules. Finally, our results obtained in the Pyrex chamber demonstrated that the channel forming acetic acid is a minor oxidation route in the atmospheric acetone + OH reaction (yield < 5%), in good agreement with the last previous studies (see also Table 1). The formation of a small amount of acetic acid cannot be excluded, in agreement with the last study of Raff et al. (21). The quantification of the products of the $\text{CD}_3\text{C}(\text{O})\text{CD}_3 + \text{OH}$ reaction showed the formation of acetic acid- d_3 with a yield of 20%, consistent with the study of Raff et al. (21) and providing confidence in the present results on acetone- h_6 and acetone- d_6 reactions with OH.

Acknowledgments

This work was supported by the Ministère chargé de la Recherche, the Région Nord-Pas-de-Calais, and the Fonds Européen de Développement Economique des Régions (FEDER) through the Contrat de Plan Etat-Région 2000-2003.

Literature Cited

- (1) Singh, H. B.; O'Hara, D.; Herth, D.; Sachse, W.; Blake, D. R.; Bradshaw, J. D.; Kanakidou, M.; Crutzen, P. J. Acetone in the

- atmosphere: Distribution, sources, and sinks. *J. Geophys. Res.* 1994, 99, 1805–1820.
- (2) Goldstein, A. H.; Schade, G. W. Quantifying biogenic and anthropogenic contributions to acetone mixing ratios in a rural environment. *Atmos. Environ.* 2000, 34, 4997–5006.
 - (3) Jacob, D. J.; Field, B. D.; Jin, E. M.; Bey, I.; Li, Q.; Logan, J. A.; Yantosca, R. M.; Singh, H. B. Atmospheric budget of acetone. *J. Geophys. Res.* 2002, 107, 4100–4118.
 - (4) Arnold, S. R.; Chipperfield, M. P.; Blitz, M. A.; Heard, D. E.; Pilling, M. J. Photodissociation of acetone: Atmospheric implications of temperature-dependent quantum yields. *Geophys. Res. Lett.* 2004, 31, L07110.
 - (5) Blitz, M. A.; Heard, D. E.; Pilling, M. J.; Arnold, S. R.; Chipperfield, M. P. Pressure and temperature-dependent quantum yields for the photodissociation of acetone between 279 and 327.5 nm. *Geophys. Res. Lett.* 2004, 31, L06111.
 - (6) Hermans, I.; Müller, J.-F.; Nguyen, T. L.; Jacobs, P. A.; Peeters, J. Kinetics of hydroxy-alkylperoxy radicals in oxidation processes. HO₂-initiated oxidation of ketones/aldehydes near the tropopause. *J. Phys. Chem. A* 2005, 109, 4303–4311.
 - (7) Folkens, I.; Chatfield, R. Impact of acetone on ozone production and OH in the upper troposphere at high NO_x. *J. Geophys. Res.* 2000, 105, 11585–11600.
 - (8) Wallington, T. J.; Kurylo, M. J. Flash photolysis resonance fluorescence investigation of the gas-phase reactions of OH radicals with a series of aliphatic ketones over the temperature range 240–440 K. *J. Phys. Chem.* 1987, 91, 5050–5054.
 - (9) Le Calvé, S.; Hittler, D.; Le Bras, G.; Mellouki, W. Kinetic studies of OH reactions with a series of ketones. *J. Phys. Chem. A* 1998, 102, 4579–4584.
 - (10) Wollenhaupt, M.; Carl, S. A.; Horowitz, A.; Crowley, J. N. Rate coefficients for reaction of OH with acetone between 202 and 395 K. *J. Phys. Chem. A* 2000, 104, 2695–2705.
 - (11) Gierczak, T.; Gilles, M. K.; Bauerle, S.; Ravishankara, A. R. Reaction of hydroxyl radical with acetone. 1. Kinetics of the reaction of OH, OD, and ¹⁸OH with acetone and acetone-*d*₆. *J. Phys. Chem. A* 2003, 107, 5014–5020.
 - (12) Yamada, T.; Taylor, P. H.; Goumri, A.; Marshall, P. The reaction of OH with acetone and acetone-*d*₆ from 298 to 832 K: Rate coefficients and mechanism. *J. Chem. Phys.* 2003, 119, 10600–10606.
 - (13) Atkinson, R.; Arey, J. Atmospheric degradation of volatile organic compounds. *Chem. Rev.* 2003, 103, 4605–4638.
 - (14) Wollenhaupt, M.; Crowley, J. N. Kinetic studies of the reactions CH₃ + NO₂ → Products, CH₃O + NO₂ → Products, and OH + CH₃C(O)CH₃ → CH₃C(O)OH + CH₃, over a range of temperature and pressure. *J. Phys. Chem. A* 2000, 104, 6429–6438.
 - (15) Vasvári, G.; Szilágyi, I.; Bencsura, Á.; Dóbe, S.; Bérces, T.; Hénon, E.; Canneaux, S.; Bohr, F. Reaction and complex formation between OH radical and acetone. *Phys. Chem. Chem. Phys.* 2001, 3, 551–555.
 - (16) Vandenberg, S.; Vereecken, L.; Peeters, J. The acetic acid forming channel in the acetone + OH reaction: A combined experimental and theoretical investigation. *Phys. Chem. Chem. Phys.* 2002, 4, 461–466.
 - (17) Tyndall, G. S.; Orlando, J. I.; Wallington, T. J.; Hurley, M. D.; Goto, M.; Kawasaki, M. Mechanism of the reaction of OH radicals with acetone and acetaldehyde at 251 and 296 K. *Phys. Chem. Chem. Phys.* 2002, 4, 2189–2193.
 - (18) Talukdar, R. K.; Gierczak, T.; McCabe, D. C.; Ravishankara, A. R. Reaction of hydroxyl radical with acetone. 2. Products and reaction mechanism. *J. Phys. Chem. A* 2003, 107, 5021–5032.
 - (19) Turpin, E.; Fittschen, C.; Tomas, A.; Devolder, P. Reaction of OH radicals with acetone: determination of the branching ratio for the abstraction pathway at 298 K and 1 Torr. *J. Atmos. Chem.* 2003, 46, 1–13.
 - (20) Turpin, E. Ph.D. Dissertation, Université des Sciences et Technologies de Lille, December 2004.
 - (21) Raff, J. D.; Stevens, P. S.; Hites, R. A. Relative rate and product studies of the OH-acetone reaction. *J. Phys. Chem. A* 2005, 109, 4728–4735.
 - (22) Masgrau, L.; González-Lafont, Á.; Lluch, J. M. Variational transition-state theory rate constant calculations with multi-dimensional tunneling corrections of the reaction of acetone with OH. *J. Phys. Chem. A* 2002, 106, 11760–11770.
 - (23) Hénon, E.; Canneaux, S.; Bohr, F.; Dóbe, S. Features of the potential energy surface for the reaction of OH radical with acetone. *Phys. Chem. Chem. Phys.* 2003, 5, 333–341.
 - (24) Canneaux, S.; Sokolowski-Gomez, N.; Hénon, E.; Bohr, F.; Dóbe, S. Theoretical study of the reaction OH + acetone: a possible kinetic effect of the presence of water? *Phys. Chem. Chem. Phys.* 2004, 6, 5172–5177.
 - (25) Taylor, W. D.; Allston, T. D.; Moscato, M. J.; Fazekas, G. B.; Kozlowski, R.; Takacs, G. A. Atmospheric photodissociation lifetimes for nitromethane, methyl nitrite, and methyl nitrate. *Int. J. Chem. Kinet.* 1980, 12, 231–240.
 - (26) Tyndall, G. S.; Cox, R. A.; Granier, C.; Lesclaux, R.; Moortgat, G. K.; Pilling, M. J.; Ravishankara, A. R.; Wallington, T. J. Atmospheric chemistry of small organic peroxy radicals. *J. Geophys. Res.* 2001, 106, 12157–12182.
 - (27) Sander, S. P.; Friedl, R. R.; Golden, D. M.; Kurylo, M. J.; Huie, R. E.; Orkin, V. L.; Moortgat, G. K.; Ravishankara, A. R.; Kolb, C. E.; Molina, M. J.; Finlayson-Pitts, B. J. Chemical kinetics and photochemical data for use in atmospheric studies. *JPL Publ.* 2003, 02–25.
 - (28) Nielsen, O. J.; Johnson, M. S.; Wallington, T. J.; Christensen, L. K.; Platz, J. U. V. absorption spectra of HO₂, CH₃O₂, C₂H₅O₂, and CH₃C(O)CH₂O₂ radicals and mechanism of the reactions of F and Cl atoms with CH₃C(O)CH₃. *Int. J. Chem. Kinet.* 2002, 34, 283–291.
 - (29) Orlando, J. J.; Tyndall, G. S.; Apel, E. C.; Riemer, D. D.; Paulson, S. E. Rate coefficients and mechanisms of the reaction of Cl-atoms with a series of unsaturated hydrocarbons under atmospheric conditions. *Int. J. Chem. Kinet.* 2003, 35, 334–353.
 - (30) Stutz, J.; Ezell, M. J.; Ezell, A. A.; Finlayson-Pitts, B. J. Rate constants and kinetic isotope effects in the reactions of atomic chlorine with n-butane and simple alkenes at room temperature. *J. Phys. Chem. A* 1998, 102, 8510–8519.
 - (31) Caralp, F.; Forst, W.; Hénon, E.; Bergéat, A.; Bohr, F. Tunneling in the reaction of acetone with OH. *Phys. Chem. Chem. Phys.* 2006, 8, 1072–1078.
 - (32) Le Calvé, S.; Le Bras, G.; Mellouki, W. Temperature dependence for the rate coefficients of the reactions of the OH radical with a series of formates. *J. Phys. Chem. A* 1997, 101, 5489–5493.
 - (33) Farkas, E.; Szilágyi, I.; Dóbe, S.; Bérces, T.; Marta, F. Kinetic isotope effect in the reaction of OH radical with acetone-*d*₆. *React. Kinet. Catal. Lett.* 2003, 80, 351–358.
 - (34) Davis, M. E.; Drake, W.; Vimal, D.; Stevens, P. S. Experimental and theoretical studies of the kinetics of the reactions of OH and OD with acetone and acetone-*d*₆ at low pressure. *J. Photochem. Photobiol. A* 2005, 176, 162–171.
 - (35) Brown, S. S.; Burkholder, J. B.; Talukdar, R. K.; Ravishankara, A. R. Reaction of Hydroxyl Radical with Nitric Acid: Insights into Its Mechanism. *J. Phys. Chem. A* 2001, 105, 1605–1614.
 - (36) Singleton, D. L.; Paraskevopoulos, G.; Irwin, R. S.; Jolly, G. S.; McKenney, D. J. Rate and mechanism of the reactions of hydroxyl radicals with formic and deuteriated formic acids. *J. Am. Chem. Soc.* 1988, 110, 7786–7790.
 - (37) Besemer, A. C.; Nieboer, H. The wall as a source of hydroxyl radicals in smog chambers. *Atmos. Environ.* 1985, 19, 507–513.
 - (38) Stangl, H.; Kotzias, D.; Van Eijk, J.; Nicollin, B.; Hjorth, J.; Ottobri, G. On the use of Teflon bags for photochemical experiments. *Chemosphere* 1987, 16, 1405–1417.
 - (39) Killus, J. P.; Whitten, G. Z. Background reactivity in smog chambers. *Int. J. Chem. Kinet.* 1990, 22, 547–575.
 - (40) Kagwade, S. V.; Clayton, C. R.; Chidambaram, D.; Halada, G. P. Photochemical breakdown of acetone on copper. *Electrochim. Acta* 2001, 46, 2337–2342.
 - (41) Xu, W.; Raftery, D. In situ solid-state nuclear magnetic resonance studies of acetone photocatalytic oxidation on titanium oxide surfaces. *J. Catal.* 2001, 204, 110–117.

Received for review January 26, 2006. Revised manuscript received May 22, 2006. Accepted July 18, 2006.

ES060183A

III.3 La réaction acide acétique + OH•

III.3.1 Sources atmosphériques de l'acide acétique

Comme l'acétone, l'acide acétique (AA) est un COV oxygéné qui a été observé partout dans la troposphère, près du sol comme vers la tropopause, et dont les niveaux de concentration, quoique généralement plus faibles que ceux de l'acétone, sont proches du ppbv (112, 161). Les émissions totales d'acide acétique sont estimées à environ 85 Tg/an (188) et les nombreuses mesures réalisées dans divers environnements indiquent que l'acide acétique est l'un des COV oxygénés les plus répandus dans l'atmosphère, et représente, avec l'acide formique, l'acide carboxylique le plus abondant (112, 189). Une campagne de mesure effectuée dans un site alpin en Europe à haute altitude a montré que les acides formique et acétique étaient les gaz acides les plus importants, devant les acides nitrique, hydrochlorique et sulfurique (190).

La source biogénique – feux de biomasse (112, 135, 191) et émissions de la végétation et des sols (112, 192) – constitue la principale source primaire d'AA. Avec l'acide formique, l'acide acétique est l'acide organique le plus important émis par la végétation. Des mesures en atmosphères marines suggèrent également une source océanique (193). Les échappements automobiles, l'élevage intensif et les installations de combustion industrielles représentent globalement des sources primaires anthropogéniques de moindre importance (194, 195), mais elles peuvent être dominantes localement (196). La production photochimique secondaire à partir de COV biogéniques (isoprène + OH• par exemple) et anthropogéniques (ozonolyse des alcènes par exemple) est significative (197, 198) et implique des réactions entre radicaux peroxy (190). Paulot *et al.* ont estimé la source secondaire à 2/3 de la source totale (188), ce qui est considérable. Le cycle de vie de l'acide acétique dans l'atmosphère (sources et puits) n'est actuellement pas encore bien compris. On peut remarquer que, lors de comparaisons mesures – modèles de chimie atmosphérique, les modèles sous-estiment fréquemment les concentrations d'acide acétique d'un facteur 3 à 9 (199, 200) et il semble que plusieurs sources d'AA ne soient pas encore prises en compte (dont peut-être un mécanisme de production hétérogène) (188, 200).

III.3.2 Réactivité et impact de l'acide acétique dans l'atmosphère

La durée de vie de l'acide acétique dans l'atmosphère est relativement courte : de quelques heures à quelques jours (193), avec une moyenne de 1,7 jours dans la couche limite atmosphérique (188). Cette durée de vie courte s'explique par l'existence de plusieurs phénomènes concomitants :

- *Les dépôts humide et sec*

L'acide acétique, comme la plupart des acides carboxyliques, présente une solubilité élevée dans l'eau, de sorte qu'on considère que le principal puits d'AA dans l'atmosphère est le dépôt humide (201). L'importance de ce phénomène varie évidemment en fonction de la pluviométrie, et, par conséquent, en fonction du territoire considéré et de la saison. Appelé aussi lessivage, le phénomène de dépôt humide d'AA a été observé par de *Gouw et al.* (191) et il est reconnu pour contribuer de façon significative (avec HCOOH) à l'acidité des précipitations dans les régions éloignées des sources de pollution anthropiques (193, 202). Le dépôt d'acide acétique à la surface de l'océan pourrait être aussi un puits important (197). Le dépôt sec sur les surfaces (sols, végétation, constructions, ...) peut parfois dépasser le dépôt humide dans des atmosphères sèches (112, 201). Enfin, des mesures de coefficients de capture à la surface d'aérosols minéraux urbains et marins montrent que le transfert de masse d'AA vers l'aérosol pourrait être compétitif par rapport aux processus en phase gazeuse (174, 203).

- *La réactivité en phase liquide*

L'AA est réparti dans l'atmosphère dans les phases gazeuses et liquides, cette répartition dépendant de la constante de Henry et de paramètres environnementaux tels que la température et le pH de l'eau. Une campagne de mesure en site semi-urbain aux Etats-Unis indique que 90% environ de l'acide acétique se trouve dans la phase gazeuse (198). La réactivité de l'acide acétique en phase liquide concerne principalement le radical OH• mais une récente étude a montré que la dégradation biologique par les microorganismes présents dans les gouttelettes d'eau des nuages pourrait représenter une voie réactionnelle équivalente à la photodégradation par le radical OH• (204).

- *La réactivité en phase gazeuse*

La réaction de l'acide acétique avec le radical OH• est plutôt lente, avec une valeur recommandée à $7,4 \times 10^{-13} \text{ cm}^3 \cdot \text{molécule}^{-1} \cdot \text{s}^{-1}$ à 298 K (85), ce qui correspond à un temps de vie d'une semaine pour une concentration moyenne de radicaux OH• de $2 \times 10^6 \text{ molécule} \cdot \text{cm}^{-3}$ (70). La constante de vitesse présente une dépendance négative assez forte avec la température, modélisée par la relation $k(T) = 4,2 \times 10^{-14} \exp(855/T) \text{ cm}^3 \cdot \text{molécule}^{-1} \cdot \text{s}^{-1}$ dans le domaine de température 220 – 300 K (85), ce qui conduit à une constante de vitesse de $2,0 \times 10^{-12} \text{ cm}^3 \cdot \text{molécule}^{-1} \cdot \text{s}^{-1}$ à 220 K. Le puits d'acide acétique via la réaction OH• + AA est donc plus important, voire majoritaire, dans la région de la haute troposphère – basse stratosphère (205).

III.3.3 Intérêt de la réaction et présentation de l'historique des différentes études

Lorsque nous avons abordé ce travail, trois études seulement traitaient des cinétiques de la réaction $\text{CH}_3\text{C}(\text{O})\text{OH} + \text{OH}^\bullet$ (**Tableau III.2**). Malgré un accord raisonnable sur la constante de vitesse à température ambiante, la dépendance en température était contradictoire entre *Dagaut et al.* (206) d'un côté (dépendance positive), et *Singleton et al.* (207) et *Butkovskaya et al.* (208) de l'autre côté (dépendance négative). Nous n'avons pas traité cette difficulté qui a été levée par d'autres études ultérieures.

Tableau III.2 : Données cinétiques disponibles sur la réaction $\text{CH}_3\text{C}(\text{O})\text{OH} + \text{OH}^\bullet$ au début de notre étude.

Référence	k (T) ($\text{cm}^3 \cdot \text{molécule}^{-1} \cdot \text{s}^{-1}$)	k(298 K) ($\text{cm}^3 \cdot \text{molécule}^{-1} \cdot \text{s}^{-1}$)
<i>Singleton et al.</i> (207)	a)	$8,7 \times 10^{-13}$
<i>Dagaut et al.</i> (206)	$1,3 \times 10^{-12} \exp(-170/T)$	$7,4 \times 10^{-13}$
<i>Butkovskaya et al.</i> (208)	$2,2 \times 10^{-14} \exp(1012/T)$	$6,6 \times 10^{-13}$

a) : pas d'expression d'Arrhenius mais valeurs de k déterminées à 5 températures différentes (296,8 K – 446,2 K) indiquant une dépendance négative de k avec T.

L'autre challenge important concernait le mécanisme de la réaction. Deux voies étaient envisagées : l'arrachement d'un atome d'hydrogène du groupement méthyl ou de la fonction acide :



L'importance de chacune de ces voies contrôle l'impact de l'acide acétique dans l'atmosphère. Très peu d'études portaient sur ce mécanisme réactionnel. Une analyse des énergies de liaisons C-H et O-H montrait que $10 \text{ kcal} \cdot \text{mol}^{-1}$ supplémentaires étaient nécessaires pour rompre la liaison O-H de la fonction acide, ce qui semblait favoriser la voie (2a). Les expériences de *Butkovskaya et al.* (208), en accord avec les prévisions de *Singleton et al.* (207), démontraient à l'inverse que la voie (2b) était prépondérante (rapport de branchement $k_{2b}/k_2 = 0,64$), probablement dû à la formation d'un complexe pré-réactif entre le radical OH^\bullet et la fonction acide.

III.3.4 Travaux réalisés

Nos travaux ont porté à la fois sur les cinétiques des réactions entre le radical OH[•], l'acide acétique et les trois isotopes deutérés de l'acide acétique (CH₃C(O)OD, CD₃C(O)OH, CD₃C(O)OD) à température ambiante, et sur le mécanisme de ces réactions. Les expériences ont été effectuées dans la chambre de simulation souple en Téflon. Le mécanisme réactionnel a été étudié de plusieurs manières :

- la mesure des quantités de CO₂ formées dans la voie b par cw-CRDS ;
- la détermination de l'effet cinétique isotopique ;
- l'observation de l'acide glyoxylique formé dans la voie (2a).

L'ensemble des résultats a fait l'objet de deux publications (**publications n°5** (58) et **n°6** (59)) et d'une participation à ouvrage (209).

III.3.5 Discussion et conclusion

Les cinétiques et le mécanisme de la réaction CH₃C(O)OH + OH[•] ont été revues dans l'article de *Carl et al.* (205). La dernière recommandation de la constante de vitesse à température ambiante, $k_2 = 7,4 \times 10^{-13} \text{ cm}^3 \cdot \text{molécule}^{-1} \cdot \text{s}^{-1}$ (85) n'est pas remise en cause par les toutes dernières publications ($6,77 \times 10^{-13} \text{ cm}^3 \cdot \text{molécule}^{-1} \cdot \text{s}^{-1}$ (210) ; $7,66 \times 10^{-13} \text{ cm}^3 \cdot \text{molécule}^{-1} \cdot \text{s}^{-1}$ (211)) et donne un temps de vie atmosphérique relatif à la réaction avec OH[•] d'environ 8 jours pour une concentration moyenne de radicaux OH[•] de $2 \times 10^6 \text{ molécule} \cdot \text{cm}^3$. La dépendance négative en température a également été confirmée (210). Un effet de pression a été mis en évidence par *Huang et al.* qui suggèrent que la réaction CH₃C(O)OH + OH[•] pourrait être plus importante que prévue dans la région de l'UTLS (211).

Toutes les études expérimentales indiquent par ailleurs que la voie d'arrachement de l'atome d'hydrogène du groupement acide est favorisée et représente environ 70% de la perte totale d'AA (58, 208, 212). Ceci est confirmé d'une part par l'effet cinétique isotopique important qui a été observé par *Singleton et al.* (207), *Vimal et Stevens* (213) et notre équipe (59), d'autre part par le calcul des surfaces d'énergie potentielle réalisé par *De Smedt et al.* (214) et *Vimal et Stevens* (213). La prédominance de la voie acide dans le mécanisme est expliquée par la formation d'un complexe pré-réactif stable à liaisons hydrogènes qui abaisse de façon significative la barrière d'énergie potentielle de la voie (2a) (205) et par l'effet tunnel, beaucoup plus important sur cette voie que sur la voie méthyl (215). L'effet tunnel permet également d'expliquer la dépendance négative en température pour $T < 500 \text{ K}$. Enfin, l'effet isotopique important observé est à mettre sur le compte d'une différence des énergies de point zéro entre les AA deutérés et l'AA non-deutééré (213).

Publication n°5
(parue dans la revue *Applied Physics B* en 2006)

S. CRUNAIRE^{1,2}
J. TARMOUL^{1,2}
C. FITTSCHEN¹
A. TOMAS^{2,✉}
B. LEMOINE³
P. CODDEVILLE²

Use of cw-CRDS for studying the atmospheric oxidation of acetic acid in a simulation chamber

¹ Laboratoire de Physico-Chimie des Processus de Combustion et de l'Atmosphère – CNRS UMR 8522,

Université des Sciences et Technologies de Lille, Lille I, Bât. C11, 59655 Villeneuve d'Ascq Cedex, France

² Département Chimie et Environnement, Ecole des Mines de Douai, 941 Rue Charles Bourseul,

B.P. 10838, 59508 Douai Cedex, France

³ Laboratoire de Physique des Lasers, Atomes et Molécules – CNRS UMR 8523,

Université des Sciences et Technologies de Lille, Lille I, Bât P5, 59655 Villeneuve d'Ascq Cedex, France

Received: 30 March 2006/Revised version: 9 May 2006
Published online: 24 June 2006 • © Springer-Verlag 2006

ABSTRACT The coupling between cavity ring-down spectroscopy (CRDS) and an environmental chamber in the investigation of photo-induced reaction mechanisms is demonstrated for the first time.

The development of the CRDS device and the corresponding analytical performances are presented. The first application is devoted to the investigation of the branching ratio of the $\bullet\text{OH}$ radical reaction of $\text{CH}_3\text{C}(\text{O})\text{OH}$ and $\text{CH}_3\text{C}(\text{O})\text{OD}$ under tropospheric conditions. An environmental chamber coupled to two complementary detection systems is used:

- gas chromatography with FTIR spectroscopy for quantitative detection of acetic acid;
- CRDS for quantitative detection of CO_2 .

Investigation of the reaction kinetics of $\bullet\text{OH} + \text{CH}_3\text{C}(\text{O})\text{OH}$ gives a rate constant of $(6.5 \pm 0.5) \times 10^{-13} \text{ cm}^3 \text{ molecule}^{-1} \text{ s}^{-1}$ (296 K) and shows good agreement with literature data. The product study indicates that the H-abstraction channel from the acid group is the dominant pathway with a branching ratio of $(78 \pm 13)\%$, whereas the corresponding D-abstraction channel in the $\bullet\text{OH} + \text{CH}_3\text{C}(\text{O})\text{OD}$ reaction represents only $(36 \pm 7)\%$. This result could be attributed to a strong kinetic isotope effect. Glyoxylic acid has also been detected for the first time as by-product.

These results illustrate the high interest of the CRDS technique in the investigation of atmospheric relevant problems.

PACS 82.33.Tb; 82.20.-w; 82.20.Tr; 07.60.-j; 07.88.+y;
42.55.Px; 42.60.Da; 42.62.Fi

1 Introduction

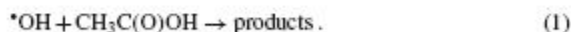
Oxygenated volatile organic compounds are trace components in the atmosphere, with ppt- to ppb-level concentrations encountered in various areas [1–4]. Nevertheless, their impact on the air quality and on the oxidative capacity of the atmosphere through the HO_x budget is considered to be significant, as oxygenated compounds are fairly reactive (with $\bullet\text{OH}$ radicals or via sunlight photolysis for carbonyls) [5] and some of them are potentially toxic [6].

Recent evidence suggests that carboxylic acids are one of the dominant classes of organic compounds found in the atmosphere, since they are present in a variety of phases (rain-water, vapor phase, aerosols, haze and dew) and they contribute to approximately a quarter of the non-methane hydrocarbon (NMHC) atmospheric mixture ([7, 8] and references therein).

Among these compounds, low molecular weight carboxylic acids like acetic acid have been recognized as potentially important especially in urban polluted atmospheres where concentrations can exceed $20 \mu\text{g m}^{-3}$ [9] and may be harmful to environment due to the acidification of the natural compartments [10, 11] and to their toxicity towards people health [12].

In the conditions of the lower troposphere, biomass burning and acetylperoxy radical reactions are recognized to be the two main sources of acetic acid [13, 14]. In particular, the reaction of $\text{CH}_3\text{C}(\text{O})\text{O}_2^\bullet$ with HO_2^\bullet is known to lead to about 20% $\text{CH}_3\text{C}(\text{O})\text{OH}$ [15]. Acetic acid in the atmosphere can also be produced by the reaction of ozone with various olefins like propene, butene [16] or isoprene [17]. A total photochemical source strength of $120 \times 10^{12} \text{ g year}^{-1}$ is reported [18]. The contribution of direct emissions from anthropogenic (biomass combustion, motor exhaust) and biogenic (bacteria metabolisms, emission from soil and vegetation) sources is evaluated to $48 \times 10^{12} \text{ g year}^{-1}$ [7].

Apart from its atmospheric sink through incorporation in water droplets, the main loss of $\text{CH}_3\text{C}(\text{O})\text{OH}$ is its reaction with $\bullet\text{OH}$ radicals:

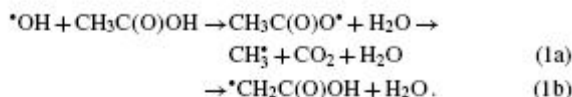


The corresponding reaction rate is now fairly well known with a recommended value of $k_1 = 8 \times 10^{-13} \text{ cm}^3 \text{ molecule}^{-1} \text{ s}^{-1}$ at $T = 298 \text{ K}$ [19], the most recent study of Butkovskaya et al. (2004) [20] showing a consistent overall rate constant of $6.6 \times 10^{-13} \text{ cm}^3 \text{ molecule}^{-1} \text{ s}^{-1}$ at 298 K. Assuming a typical tropospheric $\bullet\text{OH}$ concentration of $2 \times 10^6 \text{ molecule cm}^{-3}$ [21], an atmospheric residence time ($\tau = 1/k_1 \times [\bullet\text{OH}]$) of more than a week can be calculated. The photooxidation chain of acetic acid is expected to contribute to the production of photooxidants, thus influencing the atmospheric HO_x budget [16]. However, models usually do not

✉ Fax: +33327712914, E-mail: tomas@ensm-douai.fr

take these effects into account because too little is known about the gaseous fate of $\text{CH}_3\text{C}(\text{O})\text{OH}$ in the atmosphere. Therefore, to assess its tropospheric impact, the determination of the product distribution is needed.

Two H-abstraction channels are expected to occur in the $\cdot\text{OH}$ -initiated oxidation of acetic acid:



The rate coefficients determined by Singleton et al. (1989) [22] for the reactions of $\cdot\text{OH}$ radicals with $\text{CH}_3\text{C}(\text{O})\text{OH}$, $\text{CD}_3\text{C}(\text{O})\text{OH}$ and $\text{CD}_3\text{C}(\text{O})\text{OD}$ show that the major reaction channel involves H- (or D-) atom abstraction from the carboxylic group at room temperature. This was confirmed by the branching fraction k_{1a}/k_1 of $(64 \pm 17)\%$ determined by Butkovskaya et al. (2004) [20] over the temperature range 249–300 K and at a total pressure of 200 Torr using a high-pressure flow reactor. More recently, De Smedt et al. (2005) [23] established a branching fraction of $(64 \pm 14)\%$ at 290 K and 2 Torr for the channel (1a) using a multistage flow reactor.

In order to get insight in the $\cdot\text{OH} + \text{CH}_3\text{C}(\text{O})\text{OH}$ mechanism and to extend the pressure range, we report here a determination of the branching ratio of acetic acid oxidation by hydroxyl radicals at atmospheric conditions (296 ± 2 K and 760 Torr) in an environmental simulation chamber. For a still better understanding of the mechanism, complementary experiments using $\text{CH}_3\text{C}(\text{O})\text{OD}$ were carried out, thus allowing a comparison of the branching ratio obtained in the oxidation of the deuterated acetic acid to that obtained for the non-deuterated in the same experimental conditions.

The gas chromatography (GC) technique coupled to a Fourier transform infrared spectrometer (FTIR) was used to record acetic acid concentrations and continuous-wave cavity ring down spectroscopy (cw-CRDS) to measure CO_2 formation. The cw-CRDS analytical system was developed for the purpose to be coupled to the simulation chamber. This coupling is the first reported to our knowledge and will be described in details in the next sections.

The CRDS technique [24] is now well established as a highly sensitive way to measure weak absorption spectra. Since its discovery in 1997 [25, 26], cw-CRDS and related methods [27, 28] have been used to measure the concentration of several compounds of atmospheric relevance, as reviewed recently by Atkinson [29] and Brown [30]. The measurement of species including CH_4 , NO_2 , NO_3 , NH_3 , HCHO and CO_2 [31–36] has been demonstrated to be feasible. The detection of CO_2 at the ppm-level has also been carried out in the near-infrared range by the group of Miller [37]. The spectroscopic parameters (intensities, frequencies, etc.) of this molecule are also well known in the near infrared range [38, 39].

2 Experimental section

2.1 Experiments in the simulation chamber

Experiments were carried out in a 300 L Teflon environmental chamber enclosed in a temperature-controlled

housing and surrounded by two sets of black lamps (6 tubes Philips TMX 204 LS with emission centred on 254 nm and 6 tubes Philips TMX 200 LS with emission centred on 365 nm), distributed on both chamber sides.

Acetic acid $\text{CH}_3\text{C}(\text{O})\text{OH}$ (Acros Organics > 99%) or partly deuterated acetic acid $\text{CH}_3\text{C}(\text{O})\text{OD}$ (Acros Organics > 98% of D-atom) was introduced in the environmental chamber using a gently heated ($T \sim 330$ K) vacuum line (100 mbar) and a slight flow of purified air produced by a zero air generator (Claind 2301 HG). Initial concentrations of acetic and partly deuterated acetic acid fall in the range $(3.2 - 6.9) \times 10^{15}$ molecule cm^{-3} .

Hydroxyl radicals were produced by the photolysis of methyl nitrite (CH_3ONO) around 365 nm. CH_3ONO was synthesized using the method described by Taylor et al. [40] and kept at 255 K until use. Generally, 2 to 3 aliquots of tens of mL of gaseous CH_3ONO (resulting in CH_3ONO concentrations of about 4×10^{15} molecule cm^{-3} in the reactor) were introduced in the chamber in the course of the experiment in order to increase the $\cdot\text{OH}$ -oxidation rate of acetic acid.

Before the reaction was initiated by turning on the lights, the primary gas components were allowed to mix within the chamber for approximately one hour and several samplings of the reaction mixture were analysed in order to determine the accurate initial reactant concentration as well as to test for possible dark reactions. Negligible loss (< 2%) of acetic acid or of its d_1 -isotope has been observed. Then the bag was irradiated for two to four hours and sampling was performed at short and steady time intervals (between 15 and 30 min). After each run, the mixture was evacuated; then the bag was cleaned by flushing it with purified air for three times.

2.2 Instrumentation

Two different techniques have been used to analyse the reaction mixture. The $\text{CH}_3\text{C}(\text{O})\text{OH}$ and $\text{CH}_3\text{C}(\text{O})\text{OD}$ concentrations were determined using a GC-FTIR analytical device, whereas those of the reaction product CO_2 were measured by the cw-CRDS technique recently developed in our laboratory.

GC-FTIR. The GC-FTIR analytical device is equipped with a thermal desorption system (TCT Chrompack) allowing a 40 mL gas aliquot sampled from the photoreactor (via a sample loop) to be cryotrapped and further injected in the gas chromatographic instrument. A 50-m CP Sil 5 CB capillary column was used for the chromatographic separation combined with the following temperature program: temperature held at 50 °C during 2 min, then increased from 50 °C to 200 °C at a rate of 15 °C min^{-1} and held at 200 °C for 2 min.

Data acquisition was performed using the Omnic software (Nicolet). The Gram-Schmitt chromatogram (from the total spectral response) was built from spectra registered at steady time intervals (every 1.2 s from the average of 10 interferograms). The spectral domain of integration covers the 650 to 4000 cm^{-1} range with a resolution of 16 cm^{-1} . Functional group chromatograms were extracted from the Gram-Schmitt chromatogram in the 1600–1900 cm^{-1} spectral region (C = O band) to carry out the quantitative analysis of acetic acid.

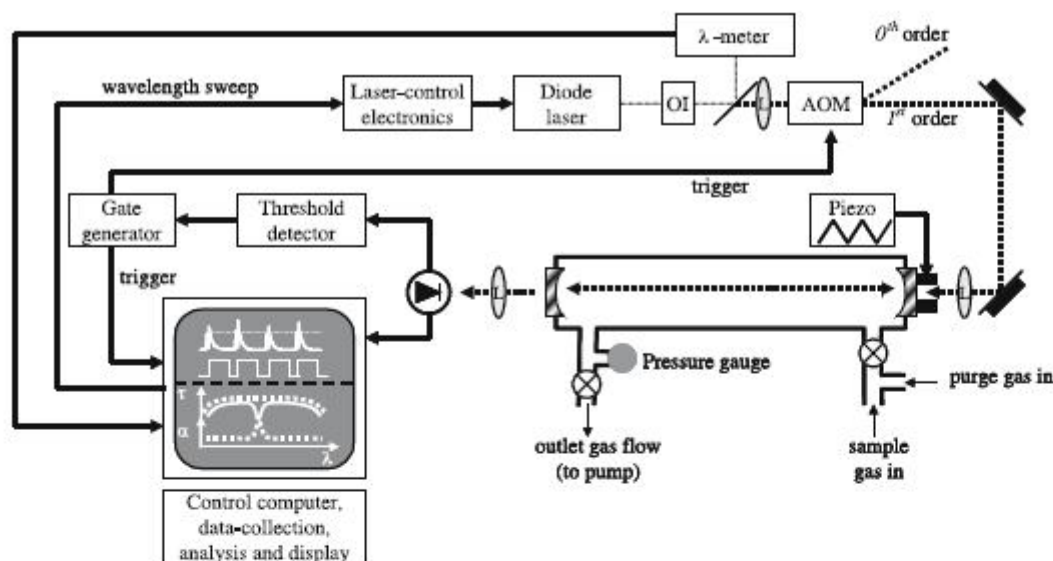


FIGURE 1 Schematic diagram of the cw-CRDS system showing the laser beam (dashed line: in fiber optic; squared line: open path) from the DFB diode laser through the high finesse cavity (absorption cell) to give the ring-down signal. Just behind the diode laser, a small fraction of the beam intensity is split off to calibrate and record the wavelength scale using a lambda-meter. OI: optical isolator; L: lens; AOM: acousto-optic modulator

cw-CRDS. Our cw-CRDS experimental apparatus is very similar to that described by Romanini et al. [26] and is illustrated in Fig. 1. It works with a cw-distributed feedback (DFB) diode laser as a light source for excitation of a high finesse optical cavity. The diode laser (NEL – NLK 1556STB) operates over the wavelength range 1569–1576 nm and generates 20 mW of laser power at the most. A fiber-coupled optical isolator (OPTIWORK – ISAD5) was placed after the laser output to reduce laser instability due to feedback into the diode laser. The laser beam was split into a zero and first order deflected beam by an acousto-optic modulator (AOM, Gooch and Housego – M040, 40 MHz), with the latter beam delivered to the ring-down cavity by a set of two mirrors. The laser beam was spatially matched to the TEM₀₀ mode of the cavity using a 30 cm focal length lens mounted on a three-dimensional translating stage. Light escaping the opposite end of the cavity was collected by a lens (focal = 5 cm) and focused onto a fast-response, near-infrared avalanche photodiode (EG&G – C30662E, 200 MHz).

For the cavity mirrors, we used a pair of dielectric coated mirrors (Layertec – A0404025) with 1 m radius of curvature and optimised for maximum reflectivity at 1570 nm. They were held within adjustable mounts, placed at a distance L of 72 cm apart on an optical breadboard and stabilised by an assembly of three Invar rods. These mirrors sealed a glass cell equipped with three ports for pressure gauge (Baratron), vacuum pumping line and gas inlets. The cavity mirrors have a reflectivity of 99.978%, which provides an effective optical absorption path length of more than 3 km.

Frequency coincidence of the cavity resonance to the laser frequency is achieved by means of a ring-shaped piezoelectric transducer (Physik Instrumente) attached to one of the

mirrors. In this way, the cavity length was continuously modulated at 50 Hz to sweep the cavity mode frequencies back and forth over one free spectral range (~ 215 MHz). Each time the transmitted light exceeds a predefined threshold indicating optimum coincidence of cavity mode and laser frequency, a trigger pulse is provided to rapidly extinguish the first-order deflected beam via the AOM, thus switching off further build-up of light intensity within the cavity. The subsequent ring-down event is captured by the detector, amplified and recorded by means of an analog-to-digital converter card (National Instrument PCI-6111, 12-bit vertical resolution) connected to a PC. The custom written LabVIEW program fitted each individual ring-down signal to single exponential functions, thus providing the decay time τ for each event. The program was also used to calculate the residual standard deviation of a group of decay rates to test the cavity stability and enable calculation of the detection sensitivity. By measuring the decay time τ_0 of the empty cell and the decay time τ of the cell containing the smog chamber sample (at reduced pressure of 40 Torr to reduce the broadening of spectral lines and thus increase the selectivity), the absorbance $\alpha(\lambda)$, and therefore the concentration can be directly determined using the following equation [41]:

$$\alpha(\lambda) = \sigma_{\text{abs}}(\lambda)[\text{abs}] = \frac{1}{c} \left(\frac{1}{\tau(\lambda)} - \frac{1}{\tau_0} \right),$$

with c the speed of light, $\sigma_{\text{abs}}(\lambda)$ the absorption cross-section at wavelength λ and $[\text{abs}]$ the concentration of the absorbent of interest.

To record a spectral line, the laser wavelength was scanned slowly across the range of interest by increasing the input voltage of the laser current driver. The laser wavelength was continuously monitored by a wavemeter (Burleigh – WA-1100).

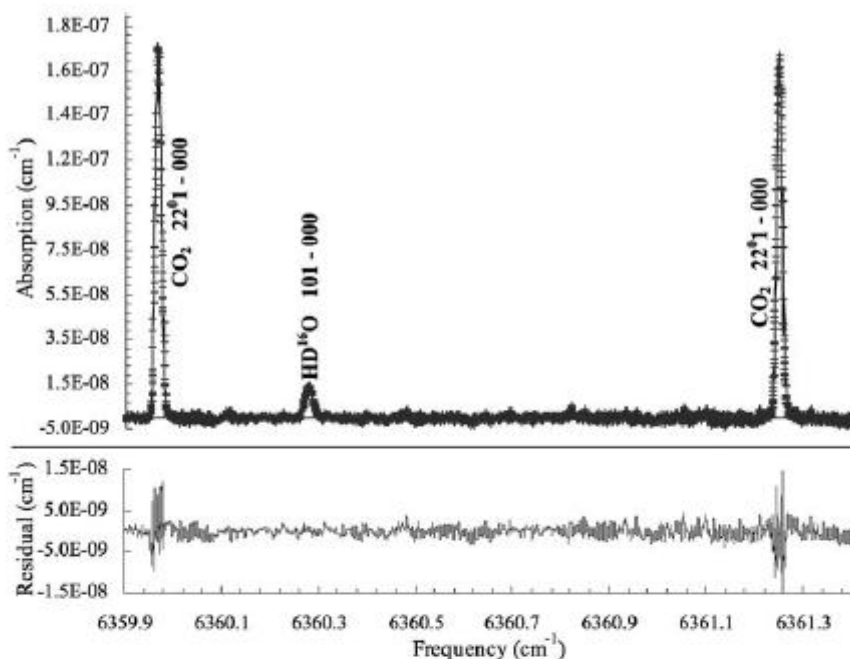


FIGURE 2 Comparison of the cw-CRDS spectrum of a sample of ambient air (pluses) at $P = 9.5$ Torr and $T = 296$ K with a simulated spectrum calculated with HITRAN 2004 data using $[\text{CO}_2] = 365$ ppmV and a relative humidity of 40% (solid line). The residual is displayed on the lower panel

2.3 Determination of the concentrations (CO_2 , CH_3COOH and CH_3COOD) and detection limits

CO_2 . For quantitative determination of the CO_2 concentrations in the photoreactor, the reaction mixture was pumped through the cavity at a flow rate of 70 mL min^{-1} using PTFE tubing.

Figure 2 shows characteristic spectral lines of CO_2 from a sample of ambient air around 6360 cm^{-1} ($\sim 1572 \text{ nm}$) obtained by cw-CRDS without any average of spectra but with an average of approximately 50 ring down events for each point on the spectrum. On the same figure, we can also see an absorption spectral line of HDO , which can prove the sensibility of the cw-CRDS technique as this species represents less than 0.03% of the water vapor content. From this measurement, the corresponding concentrations can be calculated using the database HITRAN 2004 [39,42]. Approximately 30 min are needed to scan a spectrum like that presented in Fig. 2. However, for real-time detection, it is sufficient to measure the absorption over a tighter wavelength range (less than $5 \times 10^{-3} \text{ nm}$ around the top of the spectral line). In this case, CO_2 concentrations can be determined within a few seconds. It should be pointed out that quantitative analysis does not require any calibration work: cw-CRDS directly leads to absolute concentrations, provided that the target line strength is known (from HITRAN 2004 or GEISA databases for example [42,43]). In the present work, the CO_2 absorption line at 6359.96 cm^{-1} was used with a line strength of $1.771 \times 10^{-23} \text{ cm}^{-1} \text{ molecule}^{-1} \text{ cm}^2$ [39,42] to derive the CO_2 concentration. As line strengths are given with an uncertainty of 5%, a similar uncertainty was reported on the corresponding concentration measurements.

CO_2 detection limit of our CRDS system has been calculated from the baseline noise level around 6360 cm^{-1} , by considering a signal height of three-times the noise amplitude. A detection limit of $6.6 \times 10^{13} \text{ molecule cm}^{-3}$ has been determined for CO_2 at 6359.96 cm^{-1} .

In order to evaluate the ability of our CRDS system to detect small changes in CO_2 concentrations, it was also necessary to estimate the repeatability of the measurements, as CO_2 was often present at the beginning of the experiments. The repeatability was calculated from a series of seven successive CO_2 measurements, leading to a standard deviation coefficient of 0.3%. Taking into account the uncertainties in the line strengths, the global uncertainty in CO_2 concentrations was estimated to be about 5%.

CH_3COOH and CH_3COOD . Determination of the concentrations of acetic acid and deuterated acetic acid has been performed using the thermal desorption–GC-FTIR analytical system. Calibration of the IR detector was carried out using standard solutions of these compounds in methanol. Response coefficients were obtained by plotting the area of the corresponding chromatographic peak versus the mass of the target compound at the detector. A good linearity has been obtained for both compounds.

Additional gas injections via the sample loop and the TCT injection system were carried out by sampling from the Teflon chamber filled with known amounts of acetic acid. The measured peak areas are consistent with the expected mass calculated from the concentrations of the compound in the simulation chamber. From the good agreement between the liquid and gas injections, it could be concluded that adsorption processes of acetic acid on the surface of the simulation chamber and along the Silcosteel sampling line were negligible. Un-

certainties in the quantification of acetic acids $\text{CH}_3\text{C}(\text{O})\text{OH}$ and $\text{CH}_3\text{C}(\text{O})\text{OD}$, estimated from repeated sampling from the simulation chamber and their analyses, were about 8% (2σ).

Detection limits DL were determined using a liquid standard with a concentration equal to five times the estimated DL. Seven replicate measurements of this standard were made, and the DL was calculated from the standard deviation σ of the replicate analyses as follow [44]:

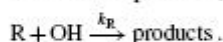
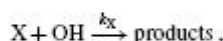
$$\text{DL} = t\sigma$$

where t is the appropriate Student's value for a 99% confidence level ($t = 3.14$). The obtained detection limits for $\text{CH}_3\text{C}(\text{O})\text{OH}$ and $\text{CH}_3\text{C}(\text{O})\text{OD}$ are 213 μg and 288 μg at the detector, which correspond, respectively, to 1.0×10^{14} and 1.3×10^{14} molecule cm^{-3} in the environmental chamber.

3 Results and discussion

3.1 $\text{CH}_3\text{C}(\text{O})\text{OH} + \cdot\text{OH}$ reaction

Determination of the rate constant. The rate constant of the $\cdot\text{OH}$ -induced oxidation of acetic acid was first determined at 296 K using the relative rate method to validate our experimental set-up. The relative method [45] is based on the simultaneous measurement of the $\cdot\text{OH}$ reaction rates of the target compound X (acetic acid in the present case) and a reference one R, the rate constant of the latter being well known and of the same order of magnitude of the investigated one.



Assuming that the reactions of the target and the reference compounds with $\cdot\text{OH}$ are the only routes of consumption of the studied compounds (photolysis processes and wall losses negligible, as checked by controlled experiments), it can be shown that:

$$\ln \frac{[\text{X}]_0}{[\text{X}]_t} = \frac{k_X}{k_R} \ln \frac{[\text{R}]_0}{[\text{R}]_t},$$

where $[\text{X}]_0$ and $[\text{R}]_0$ and $[\text{X}]_t$ and $[\text{R}]_t$ are, respectively, the concentrations of the selected compound and the reference compound at time 0 and t , and k_X and k_R the rate constants of their reaction with $\cdot\text{OH}$. A plot of $\ln([\text{X}]_0/[\text{X}]_t)$ versus $\ln([\text{R}]_0/[\text{R}]_t)$ yields a straight line with a slope of k_X/k_R .

The kinetic experiments were performed at (296 ± 2) K, using CH_3ONO as $\cdot\text{OH}$ precursor and methanol as the reference compound. The recommended value of the rate constant for the reaction of CH_3OH with $\cdot\text{OH}$ is $k_R = 9.0 \times 10^{-13}$ cm^3 molecule $^{-1}$ s $^{-1}$ with an estimated uncertainty of about 15% (1σ) [19].

Because of the high initial acetic acid concentrations employed in our experiments, the formation of the acetic acid dimer in the reaction chamber should be taken into account. The dimerization of acetic acid is a fairly well characterized process, with the preferred value for the dimerization equilibrium constant K_{eq} given as [46]:

$$K_{\text{eq}} = \frac{P_D}{P_M^2} = 7.1 \times 10^{-9} \exp\left(\frac{7705}{T}\right),$$

where P_D and P_M are, respectively, the partial pressures (in atm) of the dimer and the monomer and T is the temperature in Kelvin. At 296 K, $K_{\text{eq}} = 1432.6$ atm $^{-1}$ which is equivalent to 5.8×10^{-17} cm^3 molecule $^{-1}$ with an uncertainty of about 50%. It should be stressed that the analytical technique used in the present work to determine $\text{CH}_3\text{C}(\text{O})\text{OH}$ concentrations was not able to differentiate the dimer from the monomer (the dimer is likely decomposed into the monomer in the thermodesorption step), so that the acetic acid measured concentrations $[\text{CH}_3\text{C}(\text{O})\text{OH}]_{\text{Total}}$ were composed of the monomer and the dimer: $[\text{CH}_3\text{C}(\text{O})\text{OH}]_{\text{Total}} = [\text{monomer}] + 2[\text{dimer}]$. Combining this relation and the above equation of K_{eq} , we derived the initial concentration of the acetic acid monomer $[\text{monomer}]_0$:

$$[\text{monomer}]_0 = \frac{-1 + \sqrt{1 + 8K_{\text{eq}}[\text{CH}_3\text{C}(\text{O})\text{OH}]_{\text{Total}}}}{4K_{\text{eq}}}$$

According to Singleton et al. [22], the reaction rate constant of $\cdot\text{OH}$ radicals with the acetic acid dimer was approxi-

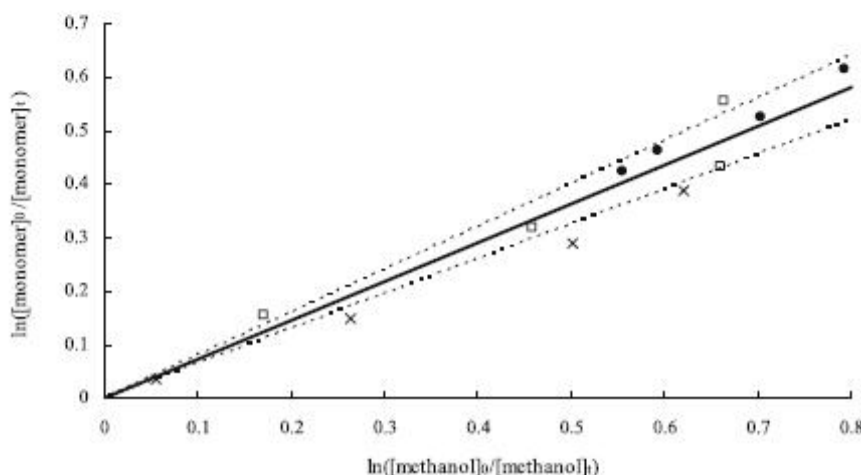


FIGURE 3 Relative rate plot for the reaction of OH with acetic acid at 296 ± 2 K using methanol as a reference compound. The different symbols represent each of the three experiments. The solid line represents the linear regression on the series of experiments and the dashed lines represent the confidence interval (2σ)

mately a hundred times less than that with the monomer ($k_{\text{dimer}} = 9.2 \times 10^{-15} \text{ cm}^3 \text{ molecule}^{-1} \text{ s}^{-1}$) at ambient temperature. Thus, we considered that the observed consumption of $\text{CH}_3\text{C}(\text{O})\text{OH}$ ($[\text{CH}_3\text{C}(\text{O})\text{OH}]_{\text{react}}$) corresponded only to the reaction of the monomer with $\cdot\text{OH}$: $[\text{CH}_3\text{C}(\text{O})\text{OH}]_{\text{react}} = [\text{monomer}]_{\text{react}}$ and $[\text{monomer}]_t = [\text{monomer}]_0 - [\text{CH}_3\text{C}(\text{O})\text{OH}]_{\text{react}}$.

Figure 3 represents the results obtained for the three experiments carried out. The resulting rate constant ratio k_1/k_R is derived from the plot of $\ln([\text{monomer}]_0/[\text{monomer}]_t)$ versus $\ln([R]_0/[R]_t)$, where R represents the methanol. A linear regression for this group of data produced a value of $k_1/k_R = 0.73 \pm 0.05$, giving a rate constant $k_1 = (6.5 \pm 0.5) \times 10^{-13} \text{ cm}^3 \text{ molecule}^{-1} \text{ s}^{-1}$ (errors are twice the standard deviation of the linear regression). This value is in very good agreement with that of Butkovskaya et al. [20] of $6.6 \times 10^{-13} \text{ cm}^3 \text{ molecule}^{-1} \text{ s}^{-1}$ and in the error limits of that recommended by Sander et al. [19] of $8.0 \times 10^{-13} \text{ cm}^3 \text{ molecule}^{-1} \text{ s}^{-1}$. This result thus tends to prove that our experimental set-up is suitable for the investigation of the branching ratio of the reaction between acetic acid and hydroxyl radicals. The good agreement of our determination of k_1 with the literature data is also a clear indication of the correctness of the equilibrium constant value K_{eq} used to determine $[\text{monomer}]_0$.

Determination of the branching ratio. The branching ratio R_1 of channel (1a) was defined as the ratio of the CO_2 formed to the $\text{CH}_3\text{C}(\text{O})\text{OH}$ consumed in reaction (1):

$$R_1 = \frac{k_{1a}}{k_{1a} + k_{1b}} = \frac{k_{1a}}{k_1} = \frac{d[\text{CO}_2]}{-d[\text{CH}_3\text{C}(\text{O})\text{OH}]} = \frac{[\text{CO}_2]_{\text{formed}}}{[\text{CH}_3\text{C}(\text{O})\text{OH}]_{\text{react}}}$$

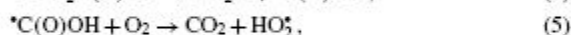
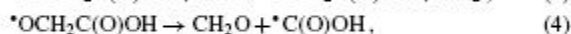
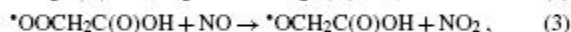
Figure 4 represents an example of the time evolutions of $[\text{CO}_2]$ and $[\text{CH}_3\text{C}(\text{O})\text{OH}]$. Before the formation of $\cdot\text{OH}$ radicals by the photolysis of CH_3ONO , both concentrations are stable; at time t_0 , CH_3ONO is injected and simultaneously $\text{CH}_3\text{C}(\text{O})\text{OH}$ starts to decrease and CO_2 to increase.

Determination of the branching ratio by the above method implies that the acetic acid consumption results only from reaction (1) and that CO_2 is only formed through channel (1a);

this assumption is discussed further on. The results are presented on Fig. 5. By averaging over all experiments, we determined the branching fraction of reaction (1a) to be $R_1 = 78 \pm 13\%$. The quoted uncertainty corresponds to the standard deviation 1σ .

The obtained branching ratios are summarised in Tables 1 and 2 together with the two values available in the literature. Even though our value is slightly higher than those obtained by Butkovskaya et al. [20] and by De Smedt et al. [23], the agreement is still good within the experimental errors. Our result also confirms former findings [22, 47, 49] on the reactivity of acid dimers (formic and acetic) compared to acid monomers, that $\cdot\text{OH}$ radicals interact mainly with the carboxylic hydrogen at ambient temperature.

The reason for the difference with the most recent investigations is not clear. First, it can be stressed that the experiments of Butkovskaya et al. [20] and De Smedt et al. [23] were carried out at low pressures (200 N₂ and 2 Torr He respectively), so that a small pressure effect on the branching ratio can be suspected. Another error source might arise from possible secondary reactions that can produce CO_2 in our reaction system. In particular, according to De Smedt et al. [23] (who referred to Peeters et al. [49] and to Olkhov et al. [50] (for reaction (5)), the pathway (1b) of the oxidation reaction could also form CO_2 in the presence of NO according to the following reaction scheme:



NO being present in our experiments due to the photolysis of CH_3ONO , the pathway (1b) could lead to the formation of CO_2 .

However, some reasons drew us to suspect that the alkoxy radical $\cdot\text{OCH}_2\text{C}(\text{O})\text{OH}$ would rather react with O_2 than decompose. First, a heat of reaction for the decomposition reaction (4) of $\Delta H_r = 51\text{--}83 \text{ kJ mol}^{-1}$ can be calculated from the heat of formation of each compound involved in the reaction: $\cdot\text{OCH}_2\text{C}(\text{O})\text{OH}$: $\Delta H_f^\circ = -(376 \pm 8) \text{ kJ mol}^{-1}$ (personal communication with Tyndall, 2005),

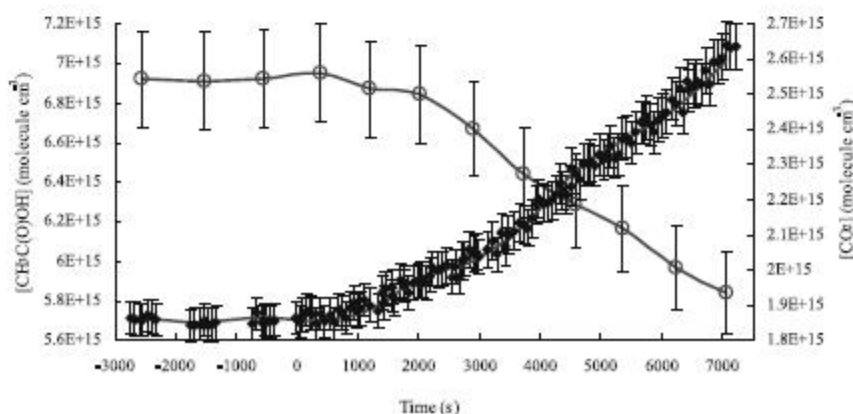


FIGURE 4 Plot of the acetic acid concentration (open circle) and CO_2 concentration (black diamond) versus reaction time. Time t_0 represents the beginning of the reaction by the photolysis of CH_3ONO and the consequent OH radical production

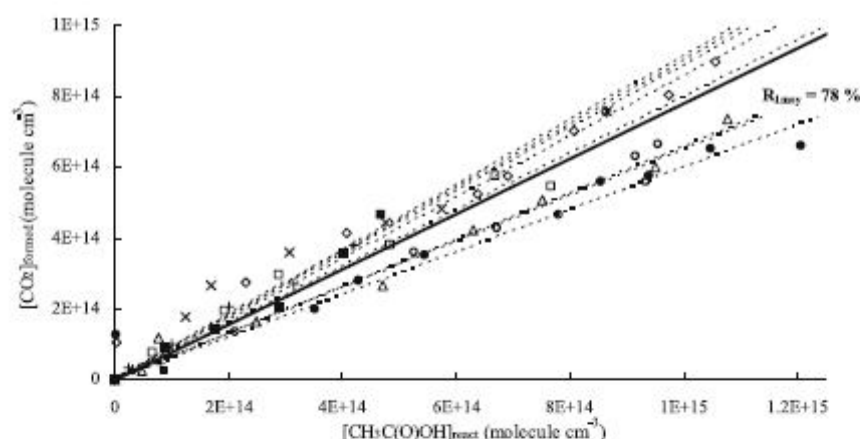
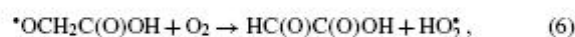


FIGURE 5 Plot of the amount of CO_2 formed against the amount of acetic acid reacted for a set of eight experiments. The *dashed lines* represent the linear regression on each experiment giving individual branching ratios and the *solid line* represents the average branching ratio

	$[\text{CH}_3\text{C}(\text{O})\text{OH}]_0$ ($\times 10^{15}$ molecule cm^{-3})	$[\text{CH}_3\text{ONO}]_0$ ($\times 10^{14}$ molecule cm^{-3})	branching fraction of channel (1a) (%)
●	6.9	24.1	60
○	5.4	99.6	65
□	5.3	57.6	80
■	3.2	1.3	89
◇	6.9	73.4	86
△	6.9	1.4	66
+	6.2	12.2	90
×	5.2	1.2	91
		mean value	78
		standard deviation	13

TABLE 1 Initial experimental conditions for the set of experiments aiming at determining the branching ratio $R_1 = k_{1a}/k_1$ for the reaction between acetic acid and OH at (296 ± 2) K and atmospheric pressure

CH_2O : $\Delta H_f^0 = -117 \text{ kJ mol}^{-1}$ [51] and $^*\text{C}(\text{O})\text{OH}$: $\Delta H_f^0 = -192 \pm 8 \text{ kJ mol}^{-1}$ [52]. So, according to the thermochemistry the reaction (4) would only be possible at higher temperature than 296 K. Secondly, Tyndall et al. [53] also reported a study of the oxidation of methyl acetate, leading to the formation of $^*\text{OCH}_2\text{C}(\text{O})\text{OCH}_3$ radicals. They found that this radical does not decompose, but reacts with O_2 to form methyl glyoxylate. Another direct piece of evidence comes from Cavalli et al. [54], who photolysed methyl bromoacetate, leading to the formation of $^*\text{OCH}_2\text{C}(\text{O})\text{OCH}_3$ radicals: they also report a preferential reaction with O_2 . Finally, it is interesting to note that we did not measure a 100% yield of CO_2 . From the thermodynamic point of view and taking into account the studies quoted above on the $^*\text{OCH}_2\text{C}(\text{O})\text{OCH}_3$ alkoxy radical reactivity, we implied that the $^*\text{OCH}_2\text{C}(\text{O})\text{OH}$ radical formed in reaction (1b) will present a similar reactivity as the $^*\text{OCH}_2\text{C}(\text{O})\text{OCH}_3$ radical and would rather react with O_2 :



to form glyoxylic acid and HO_2^* . Recently, Rosado-Reyes and Francisco (2006) [55] have performed ab-initio molecular calculations on the reaction of acetic acid with OH and have suggested that glyoxylic acid could be a major by-product of this reaction in atmospheric conditions. To test this hypothesis, we undertook complementary experiments aiming at detecting the glyoxylic acid $\text{HC}(\text{O})\text{C}(\text{O})\text{OH}$ formed in reaction (6).

In these complementary experiments, $\text{CH}_3\text{C}(\text{O})\text{OH}$ and $^*\text{OH}$ have been left to react for 2 h, and after switching off the lamps, the reaction mixture was collected using a liquid trap: 50 mL of 10% CH_3OH in water was placed in a glass bubbler connected to a Teflon line. The reaction mixture was flown through the liquid at 500 mL min^{-1} . To minimise evaporation losses, the bubbler was placed in ice water. Analysis of the solution was achieved using ionic chromatography (DIONEX equipped with a AS11-HC column) coupled to conductime-

T (K)	P (Torr)	branching ratio (%)	reference	method
249–298	200	64 ± 17	Butkovskaya et al. (2004)	high-pressure turbulent flow reactor – $[\text{CO}_2]$ determination by chemical ionization mass spectrometer
290	2	64 ± 14	De Smedt et al. (2005)	multistage fast-flow reactor – $[\text{CO}_2]$ determination by molecular beam sampling mass spectrometer
296 ± 2	760	78 ± 13	this work	atmospheric smog chamber – $[\text{CO}_2]$ determination by cw-CRDS at 6359.96 cm^{-1}

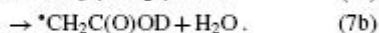
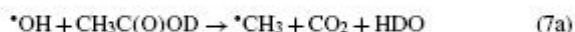
TABLE 2 Branching ratio of the reaction between $\text{CH}_3\text{C}(\text{O})\text{OH}$ and OH radicals

try detection. The elution solution consists of a concentration gradient of 1 mM of NaOH (2% MeOH) and 60 mM of NaOH (10% MeOH) flowing at 1.5 mL min⁻¹; the regeneration was obtained with a H₂SO₄ 25 mM aqueous solution.

Glyoxylic acid was clearly identified and his presence in the liquid trap solution confirmed by the standard addition method. Possible interferences with other compounds of the mixture have been examined: the glyoxalate ion does not interfere with acetate, formate, nitrates, carbonates or nitrites ions. If a collection efficiency of 100% and good linearity of the method were supposed, a formation of glyoxylic acid corresponding to a yield of approximately 10% of the consumed acetic acid can be determined. This yield is the more consistent with the branching ratio of $R_1 = 78\%$ obtained previously since possible HC(O)C(O)OH wall losses (in the photoreactor or during the sampling) and reaction with $\cdot\text{OH}$ were not taken into account in this estimation. We conclude that our results strongly support the assumption that the $\cdot\text{OCH}_2\text{C(O)OH}$ radical formed in reaction (1b) should react with O₂ and form glyoxylic acid.

3.2 CH₃C(O)OD + $\cdot\text{OH}$ reaction

H-atom abstraction from the acid group being the major reaction path, a difference in the branching ratios of the reactions of CH₃C(O)OH and CH₃C(O)OD with $\cdot\text{OH}$ can be expected due to the kinetic isotope effect (KIE):



The cw-CRDS instrument developed for the present study allowed us to measure CO₂ concentrations. The branching ratio

R_7 of the pathway (7a) is thus determined by measuring the concentration ratio of the CO₂ formed ($[\text{CO}_2]_{\text{formed}}$) to the CH₃C(O)OD reacted ($[\text{CH}_3\text{C(O)OD}]_{\text{react}}$):

$$R_7 = \frac{k_{7a}}{k_{7a} + k_{7b}} = \frac{k_{7a}}{k_7} = \frac{[\text{CO}_2]_{\text{formed}}}{[\text{CH}_3\text{C(O)OD}]_{\text{react}}} = \frac{[\text{HDO}]_{\text{formed}}}{[\text{CH}_3\text{C(O)OD}]_{\text{react}}}$$

The initial conditions and corresponding obtained branching ratios are summarised in Table 3. The results are displayed on Fig. 6 by reporting $[\text{CO}_2]_{\text{formed}}$ versus $[\text{CH}_3\text{C(O)OD}]_{\text{react}}$. A branching ratio $R_7 = (36 \pm 7)\%$ was determined. To our knowledge, this study represents the first determination of the branching ratio of the CO₂-forming pathway in the $\cdot\text{OH} + \text{CH}_3\text{C(O)OD}$ reaction. As expected for an H-atom abstraction reaction, the branching ratio R_7 for the reaction channel (7a) is smaller than that obtained for the non-deuterated acetic acid, and supports a strong primary kinetic isotope effect in the $\cdot\text{OH} + \text{CH}_3\text{C(O)OH}$ reaction. Singleton et al. [22] investigated the rate constants of the reactions of $\cdot\text{OH}$ radicals with CH₃C(O)OH, CD₃C(O)OH and CD₃C(O)OD between 297 K and 444 K and observed roughly equal rates between $\cdot\text{OH} + \text{CH}_3\text{C(O)OH}$ and $\cdot\text{OH} + \text{CD}_3\text{C(O)OH}$. They quoted furthermore “the large kinetic isotope effect observed when the carboxylic but not the alkyl hydrogen is substituted by deuterium”, for example in the case of CD₃C(O)OH and CD₃C(O)OD. It should be emphasized that a large KIE was also observed for the formic acid when substituting a deuterium in the carboxylic group [48].

As mentioned in the experimental part, HDO could easily be detected at 6360.3 cm⁻¹, as well as around 6809 cm⁻¹.

		[CH ₃ C(O)OD] ₀ (×10 ¹⁵ molecule cm ⁻³)	[CH ₃ ONO] ₀ (×10 ¹⁴ molecule cm ⁻³)	branching fraction of channel (7a) (%)
CO ₂ formation	○	5.4	57.6	28
	●	3.6	42.1	34
	△	1.2	69.1	45
	■	3.2	1.3	28
	×	5.2	1.2	42
				mean value 36 standard deviation 7

TABLE 3 Experimental conditions and corresponding branching ratios for the oxidation of CH₃C(O)OD by OH radicals at (296 ± 2) K and atmospheric pressure

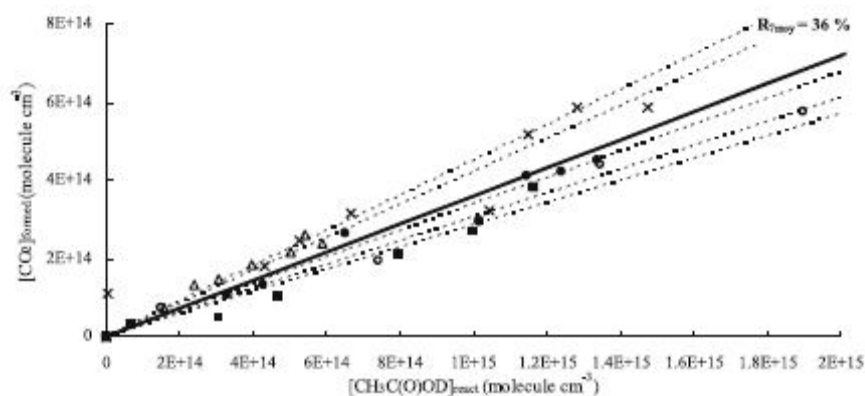


FIGURE 6 Plot of the amount of CO₂ formed against the amount of deuterated acetic acid reacted for a set of five experiments. The dashed lines represent the individual branching ratios and the solid lines the average branching ratios

The branching ratio R_7 of the pathway (7a) could thus also be determined by measuring the concentration ratio of the HDO formed ($[HDO]_{\text{formed}}$) to the $CH_3C(O)OD$ reacted. Additional experiments were then performed where both CO_2 and HDO were monitored. Consistent results were obtained when measuring HDO at 6809 cm^{-1} ($R_7 \approx 35\%$), but much smaller branching ratios were deduced from the measurements of HDO at 6360.3 cm^{-1} ($R_7 \approx 10\%$). This discrepancy could be attributed either to experimental complications or to uncertainties in the line strengths. Further experiments are in progress to resolve this disagreement.

4 Conclusion

A sensitive cw-CRDS apparatus in the near IR has been successfully built and coupled to a smog chamber to get new insights in the degradation mechanisms of atmospheric relevant organic compounds. The first study using this set-up has been devoted to the determination of the branching ratio of the $^{\bullet}OH$ oxidation reactions of $CH_3C(O)OH$ and $CH_3C(O)OD$ at atmospheric pressure and room temperature: branching fractions of $(78 \pm 13)\%$ and $(36 \pm 7)\%$ have been obtained for both acids, respectively. Glyoxylic acid has been detected for the first time as product of the pathway (1b).

Many interesting species, especially small isotopic molecules like $^{13}CO_2$, $H_2^{18}O$ and HDO can be observed in this chemical fingerprint spectral region, which can be very useful in the determination of reaction mechanisms. Possible future applications include in-situ investigation of reactions by following transient species such as HO_2^{\bullet} or $CH_3C(O)O_2^{\bullet}$ radicals [56, 57]. Advantages of using CRDS include high sensitivity ($\approx 2 \times 10^{-8}\text{ cm}^{-1}$ for our scheme but the highest sensitivity achieved using CRDS is $1 \times 10^{-12}\text{ cm}^{-1}\text{ Hz}^{-1/2}$) and rapidity of the measurement.

ACKNOWLEDGEMENTS The authors are deeply grateful to Mr. Thierry Leonardis and Dr. Olivier Briand from the Ecole des Mines de Douai and to Dr. Daniele Romanini from the Laboratoire de Spectrométrie Physique de Grenoble for their contributions to this work and their most helpful advice. Moreover, this work is jointly supported by the Nord-Pas de Calais region in the frame of the "Contrat de Plan Etat-Région, air quality axis", by the CNRS (Centre National de la Recherche Scientifique) in the frame of the "Programme National de Chimie Atmosphérique", by the CERLA (Centre d'Etudes et de Recherches Lasers et Applications - FR CNRS 2416), by the French Research Ministry and by the European funds for Regional Economic Development (FEDER). Sabine Crunaire gratefully acknowledges the financial support from the Ecole des Mines de Douai.

REFERENCES

- H.B. Singh, M. Kanakidou, P.J. Crutzen, D.J. Jacob, *Nature* 378, 50 (1995)
- M. Narukawa, K. Kawamura, S.M. Li, J.W. Bottenheim, *Atmos. Environ.* 36, 2491 (2002)
- M. Ryhl-Svendsen, J. Glasstrup, *Atmos. Environ.* 36, 3909 (2002)
- X. Yao, M. Fang, C.K. Chan, K.F. Ho, S.C. Lee, *Atmos. Environ.* 38, 963 (2004)
- A. Mellouki, G. Le Bras, H. Sidebottom, *Chem. Rev.* 103, 5077 (2003)
- G.C. Pratt, K. Palmer, C.Y. Wu, F. Ollaei, C. Hollerbach, M.J. Fenske, *Environ. Health Persp.* 108, 815 (2000)
- A. Chebbi, P. Carlier, *Atmos. Environ.* 30, 4233 (1996)
- P. Khare, N. Kumar, K.M. Kumari, S.S. Srivastava, *Rev. Geophys.* 37, 227 (1999)
- D. Grosjean, *Atmos. Environ.* 26, 3279 (1990)
- J.N. Galloway, G.E. Liens, W.C. Keene, J.M. Miller, *J. Geophys. Res.* 87, 8771 (1982)
- X. Lee, D. Qin, G. Jiang, H. Zhou, *Cold Reg. Sci. Technol.* 34, 127 (2002)
- NTP 2003, National Toxicology Program, available at <http://ntp.niehs.nih.gov/8080/index.html>
- K. Granby, C.S. Christensen, C. Lohse, *Atmos. Environ.* 31, 1403 (1997)
- K. Granby, A.H. Egekv, T. Nielsen, C. Lohse, *J. Atmos. Chem.* 28, 195 (1997)
- G.S. Tyndall, R.A. Cox, C. Granier, R. Lescaux, G.K. Moortgat, M.J. Pilling, A.R. Ravishankara, T.J. Wallington, *J. Geophys. Res.* 106, 12157 (2001)
- R. Atkinson, *J. Arey, Chem. Rev.* 103, 4605 (2003)
- E.J. Feltham, M.J. Almond, G. Marston, V.P. Ly, K.S. Wiltshire, *Spectrochim. Acta A* 56, 2605 (2000)
- E.D. Baboukas, M. Kanakidou, N. Mihalopoulos, *J. Geophys. Res.* 105, 14459 (2000)
- S.P. Sander, R.R. Friedl, D.M. Golden, M.J. Kurylo, R.E. Huie, V.L. Orkin, G.K. Moortgat, A.R. Ravishankara, C.E. Kolb, M.J. Molina, B.J. Finlayson-Pitts, *Chemical Kinetics and Photochemical Data for Use in Stratospheric Studies*, Evaluation No. 14 (JPL Publication 02-25, Pasadena, CA, 2003)
- N.I. Butkovskaya, A. Kukui, N. Pourveste, G. Le Bras, *J. Phys. Chem. A* 108, 7021 (2004)
- D.E. Heard, M.J. Pilling, *Chem. Rev.* 103, 5163 (2003)
- D.L. Singleton, G. Paraskevopoulos, R.S. Irwin, *J. Am. Chem. Soc.* 111, 5248 (1989)
- F. De Smedt, X.V. Bui, T.L. Nguyen, J. Peeters, L. Vereecken, *J. Phys. Chem. A* 109, 2401 (2005)
- A. O'Keefe, D.A.G. Deacon, *Rev. Sci. Instrum.* 59, 2544 (1988)
- D. Romanini, A.A. Kachanov, N. Sadeghi, F. Stoeckel, *Chem. Phys. Lett.* 264, 316 (1997)
- D. Romanini, A.A. Kachanov, F. Stoeckel, *Chem. Phys. Lett.* 270, 538 (1997)
- A. O'Keefe, *Chem. Phys. Lett.* 293, 331 (1998)
- J.B. Paul, L. Lapson, J.G. Anderson, *Appl. Opt.* 40, 4904 (2001)
- D.B. Atkinson, *Analyst* 128, 117 (2003)
- S.S. Brown, *Chem. Rev.* 103, 5219 (2003)
- B.L. Fawcett, A.M. Parke, D.E. Shallcross, A.J. Orr-Ewing, *Phys. Chem. Chem. Phys.* 4, 5960 (2002)
- M.I. Mazurenka, B.L. Fawcett, J.M.F. Elks, D.E. Shallcross, A.J. Orr-Ewing, *Chem. Phys. Lett.* 367, 1 (2003)
- M.D. King, E.M. Dick, W.R. Simpson, *Atmos. Environ.* 34, 685 (2000)
- R. Claps, F.V. Englich, D.P. Leleux, D. Richter, F.K. Tittel, R.F. Curl, *Appl. Opt.* 40, 4387 (2001)
- H. Barry, L. Corner, G. Hancock, R. Peverall, G.A. D. Ritchie, *Phys. Chem. Chem. Phys.* 4, 445 (2002)
- A.S.C. Cheung, T. Ma, H. Chen, *Chem. Phys. Lett.* 353, 275 (2002)
- A.R. Awatry, J.H. Miller, *Appl. Phys. B* 75, 255 (2002)
- Z. Majcherova, P. Macko, D. Romanini, V.I. Perevalov, S.A. Tashkun, J.L. Teffo, A. Campargue, *J. Mol. Spectrosc.* 230, 1 (2005)
- L.S. Rothman, D. Jacquemart, A. Barbe, D. Chris Benner, M. Birk, L.R. Brown, M.R. Carleer, C. Chackerian Jr., K. Chance, V. Dana, V.M. Devi, J.M. Flaud, R.R. Gamache, A. Goldman, J.M. Hartmann, K.W. Jucks, A.G. Maki, J.Y. Mandin, S.T. Massie, J. Orphal, A. Perrin, C.P. Rinsland, M.A.H. Smith, J. Tennyson, R.N. Tolchenov, R.A. Toth, J. Vander Auwera, P. Varanasi, G. Wagner, *J. Quantum Spectrosc. Radiat. Transf.* 96, 139 (2005)
- W.D. Taylor, T.D. Allston, M.J. Moscato, G.B. Fazekas, R. Kozlowski, G.A. Takacs, *Int. J. Chem. Kinet.* 12, 231 (1980)
- G. Berden, R. Peeters, G. Meijer, *Int. Rev. Phys. Chem.* 19, 565 (2000)
- HITRAN 2004, available at <http://www.hitran.com>
- GEISA 2003, available at <http://ara.lmd.polytechnique.fr>
- W.A. McClenny, J.D. Pleil, G.F. Evans, K.D. Oliver, M.W. Holdren, W.T. Winberry, *J. Air Waste Manage.* 41, 1308 (1991)
- R. Atkinson, W.P.L. Carter, A.M. Winer, J.N. Pitts, *J. Air Waste Manage.* 31, 1090 (1981)
- J. Chao, B.J. Zwolinski, *J. Phys. Chem. Ref. Data* 7, 363 (1978)
- G.S. Jolly, D.J. McKenney, D.L. Singleton, G. Paraskevopoulos, A.R. Bossard, *J. Phys. Chem.* 90, 6557 (1986)
- D.L. Singleton, G. Paraskevopoulos, R.S. Irwin, G.S. Jolly, D.J. McKenney, *J. Am. Chem. Soc.* 110, 7786 (1988)
- J. Peeters, G. Fantechi, L. Vereecken, *J. Atmos. Chem.* 48, 59 (2004)
- R.V. Oikhov, Q. Li, M.C. Osborne, I.W.M. Smith, *Phys. Chem. Chem. Phys.* 3, 4522 (2001)
- M.W. Chase Jr., *J. Phys. Chem. Ref. Data* 9, 1 (1998)
- Y. He, B.J. Orr, *Chem. Phys. Lett.* 319, 131 (2000)

- 53 G.S. Tyndall, A.S. Pimentel, T.J. Orlando, *J. Phys. Chem. A* **108**, 6850 (2004)
- 54 F. Cavalli, I. Barnes, K.H. Becker, T.J. Wallington, *J. Phys. Chem. A* **104**, 11 310 (2000)
- 55 M. Rosado-Reyes, J.S. Francisco, *J. Phys. Chem. A* **110**, 4419 (2006)
- 56 D.B. Atkinson, J.L. Spillman, *J. Phys. Chem. A* **106**, 8891 (2002)
- 57 S.J. Zalyubovsky, B.G. Glover, T.A. Miller, *J. Phys. Chem. A* **107**, 7704 (2003)

Publication n°6
(parue dans la revue *Reaction Kinetics and Catalysis Letters* en 2009)

RKCL5511

KINETICS OF THE $^{\bullet}\text{OH}$ -RADICAL INITIATED REACTIONS OF ACETIC ACID AND ITS DEUTERATED ISOMERS

Emese Szabó^{a,b,c,d}, Jérémy Tarmoul^{a,b,d}, Alexandre Tomas^{a,b,*},
Christa Fittschen^d, Sándor Dóbe^c and Patrice Coddeville^{a,b}

^a Université Lille Nord de France, F-59508 Douai, France

^b École des Mines de Douai, Département Chimie-Environnement, BP 10838, F-59508 Douai, France

^c Chemical Research Center, Hungarian Academy of Sciences, H-1525 Budapest, Hungary

^d Laboratoire de Physico-Chimie des Processus de Combustion et de l'Atmosphère - CNRS UMR 8522, Université des Sciences et Technologies de Lille, F-59655 Villeneuve d'Ascq, France

Received January 05, 2009, in revised form January 20, 2009, accepted January 21, 2009

Abstract

Kinetics of the $^{\bullet}\text{OH}$ -initiated reactions of acetic acid and its deuterated isomers have been investigated performing simulation chamber experiments at $T = 300 \pm 2$ K. The following rate constant values have been obtained ($\pm 1\sigma$, in $\text{cm}^3 \text{molecule}^{-1} \text{s}^{-1}$): $k_1(\text{CH}_3\text{C}(\text{O})\text{OH} + ^{\bullet}\text{OH}) = (6.3 \pm 0.9) \times 10^{-13}$, $k_2(\text{CH}_3\text{C}(\text{O})\text{OD} + ^{\bullet}\text{OH}) = (1.5 \pm 0.3) \times 10^{-13}$, $k_3(\text{CD}_3\text{C}(\text{O})\text{OH} + ^{\bullet}\text{OH}) = (6.3 \pm 0.9) \times 10^{-13}$, and $k_4(\text{CD}_3\text{C}(\text{O})\text{OD} + ^{\bullet}\text{OH}) = (0.90 \pm 0.1) \times 10^{-13}$. This study presents the first data on $k_2(\text{CH}_3\text{C}(\text{O})\text{OD} + ^{\bullet}\text{OH})$. Glyoxylic acid has been detected among the products confirming the fate of the $^{\bullet}\text{CH}_2\text{C}(\text{O})\text{OH}$ radical as suggested by recent theoretical studies.

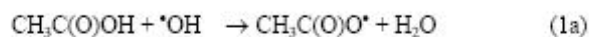
Keywords: Acetic acid, KIE, OH kinetics, glyoxylic acid

INTRODUCTION

Acetic acid ($\text{CH}_3\text{C}(\text{O})\text{OH}$) is one of the most abundant acid species in the atmosphere. As a ubiquitous compound, it has been detected both in the gaseous and condensed phases in the troposphere and up to the Upper Troposphere – Lower Stratosphere [1]. The reaction kinetics of the reaction between $\text{CH}_3\text{C}(\text{O})\text{OH}$ and the $^{\bullet}\text{OH}$ radical has been investigated in substantial detail in the past few years as it has been discussed in a recent feature article [2]. Below

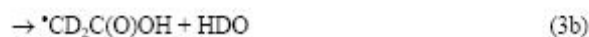
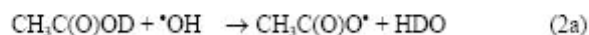
* Corresponding author. E-mail: tomas@ensm-douai.fr

~ 500 K, the rate constant presents a slightly negative temperature dependence, while above ~ 600 K, it was found to display a very sharp increase with temperature [3,4]. With the aid of quantum chemical computations, this characteristic behaviour was attributed to the formation of a pre-reactive complex between $\cdot\text{OH}$ and $\text{CH}_3\text{C}(\text{O})\text{OH}$ stabilized at low temperature and to a change in the reaction mechanism when going to higher temperatures. Concerning the reaction mechanism, $\cdot\text{OH}$ radicals are expected to react with $\text{CH}_3\text{C}(\text{O})\text{OH}$ through two H-abstraction pathways:



Contrary to what can be expected from bond dissociation energies, the dominant channel of reaction (1) has been found to be the acidic H-abstraction (channel (1a)), with a branching ratio k_{1a}/k_1 varying from 64% to 78% [4-6] around 300 K. Literature data on the $\cdot\text{OH}$ -initiated reactions of the deuterated acetic acids are very sparse [6-8], although such data would be useful for a better understanding of the reaction mechanism and in this way for assessing the impact of acetic acid on the chemistry of the atmosphere.

In this letter, we present new kinetic data on the reactions of $\cdot\text{OH}$ radicals with acetic acid and its deuterated isomers $\text{CD}_3\text{C}(\text{O})\text{OH}$, $\text{CH}_3\text{C}(\text{O})\text{OD}$ and $\text{CD}_3\text{C}(\text{O})\text{OD}$. The aim of the present study has been to propose rate constants for the four reactions under similar experimental conditions allowing direct comparison and an assessment of mechanistic features. The deuterated isotopes of acetic acid are expected to react with $\cdot\text{OH}$ also via two types of hydrogen (deuterium) abstraction reactions:

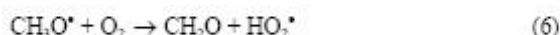
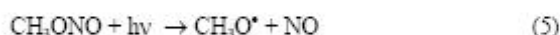


The rate constant of each reaction has been determined at laboratory temperature, with k_2 being determined for the first time, to our knowledge. In the following discussions, *AA* is used as a general abbreviation for all of the four acetic-acid isomers studied, while *d₀-AA*, *d₁-AA*, *d₂-AA*, and *d₃-AA* designate CH₃C(O)OH, CH₃C(O)OD, CD₃C(O)OH and CD₃C(O)OD, respectively.

EXPERIMENTAL

All experiments were performed using a 250 L Teflon environmental chamber. Since the experimental set-up and procedure have been described in detail in previous studies [6, 9], only the main features are presented here.

The acetic acid reactant and the reference compound were introduced into a synthetic air flow and flushed into the reactor. Methyl nitrite (CH₃ONO), used as OH precursor, was synthesised following the classical procedure [10] and stored at -30°C. It was introduced either in large quantities (up to 200 mL) at time zero, or in smaller portions (about 20 mL) every 30 min during the experiment. No difference could be observed in the results applying the two procedures. The primary gas components were allowed to mix in the chamber for about one hour before the reaction was initiated by turning on the lamps; the initial concentrations are listed in Table 1. Photolytic irradiation arising from 8 actinic lamps (300 nm < λ < 450 nm) initiated the reaction sequence by the photolysis of CH₃ONO:



The acetic acid and the reference compound were regularly measured during the reaction with gas-chromatography (GC-FID) by sampling 20 mL gas aliquots from the photoreactor followed by flash injection through a thermodesorption system (Chrompack TCT).

The kinetics of the reactions were investigated using the relative rate method. In this method, the organic reactant (*OC*) is present in the reactor along with a reference compound (*ref*) which reacts with $^\bullet\text{OH}$ at a similar rate:

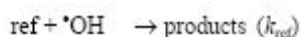
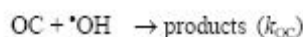


Table 1
Experimental conditions and results

Reaction (i)	Reactant	No. of Expts.	$[AA]_0$ (molecule cm^{-3})	$[ref]_0^a$ (molecule cm^{-3})	$k_i/k_{ref} \pm 1\sigma$	$(k_i \pm 1\sigma \times 10^{13})$ ($\text{cm}^3 \text{ molecule}^{-1} \text{ s}^{-1}$)
(1)	$\text{CH}_3\text{C}(\text{O})\text{OH}$	2	$(0.5-2) \times 10^{15}$	$(0.3-1.5) \times 10^{15}$	0.70 ± 0.10	6.3 ± 0.9
(2)	$\text{CH}_3\text{C}(\text{O})\text{OD}$	3	$(0.5-2) \times 10^{15}$	$(0.5-2) \times 10^{15}$	0.46 ± 0.08	1.5 ± 0.3
(3)	$\text{CD}_3\text{C}(\text{O})\text{OH}$	2	$(0.5-2) \times 10^{15}$	$(0.3-1.5) \times 10^{15}$	0.70 ± 0.10	6.3 ± 0.9
(4)	$\text{CD}_3\text{C}(\text{O})\text{OD}$	4	$(0.5-2) \times 10^{15}$	$(0.5-2) \times 10^{15}$	0.28 ± 0.04	0.90 ± 0.10

^a The reference compound, *ref*, is CH_3OH for reactions (1) and (2) and CD_3OD for reactions (3) and (4)

Assuming that the reactions with $\cdot\text{OH}$ are the only consumption reactions for the target and the reference compounds, the following simple rate equation is obtained:

$$\ln \frac{[OC]_0}{[OC]_t} = \frac{k_{OC}}{k_{ref}} \times \ln \frac{[ref]_0}{[ref]_t} \quad (\text{I})$$

where $[ref]_0$ and $[OC]_0$ and $[ref]_t$ and $[OC]_t$ are the concentrations of the reference and target molecules at time 0 and time t , respectively. Therefore, a plot of $\ln([OC]_0/[OC]_t)$ versus $\ln([ref]_0/[ref]_t)$ should yield a straight line with a slope of k_{OC}/k_{ref} . In our experiments, *OC* corresponds, e. g., to acetic acid and *ref* to methanol.

Prior to the regular experiments, test runs were carried-out in the absence of CH_3ONO : photolysis processes and wall losses were found negligible in the reaction system. Dimers of *AA* are expected to be formed in the gas phase through weak H- (or D-) bonds. Chao and Zwolinski [11], reviewing thermodynamic data for formic- and acetic acids, have proposed the following equilibrium constant, K_{eq} , for the dimerization reaction of $\text{CH}_3\text{C}(\text{O})\text{OH}$:

$$K_{eq} = \frac{P_D}{P_M^2} = 7.1 \times 10^{-9} \exp\left(\frac{7705}{T}\right) \quad (\text{II})$$

where P_D and P_M are the partial pressures (in atm) of the dimer and the monomer at temperature T (in K), respectively, giving $K_{eq} = 1012.5 \text{ atm}^{-1}$ at 300 K. Re-arrangement of equation (II) and taking into account that the measured acetic acid concentration is $[AA]_{total} = 2 \times [AA]_{monomer} + [AA]_{dimer}$ yield the following equation:

$$[AA]_{monomer} = \frac{-1 + \sqrt{1 + 8 \times K_{eq} \times [AA]_{total}}}{4 \times K_{eq}} \quad (\text{III})$$

As it has been discussed by Singleton *et al.* [7], the dimer reacts with a much slower rate with OH radicals than the monomer does. In addition, considering the concentrations of AA used under the conditions of the present study (see Table 1), the dimer represented at the most 15% of the total AA concentration. In order to take into account the dimer formation, the initial monomer concentration $[AA]_{monomer,0}$ was calculated according to equation (III) from $[AA]_{total,0}$ while $[AA]_{monomer,t}$ was obtained from $[AA]_{monomer,t} = [AA]_{monomer,0} - ([AA]_{total,0} - [AA]_{total,t})$. That is, we have assumed that the dimer does not react with $\cdot\text{OH}$. In the following considerations, $[AA]_{monomer,0}$ and $[AA]_{monomer,t}$ are designated simply as $[AA]_0$ and $[AA]_t$. For the deuterated acetic acid isomers, the same K_{eq} as used for acetic acid was assumed in the absence of other information.

Acetic acid (96%, Merck), acetic acid- d_1 (98% D, Acrôs Organics), acetic acid- d_2 (99.2% D, CDN Isotopes), acetic acid- d_4 (99.91% D, Euriso-top), methanol (99.9%, Merck) and methanol- d_4 (99.80% D, Euriso-top) were used as obtained.

RESULTS AND DISCUSSION

The kinetics of reactions (1) – (4) have been investigated at $T = (300 \pm 2) \text{ K}$ and atmospheric pressure using the relative rate method as described in the experimental section. The reference compounds were *methanol* (for the kinetic study of $\text{CH}_3\text{C}(\text{O})\text{OH}$ and $\text{CD}_3\text{C}(\text{O})\text{OH}$) and *methanol- d_4* (for $\text{CH}_3\text{C}(\text{O})\text{OD}$ and $\text{CD}_3\text{C}(\text{O})\text{OD}$). The experimental conditions and results have been summarised in Table 1. Representative plots of $\ln([AA]_0/[AA]_t)$ against $\ln([ref]_0/[ref]_t)$ are shown in Figs 1 and 2. The acetic acid isomers d_0 -AA ($\text{CH}_3\text{C}(\text{O})\text{OH}$) and d_2 -AA ($\text{CD}_3\text{C}(\text{O})\text{OH}$) present identical rate constant ratios: $k_1/k_{meth} = 0.70 \pm 0.10$ and $k_3/k_{meth} = 0.70 \pm 0.10$, while rate constant ratios for d_1 -AA ($\text{CH}_3\text{C}(\text{O})\text{OD}$) and d_4 -AA ($\text{CD}_3\text{C}(\text{O})\text{OD}$) differ by a factor of 1.6: $k_2/k_{meth-d_4} = 0.46 \pm 0.08$ and $k_4/k_{meth-d_4} = 0.28 \pm 0.04$. Using the recommended $\text{CH}_3\text{OH} + \text{OH}$ rate constant, $k_{meth} = 9.0 \times 10^{-13} \text{ cm}^3 \text{ molecule}^{-1} \text{ s}^{-1}$ [12], the respective rate constant ratios

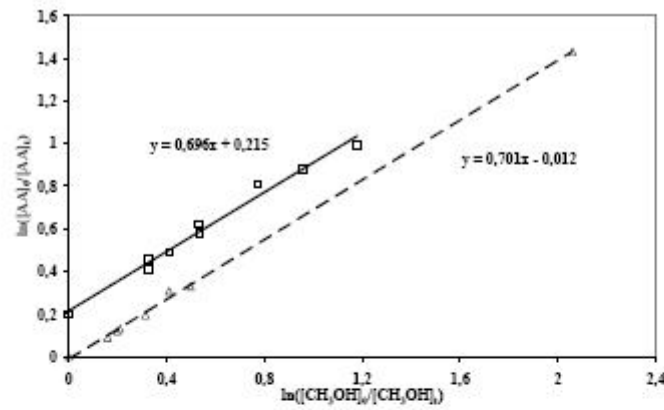


Fig. 1. Typical plots of $\ln([AA]_0/[AA])$ versus $\ln([CH_3OH]_0/[CH_3OH])$ for $AA = CH_3C(O)OH$ (squares) and $CD_3C(O)OH$ (triangles). The straight lines correspond to a linear regression on the experimental data. The $\ln([AA]_0/[AA])$ data for $CH_3C(O)OH$ have been shifted by + 0.2 for clarity

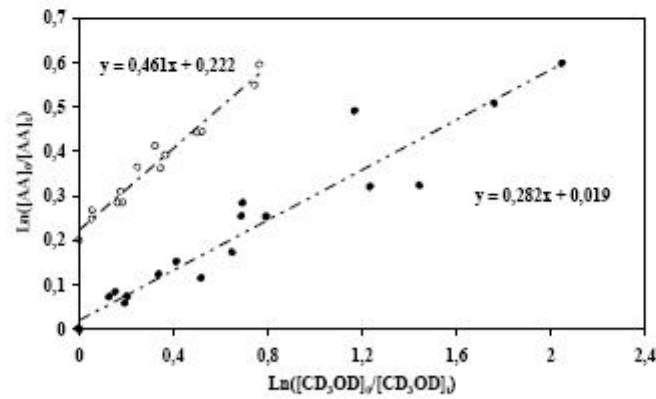


Fig. 2. Typical plots of $\ln([AA]_0/[AA])$ against $\ln([CD_3OD]_0/[CD_3OD])$ for $AA = CH_3C(O)OD$ (circles) and $CD_3C(O)OD$ (full circles). The straight lines correspond to a linear regression on the experimental data. The $\ln([AA]_0/[AA])$ data for $CH_3C(O)OD$ have been shifted by + 0.2 for clarity

translate to the absolute values of $k_1 = (6.3 \pm 0.9) \times 10^{-13}$ and $k_3 = (6.3 \pm 0.9) \times 10^{-13} \text{ cm}^3 \text{ molecule}^{-1} \text{ s}^{-1}$. For the $\text{CD}_3\text{OD} + \text{OH}$ rate constant, we took the very recent determination of Parker *et al.* [13]: $k_{\text{meth-}d4} = 3.2 \times 10^{-13} \text{ cm}^3 \text{ molecule}^{-1} \text{ s}^{-1}$ (which is in excellent agreement with Wallington *et al.* [14]: $3.23 \times 10^{-13} \text{ cm}^3 \text{ molecule}^{-1} \text{ s}^{-1}$; the other measurement by McCaulley *et al.* [15]: 1.93×10^{-13} appears much lower). The resulting k_2 and k_4 rate constants are: $k_2 = (1.5 \pm 0.3) \times 10^{-13}$, and $k_4 = (0.90 \pm 0.1) \times 10^{-13} \text{ cm}^3 \text{ molecule}^{-1} \text{ s}^{-1}$. Quoted uncertainties (1 \square) have been estimated by the statistical errors of the sampling procedure ($\sim 10\%$). They do not include the uncertainties in the reference rate constants, which are estimated to be about 15% for the methanol + OH reaction [12] and at least 30% for the methanol- d_4 + OH reaction.

Table 2

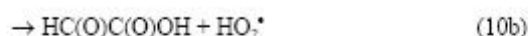
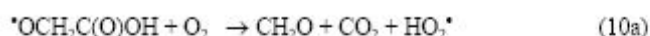
Comparison of room temperature rate constants for the reactions of OH radicals with acetic acid and deuterio acetic acids. The errors given are those reported by the authors

Reaction (i)	$10^{13} \times k$ ($\text{cm}^3 \text{ molecule}^{-1} \text{ s}^{-1}$)	Reference
OH + $\text{CH}_3\text{C}(\text{O})\text{OH}$ (1)	5.99 ± 0.39	[16]
	7.4 ± 0.3	[17]
	8.6 ± 0.3	[7]
	6.6 ± 0.4	[4]
	6.5 ± 0.3	[6]
	7.42 ± 0.06	[8]
	8.50 ± 0.45	[3]
	6.77 ± 0.14	[18]
OH + $\text{CD}_3\text{C}(\text{O})\text{OH}$ (2)	6.3 ± 0.9	This work
	8.1 ± 0.2	[7]
	7.79 ± 0.08	[8]
OH + $\text{CH}_3\text{C}(\text{O})\text{OD}$ (3)	6.3 ± 0.9	This work
OH + $\text{CD}_3\text{C}(\text{O})\text{OD}$ (4)	1.5 ± 0.3	This work
	1.09 ± 0.09	[8]
	0.90 ± 0.1	This work

Table 2 gives a comparison of all the rate constant values that have been reported for reactions (1) – (4) in previous works [3, 4, 6-8, 16-18]. The rate constant for the acetic acid + OH reaction has been determined in several investigations. The present result is in good agreement with the previous studies, though it is in the lower range of the whole interval spanning from 5.99 to $8.6 \times 10^{-13} \text{ cm}^3 \text{ molecule}^{-1} \text{ s}^{-1}$, as reported by Zetzsch and Stuhl [16] and Singleton *et al.* [7], respectively. However, we note that our rate constant agrees

very well with the very recent absolute determination of $k_1(295\text{K}) = (6.77 \pm 0.14) \times 10^{-13} \text{ cm}^3 \text{ molecule}^{-1} \text{ s}^{-1}$ by Huang *et al.* [18] who performed highly sophisticated kinetic experiments. To the best of our knowledge, the rate constant we have measured for the $d_1\text{-AA} + \text{OH}$ (2) reaction represents the first kinetic determination. Rate constants for the $d_3\text{-AA} + \text{OH}$ (3) reaction have been reported in two papers [7, 8], with which our result agrees reasonably well: our value is on average about 25% smaller. In view that Singleton *et al.* [7] and Vimal and Stevens [8] applied direct kinetic methods under very different experimental conditions, the agreement is satisfactory. Concerning the $d_4\text{-AA} + \text{OH}$ (4) reaction, the agreement with the only determination of k_4 available in the literature [8] is very good (Table 2), despite the fact that the authors used much higher acetic acid concentrations (up to 1840 ppmv) than we did in the present study (up to 81 ppm). It should be stressed that the uncertainty on $k_{\text{meth-d4}}$ is still significant (only three determinations). Application of CH_3OH as a reference for the $\text{CD}_3\text{C(O)D}$ reaction was unsuccessful because of the occurrence of significant isotope exchange reactions in the reaction system. The difference in the reactivity between $\text{CH}_3\text{C(O)OH}$ and $\text{CH}_3\text{C(O)OD}$ on the one hand, and between $\text{CD}_3\text{C(O)OH}$ and $\text{CD}_3\text{C(O)OD}$ on the other hand confirms that reactions (1) and (3) proceed essentially through the abstraction of the H-atom from the carboxylic group. This mechanistic picture is reflected also by the observed kinetic isotope effect (KIE). KIE is defined here as the rate constant ratio of the OH reactions of two acetic acid isomer molecules, one of which contains H-atom(s) while the other one D-atom(s) in the same position. This can be calculated for reactions (2) to (4) from the experimental values of k_1 to k_4 . KIE is found to be small for the hydrogen atoms in the methyl group, that is, $k_1/k_3 = 1.0$ and $k_2/k_4 = 1.6$, but large for the hydrogen atom in the carboxylic group: $k_1/k_2 = 5.2$ and $k_3/k_4 = 8.6$. Previous experimental studies on the kinetics of the reaction between OH and acetic acid provide the possibility to calculate the ratios k_3/k_4 and k_1/k_3 for comparison. From the work by Singleton *et al.* [7], one obtains $k_1/k_3 = 1.1$ and from Vimal and Stevens [8] $k_1/k_3 = 0.95$ and $k_3/k_4 = 7.1$. These KIE values are consistent with the present findings and the proposed mechanism. The observed kinetic isotope effect can be qualitatively explained by the increase of the energy barrier of the abstraction channel due to the effect of zero-point energy lowering caused by D-substituents. A strong quantum tunnelling effect has also been invoked to play a role in the reaction mechanisms at the molecular level [8,19]. It is interesting to note that a similar KIE was observed in the formic acid + OH reaction [20].

In the photooxidation reaction system, the $\text{CH}_3\text{C(O)O}^\bullet$ radical and its deuterated isomers undergo fast decomposition forming the methyl radical and CO_2 [2-4]. The further fate of the minor primary product $\text{CH}_2\text{C(O)OH}$ (and its deuterated counterparts) has been examined in the present study by product analysis.



According to the assumed reaction mechanism (8)-(10), we have searched for glyoxylic acid ($\text{HC}(\text{O})\text{C}(\text{O})\text{OH}$) among the reaction products. For this purpose, gas samples were taken from the environmental chamber after 2 to 4 h of irradiation, by pumping about 50 L of the reaction mixture through an impinger containing a mixture of water and methanol (10% w/w) cooled down to $\sim 3^\circ\text{C}$. The extraction solution was then analysed by ion chromatography (Dionex) with anion concentrator.

The ion chromatography analysis clearly showed the presence of glyoxylic acid (G_4), as confirmed by injection of a standard solution and comparison of the retention times. Similarly, $\text{HC}(\text{O})\text{C}(\text{O})\text{OD}$ was identified in the OH^{\bullet} -initiated photooxidation of $\text{CH}_3\text{C}(\text{O})\text{OD}$. These results suggest that the main fate of the ${}^{\bullet}\text{OCH}_2\text{C}(\text{O})\text{OH}$ radical is its conversion to $\text{HC}(\text{O})\text{C}(\text{O})\text{OH}$ through reaction with O_2 (reaction (10b)). This conclusion is supported also by the following considerations:

i) A heat of reaction about $51 - 83 \text{ kJ mol}^{-1}$ can be estimated for the concurrent decomposition channel (10a) using reported heats of formation of the reactants and products [21-23] indicating that this channel cannot be important under ambient conditions.

ii) The fate of the similar ${}^{\bullet}\text{OCH}_2\text{C}(\text{O})\text{OCH}_3$ alkoxy radical has been shown to be the reaction with O_2 rather than decomposition [24, 25].

Because of a lack of kinetic data on the reactivity of glyoxylic acid with ${}^{\bullet}\text{OH}$ radicals, it was not possible to determine the primary G_4 yield in the reaction system (*i.e.* to correct for consumption in the ${}^{\bullet}\text{OH}$ reaction). Calculation of the ratio of the concentration of G_4 formed and the concentration of A_4 reacted, both measured at the end of the experiment, provides the glyoxylic acid yields of 0.10 for reaction (1) and 0.15 for reaction (2). Taking into account the branching ratio of reaction (1) [4-6] and assuming channel (10a) to be negligible, G_4 yields of 0.22 to 0.36 are expected for the OH^{\bullet} -initiated oxidation of $\text{CH}_3\text{C}(\text{O})\text{OH}$. The lower experimental G_4 yields obtained in our study can be explained by considering first the G_4 wall losses and the consumption of G_4 by



Finally, we note that the non-negligible glyoxylic acid yield we have found in our experiments is in line with the recent theoretical study of Rosado-Reyes and Francisco [26] confirming their conclusion, that glyoxylic acid should be a significant organic by-product in the atmospheric oxidation of acetic acid.

Acknowledgements. This work is jointly supported by the Nord-Pas de Calais region in the frame of the IRENI research program, by the French Research Ministry and by the European Fund for Regional Economic Development (FEDER). E. Szabó thanks for financial support from the EU through project MEST-CT-2005-020659 and from the French Foreign Office and Région Nord – Pas de Calais with the framework of the ARCUS program. J. Tarmoul gratefully acknowledges the financial support from the Ecole des Mines de Douai and the CNRS.

REFERENCES

1. S. Preunkert, M. Legrand, B. Jourdain, I. Dombrowski-Etchevers: *J. Geophys. Res.*, **112**, 1 (2007).
2. S.A. Carl, L. Vereecken, J. Peeters: *Phys. Chem. Chem. Phys.*, **9**, 4071 (2007).
3. V.G. Khamaganov, X.V. Bui, S.A. Carl, J. Peeters: *J. Phys. Chem. A*, **110**, 12852 (2006).
4. N.I. Butkovskaya, A. Kukui, N. Pourvesle, G. Le Bras: *J. Phys. Chem. A*, **108**, 7021 (2004).
5. F. De Smedt, X.V. Bui, T.L. Nguyen, J. Peeters, L. Vereecken: *J. Phys. Chem. A*, **109**, 2401 (2005).
6. S. Crunaire, J. Tarmoul, C. Fittschen, A. Tomas, B. Lemoine, P. Coddeville: *Appl. Phys. B*, **85**, 467 (2006).
7. D.L. Singleton, G. Paraskevopoulos, R.S. Irwin: *J. Am. Chem. Soc.*, **111**, 5248 (1989).
8. D. Vimal, P.S. Stevens: *J. Phys. Chem. A*, **110**, 11509 (2006).
9. E. Turpin, A. Tomas, C. Fittschen, P. Devolder, J.-C. Galloo: *Env. Sci. Technol.*, **40**, 5956 (2006).
10. W.D. Taylor, T.D. Allston, M.J. Moscato, G.B. Fazekas, R. Kozlowski, G.A. Takacs: *Int. J. Chem. Kin.*, **12**, 231 (1980).
11. J. Chao, B.J. Zwolinski: *J. Phys. Chem. Ref. Data*, **7**, 363 (1978).
12. R. Atkinson, D.L. Baulch, R.A. Cox, J.N. Crowley, R.F. Hampson, R.G. Hynes, M.E. Jenkin, M.J. Rossi, J. Troe: *Atm. Chem. Phys.*, **6**, 3625 (2006).
13. A. Parker, C. Jain, C. Fittschen: *React. Kinet. Catal. Lett.*, preceding paper in this issue, (2009).
14. T.J. Wallington, P. Dagaut, M.J. Kurylo: *J. Phys. Chem.*, **92**, 5024 (1988).
15. J.A. McCaulley, N. Kelly, M.F. Golde, F. Kaufman: *J. Phys. Chem.*, **93**, 1014 (1989).
16. C. Zetzsch, F. Stuhl: 2nd European Symposium on the Physico-chemical Behavior of Atmospheric Pollutants, Ed. Dordrecht, The Netherlands (1982).
17. P. Dagaut, T.J. Wallington, R. Liu, M.J. Kurylo: *Int. J. Chem. Kin.*, **20**, 331 (1988).
18. Y. Huang, T.J. Dransfield, J.D. Müller, R.D. Rojas, X.G. Castillo, J.G. Anderson: *J. Phys. Chem. A*, **113**, 423 (2009).
19. W. Sun, M. Saeys: *J. Phys. Chem. A*, **112**, 6918 (2008).
20. D.L. Singleton, G. Paraskevopoulos, R.S. Irwin, G.S. Jolly, D.J. McKenney: *J. Am. Chem. Soc.*, **110**, 7786 (1988).

21. M.W. Chase, Jr.: *J. Phys. Chem. Ref. Data, Monograph*, **9**, 1 (1998).
22. H.-Y. He, W.-H. Fang: *J. Am. Chem. Soc.*, **125**, 16139 (2003).
23. J.J. Orlando: *Personal communication*, (2005).
24. F. Cavalli, I. Barnes, K.H. Becker, T.J. Wallington: *J. Phys. Chem. A*, **104**, 11310 (2000).
25. G.S. Tyndall, A.S. Pimentel, J.J. Orlando: *J. Phys. Chem. A*, **108**, 6850 (2004).
26. C.M. Rosado-Reyes, J.S. Francisco: *J. Phys. Chem. A*, **110**, 4419 (2006).

III.4 Cinétiques et mécanismes d'oxydation de composés multi-oxygénés

La thématique d'étude des cinétiques et mécanismes d'oxydation des composés multi-oxygénés est très récente au laboratoire. Elle a débuté dans le cadre d'un projet européen Marie Curie grâce auquel nous avons obtenu un financement pour une thèse en cotutelle entre l'Université de Lille et l'Académie des Sciences de Budapest (thèse d'E. Szabo, 2006 – 2011, (216)).

Les modèles de simulation de l'évolution du carbone organique dans l'atmosphère (type MCM) et des expériences en chambre de simulation atmosphérique montrent que l'oxydation des COV au cours de leur transport conduit à la formation d'espèces multi-oxygénées (142, 217, 218). La place de ce type de composés dans l'atmosphère est importante à de nombreux points de vue, tant en termes de qualité de l'air, de capacité oxydante de l'atmosphère et de formation des aérosols organiques secondaires. Pourtant, la réactivité des composés multi-oxygénés est souvent très peu connue et il y a aujourd'hui un réel besoin de mieux connaître la photochimie atmosphérique de ces composés. La voie de photolyse notamment peut être une voie d'oxydation très importante dans l'atmosphère pour les composés porteurs d'une fonction carbonyle. Or, quand bien même les spectres d'absorption UV-Vis sont connus, les rendements quantiques de photolyse ne sont souvent pas connus (et ils peuvent varier considérablement d'une molécule à une autre (219)), ce qui ne permet pas de déterminer précisément le devenir de ces composés. Rappelons que, lorsqu'elle a lieu, la photolyse d'un COVO est une source très importante de radicaux : dans le cas de l'acétone par exemple, elle conduit à une production nette de 3,2 radicaux HO_x contre 2 pour la voie de réaction avec le radical OH• (139). La photolyse d'espèces carbonylées et peroxydes a d'ailleurs été suggérée pour expliquer les niveaux élevés de radicaux HO_x observés dans la haute troposphère (170). Au cours de plusieurs campagnes de mesures récentes au sol, les concentrations en radicaux OH•, HO₂• et en COV ont été mesurées simultanément et comparées aux prédictions de modèles de chimie atmosphérique. Les désaccords sur les concentrations en OH• et HO₂• ont montré qu'il manquait une source importante de radicaux OH• qui pourrait être la photolyse de composés carbonylés (220, 221). Parallèlement, dans d'autres campagnes de mesures, la mesure de la réactivité totale du radical OH comparée à la réactivité calculée à partir des COV mesurés a révélé que nombreux COV réactifs n'étaient pas encore identifiés et pris en compte dans les modèles de chimie (222, 223).

Nous nous sommes focalisés dans un premier temps sur la famille des composés α -dicétones, car pour ces composés, la voie de photolyse est susceptible d'être majoritaire à cause de la présence de deux fonctions C=O. La démarche scientifique adoptée consiste à étudier les voies de

photolyse et de réaction avec le radical OH en priorité, tant d'un point de vue cinétique (pour évaluer le temps de vie) que mécanistique. Les études de produits de réaction sont envisagées dans un deuxième temps pour permettre de développer des mécanismes réactionnels et de proposer notamment des voies de sortie pour les radicaux alkoxy. Nous présentons ici une revue des sources atmosphériques des α -dicétones et de leur devenir atmosphérique, puis nous résumerons les travaux réalisés sur la 2,3-pentanedione.

III.4.1 Sources atmosphériques des composés α -dicétones

Les sources atmosphériques des composés α -dicétones sont très diverses : feux de biomasse (224), trafic routier (115) et industries agro-alimentaires et pharmaceutiques (225) ; une source marine est aussi suspectée (226). Les sources secondaires sont représentées principalement par l'oxydation des composés aromatiques et terpéniques. Plusieurs études ont montré que l'oxydation photochimique de composés hydrocarbonés (notamment les composés aromatiques avec ouverture du cycle) menait à la formation de composés carbonylés multifonctionnels, dont les α -dicarbonylés (104, 227-230).

En comparant les coefficients de partage gaz / particules mesurés et ceux calculés à partir d'un modèle d'absorption simple pour une série de composés carbonylés, *Healy et al.* ont observé des coefficients de partage expérimentaux beaucoup plus élevés que ceux calculés pour les dicarbonylés (231). Les auteurs ont attribué ces observations à une adsorption réactive de COV et à une réactivité importante en phase particulaire conduisant à la formation de ces composés carbonylés et constituant ainsi une source secondaire en phase condensée. Enfin, pour des composés multi-oxygénés de taille assez importante et présents dans la phase condensée, il est possible que la volatilisation constitue une source supplémentaire en phase gazeuse (126).

III.4.2 Réactivité des composés α -dicétones

La réactivité des α -dicétones est assez peu connue : seules quelques études ont porté sur le biacétyl $\text{CH}_3\text{C}(\text{O})\text{C}(\text{O})\text{CH}_3$, souvent considéré d'ailleurs comme composé modèle (232, 233) ; on peut mentionner aussi une étude récente sur la photolyse UV de l' α -cyclohexanedione (234). La présence de deux groupements carbonylés en α confère des caractéristiques spectrales particulières à ces composés, notamment un spectre UV qui s'étend jusque dans le visible (235). Comme la réactivité des cétones avec le radical OH est généralement faible (par exemple, $k(\text{acétone} + \text{OH}^\bullet) = 1,79 \times 10^{-13} \text{ cm}^3 \cdot \text{molécule}^{-1} \cdot \text{s}^{-1}$ (97) et $k(\text{biacétyl} + \text{OH}^\bullet) = 2,3 \times 10^{-13} \text{ cm}^3 \cdot \text{molécule}^{-1} \cdot \text{s}^{-1}$ (236)), le

processus de photolyse des α -diones dans l'atmosphère peut être significatif voire prépondérant, ce qui est le cas pour le biacétyl (226, 232, 233).

Les composés α -dicarbonylés étant des espèces polaires, ils pourront être piégés dans les hydrométéores atmosphériques et contribuer à la formation de noyaux de condensation (237). La constante de Henry de la 2,3-butanedione (56 M.atm^{-1} à 298 K (238)) est sensiblement supérieure à celle de l'acétone (32 M.atm^{-1} à 298 K (97)), ce qui indique une présence plutôt favorisée en phase gazeuse. Lorsqu'ils sont en phase aqueuse, la photolyse de ces carbonylés peut également être importante et constituer une source de radicaux peroxy (239). De façon plus générale, leur oxydation en phase aqueuse va participer à la formation de matière organique secondaire via la production de composés à faible volatilité (240).

III.4.3 Travaux réalisés

Nos premiers travaux ont commencé par l'étude de la réactivité de la 2,3-pentanedione $\text{CH}_3\text{C}(\text{O})\text{C}(\text{O})\text{C}_2\text{H}_5$ (PTD) vis-à-vis de la photolyse, de la réaction avec le radical OH^\bullet et de la réaction avec le chlore Cl^\bullet . La PTD est un composé odorant très utilisé dans l'industrie agro-alimentaire. La PTD a également été observée dans les produits de réactions d'ozonolyse d'alcènes (62) et dans les aérosols organiques secondaires produits lors de l'oxydation du toluène par le radical OH^\bullet (61). Elle est également un produit possible de l'oxydation de la 2-pentanone (issue notamment de l'oxydation du pentane (241)) par le radical OH^\bullet (242).

Nous avons déterminé les cinétiques de photolyse, réaction avec OH^\bullet et réaction avec Cl^\bullet de la PTD. Les expériences de photolyse ont été réalisées avec les lampes fluorescentes à 365 nm et 312 nm. Le taux de photolyse de la PTD dans l'atmosphère a été évalué par rapport à celui du NO_2 en utilisant les résultats de photolyse à 365 nm (243). L'ensemble des expériences ont été effectuées dans la chambre souple en Téflon. Les résultats concernant la photolyse (312 nm) et la réaction avec OH^\bullet sont repris dans l'article soumis à J. Phys. Chem., dans lequel on trouvera également les résultats obtenus à Budapest (**publication n°7**, (63)). La principale conclusion de ces travaux de cinétique est que le devenir atmosphérique de la 2,3-pentanedione est très majoritairement sa photolyse, avec un temps de demi-vie de l'ordre de la dizaine de minutes. La constante de vitesse de réaction avec OH^\bullet , bien que 10 fois supérieure à celle de la 2,3-butanedione ($2,1 \times 10^{-12} \text{ cm}^3.\text{molécule}^{-1}.\text{s}^{-1}$), reste faible mais cohérente avec la réactivité connue des cétones (80) et implique un temps de demi-vie de plusieurs jours.

Il subsiste actuellement un désaccord sur le rendement quantique de photolyse entre les données de Budapest ($\Phi \sim 0,1$ à 351 nm) et celles de Douai ($\Phi \sim 0,5 - 1$ sur 300 – 450 nm), désaccord sur lequel nous travaillerons dans le cadre de la prochaine thèse (H. Bouzidi, 2011 – 2014). Des expériences de photolyse à 365 nm réalisées récemment dans le cadre de la visite du Prof. T. Gierczak dans la chambre rigide ont permis de déterminer un rendement quantique de formation de CO de 0,1 à 5 Torr. Les prochains travaux porteront sur la détermination des produits de photolyse et de réaction avec OH^\bullet .

Publication n°7
(parue dans la revue *Journal of Physical Chemistry A* en 2011)

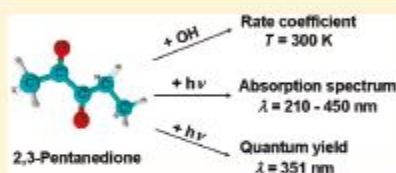
Atmospheric Chemistry of 2,3-Pentanedione: Photolysis and Reaction with OH Radicals

Emese Szabó,^{†,‡,§,||} Mokhtar Djehiche,^{†,‡} Matthieu Riva,^{†,‡} Christa Fittschen,^{†,||} Patrice Coddeville,^{†,‡} Dariusz Sarzyński,[‡] Alexandre Tomas,^{*,†,‡} and Sándor Dóbe,^{*,§}[†]Université de Lille Nord de France, F-59000, Lille, France[‡]Ecole des Mines de Douai, Département Chimie et Environnement, 941 rue Charles Bourseul, 59500 Douai, France[§]Institute of Materials and Environmental Chemistry, Chemical Research Center of the Hungarian Academy of Sciences, Pusztaszeri út 59-67, H-1025 Budapest, Hungary^{||}PhysicoChimie des Processus de Combustion et de l'Atmosphère PC2A, UMR CNRS 8522, University of Lille 1, 59650 Villeneuve d'Ascq, France[‡]Department of Physical Chemistry, Wrocław Medical University, 50-140 Wrocław, pl Nankiera 1, Poland

Supporting Information

ABSTRACT: The kinetics of the overall reaction between OH radicals and 2,3-pentanedione (1) were studied using both direct and relative kinetic methods at laboratory temperature. The low pressure fast discharge flow experiments coupled with resonance fluorescence detection of OH provided the direct rate coefficient of $(2.25 \pm 0.44) \times 10^{-12} \text{ cm}^3 \text{ molecule}^{-1} \text{ s}^{-1}$. The relative-rate experiments were carried out both in a collapsible Teflon chamber and a Pyrex reactor in two laboratories using different reference reactions to provide the rate coefficients of 1.95 ± 0.27 , 1.95 ± 0.34 , and 2.06 ± 0.34 , all given in $10^{-12} \text{ cm}^3 \text{ molecule}^{-1} \text{ s}^{-1}$.

The recommended value is the nonweighted average of the four determinations: $k_1(300 \text{ K}) = (2.09 \pm 0.38) \times 10^{-12} \text{ cm}^3 \text{ molecule}^{-1} \text{ s}^{-1}$, given with 2σ accuracy. Absorption cross sections for 2,3-pentanedione were determined: the spectrum is characterized by two wide absorption bands between 220 and 450 nm. Pulsed laser photolysis at 351 nm was used and the depletion of 2,3-pentanedione (2) was measured by GC to determine the photolysis quantum yield of $\Phi_2 = 0.11 \pm 0.02(2\sigma)$ at 300 K and 1000 mbar synthetic air. An upper limit was estimated for the effective quantum yield of 2,3-pentanedione applying fluorescent lamps with peak wavelength of 312 nm. Relationships between molecular structure and OH reactivity, as well as the atmospheric fate of 2,3-pentanedione, have been discussed.

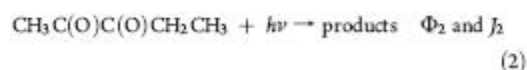


1. INTRODUCTION

2,3-Pentanedione ($\text{CH}_3\text{C}(\text{O})\text{C}(\text{O})\text{CH}_2\text{CH}_3$, 2,3PD) is a constituent of natural fragrances and synthetic flavoring agents, a selective polar solvent, and a starting material for the manufacture of dyes and pharmaceuticals.¹ It is volatile enough to escape into the atmosphere where it is expected to react primarily with OH radicals and to undergo photolysis. 2,3PD belongs to the family of α -dicarbonyls, several of which are of great importance for the chemistry of the troposphere, including glyoxal, $\text{C}(\text{O})(\text{H})\text{C}(\text{O})(\text{H})$, methyl-glyoxal, $\text{CH}_3\text{C}(\text{O})\text{C}(\text{O})\text{H}$, and biacetyl, $\text{CH}_3\text{C}(\text{O})\text{C}(\text{O})\text{CH}_3$. While these latter oxygenates have been the subjects of numerous reaction kinetic and photochemical studies, see, for example, refs 2–4 and refs 5–7, respectively, no such studies have been reported for 2,3PD in the homogeneous gas phase.

We have performed reaction kinetic and photochemical investigations of 2,3-pentanedione. The objectives of the present study were to improve our understanding of the effect of vicinal carbonyl groups on the reactivity with OH radicals and to assess the atmospheric fate of the potentially important volatile organic

compound (OVOC), 2,3PD. In this paper we present rate coefficients for the overall reaction of 2,3PD with OH radicals, k_1 , absorption cross sections as a function of wavelength, $\sigma_{2,3PD}(\lambda)$, photolysis rate coefficients, J_2 , and quantum yield, Φ_2 , at selected wavelengths, all of them determined at laboratory temperature ($T \approx 300 \text{ K}$).



Experiments were carried out both in the Chemical Research Center, Budapest (CRC, Budapest), and the École des Mines de Douai (EMD, Douai) by employing the complementary experimental techniques that are available at the two research sites.

Received: April 30, 2011

Revised: July 21, 2011

Published: July 25, 2011

Thus, kinetic experiments were carried out using the direct discharge flow method and using also relative-rate techniques to obtain rate coefficient for reaction (1). Photolysis experiments were performed employing both a pulsed laser at 351 nm and a continuous broadband irradiation source at 312 nm. The kinetic and photochemical data we present are believed to be the first determinations in the literature and, apart from the work of Jackson and Yarwood,⁸ no absorption spectrum for 2,3PD has been reported.

2. EXPERIMENTAL SECTION

Discharge Flow Technique. Absolute rate coefficient for the reaction $\text{OH} + \text{CH}_3\text{C}(\text{O})\text{C}(\text{O})\text{CH}_2\text{CH}_3$ (1) was determined in Budapest by using the low pressure fast discharge flow technique (DF) coupled with resonance fluorescence detection (RF).^{9,10}

The flow-tube reactor was constructed of Pyrex and had an inner diameter of 4.0 cm and an overall length of 60 cm. The internal surface of the reactor was coated with a thin film of halocarbon wax to reduce heterogeneous loss of OH radicals. The reactor was equipped coaxially with a movable injector; helium was the carrier gas. OH radicals were produced inside the injector by reacting H atoms with a slight excess of NO_2 : $\text{H} + \text{NO}_2 \rightarrow \text{OH} + \text{NO}$; H atoms were generated by microwave discharge of trace H_2 in helium flow. 2,3-Pentanedione was used, premixed in helium, from blackened bulb reservoirs and the concentration of the mixture was checked by GC or UV–vis absorption before use.

The OH(A–X) excitation radiation was produced by a microwave powered resonance lamp operated with flowing $\text{Ar}/\text{H}_2\text{O}$ at low pressure. The RF radiation emerging from the detection cell was passed through an interference filter centered at 307 nm and detected by a photomultiplier. The minimum detectable OH concentration was approximately 2×10^9 molecules cm^{-3} .

Relative-Rate Experiments Using a Pyrex Reactor. Kinetic experiments were performed in a 10 L Pyrex bulb, PR, to determine relative rate coefficient for reaction (1) in Budapest (RR-PR experiments). OH radicals were produced by the photo-oxidation of CH_3ONO in synthetic air. The photolytic light source was a modified movie projector operated with a 3 kW Xe arc. The irradiating light was passed through a heat reflecting mirror and three liquid filters of 12 cm optical path each in the following order: water, an aqueous solution of chrome alum, and an aqueous solution of methylene blue.¹¹ The transmitted light had a bell-shaped intensity profile with a maximum at $\lambda_{\text{max}} = 362$ nm and a full width at half-maximum of $w = 28$ nm.

The reaction mixtures contained $(5.6 - 6.0) \times 10^{15}$ molecules cm^{-3} 2,3PD, $(7.9 - 8.5) \times 10^{15}$ molecules cm^{-3} MEK (methyl ethyl ketone, reference reactant), 1.0×10^{15} molecules cm^{-3} *c*- C_4F_8 (GC standard), $\sim 4 \times 10^{16}$ molecules cm^{-3} methyl nitrite, and synthetic air made up to 1050 mbar overall pressure. The reaction temperature was measured inside the reactor using a retractable thermocouple. It was found constant and slightly above the ambient temperature ($T = 302 \pm 4$ K). Samples for analysis were withdrawn by a gastight syringe through a septum connected to a thin glass tube which reached in the middle of the bulb. Concentrations were determined by isothermal GC and flame ionization detection (FID). The GC parameters are given in Table SI-2 in the Supporting Information.

Relative-Rate and Photochemical Experiments Using a Collapsible Teflon Reactor. A collapsible Teflon reactor, TR, was used at Douai¹² to determine relative rate coefficients for

reaction 1, as well as to obtain photolysis rate coefficients for 2,3PD, J_2 . The reactor had a volume of ~ 250 L. Two types of fluorescent tubes were used for irradiation: Vilbert-Lourmat T-20 M (20 W) with peak intensity at $\lambda_{\text{max}} = 312$ nm and $w = 11$ nm, as well as Philips TL-K (40 W) with $\lambda_{\text{max}} = 365$ nm and $w = 34$ nm.

Most of the reactants were volatile liquids (2,3PD, MEK, etc.), measured amounts of which were injected in a small evacuated glass vessel first, and were then flushed into the Teflon-bag reactor one by one with a stream of purified air. In the final step, the reactor was filled to its full volume with air (or N_2 in the case of NO_2 photolysis). Concentration depletion of the organics was measured at regular intervals using online GC-FID analysis (Table SI-2 in the Supporting Information).

The following were the initial concentrations: OH-reaction (RR-TR experiments), $[2,3\text{PD}]_0 = (1.2 - 3.0) \times 10^{14}$ molecules cm^{-3} , $[\text{ethanol}]_0 = 4.3 \times 10^{14}$ molecules cm^{-3} (reference reactant), $[\text{MEK}]_0 = (2.8 - 4.2) \times 10^{14}$ molecules cm^{-3} (reference reactant), and $[\text{CH}_3\text{ONO}]_0 \approx 1 \times 10^{16}$ molecules cm^{-3} (OH radical source); continuous photolysis (CP-TR experiments): $[2,3\text{PD}]_0 = (2.5 - 6.5) \times 10^{14}$ molecules cm^{-3} .

In the NO_2 actinometry measurements, the photolysis rate coefficient, J_{NO_2} , was determined at 312 nm by monitoring the consumption of NO_2 during the irradiation of dilute NO_2/N_2 mixtures; the initial concentration was $[\text{NO}_2]_0 \approx 8 \times 10^{13}$ molecules cm^{-3} . A calibrated commercial NO_2 analyzer was used for the concentration measurements, which was operated continuously by sampling a small flow of the irradiated gas mixture from the Teflon bag.

Measurements of Absorption Cross Sections. The UV–vis absorption spectrum of 2,3PD was determined in Budapest employing a home-built gas spectrophotometer.¹⁴ Briefly, the light beam of a D_2 lamp was passed through a 50.2 cm absorption cell thermostatted to $T = 298 \pm 1$ K, dispersed by a 0.25 m monochromator, and detected by a photomultiplier interfaced to a lock-in amplifier and PC. The spectral resolution was ~ 0.4 nm. The light intensity was strongly reduced by using neutral filters to minimize potential photolysis of the analyzed samples.

Laser Photolysis Technique. Pulsed laser photolysis (PLP) at 351 nm was used to determine photolysis quantum yield for 2,3PD, $\Phi_2(351 \text{ nm})$ in Budapest. The concentration depletion was determined after a measured number of laser shots using GC analysis.^{13,14}

An exciplex laser provided the pulsed laser light; the laser was operated at 5 Hz. Photolysis was performed in a 11.6 (optical path) \times 3.6 cm (internal diameter) cylindrical quartz cell (PLP-QR experiments). A septum joint was attached to the cell for GC sampling (Table SI-2). The laser energy was measured using a calibrated laser energy meter; the energy was typically ~ 20 mJ pulse⁻¹. The photolysis was carried out in synthetic air with mixtures containing 6.3×10^{15} molecules cm^{-3} 2,3-pentanedione and 1.5×10^{15} molecules cm^{-3} *c*- C_4F_8 .

Chemicals. 2,3PD was purchased from Merck and Sigma-Aldrich with the nominal purities of ≥ 98 and 97%, respectively. The samples were purified by multiple trap-to-trap distillations in vacuum ($6\times$), retaining $\sim 2/3$ middle fraction at each step. Purity of the distilled 2,3PD was 98.5% in the liquid phase and $\geq 99.5\%$ in the gas phase. MEK (Sigma-Aldrich, $>99.7\%$), *c*- C_4F_8 (PCR Inc., 99%), methanol (Merck, 99.9%) and ethanol (Merck, 99.9%) were degassed by several freeze–pump–thaw cycles prior to use. Most of the gases were used as obtained: H_2 (99.95%, Messer-Griesheim), He (99.996%, Messer-Griesheim), synthetic air (Messer Hungaria, $\geq 99.5\%$), zero-grade air (Claid

Type AZ 2000 generator). NO₂ (Messer-Griesheim, 98%) was purified by repeated trap-to-trap distillations in vacuum from slurries kept at low temperatures. Methyl nitrite, CH₃ONO, was prepared from methanol with nitrous acid¹⁵ and was purified by trap-to-trap distillations.

Errors. Unless otherwise stated, the quoted uncertainties are two standard deviations throughout the paper and represent precision only. The errors are typically those that have returned from regression analyses and have always been propagated for the derived quantities.

3.1. KINETIC RESULTS AND DISCUSSION

3.1.1. DF-RF Determination of k_1 . The experiments were conducted at $T = 300 \pm 3$ K reaction temperature and $P = 2.49 \pm 0.06$ mbar He pressure. The standard pseudo-first-order kinetic method was employed to determine absolute rate coefficient for OH + CH₃C(O)C(O)CH₂CH₃ (1) with a large excess of [2,3PD] over the hydroxyl radical concentration of $[\text{OH}]_0 \approx 3 \times 10^{11}$ molecules cm⁻³. The experiments were performed by recording the OH resonance fluorescence signal strengths versus the varied reaction distance, z , with, $S_{\text{OH}}^{\text{on}}$, and without, $S_{\text{OH}}^{\text{off}}$ of the reactant 2,3-pentanedione flow. Under the plug-flow condition of the low-pressure DF technique, the reaction time equals $z \times v_{\text{lin}}^{-1}$, where v_{lin} is the average linear flow velocity in the flow tube. The bimolecular reaction between OH and 2,3PD was kinetically isolated from the interfering reactions in the homogeneous gas phase, but the consumption of OH was significant on the surface of the reactor, which was found to obey first-order kinetics with an effective "wall rate coefficient" of k_w .

Therefore, assuming pseudo-first-order kinetics and with the provision that the wall activity for OH was not very different in the presence and absence of 2,3PD, the experimental observables were evaluated by the eqs I–III:

$$-\ln \frac{S_{\text{OH}}^{\text{on}}}{S_{\text{OH}}^{\text{off}}} = k_1' \frac{z}{v_{\text{lin}}} \quad (\text{I})$$

$$k_1' = k_1 [2,3\text{PD}] + \text{const} \quad (\text{II})$$

$$-\ln S_{\text{OH}}^{\text{off}} = k_w \frac{z}{v_{\text{lin}}} \quad (\text{III})$$

The measured hydroxyl decays, when plotted according to eq I, displayed straight lines, indicating the validity of first-order kinetics. The slopes provided the pseudo-first-order rate coefficient, k_1' , by linear least-squares analysis (LSQ). Sample decay plots are shown in the inset of Figure 1. The main panel of this figure shows a plot of k_1' versus [2,3PD] (eq II); the bimolecular rate coefficient, k_1 , was obtained as LSQ slope. The plotted $\ln S_{\text{OH}}^{\text{off}}$ versus z data gave also straight lines, the slopes of which supplied k_w (eq III).

Large heterogeneous effects were observed in the first experiments portrayed by very high OH consumption on the surface of the reactor and a smaller than expected signal magnitudes in the experiments that were carried out in close succession to each other. Such effects are indicative of the adsorption of 2,3PD on the walls of the reactor and an enhanced heterogeneous reaction with the OH radicals. Similar behavior was reported by Stevens and co-workers for discharge flow reactions of OH with different polar reactants including carbonyls (see, e.g., ref 16 and references therein). These authors have reported the heterogeneous

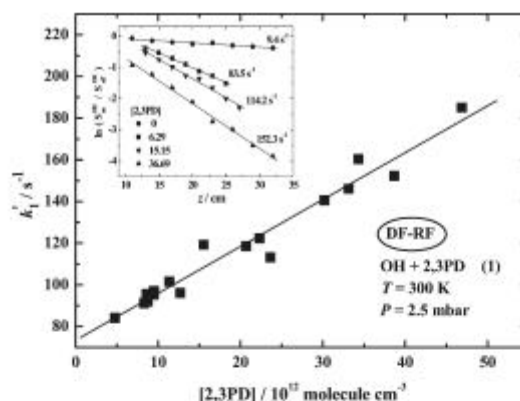
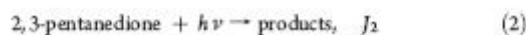
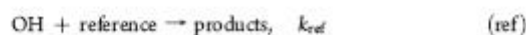
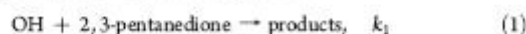


Figure 1. Plots used to determine k_1 . The figure in the inset shows representative OH-decays vs the reaction distance, where $S_{\text{OH}}^{\text{on}}$ and $S_{\text{OH}}^{\text{off}}$ are the OH signal strengths with and without 2,3PD flow, respectively, and the 2,3PD concentrations are given in 10^{12} molecules cm⁻³.

effects to be minimized by the addition of O₂. However, this option was not feasible in our current experiments because a substantial reformation of OH was observed when oxygen flow was added to the reaction system that might have caused an underestimation of the rate coefficients in the measurements. Long evacuation time and conditioning of the walls of the flow tube with OH radicals were used prior to each experiment. In this way, reasonable reproducibility was achieved, but the bimolecular rate coefficient plot showed a significant intercept (Figure 1), and the $k_w = 7\text{--}47$ s⁻¹ values were somewhat larger than the usual wall consumption of OH ($\sim 3\text{--}20$ s⁻¹) that we observed previously in DF experiments with inert wall coatings.

The experimental conditions and kinetic results are summarized in Table 1. We have not corrected the measured rate coefficient for viscous flow and axial diffusion in the present work. Instead, an 8% contribution was included in the error margins to account for such effects and other potential systematic errors by experience with previous reaction systems. Thus, the following rate coefficient is proposed by the DF-RF study for the reaction of OH radicals with 2,3-pentanedione: $k_1(300\text{ K}) = (2.25 \pm 0.44) \times 10^{-12}$ cm³ molecule⁻¹ s⁻¹ given with an overall uncertainty at the 2 σ level.

3.1.2. Relative-Rate Kinetic Studies. Relative rate coefficients for the reaction of OH with 2,3-pentanedione were determined by comparing the rate of loss of the substrate to that of a reference compound the rate coefficient for which is accurately known. 2,3PD was found to photolyze slowly at the wavelengths used to produce OH, however, no loss of the reference compounds at the time scale of the kinetic experiments was observed by test irradiations conducted in the absence of 2,3PD and the OH-source CH₃ONO.



$$\lambda_{\text{max}} = 362 \text{ and } 365 \text{ nm.}$$

Table 1. Summary of Experimental Conditions and Results for the Reaction OH + 2,3PD (1) Using the DF-RF Method ($T = 300 \pm 3$ K, $P = 2.49 \pm 0.06$ mbar He Buffer Gas)^a

η_{He} (cm s^{-1})	$[\text{OH}]_0$ (10^{11} molecules cm^{-3})	$[\text{2,3PD}]$ (10^{12} molecules cm^{-3})	k_w (s^{-1})	k_1' (s^{-1})	No. of expts	k_1 (10^{-12} cm^3 molecule $^{-1}$ s^{-1}) ^a
874–1055	2–10	4.79–46.9	7–47	84–185	17	2.25 ± 0.24

^aThe errors represent 2 σ statistical uncertainties.

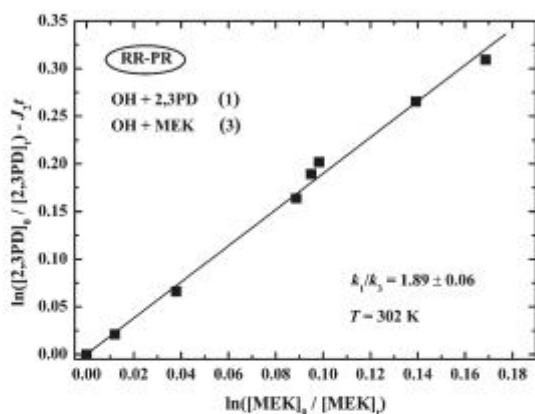


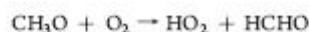
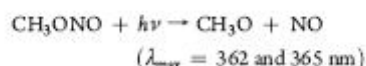
Figure 2. Plot used to determine rate coefficient ratio for the reaction of OH radicals with 2,3PD obtained from measurements using the Pyrex reactor and MEK as the reference reactant.

Provided that 2,3PD and the reference compounds are lost only by reactions with OH, neither 2,3PD, nor the reference compounds are reformed in the systems and that the photolysis of 2,3PD is slow compared to the studied chemical reactions, the following expression is obtained

$$\ln\{[2,3PD]_0/[2,3PD]_t\} - J_2 t = (k_1/k_{\text{ref}}) \times \ln\{[\text{ref}]_0/[\text{ref}]_t\} \quad (\text{IV})$$

where $[2,3PD]_0$, $[2,3PD]_t$, $[\text{ref}]_0$, and $[\text{ref}]_t$ are the concentrations of the 2,3PD and reference at time zero and t , J_2 is the photolysis rate coefficient determined from separate experiments, t is the reaction time, k_1 and k_{ref} are the rate coefficients for the 2,3PD reaction and the reference reaction, respectively. Thus, plots of the left-hand side of eq IV versus $\ln\{[\text{ref}]_0/[\text{ref}]_t\}$ should be linear with zero intercept and slope equal to k_1/k_{ref} .

OH radicals were produced by the photolysis of methyl nitrite in air



RR-PR Determination of k_1 . Relative-rate kinetic experiments were carried out in synthetic air, at $T = 302 \pm 4$ K reaction temperature and 1050 mbar overall pressure, using the Pyrex reactor. The reaction with methyl ethyl ketone, OH + MEK (3), served as reference. The measured concentration ratios plotted

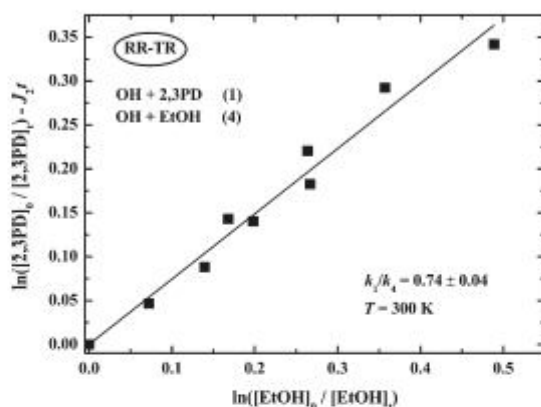


Figure 3. Plot used to determine rate coefficient ratio for the reaction of OH radicals with 2,3PD obtained from measurements using the Teflon bag reactor and EtOH as the reference reactant.

according to eq IV are presented in Figure 2. The photolysis rate coefficient needed for the data evaluation was determined by measuring the photodepletion of 2,3PD in the absence of CH_3ONO and MEK but, otherwise, under the same experimental conditions. Single exponential time dependence was observed providing $J_2(362 \text{ nm}) = (1.99 \pm 0.32) \times 10^{-5} \text{ s}^{-1}$ as the decay constant. This photolysis rate has resulted in a maximum correction of $\sim 9\%$ of the OH-reaction in eq IV. Linear least-squares analysis of the data plotted in Figure 2 have supplied $k_1/k_3 = 1.89 \pm 0.06$. The rate coefficient ratio has been put to an absolute scale by taking $k_3 = (1.09 \pm 0.18) \times 10^{-12} \text{ cm}^3 \text{ molecule}^{-1} \text{ s}^{-1}$ from ref 17 to give $k_1 = (2.06 \pm 0.34) \times 10^{-12} \text{ cm}^3 \text{ molecule}^{-1} \text{ s}^{-1}$. (The rate coefficient value we use for the reference reaction agrees within 10% with those recommended by the IUPAC and JPL data evaluations.^{18,19})

RR-TR Determination of k_1 . Two reference reactions, OH + MEK (3) and OH + $\text{C}_2\text{H}_5\text{OH}$ (EtOH; 4), were used in the relative-rate experiments that were performed in the Teflon-bag reactor. The reaction conditions were: $T = 300 \pm 2$ K and $P = 1000$ mbar overall pressure synthetic air. Similar to the Pyrex-reactor experiments, photolysis loss of 2,3PD had to be taken into account in deriving the rate coefficient ratios. The photolysis rate coefficient has been determined to be $J_2(365 \text{ nm}) = (2.01 \pm 0.08) \times 10^{-5} \text{ s}^{-1}$; the correction for photolysis was less than 15%. A plot according to eq IV is presented in Figure 3 displaying results with the application of the EtOH reference reaction. An LSQ slope of the straight line of Figure 3 provides $k_1/k_4 = 0.74 \pm 0.04$, which is resolved to the absolute rate coefficient of $k_1 = (1.95 \pm 0.27) \times 10^{-12} \text{ cm}^3 \text{ molecule}^{-1} \text{ s}^{-1}$ by taking $k_4 = (3.2 \pm 0.4) \times 10^{-12} \text{ cm}^3 \text{ molecule}^{-1} \text{ s}^{-1}$ from ref 18.

Well-obeyed straight line with zero intercept similar to those shown in Figures 2 and 3 was obtained also with the application

of the methyl ethyl ketone reference reaction¹⁷ in the Teflon-reactor experiments supplying $k_1/k_3 = 1.79 \pm 0.11$ and $k_1 = (1.95 \pm 0.34) \times 10^{-12} \text{ cm}^3 \text{ molecule}^{-1} \text{ s}^{-1}$. The relative-rate plot obtained with the OH + MEK (3) reference reaction is presented as Figure SI-2 in the Supporting Information.

3.1.3. Reactivity of 2,3-Pentanedione with OH. The absolute and relative-rate kinetic studies have provided rate coefficients for reaction (1) in good agreement with each other: DF-RF, 2.25 ± 0.44 ; RR-PR, 2.06 ± 0.34 ; RR-TR, 1.95 ± 0.27 and 1.95 ± 0.34 , all given in $10^{-12} \text{ cm}^3 \text{ molecule}^{-1} \text{ s}^{-1}$. Note also that k_1 has been found invariant to the reaction pressure in a wide range between ~ 2 and ~ 1000 mbar. The good agreement lends credence to the reliability of the results in particular that they were obtained from independent measurements in two laboratories using different experimental techniques. The recommended rate coefficient for the reaction of OH radicals with 2,3PD is the nonweighted average of the k_1 determinations:

$$k_1(300 \text{ K}) = (2.09 \pm 0.38) \times 10^{-12} \text{ cm}^3 \text{ molecule}^{-1} \text{ s}^{-1}$$

given with an overall accuracy proposed to be valid at the 95% confidence level.

To our knowledge, no prior rate coefficient has been reported for reaction (1). The only other α -diketone that has been a subject of OH-kinetic study is 2,3-butanedione ($\text{CH}_3\text{C}(\text{O})\text{C}(\text{O})\text{CH}_3$, or biacetyl). A rate coefficient of $(2.3 \pm 0.2) \times 10^{-13} \text{ cm}^3 \text{ molecule}^{-1} \text{ s}^{-1}$ ($T = 298 \text{ K}$) has been determined by Dagaut et al.⁴ for the OH + biacetyl reaction in good agreement with a previous measurement by Darnall et al.²⁰ The rate coefficient we propose from our current work for the OH + $\text{CH}_3\text{C}(\text{O})\text{C}(\text{O})\text{CH}_2\text{CH}_3$ (1) reaction is ~ 10 times higher, which can be rationalized, however, by the increased reactivity of the CH_2 group not present in the biacetyl molecule (see below).

A structural isomer of 2,3PD is 2,4-pentanedione (2,4PD), which is a β -diketone. Holloway and co-workers have carried out a detailed kinetic study of the reaction of OH with 2,4PD using both direct and relative kinetic methods.²¹ The rate coefficient they have reported is $(8.78 \pm 0.58) \times 10^{-11} \text{ cm}^3 \text{ molecule}^{-1} \text{ s}^{-1}$ ($T = 298 \text{ K}$), which is more than 40 times higher than the k_1 value we have determined for the OH + $\text{CH}_3\text{C}(\text{O})\text{C}(\text{O})\text{CH}_2\text{CH}_3$ (1) reaction. Holloway et al.²¹ have explained the high rate coefficient by that 2,4-pentanedione exists in the gas phase predominantly as the enol tautomer, $\text{CH}_3\text{C}(\text{O})\text{CH}=\text{C}(\text{OH})\text{CH}_3$, which undergoes fast addition reaction with the OH radical, while the keto-form ketones react via the slower hydrogen abstraction reaction. In contrast to 2,4PD, the vicinal diketone 2,3PD exists predominantly in the keto form with the enol form being present to a few percentages, at the most, in the gas phase at room temperature.^{22,23}

The reactivity properties of 2,3PD can be understood by the considerable knowledge that has been gathered throughout the years for the kinetics and mechanism of the reactions of OH radicals with the aliphatic monoketones, see, for example, refs 24 and 25 and also the review paper by Mellouki et al.²⁶ The $\text{C}=\text{O}$ group slightly reduces the bond dissociation energy (BDE) of a neighboring $\text{C}-\text{H}$ bond,¹⁹ but it is strongly electron withdrawing, which overrides the BDE-reducing effect, and so hydrogen abstraction by the electrophilic OH radical becomes less facile at the α -position.^{26,27} On the other hand, a characteristic feature of the OH reactions of $\text{C}_n \geq 3$ ketones is the increased reactivity of the $\text{C}-\text{H}$ bonds at the β -position.^{25,26} This latter effect is

thought to be the decisive factor in determining the pronounced reactivity of 2,3PD toward OH, compared, for example, with propane, $\text{CH}_3\text{CH}_2\text{CH}_3$, which has the same number and types of H atoms, but its rate coefficient is about half of that of the 2,3PD reaction ($k(\text{OH} + \text{propane}) = 1.1 \times 10^{-12} \text{ cm}^3 \text{ molecule}^{-1} \text{ s}^{-1}$, $T = 298 \text{ K}$ ¹⁹).

An important development for understanding the reactivity of OH radicals with polar organic molecules, including carbonyls, has been the recognition of the important role that weakly bound 'pre-reaction' (or 'pre-reactive') complexes play in the molecular mechanisms of the reactions, as it has been reviewed^{28–30} and discussed in detail, for example, in refs 31 and 32. Specifically, the role of hydrogen bonded complexes in enhancing the reactivity of the β - $\text{C}-\text{H}$ bond in the reactions of OH with aliphatic ketones has been assessed by Alvarez-Idaboy and co-workers by quantum chemical and theoretical reaction kinetics computations.³² They have shown that the β -pre-reaction complexes, $\text{C}=\text{O} \cdots \text{HO} \cdots \text{H}_\beta\text{C}_w$, significantly lower the reaction barrier via hydrogen-bond-like interactions in the transition state thus leading to increased rate coefficients.

One of the most frequently used methods to estimate OH reaction rate coefficients for gas-phase organic compounds has been Atkinson's structure–reactivity (SAR) approach,²⁷ which was found to work very well for the OH + aliphatic ketones reactions.³⁴ According to the SAR procedure, the total rate coefficient for the reaction $\text{OH} + \text{CH}_3\text{C}(\text{O})\text{C}(\text{O})\text{CH}_2\text{CH}_3$ (1) can be estimated as the sum of the following group rate coefficients ($T = 298 \text{ K}$):

$$k_1 = k_{\text{prim}}F(>\text{CO}) + k_{\text{sec}}F(>\text{CO})F(-\text{CH}_3) + k_{\text{prim}}F(-\text{CH}_2\text{C}(\text{O})-) \quad (\text{V})$$

where k_{prim} and k_{sec} are the rate coefficients per CH_3- and $-\text{CH}_2-$ groups and F_s are the substituent factors. Taking the tabulated generic rate coefficients k_{prim} , k_{sec} and the substituent factors from ref 27 one obtains $k_1 = 1.33 \times 10^{-12} \text{ cm}^3 \text{ molecule}^{-1} \text{ s}^{-1}$, which is an $\sim 50\%$ underestimate of the experimental value. We believe the reason is simply that the substituent factors currently available do not reflect the activating effect of a $-\text{C}(\text{O})\text{C}(\text{O})-$ moiety on the β - $\text{C}-\text{H}$ bond. Conversely, a $F(-\text{C}(\text{O})\text{C}(\text{O})-)$ factor can be derived by using our measured rate coefficient and the group reactivity parameters given in ref 27.

$$k_1(\text{meas}) = k_{\text{prim}}F(-\text{C}(\text{O})\text{C}(\text{O})-) + k_{\text{sec}}F(-\text{C}(\text{O})\text{C}(\text{O})-)F(-\text{CH}_3) + k_{\text{prim}}F(-\text{CH}_2\text{C}(\text{O})-) \quad (\text{VI})$$

This estimation provides $F(-\text{C}(\text{O})\text{C}(\text{O})-) = 1.55$, which indicates a definite, but smaller, activating effect than that of the $-\text{CH}_2\text{C}(\text{O})-$ group, $F(-\text{CH}_2\text{C}(\text{O})-) = 3.9$.²⁷

3.2. PHOTOCHEMICAL RESULTS AND DISCUSSION

3.2.1. UV–Vis Absorption Spectrum of 2,3-Pentanedione.

The absorption spectrum for 2,3PD was determined over the wavelength range of $\lambda = 210$ – 450 nm, at room temperature ($T = 298 \pm 1 \text{ K}$). The wavelength-dependent cross sections, $\sigma_{2,3\text{PD}}(\lambda)$, were obtained from absorption measurements applying the Beer–Lambert law:

$$\ln\{(I_0)/(I)\} = \sigma_{2,3\text{PD}}(\lambda)l[2,3\text{PD}] \quad (\text{VII})$$

where l ($= 50.2 \text{ cm}$) is the optical path length, and I_0 and I are the

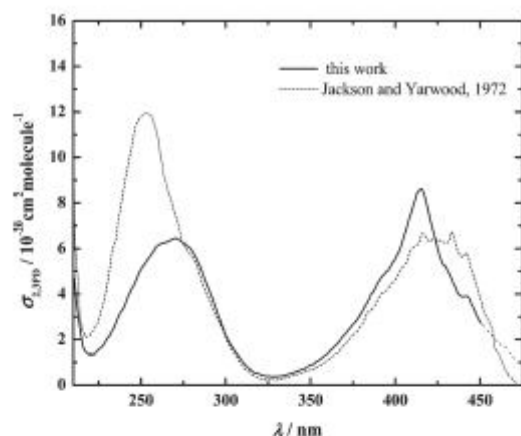


Figure 4. Absorption spectrum of 2,3-pentanedione in the gas phase at laboratory temperature: (—), this work; (·····), Jackson and Yarwood.⁸

transmitted light intensities in the absence and presence of 2,3PD, respectively. The spectrum is shown in Figure 4 and the corresponding absorption cross sections, $\sigma_{2,3PD}(\lambda)$, are tabulated in 1 nm intervals in the Supporting Information (Table SI-1) where representative Beer–Lambert (BL) plots are also presented (Figure SI-1).

As a first step, survey spectra were taken using the 2,3PD, as obtained from the supplier (nominally $\geq 98\%$ purity sample). One of the characteristic features of the spectrum determined was a strong absorption band at ~ 250 nm, which had a shoulder at ~ 270 nm. The 250 nm peak disappeared, however, when the spectrum was recorded with the purified sample and a lower-intensity unstructured band emerged with a maximum at 270 nm. The short-wavelength feature of the spectrum appeared again when the 2,3PD/He mixture applied for the analysis was prepared and stored in a bulb, which was used previously for storing other organics in gas mixtures, indicating the potential chemical transformation of 2,3PD on contaminated surfaces. Therefore, new, carefully cleaned glass parts were installed, and the absorption spectra were taken with the purified 2,3PD samples from mixtures stored for 1, 2, and 15 days, and recording of the spectra was done under static and flow-through conditions as well. The measurements have provided absorption cross sections in good agreement and so their average is proposed as the final result. This spectrum is presented in Figure 4.

As seen in Figure 4, 2,3PD has two broad absorption bands in the spectral range above ~ 220 nm: one in the UV and the other one in the visible with maximum at 270 and 415 nm, respectively. There is some indication for a vibrational structure of the second band, which may have been blurred, however, by the relatively low resolution (~ 0.4 nm) of our spectrometer. We have observed weak absorption extended to even longer wavelengths in the visible region but do not report the spectrum above 450 nm because of the large scatter and significant intercept of the BL-plots. The absorption spectrum of 2,3PD is similar to that of biacetyl in terms of the band positions, absorption cross sections and band widths.³³

The only absorption spectrum that is available for 2,3PD from the literature has been reported by Jackson and Yarwood,⁸ which is presented also in Figure 4. The UV-portion of the spectrum

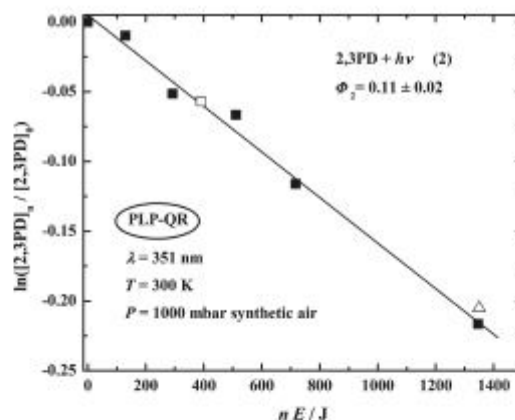


Figure 5. Depletion of 2,3PD concentration in pulsed laser photolysis experiments: n is the number of laser shots and E is the energy per pulse. The slope is proportional to the $\Phi_2(351 \text{ nm})$ photolysis quantum yield. The open symbols designate experiments performed with reaction mixtures containing 1-pentene as an OH scavenger.

reported by these authors, a large peak at 253 nm with a shoulder at 280 nm, shows close resemblance to that we observed with the 2,3PD sample when used without purification. As discussed, the strong short-wavelength band was absent in the spectrum that we obtained with the purified 2,3PD. The absorption band lying at longer wavelengths shows significant disparity as well (Figure 4). We note that we have obtained the same spectrum with the purified sample and without purification above ~ 350 nm. Clearly, this is not yet a proof for that our spectrum should be preferred at longer wavelengths as well.

3.2.2. Pulsed Laser Photolysis Results. The 351 nm PLP-QR experiments were performed at laboratory temperature ($T = 300 \pm 2$ K) in synthetic air at 1000 mbar total pressure to determine the photolysis quantum yield, $\Phi_2(351 \text{ nm})$. The concentration of 2,3PD was measured before photolysis, $[2,3PD]_0$, and after n laser shots, $[2,3PD]_n$, by GC analysis. Fresh gas mixtures were prepared for each irradiation. The experimental observables were evaluated according to eq VIII:^{13,14}

$$\ln([2,3PD]_n/[2,3PD]_0) = -C \times \Phi_2(351 \text{ nm}) \times (n \times E) \quad (\text{VIII})$$

$$\text{with } C = f_w(351 \text{ nm}) \times E_{ph}(351 \text{ nm})^{-1} \times \sigma_{2,3PD}(351 \text{ nm}) \times l \times V^{-1}$$

where E is the laser energy (mJ) per pulse, $f_w(351 \text{ nm})$ is the transmission of the entrance window (the measured value was 0.930 for one window), $E_{ph}(351 \text{ nm})$ is the energy of one photon (mJ photon⁻¹), l ($= 11.6$ cm) is the optical path length, and V is the total volume of the cell (cm³). $\Phi_2(351 \text{ nm})$ was obtained by plotting $\ln([2,3PD]_n/[2,3PD]_0)$ against $(n \times E)$ and making use of the absorption cross section measured in the present work and the known parameters in eq VIII. A plot of $\ln([2,3PD]_n/[2,3PD]_0)$ versus $(n \times E)$ is presented in Figure 5.

The reaction mixture contained 1-pentene in two experiments to trap the OH radicals potentially formed in the photo-oxidation system. Open symbols in Figure 5 represent the data obtained in the presence of OH-scavenger. The concentration of 1-pentene was 9.11×10^{14} and 8.9×10^{15} molecules cm⁻³ at low and high

2,3PD depletion, respectively. The result is seen invariant to the absence or presence of the OH scavenger 1-pentene that is believed to be a strong indication for the reliability of the quantum yield determined in the PLP-QR experiments. Linear least-squares analysis of all data in Figure 5 has provided $\Phi_2(351 \text{ nm}) = 0.11 \pm 0.01$, where the error given represents 2σ statistical uncertainty. Systematic errors were assessed for the parameters used in eq VIII, for example, it is $\pm 4\%$ for the energy measurement judged by NO_2 actinometry. Root mean squares combination of the statistical and systematic errors gives $\pm 20\%$, which is the proposed overall uncertainty at the 2σ (95% confidence) level. That is, the recommended quantum yield from our present study is:

$$\Phi_2(351 \text{ nm}) = 0.11 \pm 0.02$$

The “real” accuracy of the measurements can be considerable poorer than that given above due to the small absorption cross section of the 2,3PD molecule at the 351 nm photolysis wavelength.

3.2.3. Broadband Photolysis Results. Continuous photolysis of 2,3PD was carried out in the collapsible Teflon reactor in air buffer gas using fluorescent UV lamps with maximum emissions at 312 nm ($T = 300 \pm 2 \text{ K}$, $P = 1000 \text{ mbar}$, CP-TR experiments). The photolysis rate coefficient (“photolysis frequency”), $J_2(312 \text{ nm})$, was determined by monitoring the loss of the photolyte via online GC analysis. Experiments were performed with and without adding 1-pentene to the irradiated gas mixtures. 1-Pentene served to trap the OH radicals that potentially formed in the reaction systems. The depletion of 2,3PD concentration has been found to follow first-order kinetics as shown in Figure 6,

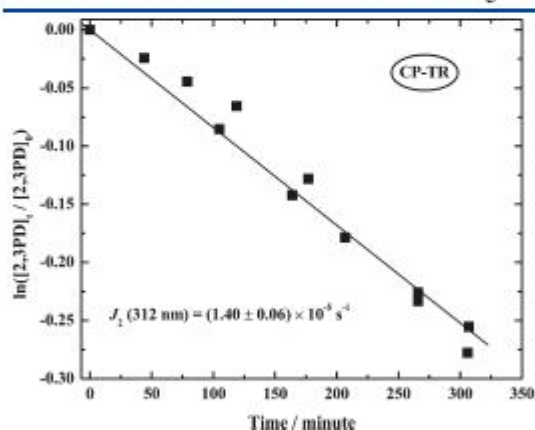


Figure 6. Depletion of 2,3PD concentration in the broadband photolysis experiments performed in the Teflon-film reactor at 312 nm. The reaction mixtures contained 1-pentene as an OH scavenger. The slope of the straight line gives the J_2 photolysis rate coefficient.

Table 2. Photolysis Rate Coefficients and Effective Quantum Yields Determined in the Collapsible Teflon Reactor at 312 nm Using Broadband Fluorescent Lamps ($T = 300 \pm 2 \text{ K}$, $P = 1000 \text{ mbar Air}$)

OH scavenger	J_2^a (10^{-5} s^{-1})	$J_{\text{NO}_2}^a$ (10^{-5} s^{-1})	$100 \times (J_2/J_{\text{NO}_2})$	Φ_2^{eff}
no scavenger	1.92 ± 0.08 (2)	0.78 ± 0.01 (9)	1.80 ± 0.12^d	0.41 ± 0.05^d
1-pentene ^c	1.40 ± 0.06 (3)			

^aThe number of experiments are given in the parentheses; $6 \times 20 \text{ W}$ lamps were used in the experiments. ^bEffective quantum yield (see text). ^cOH-scavenger: $[1\text{-pentene}]_0 = 9.1 \times 10^{14} \text{ molecules cm}^{-3}$. ^dUsing J_2 values determined in the presence of OH scavenger.

where the $\ln([2,3PD]_t/[2,3PD]_0)$ data are plotted against the reaction time, t , from two series of photolysis experiments. The J_2 values have been obtained by linear regression as the slope of the straight lines and are listed in the second column of Table 2.

The photolysis rate coefficient determined for 2,3PD is higher by $\sim 30\%$ in the absence of OH-scavenger. The OH radicals that caused the additional consumption of 2,3PD were probably formed via secondary reactions involving peroxy-radical chemistry in the photo-oxidation systems. The formation of OH by the primary photodissociation of 2,3PD can not be excluded either, but no products were determined in our current photolysis study to assess the primary and secondary photochemical processes. The photolysis rate coefficient determined in the presence of the OH scavenger is discussed next.

J_2 has been normalized to the photon flux by using NO_2 actinometry (note that the emission spectrum of the fluorescent lamps and the absorption spectra of 2,3PD and NO_2 ¹⁹ overlap in a substantial wavelength range). A dilute mixture of NO_2 in atmospheric pressure N_2 buffer gas was photolyzed in the Teflon reactor under the very same irradiation conditions than those of the 2,3PD photolysis experiments and the concentration depletion of NO_2 was measured as a function of the photolysis time up to 15–20% conversion. A plot of $\ln[\text{NO}_2]$ versus t yielded a straight line, the slope of which was equated to J_{NO_2} after minor correction for secondary reactions as proposed by Holmes et al.^{34,35} The determined J_{NO_2} photolysis frequencies along with the ratios J_2/J_{NO_2} are given in Table 2.

The J_2/J_{NO_2} values in Table 2 have been utilized to estimate an “integral” or “effective” quantum yield,^{36,37} Φ_2^{eff} , for the photolysis of 2,3PD with the broad-band fluorescent lamp with $\lambda_{\text{max}} = 312 \text{ nm}$ and $w = 12 \text{ nm}$ maximal emission wavelength and a full width at half maxima, respectively. The following expression was used:

$$\Phi_2^{\text{eff}} = \frac{J_2}{J_{\text{NO}_2}} \times \left\{ \frac{0.5\sigma_{\text{NO}_2}(\lambda_{\text{max}} - 0.5w) + \sigma_{\text{NO}_2}\lambda_{\text{max}} + 0.5\sigma_{\text{NO}_2}(\lambda_{\text{max}} + 0.5w)}{0.5\sigma_{2,3\text{PD}}(\lambda_{\text{max}} - 0.5w) + \sigma_{2,3\text{PD}}\lambda_{\text{max}} + 0.5\sigma_{2,3\text{PD}}(\lambda_{\text{max}} + 0.5w)} \right\} \times \Phi_{\text{NO}_2} \quad (\text{IX})$$

In eq IX, Φ_{NO_2} is the quantum yield for nitrogen dioxide photolysis, which was taken unity^{19,37} over the whole wavelength range studied; the absorption cross sections of NO_2 , $\sigma_{\text{NO}_2}(\lambda)$, were taken from ref 19 for the calculations and the $\sigma_{2,3\text{PD}}(\lambda)$ values from the present work (Table SI-1 in the Supporting Information). The estimated effective quantum yield is $\Phi_2^{\text{eff}}(312 \text{ nm}) = 0.41 \pm 0.05$. Trial calculations have shown only small change of the effective quantum yields when more overlap between the emission spectrum of the lamp and the absorption spectra of NO_2 and 2,3PD were taken into account.

As discussed, there was a strong, albeit indirect, indication for the formation of OH radicals in the broadband photolysis study performed at 312 nm causing a potential overestimation of the

quantum yields. In contrast, no such problem was observed in the PLP experiments at 351 nm. No obvious reason can be given to explain the diverse behavior. We just note that more photolysis channels are accessible at the lower wavelength studied (see next section) that may have led to different secondary photooxidation processes. The concentration of 1-pentene was not varied in the CP experiments, but it was assumed to be sufficiently high to scavenge all OH formed in the system. Thus, the determined quantum yield is proposed to be only an upper limit, that is, $\Phi_2^{eff}(312 \text{ nm}) \leq 0.41$.

3.2.4. Photochemistry of 2,3PD. We have determined photolysis quantum yields for 2,3-pentanedione using 351 nm XeF laser and 312 nm fluorescence lamps at room temperature ($T = 300 \pm 2 \text{ K}$) in 1000 mbar air buffer gas with the results of $\Phi_2(351 \text{ nm}) = 0.11 \pm 0.02$ and $\Phi_2^{eff}(312 \text{ nm}) \leq 0.41$. These are high values for the studied wavelengths and pressure. They appear high in comparison, for example, with the long-wavelength photolysis quantum yields of monoketones¹⁴ and the 365 nm quantum yield of the α -diketone biacetyl.³⁸ On the other side, however, high quantum yields have been reported for the photolysis of the α -ketoaldehyde, methylglyoxal, $\text{CH}_3\text{C}(\text{O})\text{C}(\text{O})\text{H}$, even at around 400 nm photolysis wavelength, although determined at lower pressures.⁶ Clearly, further investigations are needed to determine accurate photolysis quantum yields for 2,3PD. Among the quantum yields determined, we give preference to that obtained by the laser photolysis method.

Consumption yields were measured and no photolysis products were determined in our current work. Thermochemistry and the scarce information available from the literature suggest channels 2a–2d to be primary photolysis channels for 2,3PD at the relatively low excitation energies of the investigations:



The applied photolysis wavelengths of 312 and 351 nm correspond to the excitation energies of 382 and 340 kJ mol^{-1} , respectively. Three different C–C photodissociation routes are energetically accessible at 312 nm excitation, channels 2a–2c, while at 351 nm, only the formation of $\text{CH}_3\text{CO} + \text{CH}_3\text{CH}_2\text{CO}$, channel 2a, is feasible at ambient temperatures. The free radical product $\text{CH}_3\text{C}(\text{O})\text{C}(\text{O})$ formed via channel 2c may undergo decomposition depending on its excess energy^{3,40} to form CH_3CO and CO . The photoisomerization reaction 2d may take place at both excitation wavelengths studied: this channel has been proposed by Turro and Lee in a classical liquid-phase photochemical study⁴¹ (see below). (The reaction enthalpies for the different photolysis channels have been obtained by taking the recently published standard enthalpy of formation of $\Delta_f H^\circ_{298}$ (2,3PD) = $-343.7 \pm 2.5 \text{ kJ mol}^{-1}$ from ref 39 and the other enthalpy data from refs 19,39, and 40.)

Little is known about the photochemistry of 2,3PD from the literature. Turro and Lee⁴¹ have studied the photochemistry of 2,3PD in solution at 435 nm. They have shown that photolysis of 2,3PD forms 1-hydroxy-1-methyl-2-cyclobutanone via an intramolecular

photoreduction process, eq 2d, with a quantum yield of ~ 0.06 .⁴¹ Jackson and Yarwood⁴² have investigated the fluorescence and phosphorescence of 2,3PD in the gas phase at 365, 405, and 436 nm. They have derived a rate coefficient expression by the temperature dependent quenching of the phosphorescence of 2,3PD⁴² consistent with the eq 2d photoisomerization process.⁴¹ In an unpublished photo-oxidation study, performed at 254 nm in the Teflon reactor in our own laboratory, the build-up of acetaldehyde, CH_3CHO , was observed concomitant with the consumption of 2,3PD,⁴³ indicating the occurrence of photodissociation channels 2a–2c.

3.3. ATMOSPHERIC IMPLICATIONS

The absorption spectrum of 2,3-pentanedione extends to long wavelengths (Figure 4) where the solar flux increases rapidly in the troposphere, for example, the flux is ~ 150 times higher at 400 nm than that at 300 nm at the Earth's surface. Also, as presented in sections 3.2.2–3.2.4, 2,3PD undergoes photochemical changes with quantum yields that are still fairly uncertain, but they are believed significant even at relatively long wavelengths. These factors imply a likely short photolysis lifetime of 2,3PD, τ_{phot} , in the troposphere.

As discussed, we prefer the quantum yield determined with the monochromatic laser light, $\Phi_2(351 \text{ nm}) = 0.11 \pm 0.02$. We estimate τ_{phot} ⁴³ by assuming Φ_2 to be 0.1 over the whole wavelength range of 290–450 nm and utilizing the measured absorption cross sections along with tabulated actinic fluxes taken from ref 43. This estimation has provided the photolysis lifetime of less than one hour for 2,3PD during daytime at mid latitudes on the ground level. The same qualitative result is obtained assuming 0.06 for the photolysis quantum yield⁴¹ due to the significant absorption of 2,3PD and the high solar flux in the longer wavelength region.

Similar to other carbonyl molecules, OH-reaction can be an important initiation step for the tropospheric degradation of 2,3PD beside photolysis. The k_1 value determined at laboratory temperature can be used to estimate the tropospheric lifetime of 2,3PD with respect to its reaction with OH radicals, τ_{OH} . With an average global OH concentration of $[\text{OH}]_{global} = 1 \times 10^6 \text{ radicals cm}^{-3}$ (24 h average),⁴⁴ the tropospheric lifetime of $\tau_{OH} \approx 1/[k_1(300 \text{ K}) \times [\text{OH}]_{global}] = 5.3 \text{ days}$ is estimated.

In summary, our estimations show that photolysis is likely the dominant process to control the loss of 2,3PD in the troposphere. While this conclusion is believed correct in qualitative terms, accurate lifetime can not be given as yet, mostly because of the uncertainty of the photolysis quantum yields. It is noted also that the simple assessment used here is based on the assumption that 2,3PD is uniformly mixed through the troposphere that is probably not the case in view of the short lifetime of this OVOC and the average tropospheric transport time scale (1–2 months). The short lifetime indicates that 2,3PD will be removed rapidly close to its local sources in the atmosphere.

■ ASSOCIATED CONTENT

Supporting Information. Absorption cross sections for 2,3-pentanedione tabulated in 1 nm intervals along with representative Beer–Lambert plots; GC conditions; relative-rate plot to obtain $k_1(\text{OH} + 2,3\text{PD})/k_1(\text{OH} + \text{MEK})$. This material is available free of charge via the Internet at <http://pubs.acs.org>.

AUTHOR INFORMATION

Corresponding Author

*E-mail: dobe@chemres.hu; alexandre.tomas@mines-douai.fr.

ACKNOWLEDGMENT

This work has been supported in part by the Hungarian Research Fund OTKA (Contract OMF0-00992/2009). E.Sz. gratefully acknowledges the financial support from the French Foreign Office and Région Nord–Pas de Calais in the framework of the ARCUS program. The authors are indebted to the reviewers for their comments and helpful suggestions.

REFERENCES

- Burdock, G. A. *Fenaroli's Handbook of Flavor Ingredients*, 5th ed.; CRC Press: Boca Raton, FL, 2005.
- Feierabend, K. J.; Zhu, L.; Talukdar, R. K.; Burkholder, J. B. *J. Phys. Chem. A* 2008, 112, 73.
- Baena-Romero, M. T.; Glowacki, D. R.; Blitz, M. A.; Heard, D. E.; Pilling, M. J.; Rickard, A.; Seakins, P. W. *Phys. Chem. Chem. Phys.* 2007, 9, 4114.
- Dagaut, P.; Wallington, T. J.; Liu, R.; Kurylo, M. J. *J. Phys. Chem.* 1988, 92, 4375.
- Feierabend, K. J.; Flad, J. E.; Brown, S. S.; Burkholder, J. B. *J. Phys. Chem. A* 2009, 113, 7784.
- Chen, Y.; Wang, W.; Zhu, L. *J. Phys. Chem. A* 2000, 104, 11126.
- Klotz, B.; Graedler, E.; Sorensen, S.; Barnes, I.; Becker, K. H. *Int. J. Chem. Kinet.* 2001, 33, 9.
- Jackson, A. W.; Yarwood, A. J. *Can. J. Chem.* 1972, 50, 1331.
- Imrik, K.; Farkas, E.; Vasvári, G.; Szilágyi, L.; Sarzyński, D.; Dóbe, S.; Bérces, T.; Márta, F. *Phys. Chem. Chem. Phys.* 2004, 6, 3958.
- Dóbe, S.; Khachatryan, L.; Bérces, T. *Ber. Bunsen-Ges. Phys. Chem.* 1989, 93, 847.
- Pearlyn, D.; Pereira, D.; Kathirgamanathan, P. *J. Nat. Sci. Coun. Sri Lanka* 1977, 5, 41.
- Crunaire, S.; Tarnoul, J.; Fittschen, C.; Tomas, A.; Lemoine, B.; Coddeville, P. *Appl. Phys. B: Lasers Opt.* 2006, 85, 467.
- Gierczak, T.; Burkholder, J. B.; Talukdar, R. K.; Mellouki, A.; Barone, S. B.; Ravishankara, A. R. *J. Photochem. Photobiol. A* 1997, 110, 1.
- Nádasdi, R.; Züchner, G. L.; Farkas, M.; Dóbe, S.; Maeda, S.; Morokuma, K. *ChemPhysChem* 2010, 11, 3883.
- Ohbayashi, K.; Akimoto, H.; Tanaka, I. *J. Phys. Chem.* 1977, 81, 798.
- Baasan-dorj, M.; Griffith, S.; Dusanter, S.; Stevens, P. S. *J. Phys. Chem. A* 2009, 113, 10495.
- Szabó, E.; Züchner, G. L.; Szilágyi, L.; Dóbe, S.; Bérces, T.; Márta, F. *React. Kinet. Catal. Lett.* 2008, 95, 365.
- Atkinson, R.; Baulch, D. L.; Cox, R. A.; Crowley, J. N.; Hampson, R. F.; Hynes, R. G.; Jenkin, M. E.; Rossi, M. J.; Troe, J. *Atmos. Chem. Phys.* 2006, 6, 3625. IUPAC Subcommittee for Gas Kinetic Data Evaluation, <http://www.iupac-kinetic.ch.cam.ac.uk>.
- Sander, S. P.; Finlayson-Pitts, B. J.; Friedl, R. R.; Golden, D. M.; Huie, R. E.; Keller-Rudek, H.; Kolb, C. E.; Kurylo, M. J.; Molina, M. J.; Moortgat, G. K.; Orkin, V. L.; Ravishankara, A. R.; Wine, P. H. *Evaluation Number 15*, Jet Propulsion Laboratory: Pasadena, 2006.
- Darnall, K.; Atkinson, R.; Pitts, J. N. *J. Phys. Chem.* 1979, 83, 1943.
- Holloway, A.; Treacy, J.; Sidebottom, H.; Mellouki, A.; Daele, V.; Le Bras, G.; Barnes, I. *J. Photochem. Photobiol. A* 2005, 176, 183.
- Kung, J. F. T. *J. Agric. Food Chem.* 1974, 22, 494.
- Schwarzenback, G.; Wittwer, C. *Helv. Chim. Acta* 1947, 30, 656.
- Le Calvé, S.; Hittier, D.; Le Bras, G.; Mellouki, A. *J. Phys. Chem. A* 1998, 102, 4579.
- Wallington, T. J.; Kurylo, M. J. *J. Phys. Chem.* 1987, 91, 5050.
- Mellouki, A.; Le Bras, G.; Sidebottom, H. *Chem. Reviews* 2003, 103, 5077.
- Kwok, E.; Atkinson, R. *Atmos. Environ.* 1995, 29, 1685.
- Smith, I. W. M.; Ravishankara, A. R. *J. Phys. Chem. A* 2002, 106, 4798.
- Hansen, J.; Francisco, J. *ChemPhysChem* 2002, 3, 833.
- Galano, A.; Alvarez-Idaboy, J. R. *Applications of Theoretical Methods to Atmospheric Science. Adv. Quantum Chem.* 2008, 55, 245.
- Henon, E.; Canneaux, S.; Bohr, F.; Dóbe, S. *Phys. Chem. Chem. Phys.* 2003, 5, 333.
- Alvarez-Idaboy, J. R.; Cruz-Torres, A.; Galano, A.; Ruiz-Santoyo, M. E. *J. Phys. Chem. A* 2004, 108, 2740.
- Horowitz, A.; Meller, R.; Moortgat, G. K. *J. Photochem. Photobiol. A* 2001, 146, 19.
- Holmes, J. R.; O'Brien, R. J.; Crabtree, J. H.; Hecht, T. A.; Seinfeld, J. H. *Environ. Sci. Technol.* 1973, 7, 519.
- Szabó, E. Atmospheric kinetics and photochemistry of oxygenated volatile organic compounds. Ph.D. Thesis, University of Lille and University of Szeged, 2011 (submitted).
- Tadić, J.; Juranić, L.; Moortgat, G. K. *J. Photochem. Photobiol. A* 2001, 143, 169.
- Raber, W. H.; Moortgat, G. K. *Progress and Problems in Atmospheric Chemistry*; World Scientific Publishing Co.: Singapore, 1995.
- Sheats, G. F.; Noyes, W. A. *J. Am. Chem. Soc.* 1955, 77, 1421.
- Kercher, J.; Fogleman, E.; Koizumi, H.; Sztáray, B.; Baer, T. *J. Phys. Chem. A* 2005, 109, 939.
- Jaggiella, S.; Zabel, E. *Phys. Chem. Chem. Phys.* 2008, 10, 1799.
- Turro, N. J.; Lee, T.-J. *J. Am. Chem. Soc.* 1969, 91, 5651.
- Jackson, A. W.; Yarwood, A. J. *Can. J. Chem.* 1971, 49, 987.
- Finlayson-Pitts, B. J.; Pitts, J. N., Jr. *Chemistry of the Upper and Lower Atmosphere: Theory, Experiments, and Applications*; Academic Press: San Diego, 2000.
- Heard, D. E.; Pilling, M. J. *Chem. Rev.* 2003, 103, 5163.

Chapitre IV. Formation des aérosols organiques secondaires

IV.1 Rôle et importance des aérosols organiques secondaires

IV.1.1 Les aérosols atmosphériques : caractéristiques et impacts

L'atmosphère de la Terre présente, au sein de la phase gazeuse, une partie solide et liquide sous la forme de particules dont le diamètre est compris entre quelques nanomètres et 100 μm environ. Au-delà de 100 μm , les particules sédimentent rapidement, ce qui réduit fortement leur temps de résidence et leurs éventuels effets sur l'atmosphère. Les aérosols atmosphériques, définis comme des suspensions relativement stables de particules solide ou liquide dans l'atmosphère (jusqu'à 10^8 particules. cm^{-3}), ont des origines très diverses, comme l'érosion des sols, les océans, la conversion gaz/particule ... et des constituants très variés, comme des sels inorganiques, des métaux, du carbone élémentaire et de la matière organique. Ces dernières années, l'intérêt scientifique (et politique) porté aux particules atmosphériques s'est fortement accentué, compte tenu de leur impact sur la qualité de l'air et de leurs effets sur le climat, effets comportant des incertitudes encore importantes.

L'impact des aérosols atmosphériques comporte essentiellement deux volets : la qualité de l'air et le climat. De nombreuses études épidémiologiques réalisées dans les deux dernières décennies démontrent une association étroite entre l'accroissement des taux de morbidité et mortalité et l'exposition à la pollution particulaire atmosphérique, même à des niveaux très faibles de concentration (244, 245). On sait aujourd'hui qu'il y a une relation continue entre niveaux d'exposition aux particules et niveaux de risque, sans limite inférieure (comme cela semble être le cas pour l'ozone également) (127). En comparant les niveaux de pollution en $\text{PM}_{2,5}$ dans 51 villes des USA entre 1980 et 2000, *Pope et al.* ont montré qu'une diminution de $10 \mu\text{g}.\text{m}^{-3}$ entraînait une augmentation de l'espérance de vie moyenne de 0,61 an (246). Les particules atmosphériques sont en effet suffisamment petites pour pénétrer – certaines profondément – dans le système respiratoire des êtres humains et entraîner des maladies cardiovasculaires, respiratoires et des cancers. Certaines personnes / groupes de personnes sont plus sensibles à la pollution particulaire : les enfants et les personnes âgées, les personnes déjà touchées par une maladie cardiovasculaire ou respiratoire (247, 248). Une étude très récente s'est attachée à observer les effets (encore très peu étudiés) d'une exposition régulière à la pollution particulaire sur le cerveau : cette exposition serait susceptible de provoquer des troubles psychologiques sur l'être humain (249).

Le deuxième impact des aérosols atmosphérique touche au climat de la Terre. En effet, les particules sont à même de diffuser et absorber le rayonnement solaire, ce qui a pour effet de réduire l'énergie solaire parvenant sur la Terre (forçage négatif) et de diminuer la visibilité (30). Le forçage

radiatif dû aux aérosols atmosphériques est estimé à $-1,1 \text{ W.m}^{-2}$, ce qui signifie un refroidissement de l'atmosphère (250). Pour comparaison, le forçage radiatif positif dû au dioxyde de carbone est de $1,7 \text{ W.m}^{-2}$ (250). Les aérosols agissent également dans le processus de formation des nuages en jouant le rôle de noyaux de condensation, ce qui a pour effet d'augmenter la concentration en nombre de gouttelette et de diminuer leur taille. La réflexion du rayonnement solaire est ainsi accrue et on estime que le phénomène de précipitations est altéré (251).

On regroupe habituellement l'aérosol atmosphérique sous 3 modes (**Figure IV.1**) : le mode grossier (diamètre des particules $d > 1 \mu\text{m}$), le mode accumulation ($0,1 \mu\text{m} < d < 1 \mu\text{m}$) et le mode nucléation ($d < 0,1 \mu\text{m}$).

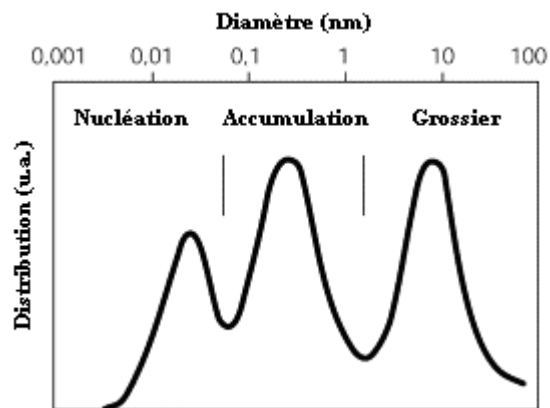


Figure IV.1 : Granulométrie typique d'un aérosol atmosphérique (adapté de (252))

Chacun de ces modes est 'alimenté' par des sources assez spécifiques : de façon schématique, le mode grossier représente plutôt des particules générées mécaniquement (érosion, volcans, végétation, ...), le mode accumulation est issu de phénomènes de coagulation entre particules, le mode nucléation apparaît lors de la conversion gaz – particules de vapeurs organiques et inorganiques.

En fonction de l'impact de l'aérosol atmosphérique considéré, c'est l'une ou l'autre de ses propriétés physiques (taille, surface spécifique, ...) qui devra être prise en compte. Par exemple, dans leur interaction avec le rayonnement solaire, c'est la taille des particules et leur composition chimique qui vont être prépondérantes. La surface, le volume et la morphologie des particules seront des paramètres déterminants dans les réactions de surface et les réactions ayant lieu à l'intérieur des particules. Quant à la qualité de l'air, c'est la concentration massique en particules

qui est la donnée aujourd'hui prise en compte pour son évaluation dans les réglementations française et européenne.

IV.1.2 Les aérosols organiques secondaires (AOS)

Une fraction importante de l'aérosol atmosphérique – environ 50% en masse – est constituée de matière organique pouvant comprendre des centaines de composés organiques différents (23). Cette fraction est très variable selon les environnements. On distingue les émissions directes d'aérosol organique, appelées aérosols organiques primaires (AOP), des émissions indirectes issues de précurseurs gazeux et appelées aérosols organiques secondaires (AOS), sur lesquels nous focaliserons notre attention.

D'un point de vue global, *Kanakidou et al.* ont estimé que 60% de la masse d'aérosol organique serait d'origine secondaire (253) ; cette fraction pourrait être même plus élevée régionalement, jusqu'à 90% en zone urbaine (254). Depuis l'ère préindustrielle, *Hoyle et al.* ont calculé, au moyen d'un modèle de chimie transport, que la quantité moyenne annuelle d'AOS avait augmenté de plus de 50 % dans l'atmosphère, avec un effet plus marqué sur les régions industrialisées ou fortement émettrices de composés biogéniques (255). La fraction secondaire de l'aérosol organique est généralement plus élevée l'été que l'hiver du fait de la photochimie (256). Les aérosols organiques secondaires formés sont souvent constitués de très fines particules (diamètre < 100 nm). Plusieurs équipes ont montré que les effets sur la santé de ces particules ultrafines sont distincts des effets des autres particules plus grosses ou des composés toxiques et que c'est le mode nucléation qui comporte le plus de risques sanitaires (16, 257-259). Par ailleurs, si les particules ultrafines contribuent peu à la masse totale des aérosols atmosphériques, leur concentration en nombre et la surface développée sont beaucoup plus grandes et il conviendrait peut-être de prendre en compte la concentration de surface, voire la concentration en nombre plutôt que la concentration massique dans la réglementation de la qualité de l'air (260, 261). Une étude récente a ainsi montré une forte corrélation entre la concentration en nombre de particules et les admissions hospitalières et la mortalité cardiovasculaire (262).

La quantification de l'impact climatique des particules secondaires est encore sujette à des incertitudes significatives (250) ; il semble néanmoins que le forçage radiatif des AOS soit plus important que celui calculé pour les aérosols organiques primaires (255). Par ailleurs, la présence de matière organique dans une particule de carbone augmente l'absorption du rayonnement solaire (263) et diminue l'efficacité des noyaux de condensation (à l'origine de la formation des nuages) des particules du fait de la baisse de l'hygroscopicité (264). Toutefois, ceci est à pondérer car la

variabilité de la composition chimique des aérosols atmosphériques entraîne une variabilité de l'efficacité des noyaux de condensation.

Les AOS sont produits schématiquement en deux étapes distinctes :

1. un précurseur organique gazeux réagit avec un oxydant de l'atmosphère (ex. : OH[•]) pour former un ou plusieurs composés de faible volatilité, qui s'accumulent au cours de la réaction ;
2. ces produits de réaction faiblement volatils se partagent entre les phases gazeuse et particulaire selon des processus physico-chimiques qui dépendent de nombreux paramètres, dont l'existence d'une phase condensée au sein de l'atmosphère. C'est ce transfert de masse gaz – particules qui forme les AOS.

Cette deuxième étape peut se subdiviser en trois sous-étapes : (i) la nucléation homogène (avec une faible participation d'espèces chargées) formant des clusters, (ii) une phase de croissance des particules jusqu'à 20 nm (iii) une deuxième phase de croissance principalement par condensation (265). Les phases de nucléation et de croissance semblent être découplées, ce qui indique que les composés impliqués sont différents (265).

La formation des aérosols organiques secondaires dans l'atmosphère est loin d'être un processus irréversible et figé ; au contraire, la composition et la taille des particules vont évoluer au cours de leur transport par des phénomènes d'oxydation hétérogène (réactivité OH[•] + particules par exemple), par des processus oxydants ou non (formation d'oligomères) au sein de la phase condensée et par une re-volatilisation de composés organiques (174, 266-268). Ce dernier phénomène est toutefois sujet à questionnement (269).

En dépit d'efforts considérables ces dix dernières années, les mécanismes précis de formation des aérosols organiques secondaires dans l'atmosphère à partir de composés organiques semi-volatils (COSV) demeurent peu compris. Deux processus majeurs semblent avoir lieu : (i) la nucléation homogène ou induite par des ions, qui forme de très petites particules (< 1 nm) par « addition » des molécules les unes aux autres (conversion gaz – particules) et (ii) la condensation des COSV sur des particules préexistantes, par exemple minérales ou carbonées, conduisant à l'accroissement en taille des nanoparticules (270, 271). Notre connaissance actuelle sur la formation des AOS ne permet pas d'expliquer les niveaux d'aérosols organiques élevés observés dans l'atmosphère (272), ce qui indique notamment :

- qu'un nombre important de COV ne sont actuellement pas pris en compte dans les modèles de chimie atmosphérique impliquant des réactions formant des AOS (218, 273).
- que les processus de formation des AOS – nucléation homogène/hétérogène, ... – ne sont pas encore correctement modélisés (23, 274).

Des évènements de nucléation ont été observés partout sur la Terre, de façon régulière et dans des environnements très variés, le jour comme la nuit (274-276) : dans les régions polaires, dans des centres urbains pollués (même en présence de particules préexistantes : à Pékin : (277) et dans la vallée du Pô en Italie : (278)) comme aussi à l'intérieur de bâtiments (279). Les principaux COV précurseurs d'aérosols organiques secondaires sont les monoterpènes et les aromatiques. Plusieurs de ces évènements de nucléation ont été corrélés avec l'irradiance entre 300 et 340 nm (280). L'acide sulfurique joue un rôle prépondérant dans la formation des nouvelles particules (nucléation binaire H_2O/H_2SO_4 et ternaire $H_2O/H_2SO_4/NH_3$), mais dans les atmosphères pauvres en soufre, les composés organiques contribuent de façon notable à la formation et à la croissance des nouvelles particules (271, 281, 282).

Du point de vue de la modélisation de la chimie atmosphérique et dans une optique d'amélioration de la qualité de l'air, une donnée intéressante est la capacité d'un précurseur gazeux à produire des aérosols organiques secondaires lors de son oxydation. Ce paramètre est évalué expérimentalement au travers de la notion de rendement en aérosol, noté Y, et défini par l'équation :

$$Y = \frac{\Delta M_0}{\Delta COV} \quad (\text{Eq. XI})$$

Dans cette équation, ΔM_0 représente la concentration massique en aérosol organique formée ($\mu\text{g m}^{-3}$) et ΔCOV la concentration massique du COV précurseur ayant réagi ($\mu\text{g m}^{-3}$). Les valeurs de rendement en aérosol ne sont disponibles que pour un nombre assez restreint de composés et pour des conditions expérimentales particulières et sont souvent très variables d'une étude à l'autre, voire au sein d'une même étude. *Odum et al.* a développé une relation semi-empirique explicitant Y en fonction des coefficients de partage $K_{mo,i}$ de chaque espèce organique i impliquée (283) :

$$Y = M_0 \sum_i \left(\frac{\alpha_i K_{mo,i}}{1 + K_{mo,i} M_0} \right) \quad (\text{Eq. XII})$$

M_0 représente la masse de matière organique particulaire présente et α_i le rapport entre la concentration en composé i formé et ΔCOV . Bien que la phase particulaire puisse contenir des dizaines de composés organiques différents, les courbes de rendements Y vs M_0 sont souvent simulées avec un modèle à un ou deux composés types en ajustant α_i et $K_{\text{mo},i}$:

$$Y = M_0 \left(\frac{\alpha_1 K_{\text{mo},1}}{1 + K_{\text{mo},1} M_0} + \frac{\alpha_2 K_{\text{mo},2}}{1 + K_{\text{mo},2} M_0} \right) \quad (\text{Eq. XIII})$$

Les coefficients de partage $K_{\text{mo},i}$ peuvent aussi être calculés à partir de l'expression suivante :

$$K_{\text{mo},i} = \frac{760RT}{M_{\text{w,mo}} 10^6 \zeta_i p_i^0} \quad (\text{Eq. XIV})$$

R est la constante des gaz parfaits, T la température, $M_{\text{w,mo}}$ la masse molaire moyenne de la matière organique particulaire, ζ_i le coefficient d'activité du composé i dans la phase condensée et p_i^0 la pression de vapeur saturante du composé i liquide.

IV.2 Ozonolyse des catéchols

IV.2.1 Sources et importance atmosphérique des catéchols

Les catéchols sont des composés aromatiques dont le représentant le plus simple est le 1,2-dihydroxybenzène. Les autres membres de cette famille sont constitués des dérivés alkylés du 1,2-dihydroxybenzène (**Figure IV.2**).

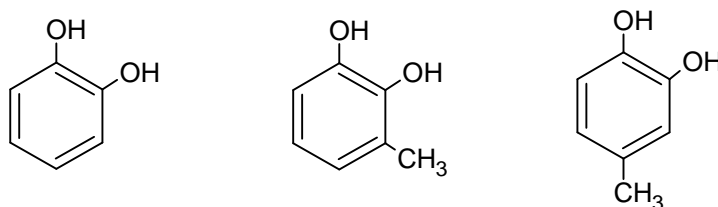


Figure IV.2 : Représentations développées des catéchols : 1,2-dihydroxybenzène, 3-méthyl-1,2-dihydroxybenzène et 4-méthyl-1,2-dihydroxybenzène

Les catéchols sont synthétisés et utilisés dans l'industrie comme précurseurs réactifs dans la production des pesticides (environ 50% de la production) et dans la chimie fine (parfums, pharmacie, adhésifs, etc.). Leur production se monte à quelques milliers de tonnes par an (284). Ils sont également présents dans les émissions de certaines espèces végétales (chêne, saule, champignons) et ont été détectés dans la fumée de cigarette et dans les fumées de combustion de bois et de biomasse (285, 286).

La source secondaire est potentiellement plus importante. En effet, les hydrocarbures aromatiques dont ils font partie représentent une classe très importante des composés organiques volatils (COV), principalement émis dans l'atmosphère suite aux activités humaines (68). Les composés aromatiques possèdent les potentiels de formation d'ozone parmi les plus élevés (287). Leur oxydation atmosphérique par le radical OH^\bullet conduit à des composés oxygénés à basse pression de vapeur qui peuvent former des aérosols organiques secondaires (68). Ils sont considérés aujourd'hui comme une source majeure d'AOS dans les atmosphères urbaines, pouvant représenter jusqu'à 80% des précurseurs d'AOS dans ce type d'environnement (23, 273). Si de nombreuses études en chambres de simulation atmosphérique ont été réalisées sur l'oxydation des hydrocarbures aromatiques, la littérature est bien plus réduite en ce qui concerne le devenir de leurs produits d'oxydation, notamment vis-à-vis de la formation des aérosols organiques secondaires (288).

Dans l'atmosphère, le benzène et ses dérivés alkylés comme le toluène et les xylènes réagissent principalement avec le radical OH^\bullet pendant la journée. Ces réactions conduisent à la formation d'autres composés aromatiques de type phénol, crésols et diméthylphénols avec des rendements importants, jusqu'à 60% (289, 290) en fonction des concentrations d'oxydes d'azote atmosphériques. Ces composés aromatiques monohydroxylés réagissent lentement avec l'ozone, mais leur réaction avec les radicaux OH^\bullet et NO_3^\bullet est rapide, ce qui entraîne des temps de vie pour le phénol, les crésols et les diméthylphénols dans la troposphère beaucoup plus courts que ceux de leurs précurseurs (68). *Henze et al.* ont estimé que le benzène est le composé aromatique le plus important au regard de la formation d'AOS, avec une production équivalente à celles du toluène et des xylènes combinées (291).

Au début des années 2000, *Olariu et al.* (292) ont montré que le phénol et les crésols produisaient des catéchols (**Figure IV.3**) avec des rendements très élevés, de l'ordre de 80%, résultats confirmés une année plus tard par *Bernd et Böge* (293). Les catéchols constituent donc des produits secondaires très importants dans la dégradation du benzène et de ses dérivés alkylés par le

radical OH^\bullet . Afin d'avoir une vue complète de l'impact des aromatiques sur la chimie troposphérique, il convenait d'étudier la réactivité des catéchols.

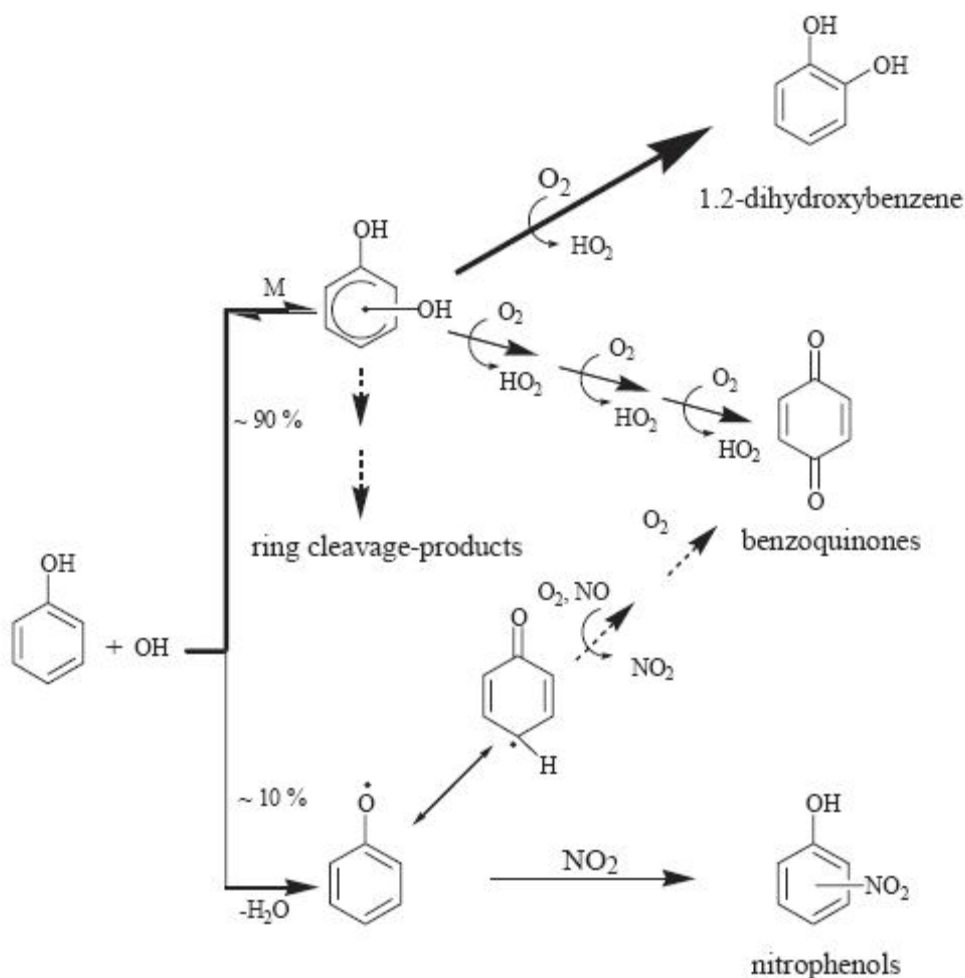


Figure IV.3 : Mécanisme simplifié proposé par Olariu *et al.* pour l'oxydation du phénol par le radical OH^\bullet (292)

Les cinétiques d'oxydation des trois représentants des catéchols avec le radical OH^\bullet ont été étudiées en chambre de simulation atmosphérique par l'équipe de I. Barnes. Les constantes de vitesse à température ambiante du 1,2-dihydroxybenzène, du 3-méthyl-1,2-dihydroxybenzène et du 4-méthyl-1,2-dihydroxybenzène sont respectivement de $1,04 \times 10^{-10}$, $2,05 \times 10^{-10}$ et $1,56 \times 10^{-10}$ $\text{cm}^3 \cdot \text{molécule}^{-1} \cdot \text{s}^{-1}$ (294). A la suite de l'étude cinétique de Olariu *et al.* sur l'oxydation par OH^\bullet des catéchols, nous nous sommes intéressés sur la réactivité avec le radical nitrate NO_3^\bullet qui peut être importante la nuit. Lors des premières expériences dans lesquelles O_3 (puis NO_2 pour former NO_3) était introduit dans le réacteur, nous avons constaté que l'ozone comme le 1,2-dihydroxybenzène disparaissaient rapidement tout en formant des quantités importantes d'aérosols. Une publication

assez ancienne de *Yamamoto et al.* portant sur l'ozonolyse de composés aromatiques hydroxylés en phase aqueuse relevait que les catéchols étaient plus réactifs avec l'ozone que le phénol (295). Cette observation, ainsi que nos propres expériences nous ont incités à rechercher si l'ozonolyse des catéchols pouvait représenter un puits significatif dans l'atmosphère.

IV.2.2 Cinétique d'ozonolyse des catéchols

Les réactions d'ozonolyse des composés aromatiques sont la plupart du temps négligeables dans l'atmosphère, les constantes de vitesse possédant des valeurs inférieures à 10^{-20} $\text{cm}^3 \cdot \text{molécule}^{-1} \cdot \text{s}^{-1}$ (68). Les seuls composés aromatiques réagissant significativement avec O_3 sont ceux contenant une (ou plusieurs) liaison C-C insaturée, comme par exemple le styrène et l'indène, ce qui permet à la molécule d'ozone de s'additionner sur la double liaison, à l'instar des hydrocarbures oléfiniques. Dans ce cas, la constante de vitesse d'ozonolyse du composé aromatique est de l'ordre de 10^{-19} $\text{cm}^3 \cdot \text{molécule}^{-1} \cdot \text{s}^{-1}$ (68).

L'étude que nous avons menée en chambre de simulation a permis de montrer que la réactivité des catéchols avec l'ozone est bien plus élevée que celle observée pour les alkylbenzènes et les phénols, confirmant leur réactivité élevée en phase aqueuse (295). Cette réactivité particulière semble être liée à la présence des deux fonctions $-\text{OH}$ en *ortho* sur le cycle benzénique qui augmentent la densité électronique dans leur voisinage et facilitent ainsi l'approche d'un réactif électrophile comme l'ozone. Des expériences réalisées avec le 1,4-dihydroxybenzène (groupes OH en *para*) montrent une réactivité beaucoup plus faible, ce qui confirme cette analyse. Les constantes de vitesse obtenues permettent de calculer un temps de demi-vie des catéchols dans l'atmosphère. Par comparaison avec la réactivité avec le radical OH^\bullet , on estime que la fraction de catéchol qui réagira avec l'ozone dans un environnement moyennement pollué ($[\text{O}_3] = 100$ ppb, $[\text{OH}^\bullet] = 1,6 \times 10^6$ $\text{molécule} \cdot \text{cm}^{-3}$) est de 10 à 20 %.

Ces travaux ont fait l'objet d'une publication dans la revue *International Journal of Chemical Kinetics* (**publication n°8**, (64)).

IV.2.3 Formation des aérosols organiques secondaires

Comme mentionné précédemment, les premières expériences impliquant le 1,2-dihydroxybenzène et l'ozone révélèrent une formation importante de particules ultrafines. Nous avons donc réalisé dans un premier temps des expériences dans la chambre de simulation européenne Euphore (dans le cadre de mon post-doctorat), puis, dans un deuxième temps, des expériences dans les chambres de simulation à Wimereux et à Cork (dans le cadre de la thèse d'A.

Guilloteau et du post-doctorat du Dr. N. Visez). Ces travaux sont brièvement résumés dans les deux paragraphes suivants ; les résultats détaillés sont donnés dans les publications jointes auxquels ils ont donné lieu.

IV.2.3.1 Etude au Centre de Recherche Européen Euphore à Valencia (Espagne)

La chambre de simulation européenne Euphore est l'une des plus grandes chambres existantes avec un volume de 200 m³ environ et équipée d'une panoplie de matériels d'analyse de pointe. C'est un outil extrêmement précieux au niveau européen, car il permet de travailler dans des conditions expérimentales beaucoup plus proches de la réalité en termes de concentrations notamment. Par ailleurs, dans le cadre d'études impliquant des aérosols, le faible rapport surface/volume (0,4 m⁻¹, cf. **Tableau IV.1**) est un atout considérable. Mon post-doctorat s'effectuant au sein du projet européen EXACT (Effects of the oXidation of Aromatic Compounds in the Troposphere), nous avons bénéficié d'un financement pour réaliser une série d'expériences d'ozonolyse des catéchols à Euphore. L'objectif de ces expériences était de confirmer les premières observations faites à Wuppertal et de caractériser (distribution en taille et rendement) les aérosols organiques formés lors de ces réactions. Quelques indications concernant les produits de réaction ont également pu être retirées des analyses chimiques réalisées par HPLC et GC-MS.

Les rendements en aérosols organiques secondaires déterminés sont significatifs (~ 20 – 60 %) Les résultats ont été publiés dans le rapport annuel de recherche 2003 du centre Euphore (**publication n°9**, (65)).

IV.2.3.2 Etudes à Cork et Wimereux

L'objectif des études à Cork et à Wimereux était de confirmer (sur le 1,2-dihydroxybenzène seulement) les résultats obtenus à Euphore dans des réacteurs de plus petits volumes (resp. 3,9 m³ et 8 m³) et d'étudier les produits d'ozonolyse dans les phases gazeuse et particulaire. Les différences de conditions expérimentales et d'équipements d'analyse sont résumées dans le **Tableau IV.1**.

Un très bon accord entre les 3 séries d'expériences a été obtenu : les rendements en aérosols sont du même ordre de grandeur et les courbes des rendements ont été simulées selon le formalisme de *Odum et al.* (283) avec un seul composé type. Ces résultats ont été publiés dans la revue *Atmospheric Environment* (**publication n°10**, (66)). Des composés carbonylés (cyclopentène-3,5-dione et o-benzoquinone) et des acides organiques ont été détectés dans les phases gazeuse et particulaire ; par manque de temps, ces analyses n'ont pu être davantage développées (296).

Tableau IV.1 : Synthèse des conditions expérimentales lors des expériences d’ozonolyse du catéchol effectuées dans trois réacteurs différents et outils d’analyse utilisés

	[O ₃] ₀ (ppm)	[Catéchol] ₀ (ppm)	Rapport S/V du réacteur (m ⁻¹)	Outils d’analyse
Euphore	0,17 – 1,1	0,31 – 1,4	0,4	IRTF in situ, SMPS, prélèvements sur filtre et analyse GC-MS, prélèvements sur cartouches DNPH et analyse HPLC, analyseur d’O ₃
Cork	0,61 – 2,3	0,78 – 1,3	4,2	IRTF in situ, SMPS, prélèvements sur denuder/filtre et analyse GC-MS, analyseur d’O ₃
Wimereux	0,10 – 0,37	0,06 – 0,90	3,0	SMPS, prélèvement sur cartouche et analyse GC-FID/MS, analyseur d’O ₃

IV.2.3.3 Conclusions et dernières publications dans la littérature

Les différentes études menées au sein de plusieurs laboratoires ont permis de mettre en évidence une nouvelle source atmosphérique d’aérosols organiques secondaires. Alors que l’ozonolyse des composés aromatiques est habituellement négligeable, ces travaux illustrent notre connaissance encore lacunaire de la chimie atmosphérique et la nécessité de poursuivre les études cinétiques et mécanistiques de dégradation des COV. La cohérence des résultats obtenus sur l’AOS dans trois laboratoires différents démontre la pertinence de ces études et l’intérêt d’effectuer des expériences similaires avec des outils complémentaires.

Récemment, une étude réalisée au LPCA à Dunkerque sur l’ozonolyse du 3-méthylcatéchol et du 4-méthylcatéchol a reporté des valeurs de rendements en aérosols similaires à celles obtenues pour le catéchol (297). Par ailleurs, deux études en chambre de simulation atmosphérique et en réacteur à écoulement ont porté sur la caractérisation physico-chimique de la matière organique dans les AOS formés lors de l’ozonolyse du catéchol, en utilisant des techniques d’analyse très poussées (ATR-FTIR, MEB, ...) (298, 299). Il apparaît que les particules formées revêtent une forme sphérique, ce qui est cohérent avec une conversion gaz-particules (186). Par ailleurs, l’étude de la composition de la phase particulaire révèle la présence de composés à poids moléculaires

élevés et très oxydés, dont des carbonylés et des acides carboxyliques (298, 299), confirmant ainsi nos propres résultats préliminaires (296).

Publication n°8
(parue dans la revue *International Journal of Chemical Kinetics* en 2003)

Kinetics of the Reaction of O₃ with Selected Benzenediols

ALEXANDRE TOMAS, ROMEO I. OLARIU, IAN BARNES, KARL H. BECKER

Bergische Universität Wuppertal, Physikalische Chemie - FB 9, Gaußstraße 20, D-42097 Wuppertal, Germany

Received 27 December 2002; accepted 11 February 2003

DOI 10.1002/kin.10121

ABSTRACT: The kinetics of the reaction of O₃ with the aromatic vicinal diols 1,2-benzenediol, 3-methyl-1,2-benzenediol, and 4-methyl-1,2-benzenediol have been investigated using a relative rate technique. The rate coefficients were determined in a 1080-L smog chamber at 298 K and 1 atm total pressure of synthetic air using propene and 1,3-butadiene as reference compounds. The following O₃ reaction rate coefficients (in units of cm³ molecule⁻¹ s⁻¹) have been obtained: $k(1,2\text{-benzenediol}) = (9.60 \pm 1.12) \times 10^{-18}$, $k(3\text{-methyl-1,2-benzenediol}) = (2.81 \pm 0.23) \times 10^{-17}$, $k(4\text{-methyl-1,2-benzenediol}) = (2.63 \pm 0.34) \times 10^{-17}$. Absolute measurements of the O₃ rate coefficient have also been carried out by measuring the decay of the dihydroxy compound in an excess of O₃. The results from these experiments are in good agreement with the relative determinations. Atmospheric implications are discussed. © 2003 Wiley Periodicals, Inc. *Int J Chem Kinet* 35: 223–230, 2003

INTRODUCTION

Aromatic hydrocarbons are significant constituents of lead-free gasoline. It has been recently shown that the organic aerosol arising from the atmospheric oxidation of a gasoline vapor can be accounted for solely by the aromatic content [1]. In addition, because of their high ozone formation potential, the contribution of aromatics to the ozone formation in the troposphere is believed to be quite substantial [2]. The major sink of aromatic compounds in the daytime is their reaction

with the OH radical, leading to numerous ring-retaining and ring-cleavage products. However, in many cases, the main OH reaction products are not well characterized and carbon balances are generally very poor [3,4]. In the case of benzene and toluene, which are the major aromatic compounds found in the troposphere, the addition of OH to the aromatic ring is known to produce phenol and the cresol isomers with yields of the order of up to 50% [3–6] and 20% [7], respectively. The further oxidation of these monohydroxylated aromatic compounds is now known to lead to the formation of vicinal diols, i.e. 1,2-benzenediols (also known as catechols), in high yields of about 80% [8–10], thus rendering them important ring-retaining products in the oxidation of benzene and toluene.

Generally, the reaction of O₃ with aromatic compounds is expected to be very slow [3,4,11]. Up to now, the only aromatic compounds known to react significantly with O₃ in the atmosphere are those that contain substituents with unsaturated >C=C< bonds, e.g. styrene and indene, thus allowing the O₃ molecule to

Correspondence to: Ian Barnes; e-mail: barnes@uni-wuppertal.de

Present address of Alexandre Tomas: Ecole des Mines de Douai, Département Chimie et Environnement, 941, rue Charles Bourseul, B.P. 838, 59508 Douai Cedex, France.

Present address of Romeo I. Olariu: Department of Analytical Chemistry, Faculty of Chemistry, "A.I. Cuza" University of Iasi, Carol I Boulevard, 11, 6600, Iasi, Romania.

Contract grant sponsor: Project EXACT, 5th Framework Programme, European Commission.
© 2003 Wiley Periodicals, Inc.

add to the aliphatic double bond. For aromatic hydrocarbons with such substituents, the O_3 reaction rate coefficient is generally estimated to be less than $10^{-19} \text{ cm}^3 \text{ s}^{-1}$ [3,4,8], so that the reaction of these compounds with O_3 represents a negligible removal reaction pathway in the troposphere relative to reaction with OH and NO_3 radicals.

In this work, we have investigated the kinetics of the reaction of O_3 with three vicinal benzenediols: 1,2-benzenediol, 3-methyl-1,2-benzenediol, and 4-methyl-1,2-benzenediol, using a smog chamber facility and *in situ* FT-IR detection of reactants. These investigations were motivated by some observations from studies on the kinetics of NO_3 radicals with benzenediols in which the NO_3 radical was generated via the reaction of NO_2 with O_3 . During these studies it was noted that when O_3 was added to the benzenediol in the reactor in air, both the diol and O_3 were consumed with the simultaneous formation of high yields of aerosol. Yamamoto et al. [12] noted in their study of the ozonolysis of hydroxylated aromatic compounds in water that 1,2-benzenediols were more reactive toward ozone than phenol. Therefore, in order to determine whether the gas-phase reactions of O_3 with benzenediols could represent an important loss pathway for benzenediols in polluted atmospheres a kinetic study on these reactions was undertaken.

EXPERIMENTAL

The experimental setup has been described in detail elsewhere [13] and only the main features will be outlined here.

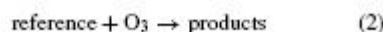
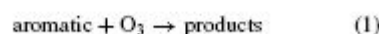
All experiments were performed in a darkened cylindrical quartz reactor with a volume of 1080 L (6.2 m length and 47 cm inner diameter) in 760 \pm 10 Torr of synthetic air (99.99% purity, Messer) at 298 \pm 3 K. The aromatic compounds investigated being solid were transferred into the gas phase by gently heating weighed amounts in a low-pressure nitrogen flow. Other gaseous and liquid reagents were introduced using calibrated syringes with the reactor under reduced pressure. Ozone was produced by flowing O_2 (99.998% purity, Messer) through an electrical discharge ozonizator and was added to the reaction mixture. This procedure took 20–60 s. The amount of ozone introduced into the chamber was varied between 3 and 13 ppmv (1 ppmv = $2.46 \times 10^{13} \text{ molecule cm}^{-3}$ at 298 K and 1 atm). As benzenediols deposit fairly rapidly on the reactor wall (wall loss rate coefficients $\approx 5 \times 10^{-4} \text{ s}^{-1}$), the initial amount of ozone had to be high enough so that the ozone reaction rate was higher than the wall loss rate, i.e., the conditions had to be

set so that the wall loss process did not dominate the overall aromatic decay. The gas mixture was continuously stirred by three fans at the ends and in the middle of the reactor, thus ensuring a homogeneous mixing of the reactants.

Reactants were monitored using a White-type optical mirror system (optical path length of $484.7 \pm 0.8 \text{ m}$) coupled to an FT-IR absorption spectrometer (Bruker IFS 88) operated at a resolution of 1 cm^{-1} . Between 10 and 15 spectra were recorded in each experiment, corresponding to reaction times of 10–15 min. The relative concentrations of reactants were obtained by using a subtraction procedure. Sharp spectral features in the region 1200–700 cm^{-1} were used to monitor the reactants. Interference of these features by product absorptions was minimal in this region and relatively clean spectral subtraction was possible in all cases. Ozone was generally added after the first spectrum was recorded. However, for some experiments, about 15 spectra were recorded before ozone was added, thus allowing the wall loss rates of the reactants to be determined. In the experiments the concentration of the catechols were varied in the range $(0.4\text{--}5) \times 10^{13} \text{ molecule cm}^{-3}$ and those of the reference hydrocarbons in the range $(3.76\text{--}7.52) \times 10^{13} \text{ molecule cm}^{-3}$. The compounds studied (1,2-dihydroxybenzene, 3-methyl-1,2-dihydroxybenzene, 4-methyl-1,2-dihydroxybenzene, and 1,4-benzoquinone) were supplied by Aldrich Chemical Co. with stated purities of >98% and were used without further purification. The reference hydrocarbons propene and 1,3-butadiene with stated purities of >99% were used as supplied by Messer-Griesheim and Aldrich, respectively.

The rate coefficients for the reaction of O_3 with 1,2-benzenediol, 3-methyl-1,2-benzenediol, and 4-methyl-1,2-benzenediol were determined using the relative method. Two reference compounds have been employed in this work: propene and 1,3-butadiene. The recommended rate coefficients used in this study are $k(\text{propene} + O_3) = 1.01 \times 10^{-17}$ and $k(1,3\text{-butadiene} + O_3) = 6.3 \times 10^{-18} \text{ cm}^3 \text{ s}^{-1}$ [14].

In the presence of ozone, both the aromatic and the reference compounds will react:



The aromatic compounds are also lost to the surface of the reactor:



No wall deposition was observed for both reference hydrocarbons.

For the aromatic hydrocarbon and the reference compounds, the following kinetic equations are valid:

$$-\frac{d[\text{aromatic}]_t}{dt} = k_1 \times [\text{aromatic}]_t \times [\text{O}_3]_t + k_3 \times [\text{aromatic}]_t$$

$$-\frac{d[\text{reference}]_t}{dt} = k_2 \times [\text{reference}]_t \times [\text{O}_3]_t$$

where $[\text{aromatic}]_t$ and $[\text{reference}]_t$ are the concentrations of the aromatic hydrocarbon and reference compounds at time t .

Integrating and combining these two equations yields the following relation between the aromatic hydrocarbon and reference concentrations and the O₃ reaction rate coefficients:

$$\ln \frac{[\text{aromatic}]_0}{[\text{aromatic}]_t} - k_3 \times t = \frac{k_1}{k_2} \times \ln \frac{[\text{reference}]_0}{[\text{reference}]_t} \quad (\text{I})$$

where $[\text{aromatic}]_0$ and $[\text{reference}]_0$ are the initial concentrations of the aromatic and reference compounds. The relative O₃ reaction rate coefficient ratio k_1/k_2 can then be derived from plots of $\ln([\text{aromatic}]_0/[\text{aromatic}]_t) - k_3 \times t$ as a function of $\ln([\text{reference}]_0/[\text{reference}]_t)$. Generally, this was the preferred method to determine the rate coefficient k_1 .

Additional experiments were also performed in the presence of an excess of O₃, i.e., a factor of at least 10 more than the initial aromatic hydrocarbon concentration. In these experiments, the concentration of ozone did not vary more than 10% and was thus assumed to be constant for the time period of the experiment. As described above, the aromatic hydrocarbon decay is due to reaction with O₃ and wall loss:

$$-\frac{d[\text{aromatic}]_t}{dt} = k_1 \times [\text{O}_3] \times [\text{aromatic}]_t + k_3 \times [\text{aromatic}]_t$$

In this case, the equation can be simplified by replacing $k_1 \times [\text{O}_3]$ by the pseudo-first-order rate coefficient,

$$k'_1 = k_1 \times [\text{O}_3]$$

yielding

$$-\frac{d[\text{aromatic}]_t}{dt} = k'_1 \times [\text{aromatic}]_t + k_3 \times [\text{aromatic}]_t$$

which on integration gives

$$\ln \left(\frac{[\text{aromatic}]_0}{[\text{aromatic}]_t} \right) - k_3 \times t = k'_1 \times t$$

The rate coefficient k_1 is then deduced from the straight line of the plot of $\ln([\text{aromatic}]_0/[\text{aromatic}]_t) - k_3 \times t$ as a function of t .

As the reaction of O₃ with all these compounds (the reference compounds, possibly the aromatic hydrocarbons under investigation and the products of reaction) could lead to the formation of OH radicals [7,14], it was necessary to perform the experiments in the presence of an OH-radical scavenger. The scavenger will react with the OH radicals that possibly arise from the O₃ reactions. 1,3,5-Trimethylbenzene was mainly employed as the scavenger, although 1,2,3-trimethylbenzene and *m*-cresol were also used in some experiments. Different OH-radical scavengers were used to check for possible influences of the scavengers on the kinetic results. The ratio $[\text{scavenger}]/[\text{catechol}]$ was varied between 10 and about 300; however, values around 150 were generally used. No influence on the results was observed from any of the scavengers. Under the experimental conditions employed, generally more than 90% of any OH radicals formed would react with the scavenger so that the contribution of any OH reaction to the decays of the aromatic and reference compounds are relatively small.

RESULTS AND DISCUSSION

Plots of the results according to Eq. (I) are displayed in Figs. 1–3 for 1,2-benzenediol, 3-methyl-1,2-benzenediol, and 4-methyl-1,2-benzenediol, respectively. The plots presented in Figs. 1–3 exhibit a good linear dependence between $\ln([\text{aromatic}]_0/[\text{aromatic}]_t) - k_3 \times t$ and $\ln([\text{reference}]_0/[\text{reference}]_t)/k_2$. The larger scatter in Fig. 1 compared to the other figures is due to the slower rate for this compound. For each aromatic compound, at least nine experiments were performed using different aromatic hydrocarbon and O₃ concentrations. Within the concentration ranges employed, no significant influence of changes in concentration on the resulting O₃ reaction rate coefficient was observed. Using the recommended rate coefficient values for k_2 , a least-square analysis of the experimental data yields the average values k_1 reported in Table I for the O₃ reaction rate coefficients.

The quoted uncertainties represent only the statistical error (2σ) from the average of the rate coefficients of all individual experiments, at the 97.5% confidence level. The main systematic uncertainty

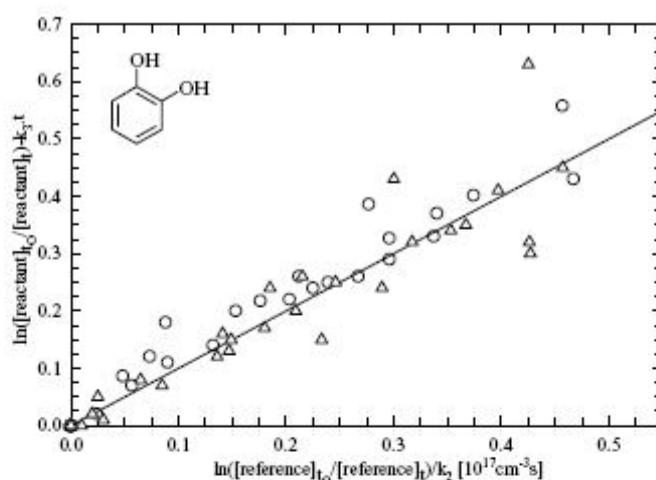


Figure 1 Plot of Eq. (I) for the reaction of 1,2-benzenediol with O_3 ; reference hydrocarbons are 1,3-butadiene for circles and propene for triangles.

arose from uncertainties in the FT-IR subtraction procedure of both the aromatic hydrocarbon and the reference compound (about 15%). Wall loss deposition rates of all the 1,2-benzenediols were fairly high compared to the O_3 reaction rates, about 20–30%, thus providing an additional 10% uncertainty in the O_3 reaction rate coefficient. An uncertainty of 25% has been attributed to the reference reaction rate coefficient k_2 [14]. The global uncertainty for each O_3 reaction rate coefficient determined in this work is estimated to be about 30–40%.

As can readily be seen in Table I, there seems to be a systematic discrepancy between the rate coefficients k_1 arising from the propene experiments and those from the 1,3-butadiene experiments (ca. 20% for 1,2-benzenediol). This discrepancy probably lies in the uncertainties in the reference O_3 reaction rate coefficients k_2 that are of the order of 25%.

To check the relative kinetic measurements a few additional experiments were also performed under pseudo-first-order conditions, the O_3 concentration being in excess (a factor of 10) and assumed to be constant

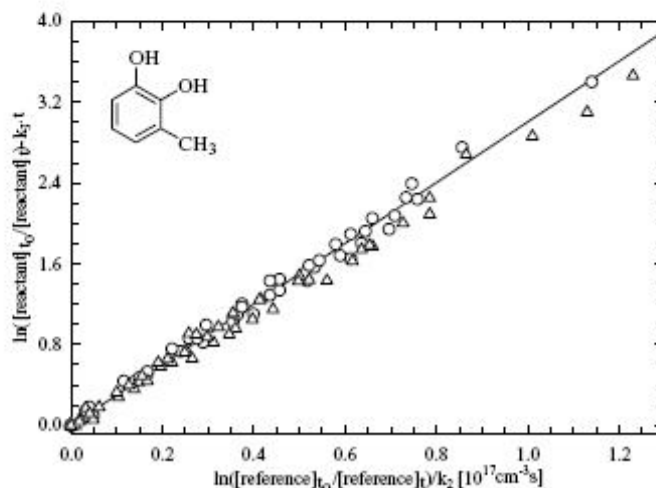


Figure 2 Plot of Eq. (I) for the reaction of 3-methyl-1,2-benzenediol with O_3 ; reference hydrocarbons are 1,3-butadiene for circles and propene for triangles.

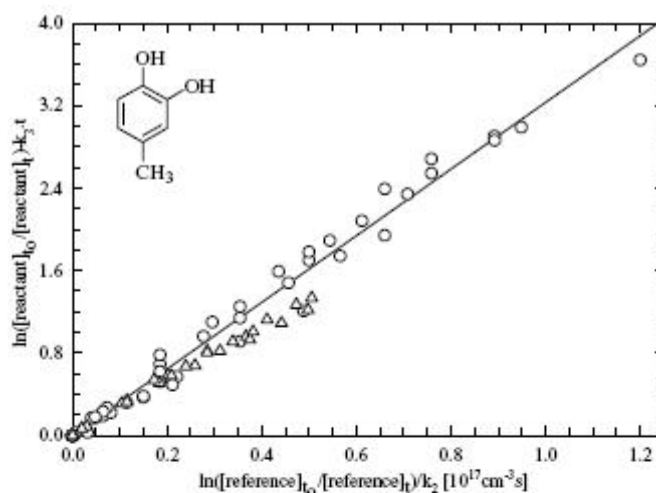


Figure 3 Plot of Eq. (1) for the reaction of 4-methyl-1,2-benzenediol with O₃; reference hydrocarbons are 1,3-butadiene for circles and propene for triangles.

within 10% during the experiment. Figure 4 shows an example of one of these experiments. As can be seen in Table I, the O₃ reaction rate coefficients obtained from such experiments are in good agreement with those obtained using the relative kinetic method, thus providing extra confidence in the results from the relative determination. Some of these experiments were carried out in the absence of an OH-radical scavenger. Given the fairly large experimental uncertainties it is difficult to interpret the differences observed in the rate coefficient values in the presence and in the absence of the OH-radical scavenger. The rate coefficient values derived from the experiments without any scav-

enger were generally somewhat higher than those derived from the experiments with a scavenger: 10% for the methyl-substituted benzenediols (which is within the error range) and 30% for 1,2-benzenediol. In the FT-IR residual spectra from these experiments none of very characteristic product bands expected from reaction of OH with 1,2-benzenediols could be observed (R. I. Olariu, A. Tomas, and I. Barnes, unpublished results). The observations support that the yield of OH radicals in the ozonolysis of 1,2-benzenediols must be fairly low.

The measured gas-phase rate coefficients for the reaction of O₃ with vicinal aromatic diol compounds

Table I Experimental O₃ Reaction Rate Coefficients Obtained in the Present Study

Aromatic Compound	Reference Hydrocarbon	k_1/k_2	k_1^a (cm ³ molecule ⁻¹ s ⁻¹)	k_1^b (cm ³ molecule ⁻¹ s ⁻¹)
1,2-Benzenediol	Propene	0.85 ± 0.08	(8.54 ± 0.84) × 10 ⁻¹⁸	(9.60 ± 1.12) × 10 ⁻¹⁸
	1,3-Butadiene ^c	1.69 ± 0.22	(1.07 ± 0.14) × 10 ⁻¹⁷ 8.59 × 10 ^{-18d}	
3-Methyl-1,2-benzenediol	Propene	2.70 ± 0.33	(2.73 ± 0.33) × 10 ⁻¹⁷	(2.81 ± 0.23) × 10 ⁻¹⁷
	1,3-Butadiene ^c	4.60 ± 0.22	(2.90 ± 0.14) × 10 ⁻¹⁷ (2.78 ± 0.30) × 10 ⁻¹⁷	
4-Methyl-1,2-benzenediol	Propene	2.51 ± 0.24	(2.54 ± 0.25) × 10 ⁻¹⁷	(2.63 ± 0.34) × 10 ⁻¹⁷
	1,3-Butadiene ^c	4.68 ± 0.55	(2.95 ± 0.35) × 10 ⁻¹⁷ (2.39 ± 0.41) × 10 ⁻¹⁷	

Note. Quoted uncertainties are 2σ.

^a $k(\text{propene} + \text{O}_3) = 1.01 \times 10^{-17}$ and $k(1,3\text{-butadiene} + \text{O}_3) = 6.3 \times 10^{-18}$ cm³ molecule⁻¹ s⁻¹ [11].

^bAverage of both relative measurements.

^cPseudo-first-order experiments (no reference hydrocarbon).

^dAverage of two measurements only.

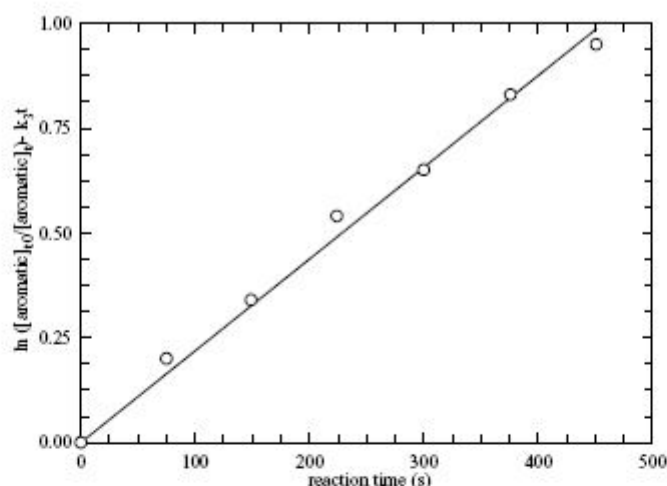


Figure 4 Typical plot obtained in an experiment carried out with an excess of O_3 without scavenger. Concentrations were $[1,2\text{-benzenediol}]_0 = 650$ ppb, $[O_3] = 8.3$ ppm; Resulting rate coefficient: $k = 1.00 \times 10^{-17} \text{ cm}^3 \text{ molecule}^{-1} \text{ s}^{-1}$.

are much higher than what is normally observed for the reactions of O_3 with alkylbenzenes and monohydroxy aromatic compounds (phenol/cresols). Rate coefficients for these reactions are generally of the order of $10^{-19} - 10^{-20} \text{ cm}^3 \text{ molecule}^{-1} \text{ s}^{-1}$ [3,7,11]. This low reactivity of aromatic compounds towards ozone has been related to the aromaticity of the benzene ring. When the aromaticity is broken, as is the case for 1,3-cyclohexadiene, the rate coefficient becomes much higher ($k_{O_3+cyclohexadiene} = 1.22 \times 10^{-15} \text{ cm}^3 \text{ molecule}^{-1} \text{ s}^{-1}$; [14]). In the case of the monohydroxy cresol isomers, the O_3 rate coefficients are 3×10^{-19} , 2×10^{-19} , and $5 \times 10^{-19} \text{ cm}^3 \text{ molecule}^{-1} \text{ s}^{-1}$ (uncertainty factor of 2) for *o*-cresol, *m*-cresol, and *p*-cresol [3,4], respectively, which are factors of between 20 and 100 less than the rate coefficients measured in this study for the diols. The rate coefficient for the gas-phase reaction of O_3 with phenol is not known.

The two OH groups in the benzenediols investigated are vicinal, i.e., *ortho*, to one another. Some experiments were also performed on the reaction of O_3 with 1,4-benzenediol where the OH groups are *para* to one another. These experiments were difficult and not very successful because of wall problems with the compound but they did demonstrate that the 1,4-isomer reacts very much slower with O_3 than the 1,2-isomer. Other experiments performed with 1,4-benzoquinone showed that this molecule also does not present any reactivity towards O_3 , even though its aromaticity is not so strong as in the case of benzene and toluene, because of the presence of the carbonyl functional groups.

At this stage it is instructive to compare the present gas-phase rate coefficients with those determined in the aqueous phase. The rate coefficients reported for the reaction of O_3 with 1,2- and 1,4-benzenediol in the aqueous phase are much larger than those in the gas phase, and in stark contrast to the present study the reaction of O_3 with 1,4-benzenediol is approximately a factor of 5 faster than that for 1,2-benzenediol [15]. No aqueous phase data could be found for 3-methyl- and 4-methyl-1,2-benzenediol. However, when making this comparison it should be borne in mind that the kinetic database is very small and that the diols will dissociate in water, which can result in a mechanistic change compared to the gas-phase reaction or even a mixture of mechanisms. The investigations in the present work were performed under very dry conditions. Because of the FT-IR analytical method employed for the analysis it was not possible to perform the reactions under the high relative humidity conditions often found in the atmosphere since the H_2O bands saturate large sections of the infrared spectral region. Of the many gas-phase kinetic studies on the ozonolysis of alkenes [16] and phenolic compounds [7] no indication has yet been found for the influence of water vapor. The reaction of O_3 with alkenes proceeds via electrophilic addition of O_3 to the double bond, and the ozonation of phenols and aromatic 1,2-diols, based on observed products, has also been proposed to proceed via addition of O_3 to the aromatic ring, the O_3 adding to the ring across the carbons bearing the OH groups [17]. If such a mechanism is occurring water will not affect

the primary rate-controlling step but could influence the product distribution by involvement in secondary reaction steps as is well documented for alkenes [16]. Addition of O₃ across the OH groups is not surprising since the juxtaposition of the hydroxyl groups in the catechols raises the electron densities at these sites and facilitates reactivity towards electrophilic reagents like O₃. If the mechanistic considerations are correct then enhanced gas-phase reactivity towards O₃ would be expected for other aromatic compounds containing electron-donating groups such as -OCH₃ and -NH₂ in a 1,2 site configuration. To our knowledge no investigation on the gas-phase kinetics of such compounds have been reported to date.

The infrared product spectrum observed from the ozonation of 1,2-benzenediol is relatively simple with a broad carbonyl absorption band around 1800–1600 cm⁻¹ and absorptions in the OH stretching region that are typical for carboxylic acids. A preliminary GC-MS analysis has shown that muconic acid (2,4-hexadienedicarboxylic acid) is a product, which would support that the addition of O₃ to the ring across the carbons bearing the OH groups is occurring followed by subsequent ring fragmentation.

Based on the available evidence, it would appear that the vicinal nature of the two OH groups in aromatic diols rather than a decrease of the aromaticity is responsible for the enhanced reactivity of these 1,2-benzenediols towards O₃.

It is also interesting to note that the rate coefficients for the methylated 1,2-benzenediols are about three times greater than for 1,2-benzenediol. The same trend has been observed in the ozonolyses of benzenols (phenols) [17] where the presence of the methyl group increases the reactivity towards O₃; this effect has also been observed for the reactivity of 1,2-benzenediols towards OH radicals [18].

ATMOSPHERIC IMPLICATIONS

The benzenediol compounds investigated in the present study are the major degradation products of the

OH-initiated oxidation of phenol and the cresol isomers. The yields of formation of these products are now known to be between 70 and 80% [8-10], making them important atmospheric secondary oxidation products. The reaction rate coefficient of 1,2-benzenediol, 3-methyl-1,2-benzenediol, and 4-methyl-1,2-benzenediol with the OH radical are 1.04×10^{-10} , 2.05×10^{-10} , and 1.56×10^{-10} cm³ molecule⁻¹ s⁻¹, respectively [18]. Using this kinetic data for OH and the O₃ kinetic data from this study, atmospheric residences τ_i for the benzenediols with respect to reaction with OH and O₃ can be calculated according to the relationship $\tau_i = (k_i [\text{OH or O}_3])^{-1}$. Table II shows residence times based on an average tropospheric hydroxyl radical concentration of 1.6×10^6 cm⁻³ [19,20] and an O₃ concentration of 2.46×10^{12} cm⁻³ (~100 ppb at 298 K and atmospheric pressure), which is of the order of magnitude of the O₃ concentrations often encountered in polluted areas [21].

It is evident that the contribution of O₃ reaction to the overall oxidation of these aromatics can be fairly significant and could be potentially much greater for severe smog events. As aromatic compounds are emitted principally from car gas exhaust, a lot of their photooxidation will occur in areas where ozone levels can be very high.

As mentioned in the introduction aromatic compounds comprise a significant proportion of the secondary organic aerosol (SOA) formation observed in urban areas, the identity of which is still uncertain [22-24]. The observation of substantial aerosol formation from the reaction of ozone with the benzenediols was the main incentive for the present kinetic investigation. As mentioned earlier, preliminary results indicate that a major component of the aerosol is probably muconic acid and work is currently ongoing to quantify and identify the main components of the aerosol formed from the reaction of O₃ with benzenediols. These investigations will allow an evaluation of the contribution of such previously unconsidered reactions to the SOA formation from the photooxidation of the simple alkylbenzenes (benzene, toluene, and the xylene isomers).

Table II Comparison Between Atmospheric Lifetimes in Relation to OH Radical and O₃ Molecule Oxidation of Benzenediol Compounds

Aromatic Compound	Lifetime with Respect to OH Radical Oxidation ^a (h)	Lifetime with Respect to O ₃ Oxidation ^b (h)	Contribution of O ₃ Reaction (%)
1,2-Benzenediol	1.67	11.76	12
3-Methyl-1,2-benzenediol	0.85	4.02	17
4-Methyl-1,2-benzenediol	1.11	4.29	20

^aAverage concentration of OH radicals: 1.6×10^6 molecule cm⁻³; rate coefficients are from Ref. [18].

^bAverage concentration of O₃: 100 ppb (polluted atmosphere).

BIBLIOGRAPHY

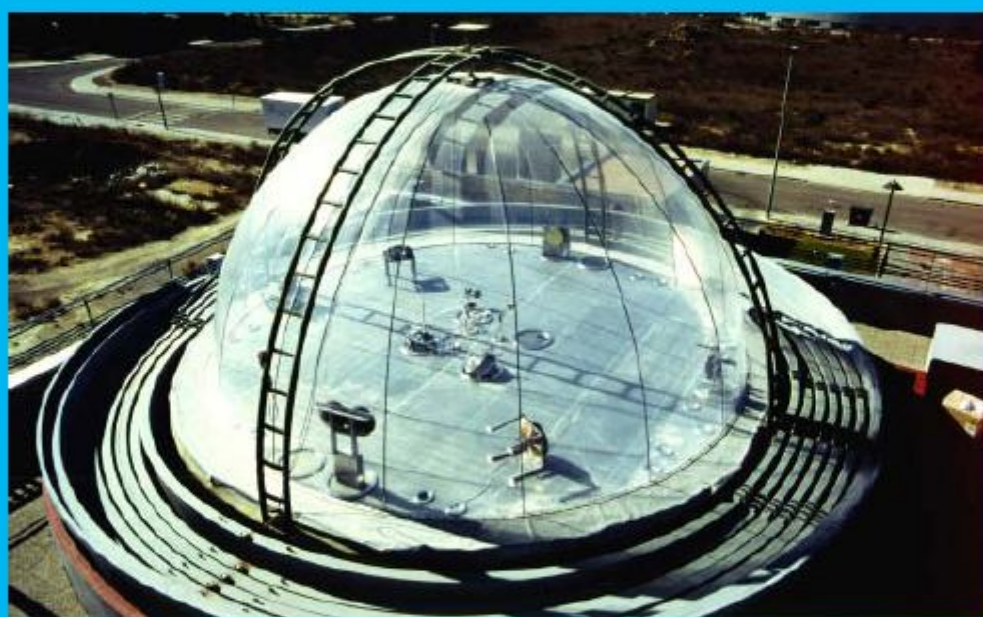
1. Odum, J. R.; Jungkamp, T. P. W.; Griffin, R. J.; Flagan, R. C.; Seinfeld, J. H. *Science* 1997, 276, 96.
2. Derwent, R. G.; Jenkin, M. E.; Saunders, S. M. *Atmos Environ* 1996, 30, 181.
3. Atkinson, R. *J Phys Chem Ref Data, Monograph 2*, 1994, 1.
4. Volkamer, R.; Klotz, B.; Barnes, I.; Imamura, T.; Wirtz, K.; Washida, N.; Becker, K. H.; Platt, U. *Phys Chem Chem Phys* 2002, 4, 1598.
5. Klotz, B.; Volkamer, R.; Hurley, M. D.; Sulbaek, Andersen, M. P.; Nielsen, O. J.; Barnes, I.; Imamura, T.; Wirtz, K.; Becker, K. H.; Platt, U.; Wallington, T. J.; Washida, N. *Phys Chem Chem Phys* 2002, 4, 4399.
6. Berndt, T.; Böge, O. *Phys Chem Chem Phys* 2001, 3, 4946.
7. Calvert, J. G.; Atkinson, R.; Becker, K. H.; Kamens, R. M.; Seinfeld, J. H.; Wallington, T. J.; Yarwood, G. *Mechanisms of Atmospheric Oxidation of Aromatic Hydrocarbons*; Oxford University Press: New York, 2002.
8. Olariu, R. I.; Barnes, I.; Becker, K. H.; Klotz, B.; Mocanu, R. *Proceedings of the EC/EUTROTRAC-2 Joint Workshop, EC Cluster 4: Chemical Processes and Mechanisms, EUTROTRAC-2: Chemical Mechanism Development, EPFL, Lausanne-Ecublens, Switzerland, Sept. 11–13, 2000*; pp. 60–63.
9. Olariu, R. I.; Klotz, B.; Barnes, I.; Becker, K. H.; Mocanu, R. *Atmos Environ* 2002, 36, 3685.
10. Berndt, T.; Böge, O. *Phys Chem Chem Phys* 2003, 5, 342–350.
11. Atkinson, R.; Carter, W. P. L. *Chem Rev* 1984, 84, 437.
12. Yamamoto, Y.; Niki, E.; Shiokawa, H.; Kamiya, Y. *J Org Chem* 1979, 44, 2137.
13. Barnes, I.; Becker, K. H.; Mihalopoulos, N. *J Atmos Chem* 1994, 18, 267.
14. Atkinson, R. *J Phys Chem Ref Data* 1997, 26, 215.
15. Retrieved January 2003 from <http://kinetics.nist.gov/solution/index.php>. January 2003.
16. Calvert, J. G.; Atkinson, R.; Kerr, J. A.; Madronich, S.; Moortgat, G. K.; Wallington, T. J.; Yarwood, G. *The Mechanism of Atmospheric Oxidation of the Alkene*; Oxford University Press: New York, 2000.
17. Bailey, P. S. *Ozonation in Organic Chemistry, Vol. II: Nonolefinic Compounds*; Academic Press: New York, 1982.
18. Olariu, R. I.; Barnes, I.; Becker, K. H.; Klotz, B. *Int J Chem Kinet* 2000, 32, 696.
19. Prinn, R.; Cunnold, D.; Simmonds, P.; Alyea, F.; Boldi, R.; Crawford, A.; Fraser, P.; Gutzler, D.; Hartley, D.; Rosen, R.; Rasmussen, R. *J Geophys Res* 1992, 97, 2445.
20. Crutzen, P. J.; Zimmermann, P. H. *Tellus* 1991, 43A, 136.
21. Lin, C.-Y. C.; Jacob, D. J.; Fiore, A. M. *Atmos Environ* 2001, 35, 3217.
22. Yu, J.; Jeffries, H. E.; Sexton, K. G. *Atmos Environ* 1997, 31, 2261.
23. Yu, J.; Jeffries, H. E. *Atmos Environ* 1997, 31, 2281.
24. Jang, M.; Kamens, R. M. *Environ Sci Technol* 2001, 35, 3626.

Publication n°9

(parue dans le *Rapport annuel 2001 du centre de recherche européen EUPHORE* en 2003)

The European Photoreactor EUPHORE

4thREPORT 2001



Editor: Ian Barnes

Compiled by:
Institute of Physical Chemistry, Bergische Universität Wuppertal
Wuppertal, November 2003

The European Photoreactor

EUPHORE

4th Report 2001

Editor: Ian Barnes

Compiled and Produced by:
Institute of Physical Chemistry, Bergische Universität Wuppertal
Wuppertal, November 2003

PDF copies of the report can be downloaded from the web site:
http://www.physchem.uni-wuppertal.de/PC-WWW_Site/Publications/Publications.html

*Hard copies of the report can be obtained from Dr. Barnes, Bergische Universität Wuppertal,
Physikalische Chemie / FB 9, Gauss Str. 20, 42097 Wuppertal, Germany*

e-mail: becker@uni-wuppertal.de; barnes@uni-wuppertal.de

3.5 Atmospheric Ozone Degradation Reaction of 1,2-dihydroxybenzene: Aerosol Formation Study

R.I. Olariu, "A.I.I. Cuza" University of Iasi, Department of Analytical Chemistry, Faculty of Chemistry, Romania

Al. Tomas, Ecole des Mines de Douai, Département Chimie et Environnement, France.

I. Barnes, I. Bejan, K.H. Becker, Bergische Universität Wuppertal, Germany.

K. Wirtz, EUPHORE Laboratories. Fundación Centro de Estudios Ambientales del Mediterráneo., Charles R. Darwin, 14, 46980 Paterna, Valencia, Spain.

Objective

The main objective of the present study was to quantify the particles formed from the ozonolysis of 1,2-dihydroxybenzene in purified air in the EUPHORE chamber facilities. The work was performed within the frame of the EAXT project in order to improve the understanding of the mechanisms of SOA formation from the photooxidation of aromatic hydrocarbon systems.

Introduction

The presence of aromatic hydrocarbons, principally benzene, toluene and xylene isomers (BTX), in urban areas is directly correlated with anthropogenic activities. This class of hydrocarbon is assumed to be responsible for two main aspects of air pollution. One is their role as precursors in the formation of photo-oxidants (Derwent *et al.*, 1998) and the second is their contribution to secondary organic aerosol (SOA) formation (Odum *et al.*, 1997a,b; Forstner *et al.*, 1997; Hurley *et al.*, 2001). The aromatic hydrocarbons are believed to be a major anthropogenic source of secondary organic aerosol in urban areas (Seinfeld and Pandis, 1998). Many important aspects of the reaction and SOA formation mechanisms still need to be clarified.

Recent findings on the photo-oxidation of aromatic hydrocarbons (Klotz *et al.*, 2002, Volkamer *et al.*, 2002) have shown that it is necessary to reconsider the importance of the ring-retaining degradation pathways of aromatic hydrocarbon systems under atmospheric conditions. In the case of benzene, for example, experimentally obtained phenol yields under near atmospheric conditions are in the range 0.24 – 0.53 (Atkinson, 1994; Bohn *et al.*, 1999, Volkamer *et al.*, 2002). The further OH-radical initiated oxidation of phenol is now believed to lead to the formation of 1,2-dihydroxybenzene in yields between 73-80% (Olariu *et al.*, 2001a;

Olariu *et al.*, 2002a; Berndt and Børge, 2003) thus rendering them very important secondary ring-retaining products in the oxidation of benzene.

It is known that (e.g. phenol) do not contribute as efficiently to photo-oxidant formation as the products formed after ring-cleavage, but it has been always suggested that the ring-retaining products should have an important role in the SOA formation processes. While it has been known for some time that the atmospheric oxidation of aromatic species leads to aerosol formation, the exact mechanism by which aerosol is formed is unclear.

Secondary organic aerosols result from the atmospheric oxidation of primary organic compounds whose molecules are sufficiently large to lead to products with vapor pressures low enough to enable them to condense into the aerosol phase. From this point of view, it is interesting to note the relationship between the vapor pressure and the changes in molecular structure as the oxidation process is proceeding. For BTX there are large decreases in vapor pressure as $-OH$ and $-NO_2$ groups are added to the aromatic ring structure (Yaws *et al.*, 1999).

Results from recent studies performed in the EUPHORE chamber on the aerosol formation from the photo-oxidation of the phenol initiated by OH radicals under different conditions indicate that the formation of 1,2-dihydroxybenzene, as the main primary gas-phase product (about 80% molar yield, Olariu *et al.*, 2001a) is probably crucial in the initiation of the aerosol formation processes from such systems. Little is currently known about the atmospheric chemistry of 1,2-dihydroxybenzene. Gas-phase kinetic studies of 1,2-dihydroxy(alkyl)benzenes have shown that these compounds react rapidly with OH radicals (Olariu *et al.*, 2000), NO_3 radicals (Olariu *et al.*, 2002b) and with O_3 (Tomas *et al.*, 2003). Therefore, 1,2-dihydroxybenzenes will contribute significantly to the fast secondary chemistry in alkylbenzene photooxidation systems and, depending on the products, could make a sizeable contribution to the SOA formation observed in such systems (Olariu *et al.*, 2001b).

In a series of experiments to determine and quantify pathways leading to aerosol formation in the oxidation of aromatic hydrocarbons we report here on investigations of SOA formation from the ozonolysis of 1,2-dihydroxybenzene in the EUPHORE outdoor smog chamber facility.

Experimental

A total of 5 experiments on the reaction of 1,2-dihydroxybenzene with O_3 were conducted in EUPHORE chamber B. A detailed description of the experimental set-up is available elsewhere (Becker, 1996). A brief description including only the analytical instruments used in the present study is given below.

The reaction mixtures were monitored by long path in-situ IR-spectroscopy (Nicolet Magna 550 spectrometer, mercury-cadmium-tellurium (MCT) detector, spectral resolution 1 cm^{-1} , optical path of 553.5 m). The spectra were derived from 300 co-added interferograms. FT-IR analyses were carried out by computer-aid subtraction of calibrated reference spectra. The concentrations of the aromatic compounds were calculated using FT-IR integral and absolute cross section taken from the literature (Olariu et al., 2002a).

For the analyses of the gas-phase products as well as for the aerosol products, the reaction mixture was sampled in three different ways: sampling on Teflon filters, followed by GC-MS analysis; sampling on DNPH cartridges, followed by HPLC – UV detector analysis and on-line sampling for TGA (Trace Gas Analyzer).

A NO_x analyzer (ECO-Physics CLD 770 AL NO -analyzer with photolytic NO_2 converter PLC 760) and an ozone analyzer (Monitor Labs) were in operation during the experiments.

For analysis of the aerosol size distribution an SMPS system (TSI 3934), consisting of an electrostatic classifier (TSI 3071A) and a condensation particle counter (TSI 3022A) was used. The sampling line was a straight $\frac{1}{4}$ inch stainless steel tube of 1.5 m length. The sampling site was located ca. 0.5 m above the chamber floor and about 1 m away from the FEP wall. SMPS sampling was timed to coincide with the recording of the FT-IR spectra, resulting in sampling times of 5 min.

The experimental procedure was as follows: Prior to injection of 1,2-dihydroxybenzene, a weighed amount of the compound was dissolved in a small volume of distilled water which was then added to the chamber using a spray inlet system. For some experiments cyclohexane (used as scavenger for any OH radicals produced from the ozonolysis) was then injected by a syringe into a glass tube (impinger) connected to the chamber by a Teflon line and flushed into the chamber in flow of purified warm air. 1,2-Dihydroxybenzene and cyclohexane were used as supplied by Aldrich Chemical Company and had stated purities of $> 98\%$. O_3 , produced by the photolysis of O_2 at 184.9 nm using a commercial Pen-ray low-pressure mercury lamp, was then added directly to the chamber through a Teflon line for about 10-15 min. Subsequent losses of 1,2-dihydroxybenzene as well as the formation of aerosols were monitored over time period of 1-2 hours.

The relative humidity (RH) in the chamber during the experiment runs was less than 2 %. The experiments were terminated by addition of large amount of NO to the chamber. The decay of the aerosol in the dark was then monitored for a short period.

The reaction chamber was pressurized continuously during the experiments to compensate for losses due to sampling and leaks. This dilution was monitored by FT-IR using SF₆ as an inert tracer gas; the loss rate was typically about 3 % h⁻¹.

The reactant concentrations employed in the EUPHORE experiments are given in Table 1. Also listed in this Table are the reacted fractions of the 1,2-dihydroxybenzene and the maximum and final O₃ concentrations.

Table 1. Overview of the experimental conditions employed for the aerosol study of the O₃-initiated oxidation of 1,2-dihydroxybenzene (DHBZ) performed in Chamber B at CEAM institute Valencia/Spain in May 07-14, 2001.

experiment name	reaction	DHBZ (ppb)	O ₃ max. (ppb)	DHBZ reacted %	O ₃ end (ppb)
cat1 (07/05/01)	1,2 DHBZ + O ₃	1370	242	21	116
cat2 (08/05/01)	1,2 DHBZ (cyclohexane-160 ppm) + O ₃	307	170	20	114
cat3 (09/05/01)	1,2 DHBZ + O ₃	309	190	30	123
cat4 (10/05/01)	1,2 DHBZ + O ₃	314	1062	~90	735
cat5 (15/05/01)	1,2 DHBZ (cyclohexane-360 ppm) + O ₃	294	242	17	112

In the experiments the initial 1,2-dihydroxybenzene concentration and the maximum O₃ concentration added were varied by almost a factor of five. In one experiment the input order of the reactants 1,2-dihydroxybenzene and O₃ was reversed. In the experiment performed on 10/05/01, a large amount of ozone (about 1062 ppb) was added first and then 1,2-dihydroxybenzene. The reason for this experiment was to look for possible influences of the addition order of the reactants on the aerosol formation processes.

Since the ozonolysis of alkenes produces OH radicals (Atkinson, 1997) cyclohexane was used in 2 experiments (cat2 and cat5) as an OH scavenger to check for possible OH radical formation in the reaction of O₃ with 1,2-dihydroxybenzene. Ratios [scavenger]/[1,2-dihydroxybenzene] of 160 and 360 were used for cat2 and cat5, respectively. Under these conditions more than 95% of any OH radicals formed will react with the scavenger thus rendering the contribution of any OH reaction to the decays of the aromatic negligible.

Results and discussions

Figure 1 shows typical concentration-time profiles of 1,2-dihydroxybenzene and O₃, the particle number and the measured aerosol mass.

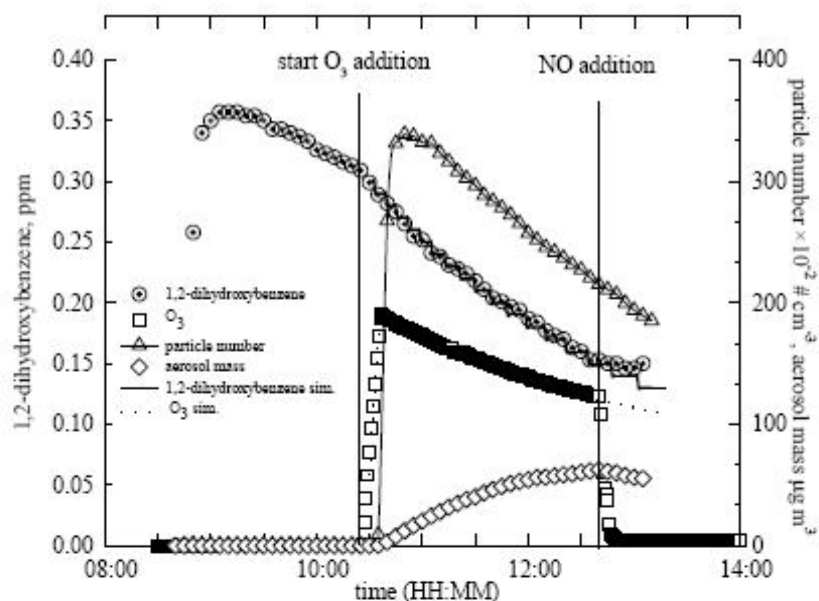


Figure 1. Concentration-time profiles of reactants and formation of particles recorded during one experiment performed in EUPHORE chamber B (experiment cat3, performed on the 09/05/2001).

Aerosol formation was observed in all experiments within this study. Particle formation only occurred after addition of O_3 . The formation was observed 5 min after the addition of O_3 (see Figure 1). In all the experiments the particle-time profiles show a rapid increase in the particle number concentration followed by a rapid decrease. The initial particles observed were small, with diameters of about 70 nm. Rapid growth led to particles with a final mean diameter of around 170 ± 20 nm. A time series of aerosol size distributions measured during a typical experiment is shown in Figure 2.

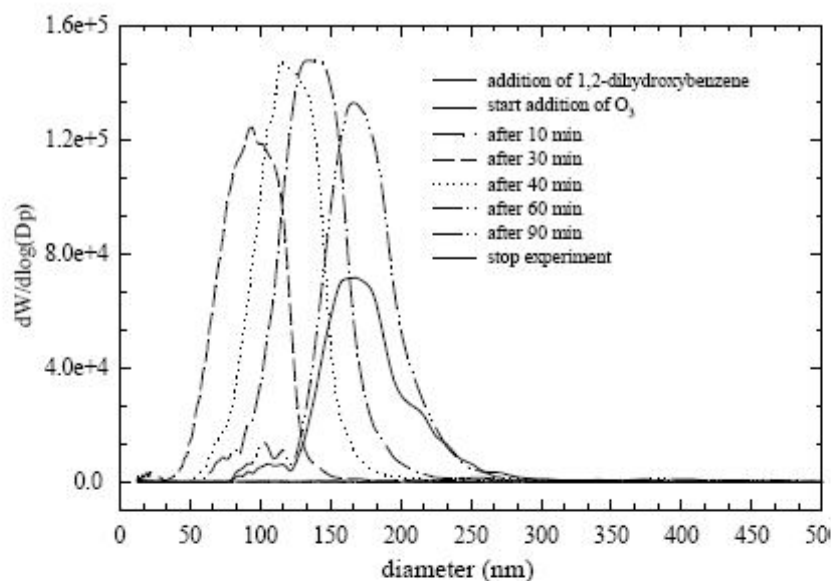


Figure 2. Aerosol distributions observed in the EUPHORE chamber from a reaction mixture containing 309 ppb 1,2-dihydroxybenzene and 190 ppb added O_3 (exp cat3 performed on the 09/05/01).

The aerosol mass formed during the reaction time has been obtained from the aerosol volume distribution assuming unity density. The shape of the aerosol mass curves depends on both the aerosol production from 1,2-dihydroxybenzene oxidation, aerosol loss processes like wall deposition and dilution. In deriving the aerosol formation yields, these secondary processes need to be considered. Aerosol wall deposition and dilution rates were determined by observing the decay of the aerosol in the dark, after termination of the experiment by addition of large amount of NO to destroy O_3 . Corrections for dilution and wall deposition were made to the aerosol and reactant data.

The corrected aerosol masses from all the experiments are plotted against the amounts of 1,2-dihydroxybenzene reacted in Figure 3. Aerosols formation yields were derived from the linear sections of the slopes. Table 2 gives an overview of the results obtained. The aerosol yields generally varied from 20% to 27% with slightly higher values when cyclohexane is not present. A very high yield was obtained (58.5 %) when $[O_3]$ was very high (experiment cat4: 1,2-dihydroxybenzene ~90% consumed).

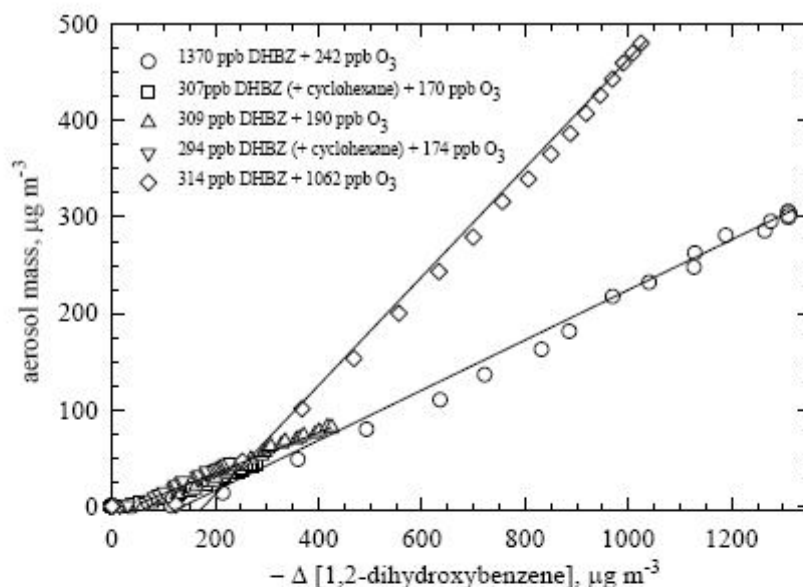


Figure 3. Aerosol mass from the O₃-initiated oxidation of 1,2-dihydroxybenzene as a function of 1,2-dihydroxybenzene consumption.

Table 2. Overview of the results obtained from the aerosol studies on the O₃-initiated oxidation of 1,2-dihydroxybenzene.

experiment name	reaction	mass DHBZ reacted (µg m ⁻³)	mass aerosol (µg m ⁻³)	aerosol yield (%)
cat1 (07/05/01)	1,2 DHBZ + O ₃	1308	299.6	27.6
cat2 (08/05/01)	1,2 DHBZ (cyclohexane-160ppm) + O ₃	279	44.3	19.9
cat3 (09/05/01)	1,2 DHBZ + O ₃	422	85.3	23.7
cat4 (10/05/01)	1,2 DHBZ + O ₃	1084	550.0	58.5
cat5 (15/05/01)	1,2 DHBZ (cyclohexane-360ppm) + O ₃	229	44.7	24.8

The present study gives little information on the chemical composition of the gas-phase and particle products. The IR residual product spectra could not be evaluated because of the overlap with the spectral features of H₂O. Small aldehydes were identified, formaldehyde, acetaldehyde and glyoxal from the analyses of DNPH cartridge samples. A preliminary GC-MS analysis of the Teflon filter samples has shown, based on MS library data, that a large body of ring-cleavage products such as carboxylic acids, e.g. muconic acid (2,4-hexadienedicarboxylic acid), were formed in the gas-phase as well as in the aerosol phase. Quantification of the products identified by HPLC and GC-MS is currently ongoing.

OH radical reaction influence on aerosol formation

Formation of OH radicals during the experimental runs has been confirmed by the chromatograms obtained from the TGA sample analyses which show the formation of cyclohexanone in the reaction system. The OH radicals produced in the system could be formed by the reaction of O₃ with the reactant or unsaturated products and/or its photolysis since the chamber is not completely dark. Because of the high magnitude of the OH radical reaction rate coefficient, $k_{OH} = 1.04 \cdot 10^{-10} \text{ cm}^3$ (Olariu *et al.*, 2000) both ozone and OH reactions will contribute to the decay of 1,2-dihydroxybenzene during the experiment runs without scavenger.

To estimate the relative contributions of the 2 possible decay pathways of 1,2-DHBZ, i.e. ozonolysis versus OH radical reaction, the decay of 1,2-dihydroxybenzene has been simulated in a first step assuming that the 1,2-dihydroxybenzene compound reacts only with O₃. The O₃ + 1,2-dihydroxybenzene rate constant derived from the simulations of the experiments without scavenger (cat2 and cat5) was always higher than that determined in the kinetic study of Tomas *et al.* (2003) by a factor of about 1.5. In a second step the contribution of the OH radical reaction to the 1,2-dihydroxybenzene decay was taken into account for the simulation. The rate constant used in the simulation was $k_{O_3} = 9.6 \times 10^{-18} \text{ cm}^3$ (Tomas *et al.*, 2003). In this case, an excellent fit between simulation and the experimental data points was obtained. The magnitude of the [OH] radical concentration has been estimated to be $7.0 \cdot 10^{-3} \text{ ppt}$ using a rate coefficient of $k_{OH} = 1.04 \cdot 10^{-10} \text{ cm}^3$ (Olariu *et al.*, 2000). The ratios of the OH radical reaction and the ozonolysis of 1,2-dihydroxybenzene as obtained from simulations are given in Table 3. The solid line in Figure 1 is the simulation for the experiment performed on 09/05/2001.

Considering the simulation results from the present experimental data it can be concluded that during the ozonolysis of 1,2-dihydroxybenzene OH radicals are formed and that they contribute approximately 30% to the decay of the aromatic compound. From Table 2 it can be seen that the aerosol yield measured in the absence of the scavenger are slightly higher than those measured in the presence of the scavenger. This indicates that the aerosol formed in the reaction mixture involves both reactions with O₃ and OH radical, and suggests that they could have the same magnitude with respect to secondary organic aerosol formation.

Table 3. Overview of the results obtained from the aerosol studies on the O₃-initiated oxidation of 1,2-dihydroxybenzene.

experiment name	Reaction	Simulation 1 α_1 ^a	Simulation 2		
			$\alpha_2(\%)$ ^b	$K(\text{m}^3 \mu\text{g}^{-1})$	p_i (torr)
cat1 (07/05/01)	1,2 DHBZ + O ₃	0.41	26.68	1.9×10^{-2}	8.8×10^{-6}
cat2 (08/05/01)	1,2 DHBZ (cyclohexane) + O ₃	-	18.21	1.2×10^{-1}	1.4×10^{-6}

cat3 (09/05/01)	1,2 DHBZ + O ₃	0.44	26.65	4.4×10 ⁻²	3.8×10 ⁻⁶
cat4 (10/05/01)	1,2 DHBZ + O ₃	0.46	60.10	7.7×10 ⁻³	2.5×10 ⁻⁵
cat5 (15/05/01)	1,2 DHBZ (cyclohexane) + O ₃	-	24.34	1.0×10 ⁻¹	1.6×10 ⁻⁶

Note: a: α_1 is the ratio: $k_{OH} \times [OH] / k_{O_3} \times [O_3]$.

b: α_2 is the % molar yield of the major product in the ozonolysis of 1,2-dihydroxy(alkyl)benzene that is expected to partition into gas and condensed phases.

Aerosol as secondary product

Using the aerosol volume distribution and assuming unity density, qualitative information concerning the aerosol yield from the ozonolysis of 1,2-dihydroxybenzene has been obtained. The gas/phase adsorption model proposed by Odum *et al.* (1996) has been used. In this model the fractional aerosol yield (Y) is defined as the amount of reacted reactive organic (Δ ROG) which is converted into aerosol and the aerosol yield is given by:

$$Y = \frac{\Delta M_0}{\Delta \text{ROG}} \quad (\text{I})$$

where ΔM_0 is the organic aerosol mass concentration ($\mu\text{g m}^{-3}$) produced for a given amount of compound reacted, ΔROG ($\mu\text{g m}^{-3}$).

The essence of the gas/particle model proposed by Odum *et al.* (1996) is that the gas phase oxidation of the parent compound produces semi-volatile compounds which partition between the gas and the organic aerosol phases. Taking this into account, the model proposed an expression that includes the total aerosol yield in terms of the individual product mass-based stoichiometric coefficients α_i , and the partitioning coefficients K_i , and the total organic aerosol mass concentration M_0 :

$$Y = M_0 \sum_{i=1}^n \frac{\alpha_i K_i}{1 + K_i M_0} \quad (\text{II})$$

Figure 4 shows examples of plots of the aerosol yield, as defined above, as a function of the secondary aerosol mass concentration M_0 ($\mu\text{g m}^{-3}$) for experiments performed on O₃ reaction with 1,2-dihydroxybenzene.

Although the organic aerosol phase is often comprised of dozens of oxidation products (Forstner *et al.*, 1997), the aerosol yield data measured in aromatic compound systems have usually been fitted assuming that there are only two hypothetical products (Odum *et al.*, 1997 a,b).

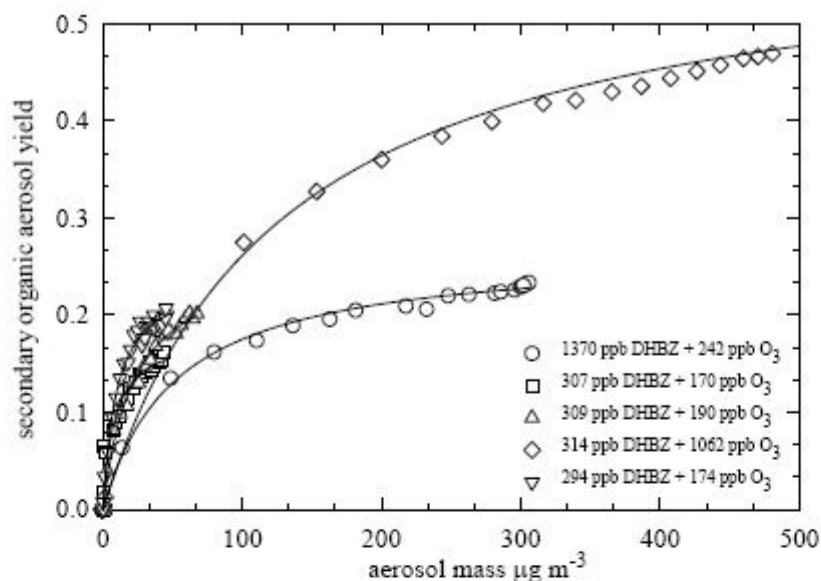


Figure 4. Secondary organic aerosol yields from the O₃-initiated oxidation of 1,2-dihydroxybenzene as a function of aerosol mass concentration.

In very recent results from Ferry *et al.* (2001) and Olariu *et al.* (2001b) it was indicated that the aerosol yield obtained in aromatic photooxidation systems could be well described by assuming only one hypothetical product. In the present study the results can be simulated using an expression of type:

$$y = \frac{ax}{b+x} \quad (\text{III})$$

which includes only two parameters: a is the individual product mass-based stoichiometric coefficient α and b is the partitioning coefficient K (y and x are Y and M_0 , respectively). As can be seen in the Figure 4, the aerosol yield data can be well characterized by assuming that there is only one semi-volatile major product formed in the ozonolysis of 1,2-DHBZ. The use of two or more products in the model does not improve the quality of the fits. The parameters α and K derived from the fits of the experimental data are presented in Table 3 (α is listed as α_2 in the table).

At this stage it is important to compare the measured aerosol yield and the stoichiometric coefficient α . It is known that the stoichiometric coefficient α depends on the gas-phase chemical reaction mechanism and represent the total amount of the semi-volatile product formed in both the gas- and aerosol-phase, per amount of parent organic compound reacted, whereas the yield Y measures only the semi-volatile products that have been formed during the oxidation period and depends on both the gas-phase chemical reaction and the amount of organic mass available as adsorption

medium. The values of Y (see Table 3) compared with those of α_2 (see Table 2) are slightly higher. This observation together with the results from the gas/aerosol adsorption model (see above) suggests that the “lumped” low-volatile compound that is generated in the system via the ozonolysis of 1,2-dihydroxybenzene will probably go almost completely into the particle phase. The reactions of ozone with unsaturated species generally produce higher molecular weight and hence lower volatility compounds (Hoffmann *et al.*, 1997). The preliminary product data suggest that one such low-volatile compound could be muconic acid. Formation of muconic acid in the reaction system could be expected to come from the ozonolysis of *o*-quinone (Bailey, 1982).

Considering only the aerosol phase the partitioning coefficient K_i ($\text{m}^3 \mu\text{g}^{-1}$) can be expressed in terms of mean molecular weight \overline{M}_w (g mol^{-1}), vapor pressure p_i (torr), activity coefficient γ_i , temperature T (K), and the ideal gas constant R ($6.2 \times 10^{-2} \text{ torr m}^3 \text{ mol}^{-1} \text{ K}^{-1}$) (Calvert *et al.*, 2002):

$$K_i = \frac{RT}{\overline{M}_w \gamma_i p_i} 10^{-6} \quad (\text{IV})$$

Using this relation together with the partitioning coefficient values obtained from the above simulation results (see Table 3), the partial pressure p_i (torr) of the “lumped” low-volatile compound has been calculated for all the experiments performed in the EUPHORE chamber assuming that the mean molecular weight of the aerosol mass is the same as that of 1,2-dihydroxybenzene and that the activity coefficient γ_i is unity. The vapor pressure values obtained for the one compound formed in the gas-phase are indicated in Table 3. They fall into the range 10^{-5} - 10^{-6} torr which is reasonable for secondary oxidation products (Calvert *et al.*, 2002). It is known that compounds with vapor pressures less than 1×10^{-3} torr are often found in the aerosol phase. At this point it is necessary to indicate that while the simple model considers only one low volatility secondary oxidation product, it is well established that in reality the aerosol is composed of many different chemical compounds (Forstner *et al.*, 1997). The model that has been employed is the simplest which captures the essential features of aerosol formation.

The aerosol profiles shown in Figure 1 are unlike primary product profiles observed in gas phase studies. Primary product profiles pass through the origin and are independent of initial reactant concentration. Using the simple conceptual model proposed by Hurley *et al.* (2002), it is possible to interpret the aerosol mass formation as resulting from secondary chemistry involving one primary product, i.e. from the ozonolysis of 1,2-dihydroxybenzene. Based on the following analytical expressions:





primary (P) and secondary (S) oxidation product profiles can be generated from the initial reactant concentration $[R]_0$ and the rate constants k_1 and k_2 .

If during the experimental runs reaction with O_3 is the major loss process for both reactant and primary product, then the concentration profile of the product P can be described by:

$$[P] = \frac{\alpha}{(1 - k_{ratio})} (1 - x) [(1 - x)^{(k_{ratio} - 1)} - 1] [R_0] \quad (V)$$

where x is defined as the conversion of R, $\Delta[R]/[R]_0$, α is the yield of P and k_{ratio} is the rate constant ratio, k_2/k_1 . Since α is the yield of P, the concentration of S is given by:

$$[S] = \alpha(\Delta[R]) - [P] \quad (VI)$$

Figure 5 shows the predicted primary and secondary product profiles calculated using equations (V) and (VI). The profiles P and S are shown for the case where $\alpha = 0.25$ (taking into account the values of α_2 obtained in Table 3) and $k_2/k_1 = 50$ (see later in text).

The secondary product S profile in Figure 5 is for gas phase, while what is observed experimentally is the aerosol mass formation. Secondary product S is initially formed in the gas phase and it does not go in the aerosol phase (to contribute to the aerosol mass) until the concentration of S exceeds its vapor pressure. Partitioning of S between the gas and condensed phase will then occur. This phenomenon would appear as an offset between the secondary product profile and the aerosol mass profile. Furthermore, if this offset has the properties of a vapor pressure, it will be independent of initial reactant concentration but it must be directly correlated with the nature of the gas-phase compound as well as particle phase existing in the reaction mixture. Equation (VI) can be expanded to incorporate this secondary product offset. If p is the concentration offset then this offset can be incorporated into equation (VI) to arrive at an expression for aerosol mass M_0 formed from the condensation of the secondary product S:

$$[M_0] = \{\alpha(\Delta[R]) - [P]\} - p \quad (VII)$$

Considering the similarity between α (α_2 in fact) and Y (see Table 2 and 3), it was also assumed that S goes predominately into the condensed phase and reaction of S in the gas phase has a small impact on the total S concentration. Figure 5 shows an example of the predicted aerosol profile using equation (VII) where the parameter p has been converted into $\mu\text{g m}^{-3}$ units using the values given in Table 3. The predicted particle profile agrees fairly well with the observed aerosol behavior.

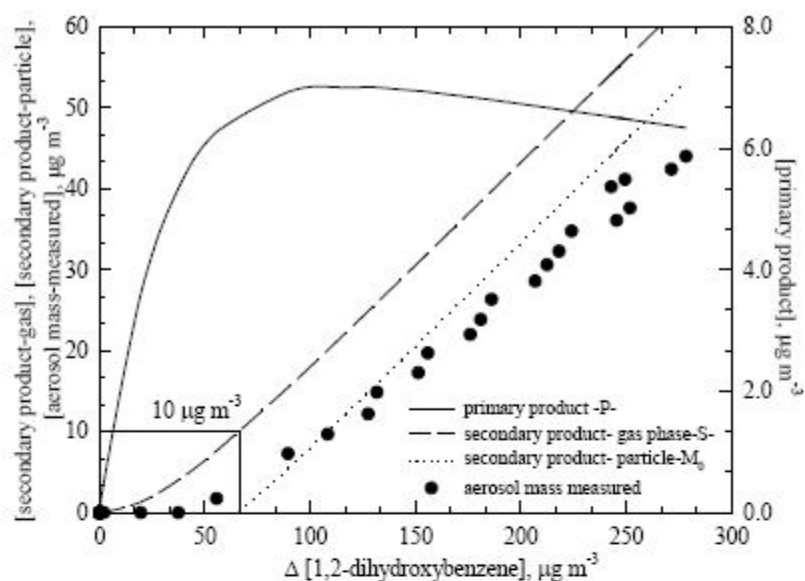


Figure 5. Primary and secondary product profiles calculated for the experiment performed on the 08/05/01.

The offset for M_0 corresponds to the early stages of the 1,2-dihydroxybenzene oxidation when the aerosol precursor material already exists in the gas phase, but in concentrations too small to form the first nucleation particles. In all the experiments about $40 \mu\text{g m}^{-3}$ of dihydroxybenzene should have reacted in order to see the formation of particles. For all the experiments good fits of the predicted particle profile with the aerosol mass measured have been obtained for p in the range of 10- to $50 \mu\text{g m}^{-3}$. There was one exception, this was for the experiment performed on 10/05/2001 when the O_3 was first added in a large quantity and about $180 \mu\text{g m}^{-3}$ of dihydroxybenzene reacted before formation of particles occurred. In this case the best-fit curve for the predicted particle profile with the experimental aerosol mass corresponds to a p value of about $125 \mu\text{g m}^{-3}$. Aerosol formation in this experiment arises from reaction with ozone and OH radical as well. This latter experiment corresponds to a case where radical concentrations were very high and probably the overall mechanism had changed, so that the compounds going into the condensed phase were somewhat different (therefore a different p value).

At this stage of knowledge regarding the atmospheric chemistry of 1,2-dihydroxybenzene, it is difficult to give an explanation for the differences in the values of the parameter p , but it can be suggested that two factors at least can contribute to this effect. One of these factors is that the secondary oxidation product(s) formed in the presence of OH radicals is competitive with the one whom is

formed in the absence of OH radicals, and even if its vapor pressure seems to be substantially higher than that in the pure "ozone" system, it must be formed much rapidly and in a higher yield. Another factor is that in both systems the same secondary oxidation product(s) is formed.

Summary

- The aerosol formation yield from the O₃-initiated oxidation of 1,2-dihydroxybenzene was slightly sensitive to the presence of the OH radicals in the reaction mixture. There was no discernable effect of the initial concentration of 1,2-dihydroxybenzene. Aerosol formation was observed with yields varying from about 20% to about 27%, the yields being slightly higher when cyclohexane was not present. A high yield (about 58%) was obtained when the initial O₃ concentration was high.
- The O₃-initiated oxidation of 1,2-dihydroxybenzene gives a variety of primary products including aldehydes (e.g. formaldehyde, acetaldehyde, glyoxal) and carboxylic acids (e.g. muconic acid). No quantitative data related to product yields have been obtained.
- Using the Odum gas/particle-partitioning model of secondary organic aerosol formation (Odum et al., 1996) the present data were simulated using a two-parameter equation (only one compound with a low vapor pressure), indicating that the aerosol phase is mainly comprised of one major product.
- The experimental data presented herein indicate that the aerosol phase is composed of secondary products coming from the reaction of primary products with O₃ and OH. A simple conceptual model is presented to explain the results. In the simple analytical model used, the observed aerosol mass has been rationalized by invoking the reaction of O₃ with one primary product and using a reactivity towards O₃ 50 times higher than that of 1,2-dihydroxybenzene. Using $k(\text{O}_3 + 1,2\text{-dihydroxybenzene}) = (9.6 \pm 1.1) \times 10^{-13} \text{ cm}^3 \text{ molecule}^{-1} \text{ s}^{-1}$ (Tomas *et al.*, 2003) gives $k(\text{O}_3 + \text{primary product(s)}) = (4.8 \pm) \times 10^{-16} \text{ cm}^3 \text{ molecule}^{-1} \text{ s}^{-1}$ which could be the magnitude of the O₃ rate constant reaction for one of the primary oxidation product (Atkinson, 1994). This model explains fairly well the experimental aerosol mass generated in the studied system.

Working results is that ozone reaction of primary products of the O₃ initiated oxidation of 1,2-dihydroxybenzenes is a significant source of aerosol. The results indicated also that the secondary chemistry involving OH oxidation of the 1,2-dihydroxybenzene and the primary products is an important factor with regard of the increase in the aerosol mass formed. Future work is needed to establish whether the

findings presented herein could be representative for aromatic oxidations under atmospheric conditions.

Bibliography

- Atkinson, R.,
Gas-phase tropospheric chemistry of organic compounds,
Journal of Physical Chemistry Reference Data, Monograph No. 2, 1-216,
1994.
- Atkinson, R.,
Journal of Physical Chemistry Reference Data, 26, 215, 1997.
- Atkinson, R., Aschmann, S.M., Arey, J.,
Reactions of OH and NO₃ radicals with phenol, cresols, and 2-nitrophenol at
296 ± 2 K,
Environmental Science & Technology, 26, 1397-1403, 1992.
- Bailey, P.S.
Ozonation in Organic Chemistry, Vol. II, Nonolefinic Compounds,
Academic Press, New York, 1982.
- Becker, K. H.,
The European Photoreactor "EUPHORE", Final report, EC contract EV5V-
CT92-0059, University of Wuppertal, 1996.
- Berndt, T., and Böge O.,
Gas-phase reaction of OH radicals with phenol.
Physical Chemistry Chemical Physics, 5, 342-350, 2003.
- Bohn, B., and C. Zetzsch,
Gas-phase reaction of the OH-benzene adduct with O₂: reversibility and
secondary formation of HO₂.
Physical Chemistry Chemical Physics, 1, 5097-5107, 1999.
- Calvert, J., Atkinson, R., Becker, K.H., Kamens, R., Seinfeld, J., Wallington, T.,
Yarwood, G.,
Mechanisms of Atmospheric Oxidation of Aromatic Hydrocarbons,
Oxford University Press, 2002.
- Derwent, R.G., Jenkin, M.E., Saunders, S.M., Pillings, M.J.,
Photochemical ozone creation potentials for organic compounds in Northwest
Europe calculated with a master chemical mechanism,
Atmospheric Environment, 32, 2429-2441, 1998.
- Ferri, D., Astorga, C., Tedeschi, R., Winterhalter, R., Viidanoja, J., Bolzacchini, E.,
Jensen, N.R., Larsen, B.R., Hjorth, J.,

Photo-oxidation of Benzene, Toluene and Benzaldehyde: Identification and Quantification of Reaction Products in the Gas-Phase and in Particle.

Poster at A Changing Atmosphere, 8th European Symposium on the Physico-Chemical Behaviour of Atmospheric Pollutants, Torino, Italia, 17-20 September 2001,

- Forstner, H.J.L., Flagan, R.C., Seinfeld, J.H.,
Secondary organic aerosol from the photo-oxidation of aromatic hydrocarbons: Molecular composition.
Environmental Science & Technology, **31**, 1346-1358, 1997.
- Hoffmann, T.; Odum, J. R.; Bowman, F.; Collins, D.; Klockow, D.; Flagan, R. C.; Seinfeld, J. H.,
Formation of organic aerosols from the oxidation of biogenic hydrocarbons,
Journal of Atmospheric Chemistry, **26**, 189-222. 1997.
- Hurley, M.D., Sokolov, O., Wallington, T.J., Takekawa, H., Karasawa, M., Klotz, B., Barnes, I., Becker, K.H.,
Organic Aerosol Formation During the Atmospheric Degradation of Toluene,
Environmental Science & Technology, **35**, 1358-1366, 2001.
- Klotz, B., Volkamer, R., Hurley, M., Andersen, M., Nielsen, J., Barnes, I., Imamura, T., Wirtz, K., Becker, K. H., Platt, U., Wallington, T., Washida, N.,
OH-initiated oxidation of benzene, Part II. Influence of elevated NOx concentrations.
Physical Chemistry Chemical Physics, **4**, 4399-4411, 2002.
- Odum, J.R., Hoffmann, T., Bowman, F., Collins, D., Flagan, R.C., Seinfeld, J.H.,
Gas/particle partitioning and secondary organic aerosol yields,
Environmental Science & Technology, **30**, 2580-2585, 1996.
- Odum, J.R., Jungkamp, P.W., Griffin, R.J., Forstner, H.J.L., Flagan, R.C., Seinfeld, J.H.,
The atmospheric aerosol-forming potential of whole gasoline vapour.
Science, **276**, 96-99, 1997a.
- Odum, J.R., Jungkamp, P.W., Griffin, R.J., Forstner, H.J.L., Flagan, R.C., Seinfeld, J.H.,
Aromatics, reformulated gasoline, and atmospheric organic aerosol formation,
Environmental Science & Technology, **31**, 1890-1897, 1997b.
- Olariu, R.I., Barnes, I., Becker, K.H., Klotz, B.,
Rate coefficients for the gas-phase reaction of OH with selected dihydroxybenzenes and benzoquinones,
International Journal of Chemical Kinetics, **32**, 696-702, 2000.

- Olariu, R.I., Barnes, I., Arsene, C., Becker, K.H., Wirtz, K., Maldonado, C., Ponds, M.,
 Studies on the Atmospheric Oxidation of Phenol: I. Gas-Phase Product Analysis
 The European Photoreactor EUPHORE, 3RD REPORT 2000, Ian Barnes and Howard Sidebottom, Compiled and Produced by Institute of Physical Chemistry, Bergische Universitat Wuppertal, Germany, pp. 16-26, 2001a.
- Olariu, R.I., Barnes, I., Arsene, C., Becker, K.H., Wirtz, K.,
 Studies on the Atmospheric Oxidation of Phenol: II. Secondary Organic Aerosol Formation.
 The European Photoreactor EUPHORE, 3RD REPORT 2000, Ian Barnes and Howard Sidebottom, Compiled and Produced by Institute of Physical Chemistry, Bergische Universitat Wuppertal, Germany, pp. 27-38, 2001b.
- Olariu, R.I., Klotz, B., Barnes, I., Becker, K. H., Mocanu, R.,
 FT-IR study of the ring-retaining products from the reaction of OH radical with phenol, o-, m-, and p-cresol,
 Atmospheric Environment, **36**, 3685. 2002a.
- Olariu, R., Barnes, I., Bejan, I., Becker, K.H., Wirtz, K.,
 Rate Constants for the Gase-Phase Reaction of the NO₃ Radicals with a Series of Benzenediol Compounds.
 Poster presented at the 17th International Symposium on Gas Kinetics, Essen, Germany, 25-28 August 2002b.
- Seinfeld, J.H., Pandis, S.P.,
 Atmospheric Chemistry and Physics,
 John Wiley and Sons, New York, 1998.
- Tomas, A. Olariu, R.I., Barnes, I., Becker, K.H.,
 Kinetics of the Reaction of O₃ with selected Benzenediols,
 Accepted for publication in the International Journal of Chemical Kinetics, 2003.
- Volkamer, R., Klotz, B., Barnes, I., Imamura, T., Wirtz, K., Washida, N., Becker, K. H., Platt, U.,
 OH-initiated oxidation of benzene, Part I. Phenol formation under atmospheric conditions.
 Physical Chemistry Chemical Physics, **4**, 1598-1610, 2002.
- Yaws, C.L., Lin, X., Bu, L., Balundgi, D.R., Tripathi S.,
 Vapor pressures.
 Chemical Properties Handbook, McGraw-Hill, 1999.

Publication n°10
(parue dans la revue *Atmospheric Environment* en 2009)



Aerosol formation yields from the reaction of catechol with ozone

Cécile Coeur-Tourneur^{a,*}, Alexandre Tomas^b, Angélique Guilloteau^{b,d}, Françoise Henry^a, Frédéric Ledoux^a, Nicolas Visez^b, Véronique Riffault^b, John C. Wenger^c, Yuri Bedjanian^d

^a Laboratoire de Physico-Chimie de l'Atmosphère, UMR CNRS 8101, Université du Littoral Côte d'Opale, 32 avenue Foch, 62 930 Wimereux, France

^b Département Chimie et Environnement, École des Mines de Douai, 941 rue Charles Bourseul, 59 508 Douai, France

^c Department of Chemistry and Environmental Research Institute, University College Cork, Cork, Ireland

^d Institut de Combustion, Aérodynamique, Réactivité et Environnement, CNRS, 1C avenue de la Recherche Scientifique, 45 071 Orléans, France

ARTICLE INFO

Article history:

Received 22 July 2008

Received in revised form

21 November 2008

Accepted 24 December 2008

Keywords:

Catechol

Secondary organic aerosol yields

Smog chamber

ABSTRACT

The formation of secondary organic aerosol from the gas-phase reaction of catechol (1,2-dihydroxybenzene) with ozone has been studied in two smog chambers. Aerosol production was monitored using a scanning mobility particle sizer and loss of the precursor was determined by gas chromatography and infrared spectroscopy, whilst ozone concentrations were measured using a UV photometric analyzer. The overall organic aerosol yield (Y) was determined as the ratio of the suspended aerosol mass corrected for wall losses (M_0) to the total reacted catechol concentrations, assuming a particle density of 1.4 g cm^{-3} . Analysis of the data clearly shows that Y is a strong function of M_0 and that secondary organic aerosol formation can be expressed by a one-product gas–particle partitioning absorption model. The aerosol formation is affected by the initial catechol concentration, which leads to aerosol yields ranging from 17% to 86%. The results of this work are compared to similar studies reported in the literature.

© 2009 Elsevier Ltd. All rights reserved.

1. Introduction

Aromatic hydrocarbons are an important class of volatile organic compounds (VOCs) that are emitted into the troposphere as a result of anthropogenic activities (Piccot et al., 1992). Atmospheric oxidation of these hydrocarbons leads to the production of ozone as well as low-volatility species which can then partition into the condensed phase, forming secondary organic aerosol (SOA). The aromatics are believed to be a major anthropogenic source of SOA in urban areas (Seinfeld and Pandis, 1998). Despite considerable efforts over the last 10 years, the basic underlying mechanisms of secondary organic aerosol formation and growth from aromatic precursors remain poorly understood. Besides, the present knowledge on the formation of SOA is not able to explain the observed levels of SOA in the atmosphere, thus indicating that a large number of VOCs (especially those from anthropogenic sources) are currently not taken into account in the SOA-forming reactions included in the existing models (Volkamer et al., 2006; Weitkamp et al., 2007).

In the atmosphere, benzene and the alkyl substituted benzenes such as toluene, the xylenes and trimethylbenzenes react mainly with the hydroxyl radical (OH) during the day. In addition, reaction

with the nitrate radical (NO_3) can contribute to their degradation mainly during the night. The reaction with OH leads to the formation of phenol, cresols and dimethylphenols in significant yields (up to 60%) from benzene, toluene and xylenes, respectively (Berndt and Böge, 2001; Klotz et al., 2002; Smith et al., 1999, 1998; Volkamer et al., 2002a,b). These monohydroxylated aromatic compounds react only slowly with O_3 (Calvert et al., 2002) and their reaction with OH and NO_3 radicals are rapid and result in phenol, cresol and dimethylphenol lifetimes in the troposphere which are significantly shorter than those of their parent aromatic hydrocarbons (Calvert et al., 2002). The reaction of benzene, phenol and cresols with OH has been shown to produce 1,2-benzenediols (also known as catechols) with high yields, around 80% (Berndt and Böge, 2003; Olariu et al., 2002).

The reactivity of 1,2-benzenediol compounds with O_3 is much higher than what is normally observed for the reaction of O_3 with alkylbenzenes, phenols and cresols (Calvert et al., 2002; Tomas et al., 2003). This is linked to the two neighboring OH groups that raise the electron density at these sites and facilitate reactivity toward electrophilic reagents like O_3 . Interestingly, preliminary investigations performed at the European Photoreactor (EUPHORE), showed that the gas-phase reaction of catechol with ozone produced significant amounts of secondary organic aerosol (Olariu et al., 2003). Until recently, the formation of SOA from aromatic compounds has been mainly focused on the alkylbenzenes (Hu and Kamens, 2007; Hurley et al., 2001; Jang and Kamens,

* Corresponding author. Tel.: +33 321 99 64 05; fax: +33 321 99 64 01.
E-mail address: coeur@univ-littoral.fr (C. Coeur-Tourneur).

2001; Johnson et al., 2005; Kleindienst et al., 1999; Martin-Reviejo and Wirtz, 2005; Ng et al., 2007; Odum et al., 1996, 1997b; Song et al., 2005, 2007a,b; Takekawa et al., 2003), with little attention paid to their oxidation products, although the formation of SOA from the OH initiated oxidation of the cresols was recently studied in our laboratory (Henry et al., 2008). In this work, we have investigated the formation of SOA from the reaction of ozone with catechol in two different smog chambers. SOA formation yields obtained in the two chambers have been compared and analyzed using the absorptive gas–particle partitioning model (Odum et al., 1996; Pankow, 1994a,b).

2. Experimental

The study was carried out using mainly the smog chamber at the Laboratoire de Physicochimie de l'Atmosphère of the Université du Littoral Côte d'Opale, France (LPCA–ULCO). Additional experiments were performed at the Centre for Research into Atmospheric Chemistry (CRAC), University College Cork, Ireland. The experimental facilities in these two laboratories provide complementary information concerning secondary organic aerosol formation during the ozone-initiated oxidation of catechol.

2.1. Smog chamber at the LPCA

Experiments at the LPCA were performed in a darkened 8 m³ cubic evacuable Plexiglas reaction chamber, at atmospheric pressure, room temperature (294 ± 2 K) and low relative humidity (5–10%). The gas mixture was continuously stirred by a fan at the bottom of the reactor, thus ensuring a homogeneous mixing of the reactants. The smog chamber has been described in detail elsewhere (Coeur-Tourneur et al., 2006).

The experimental procedure was as follows: first, ozone was introduced into the chamber by passing clean air through a mercury lamp O₃ generator (Thermo Environmental Instruments Inc. Dynamic Gas Calibration System – Model 146). Secondly a known volume of catechol dissolved into water (solution at 25%) was injected into the chamber after vaporization at 553 K. Its introduction corresponded to the beginning of the reaction. Chemicals used and their purity levels were as follows: catechol >99% (Merck products). All experiments were carried out in the absence of inorganic seed aerosol and were conducted until the suspended aerosol mass (corrected for wall losses) M_0 was constant (corresponding to approximately 6 h of reaction).

The loss of reactants and formation of aerosol was monitored throughout the experiments. The catechol concentration was determined by gas–chromatography with flame ionisation detection (Perkin Elmer, Turbomatrix-GC-FID). The catechol was collected at room temperature, onto stainless steel tubes filled with Tenax TA (60–80 mesh) and thermally desorbed onto a 30 m DB-5 Megabore fused silica capillary column held at 313 K for 5 min and then programmed to 523 K at 5 K min⁻¹. Ozone concentrations were measured by a UV photometric analyzer (Thermo Electron Corporation O₃ Analyzer – Model 49C). Particle size distributions (in the 11–1083 nm diameter range) and concentrations were monitored with a Scanning Mobility Particle Sizer (SMPS, GRIMM, CPC 5.404). The SMPS sampled every 6 min with a 1 min delay between samples. The aerosol mass formed during the reaction time was obtained from the aerosol volume concentration assuming a density of 1.4 g cm⁻³ for the organic aerosol, which has been shown by Bahreini et al. (2005) to be a reasonable approximation.

Reactor walls could be a source of gas and/or particles, due to either the offgassing of compounds that react to form SOA or the direct release of particles. Moreover, the impurities in the air of the

chamber can also react with ozone to form SOA. As a result, a number of preliminary experiments and tests were performed in the smog chamber. Before an experimental run, the chamber was flushed for 24 h with purified air produced by a pure air generator (Dominick Hunter LGCAD 140). The amount of particles in the background air was determined by SMPS to be very small, with typical particle number concentrations less than 10 cm⁻³. Controlled experiments in which ozone and purified air were mixed for 6 h were performed. The aerosol mass concentration determined in these tests was lower than 3 µg m⁻³, with a mean diameter of about 50 nm. This background is negligible compared to the SOA mass formed during the ozone reaction with catechol.

The aerosol concentration was determined from the measured values corrected for aerosol deposition on the walls of the chamber. Wall losses are described by a first order law, with a dependence on the aerosol size. The deposition rates of secondary organic aerosol were measured in the dark by observing the decay of the aerosol concentration at the end of the experiments after addition of NO to destroy O₃. The deposition rate constants determined in this work were about 3–4% h⁻¹ for the LPCA chamber. These values are within the range reported for other large chamber facilities (Henry et al., 2008; Hurley et al., 2001; Takekawa et al., 2003).

Catechol wall loss rates of about 8–9% h⁻¹ were also determined in the dark over a period of 6 h. Corrections for wall losses were applied to both catechol and SOA data.

2.2. Smog chamber at the CRAC

Complementary experiments were performed at the CRAC chamber which is a cylindrical 3.9 m³ reactor made of FEP foil operated at atmospheric pressure, room temperature (295 ± 2 K) and low relative humidity (0.03–3%). Only the main features of the experimental set-up will be provided here; a more detailed description can be found elsewhere (Thüner et al., 2004).

Prior to the addition of reactants, the chamber was flushed with purified air for at least 4 h at 150 L min⁻¹ and analysis of the contents was carried out to ensure that no impurities (hydrocarbons, NO_x or particles) were present. Weighed amounts of catechol were introduced in the chamber via a small air flow by using a heated impinger. Around 30 min was allowed for the catechol to reach a stable concentration inside the reactor, as no mixing fans were present at the time of the experiments. Wall loss rates were determined for the next 30 min and ranged from 14 to 34% h⁻¹ in the different experiments. Ozone was then injected and started immediately to react with catechol. Reactant concentrations were monitored by *in situ* FTIR spectroscopy (BioRad spectrometer, 1 cm⁻¹ resolution, coupled to a 229.6 m long White cell) using integrated band intensities between 1112 and 1653 cm⁻¹ for catechol and the absorption cross-section at 1055 cm⁻¹ for ozone ($\sigma = 2 \times 10^{-20}$ cm² molecule⁻¹) (Olariu, 2001). Aerosol size distributions and particle numbers were determined by a TSI 3080 Scanning Mobility Particle Sizer (SMPS) with a time resolution of 3 min. Aerosol wall losses were determined at the end of the reaction and allowed for the correction of the organic aerosol mass formed. The aerosol wall loss rate was typically 72% h⁻¹.

3. Results and discussion

3.1. Aerosol formation profiles

A series of seven experiments were conducted at the LPCA and three at the CRAC. The experimental conditions are reported in Table 1. Initial concentrations of catechol and ozone varied significantly, from 61 to 1293 ppbV and from 102 to 1400 ppbV, respectively. In the case of the first two CRAC experiments, large

Table 1
Initial conditions for the experiments performed in the LPCA and CRAC smog chambers.

Expt.	[catechol] ₀ ^a		[ozone] ₀ ^b		OH scavenger ^c
	ppbV	μg m ⁻³	ppbV	μg m ⁻³	
LPCA					
LPCA-1	897	4112	374	748	-
LPCA-2	669	3066	102	204	-
LPCA-3	646	2960	340	680	-
LPCA-4	320	1468	250	500	-
LPCA-5	280	1283	200	400	-
LPCA-6	160	735	201	402	-
LPCA-7	61	281	206	412	-
CRAC					
CRAC-1	742	3399	1400	2800	2.5
CRAC-2	219	1004	498	996	2.5
CRAC-3	1283	5926	610	1220	-

^a Initial catechol concentrations.

^b Initial ozone concentrations. For the CRAC experiments, ozone was undergoing reaction with catechol as it was being added to the chamber. The value corresponds to the maximum observed concentration.

^c CO was used as OH scavenger in the experiments performed at the CRAC. No scavenger was used at LPCA.

amounts of CO (2.5%) were added to scavenge the OH radicals which could be formed from the catechol ozonolysis.

Fig. 1 shows typical concentration-time profiles obtained at the LPCA for catechol, O₃ and the measured aerosol mass (experiment LPCA-5). The corresponding time-series of aerosol size distributions is shown in Fig. 2. Similar plots were obtained at CRAC. In all the experiments SOA formation was observed immediately after the addition of the second reactant (i.e. catechol for the LPCA experiments, ozone for the CRAC experiments). In the first few minutes there was a very fast increase in the particle number concentration followed by a gradual decrease throughout the experiment. This observation is consistent with an initial nucleation step producing a burst of nano-particles, followed by coagulation of these particles which results in an increase in the mean particle size, along with a corresponding decrease in the number. The initial particles observed were fairly small, with mean diameters starting at about 90 nm for the smallest initial reactant

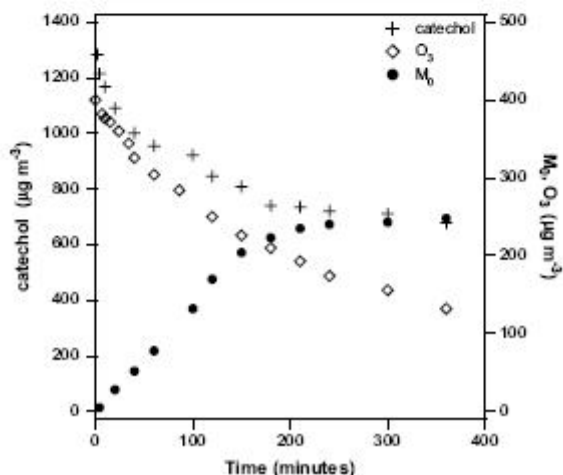


Fig. 1 Reaction-time profile of a typical photooxidation experiment (LPCA-5, initial conditions: 1283 μg m⁻³ catechol and 400 μg m⁻³ ozone).

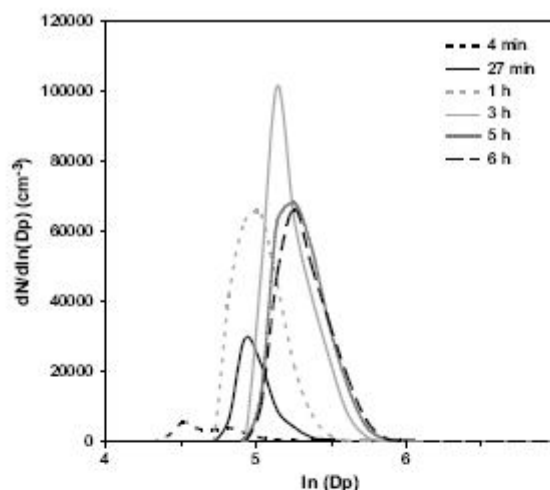


Fig. 2 Aerosol size distributions of a typical photooxidation experiment (experiment LPCA-5, initial conditions: 1283 μg m⁻³ catechol and 400 μg m⁻³ ozone).

concentrations. Rapid growth led to particles with a final mean diameter of around 190 nm.

Two plots of the organic aerosol mass formed (M_0) as a function of the catechol mass reacted ($\Delta[\text{cat}]$) are provided in Fig. 3, corresponding to experiments LPCA-5 and CRAC-1. These plots reveal that an initial amount of reacted catechol is required before the rise of the aerosol mass is measured. This reacted amount is about 160–300 μg m⁻³, depending on the initial catechol and ozone concentrations.

Time-dependent growth curves of aerosol mass versus hydrocarbon consumption have been plotted by Ng et al. (2006) in their study of the ozonolysis of ten biogenic hydrocarbons with at least one double bond. Most experiments were performed in low-RH ammonium sulfate seeded conditions and for ozone concentrations largely exceeding (about three times) those of the hydrocarbon. Two different types of curves have been established: (i) compounds with one double bond mainly exhibiting a linear growth in aerosol mass after the initiation period and (ii) compounds with at least two double bonds presenting a linear growth followed by a curve region where no hydrocarbon consumption is observed and yet the SOA mass is still increasing. A possible explanation discussed by Ng et al. (2006) is that SOA formation in these later stages is due to further oxidation of the unsaturated first-generation products. In our study three experiments have been carried out where the ozone concentration is in excess, by a factor of 2–3 (LPCA-7, CRAC-1, and CRAC-2). A typical growth curve for this case (CRAC-1 experiment) is shown in Fig. 3b. The last part of the plot clearly shows that the aerosol mass continues to accumulate whilst the catechol reactivity has stopped, which seems to indicate the further oxidation by O₃ of gaseous unsaturated products leading to semi-volatile compounds. In the only previous study of SOA formation from the reaction of catechol with ozone, performed at EUPHORE (Olariu et al., 2003), one experiment was carried out in excess of ozone (EUPHORE-5), but the observed growth in aerosol mass was solely linear. However, less than 20% of catechol was consumed in this particular experiment, providing little opportunity for any secondary chemistry to contribute to SOA formation.

Fig. 3b suggests that the SOA formation from the reaction of catechol with O₃ appears to result from two sources: (i) the

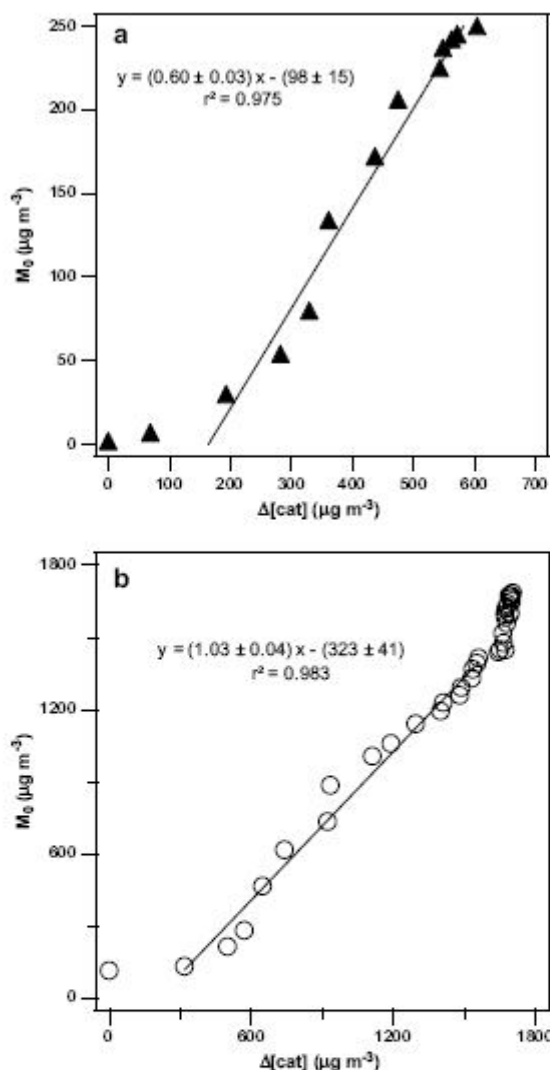


Fig. 3. Plots of the SOA mass concentration (M_0) against the reacted catechol concentration ($\Delta[\text{cat}]$). (a): experiment LPCA-5 (the straight line represents a linear regression on all the data points except the first two); (b): experiment CRAC-1 (the straight line represents a linear regression on the data points for $\Delta[\text{cat}] = (300\text{--}1600) \mu\text{g m}^{-3}$).

primary reaction after the saturation vapour pressure of the products is reached and (ii) further reaction of the first generation products, possibly quinones or ring opening products.

Fig. 4 presents the plot of the SOA mass concentration (M_0) against the reacted catechol concentration ($\Delta[\text{cat}]$) at the end of each experiment. This figure shows strong linear correlations for the LPCA ($R^2 = 0.92$) and CRAC data ($R^2 = 0.99$), with slopes of 0.82 and 0.88 respectively. These values correspond to the highest aerosol yields determined in both smog chambers. This figure also displays that the aerosol mass produced in the smog chamber starts to be substantial after a certain amount (about $180 \mu\text{g m}^{-3}$) of the reacting organic gas has been oxidized. This value is in accordance

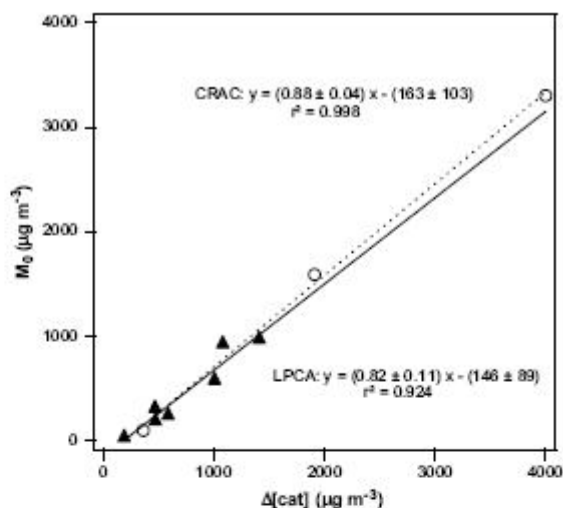


Fig. 4. Plot of the SOA mass concentration against the reacted catechol concentration measured at the end of the experiments. Each data point represents a separate experiment. LPCA (\blacktriangle); CRAC (\circ).

with those observed in the individual experiments in LPCA and CRAC (Fig. 3).

3.2. SOA yield parameters

SOA yields (Y) can be determined experimentally by calculating the ratio of the organic aerosol mass concentration M_0 (in $\mu\text{g m}^{-3}$) to the amount of catechol reacted $\Delta[\text{cat}]$ at the end of each experiment:

$$Y = \frac{M_0}{\Delta[\text{cat}]} \quad (1)$$

SOA yields can also be described by a semi-empirical model based on absorptive gas–particle partitioning of semi-volatile products (Odum et al., 1996; Pankow, 1994ab):

$$Y = \sum_i M_0 \frac{\alpha_i K_{om,i}}{1 + K_{om,i} M_0} \quad (2)$$

in which α_i is the mass-based gas-phase stoichiometric fraction for semi-volatile species i and $K_{om,i}$ is the gas–particle partitioning coefficient for species i . This equation can be used to fit the experimental yield data and determine values for α_i and $K_{om,i}$. Fig. 5 displays the SOA yield versus the concentration of organic aerosol M_0 formed from the ozone + catechol reaction in the LPCA and CRAC chambers. The data from the EUPHORE chamber experiments (Olariu et al., 2003) are included for comparison. The simulation of all the data $Y = f(M_0)$ from the present experimental study demonstrates that a one-product model is able to accurately reproduce the data; the use of two or more products in the model did not improve the quality of the fits. The following SOA yield parameters have been determined: $\alpha = 0.91 \pm 0.15$ and $K_{om} = (4.8 \pm 2.9) \times 10^{-3} \text{ m}^3 \mu\text{g}^{-1}$ at the 95% confidence level. It is interesting to note that when considering only the LPCA data, values of α and K_{om} remain the same and only the corresponding uncertainties increase by a factor of 2.5. Many studies on SOA yields from aromatic compounds have reported that the aerosol yield data should be fitted assuming two hypothetical products (Odum et al.,

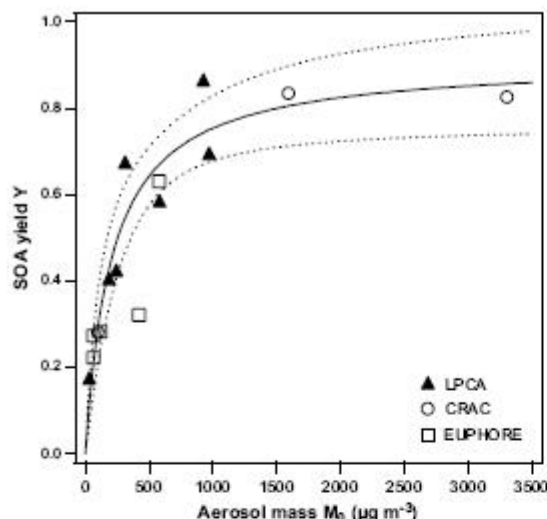


Fig. 5. Aerosol yield (Y) as a function of the organic aerosol mass formed (M_0). LPCA (\blacktriangle), CRAC (\circ) and EUPHORE (\square) (Olariu et al., 2003). The solid line represents the best fit to the LPCA and CRAC data considering one semi-volatile major product ($\alpha=0.91$; $K_{om}=4.8 \times 10^{-3} \text{ m}^3 \mu\text{g}^{-1}$). The dotted lines represent the upper and lower limits for the 95% confidence interval.

1997a,b; Song et al., 2005). However, a number of recent studies have shown that the organic aerosol yield formed in aromatic photooxidation systems could be well described by assuming only one hypothetical product (Ferri et al., 2001; Henry et al., 2008; Olariu et al., 2001; Takekawa et al., 2003). Although the organic aerosol phase is often composed of many oxidation products (Forstner et al., 1997), the present simulation with the one-product model indicates either that one semi-volatile organic compound is the major component of the condensed phase or that the few organics composing the SOA phase have similar α and K_{om} values. In this latter case, the obtained constants α and K_{om} would not have any intrinsic physical meaning but would rather represent mean values.

It is noteworthy that the value of α (0.91) is very close to that of the slope on Fig. 4 (~ 0.85) which corresponds to the highest aerosol yields determined in both smog chambers. Considering that Y is the SOA yield (for the particle phase) and α is the stoichiometric fraction for all semi-volatile species (α takes into account compounds formed in the gas and aerosol phases), this suggests that the low-volatile compounds formed in the reaction of catechol with ozone are transferred almost completely into the particle phase. The same observations have been made for the catechol+ O_3 (Olariu et al., 2003) and cresol+OH reactions (Henry et al., 2008).

As shown in Figs. 4 and 5, a fairly good agreement was observed between the two sets of experiments performed under different conditions in the LPCA and the CRAC smog chambers.

In the CRAC chamber, two experiments were conducted with CO as OH scavenger. The SOA formation yields determined from these two data sets displayed values which can be fit very well with those without OH scavenger. This indicates that either the OH radical production is not significant in the catechol ozonolysis or that the OH reaction with catechol leads to similar SOA yields than the one with ozone. In previous experiments performed at EUPHORE, Olariu et al. (2003) have shown OH formation from catechol ozonolysis and they have observed slightly higher aerosol yields

Table 2

Experimental results obtained in the LPCA and CRAC smog chambers; EUPHORE data from Olariu et al. (2003) have been added for comparison.

Expt.	$\Delta[\text{cat}]^a$			$\Delta[\text{ozone}]^b$			M_0^c		Y^d
	ppbV	$\mu\text{g m}^{-3}$	%	ppbV	$\mu\text{g m}^{-3}$	%	$\mu\text{g m}^{-3}$	%	
LPCA – This work									
LPCA-1	235	1076	26	281	562	75	925	86	
LPCA-2	101	463	15	47	94	46	310	67	
LPCA-3	307	1406	47	222	444	65	970	69	
LPCA-4	218	1000	68	138	276	55	580	58	
LPCA-5	126	579	45	113	226	57	243	42	
LPCA-6	101	465	63	116	332	58	186	40	
LPCA-7	40	182	65	76	152	37	31	17	
CRAC – This work									
CRAC-1	416	1906	56	1000	2000	71	1590	83	
CRAC-2	78	356	35	200	400	40	100	28	
CRAC-3	873	4000	67	200	400	33	3302	83	
EUPHORE – Olariu et al. (2003)									
EUPHORE-1	285	1308	21	n.a.	–	–	419	32	
EUPHORE-2	61	279	20	n.a.	–	–	62	22	
EUPHORE-3	92	422	30	n.a.	–	–	119	28	
EUPHORE-4	267	1084	85	n.a.	–	–	770	63	
EUPHORE-5	50	229	17	n.a.	–	–	63	27	

^a Reacted catechol concentrations.

^b Reacted ozone concentrations. CRAC values are estimated as ozone already started to react before reaching its maximum concentration. EUPHORE data were not available (n.a.).

^c Organic aerosol mass concentration (corrected for wall losses and assuming a particle density of 1.4 g cm^{-3}).

^d SOA yield calculated as the ratio of M_0 to the total reacted catechol concentration.

without OH radical scavenger (with cyclohexane used as OH scavenger).

A summary of experimental results obtained in the experiments performed in the two chambers is provided in Table 2. The results reported from experiments performed in the EUPHORE chamber have also been included for comparative purposes. SOA yields obtained in the EUPHORE experiments have been recalculated using a particle density of 1.4 g cm^{-3} . There is good agreement between the 3 sets of data (except one EUPHORE experimental run) even though the chamber volume, reaction conditions and analytical techniques were somewhat different in each case.

4. Summary and conclusions

The ozonolysis of catechol has been investigated in environmental smog chamber experiments and has been shown to produce large amounts of secondary organic aerosol. The aerosol yields have been measured under NO_x -free, low-RH, and non-seeded conditions and values as high as 86% have been obtained. Therefore, the reaction of O_3 with catechol (and probably its methylated counterparts, Olariu et al., 2003) could contribute significantly to the aerosol loading of the lower troposphere in polluted areas, where ozone concentrations could be high. A one-product gas–particle partitioning model has been successfully applied to explain SOA formation. Further investigation of the composition of both the gas and particulate phases would be necessary to identify the possible intermediates and supply data to model multiple oxidation steps leading to SOA formation.

Acknowledgements

The LPCA and EMD participate in the Research Institute of Industrial Environment (IRENI) which is financed by the

Communauté Urbaine de Dunkerque, the Nord-Pas de Calais Regional Council, the French Ministry of Education and Research, and European funds (FEDER). Funding has also been received from the National Program "LEFE-CHAT". N. Visez wishes to thank ARMINES and the Ecole des Mines de Douai for his postdoctoral fellowship. A. Guilloreau gratefully acknowledges financial support from the European Science Foundation programme INTROP in the form of an exchange grant.

References

- Bahreini, R., Keywood, M.D., Ng, N.L., Varutbangkul, V., Gas, S., Flagan, R.C., Seinfeld, J.H., Worsnop, D.R., Jimenez, J.L., 2005. Measurements of secondary organic aerosol from oxidation of cycloalkenes, terpenes, and *m*-xylene using an aerodyne aerosol mass spectrometer. *Environmental Science and Technology* 39, 5674–5688.
- Berndt, T., Böge, O., 2001. Gas-phase reaction of OH radicals with benzene: products and mechanism. *Physical Chemistry Chemical Physics* 3, 4946–4959.
- Berndt, T., Böge, O., 2003. Gas-phase reaction of OH radicals with phenol. *Physical Chemistry Chemical Physics* 5, 342–350.
- Calvert, J.G., Atkinson, R., Becker, H., Kamens, R.M., Seinfeld, J.H., Wallington, T.J., Yarwood, G., 2002. *Mechanisms of Atmospheric Oxidation of Aromatic Hydrocarbons*. Oxford University Press, New York.
- Coeur-Tourneur, C., Henry, F., Janquin, M.-A., Brutier, L., 2006. Gas-phase reaction of hydroxyl radicals with *m*-, *o*- and *p*-cresol. *International Journal of Chemical Kinetics* 38, 553–562.
- Ferri, D., Astorga, C., Tedeschi, R., Winterhalter, R., Viñanoja, J., Bolzacchini, E., Jensen, N.R., Larsen, B.R., Hjorth, J., 2001. Photo-oxidation of benzene, toluene and benzaldehyde: identification and quantification of reaction products in the gas-phase and in particles. In: Eighth European Symposium on the Physico-Chemical Behaviour of Atmospheric Pollutants, Torino, Italia, 17–20 September 2001.
- Forstner, H.J.L., Flagan, R.C., Seinfeld, J.H., 1997. Molecular speciation of secondary organic aerosol from photooxidation of the higher alkenes: 1-octene and 1-decene. *Atmospheric Environment* 31, 1953–1964.
- Henry, F., Coeur-Tourneur, C., Ledoux, F., Tomas, A., Menu, D., 2008. Secondary organic aerosol formation from the gas phase reaction of hydroxyl radicals with *m*-, *o*- and *p*-cresol. *Atmospheric Environment* 42, 3035–3045.
- Hu, D., Kamens, R.M., 2007. Evaluation of the UNC toluene-SOA mechanism with respect to other chamber studies and key model parameters. *Atmospheric Environment* 41, 6465–6477.
- Hurley, M.D., Sokolov, O., Wallington, T.J., Takekawa, H., Karasawa, M., Klotz, B., Barnes, I., Becker, K.H., 2001. Organic aerosol formation during the atmospheric degradation of toluene. *Environmental Science and Technology* 35, 1358–1366.
- Jang, M., Kamens, R., 2001. Characterization of secondary aerosol from the photo-oxidation of toluene in the presence of NO₂ and 1-propene. *Environmental Science and Technology* 35, 3626–3639.
- Johnson, D., Jenkin, M.E., Wirtz, K., Martin-Reviejo, M., 2005. Simulating the formation of secondary organic aerosol from the photooxidation of aromatic hydrocarbons. *Environmental Chemistry* 2, 35–48.
- Kleindienst, T.E., Smith, D.F., Edney, E.O., Driscoll, D.J., Speer, R.E., Weathers, W.S., 1998. Secondary organic aerosol formation from the oxidation of aromatic hydrocarbons in the presence of dry submicron ammonium sulfate aerosol. *Atmospheric Environment* 33, 3669–3681.
- Klotz, B., Volkamer, R., Hurley, M.D., Andersen, M.P.S., Nielsen, O.J., Barnes, I., Imamura, T., Wirtz, K., Becker, K.H., Platt, U., Wallington, T.J., Washida, N., 2002. OH-initiated oxidation of benzene Part II. Influence of elevated NO_x concentrations. *Physical Chemistry Chemical Physics* 4, 4399–4411.
- Martin-Reviejo, M., Wirtz, K., 2005. Is benzene a precursor for secondary organic aerosol? *Environmental Science and Technology* 39, 1045–1054.
- Ng, N.L., Kroll, J.H., Keywood, M.D., Bahreini, R., Varutbangkul, V., Flagan, R.C., Seinfeld, J.H., Lee, A., Goldstein, A.H., 2006. Contribution of first- versus second-generation products to secondary organic aerosols formed in the oxidation of biogenic hydrocarbons. *Environmental Science and Technology* 40, 2283–2297.
- Ng, N.L., Kroll, J.H., Chan, A.W.H., Chhabra, P.S., Flagan, R.C., Seinfeld, J.H., 2007. Secondary organic aerosol formation from *m*-xylene, toluene, and benzene. *Atmospheric Chemistry and Physics* 7, 3909–3922.
- Odum, J.R., Hoffmann, T., Bowman, F.M., Collins, D., Flagan, R.C., Seinfeld, J.H., 1996. Gas/particle partitioning and secondary organic aerosol yields. *Environmental Science and Technology* 30, 2580–2585.
- Odum, J.R., Jungkamp, T.P.W., Griffin, R.J., Flagan, R.C., Seinfeld, J., 1997a. The atmospheric aerosol-forming potential of whole gasoline vapor. *Science* 276, 96–99.
- Odum, J.R., Jungkamp, T.P.W., Griffin, R.J., Forstner, H.J.L., Flagan, R.C., Seinfeld, J.H., 1997b. Aromatics, reformulated gasoline, and atmospheric organic aerosol formation. *Environmental Science and Technology* 31, 1890–1897.
- Olariu, R.I., 2001. *Atmospheric Oxidation of Selected Aromatic Hydrocarbons*. PhD thesis, University of Wuppertal, Germany.
- Olariu, R.I., Barnes, I., Arsene, C., Becker, K.H., Wirtz, K., 2001. Studies on the atmospheric oxidation of phenol: II. Secondary organic aerosol formation. In: The European Photoreactor EUPHORE, 3rd Report 2000. Ed. Institute of Physical Chemistry, Bergische Universität Wuppertal, Germany, pp. 27–38.
- Olariu, R.I., Klotz, B., Barnes, I., Becker, K.H., Mocanu, R., 2002. FT-IR study of the ring-retaining products from the reaction of OH radicals with phenol, *o*-, *m*-, and *p*-cresol. *Atmospheric Environment* 36, 3685–3697.
- Olariu, R.I., Tomas, A., Barnes, I., Wirtz, K., 2003. Atmospheric ozone degradation reaction of 1,2-dihydroxybenzene: aerosol formation study. In: The European Photoreactor EUPHORE, fourth report 2001. Ed. Institute of Physical Chemistry, Bergische Universität Wuppertal, Germany, pp. 54–71.
- Pankow, J.F., 1994a. An absorption model of gas/particles partitioning of organic compounds in the atmosphere. *Atmospheric Environment* 28, 185–188.
- Pankow, J.F., 1994b. An absorption model of the gas/aerosol partitioning involved in the formation of secondary organic aerosol. *Atmospheric Environment* 28, 189–193.
- Picot, S.D., Watson, J.J., Jones, J.W., 1992. A global inventory of volatile organic compound emissions from anthropogenic sources. *Journal of Geophysical Research* 97, 9897–9912.
- Seinfeld, J., Pandis, S.N., 1998. *From Air Pollution to Climate Change*. Atmospheric Chemistry and Physics. J. Wiley, New York.
- Smith, D.F., Kleindienst, T.E., McIver, C.D., 1999. Primary product distributions from the reaction of OH with *m*-, *p*-xylene, 1,2,4- and 1,3,5-trimethylbenzene. *Journal of Atmospheric Chemistry* 34, 339–364.
- Smith, D.F., McIver, C.D., Kleindienst, T.E., 1998. Primary product distribution from the reaction of hydroxyl radicals with toluene at ppb NO_x mixing ratios. *Journal of Atmospheric Chemistry* 30, 209–228.
- Song, C., Na, K., Cocker, D.R., 2005. Impact of the hydrocarbon to NO_x ratio on secondary organic aerosol formation. *Environmental Science and Technology* 39, 3143–3149.
- Song, C., Na, K., Warren, B., Malloy, Q., Cocker, D.R., 2007a. Secondary organic aerosol formation from *m*-xylene in the absence of NO_x. *Environmental Science and Technology* 41, 7409–7416.
- Song, C., Na, K., Warren, B., Malloy, Q., Cocker, D.R., 2007b. Secondary organic aerosol formation from the photooxidation of *p*- and *o*-xylene. *Environmental Science and Technology* 41, 7403–7408.
- Takekawa, H., Minoura, H., Yamazaki, S., 2003. Temperature dependence of secondary organic aerosol formation by photo-oxidation of hydrocarbons. *Atmospheric Environment* 37, 3413–3424.
- Thüner, L.P., Bardini, P., Rea, G.J., Wenger, J.C., 2004. Kinetics of the gas-phase reactions of OH and NO₃ radicals with dimethylphenols. *Journal of Physical Chemistry A* 108, 11019–11025.
- Tomas, A., Olariu, R.I., Barnes, I., Becker, K.H., 2003. Kinetics of the reaction of O₃ with selected benzenediols. *International Journal of Chemical Kinetics* 35, 223–230.
- Volkamer, R., Jimenez, J.L., Dzepina, K., Salcedo, D., SanMartini, F.M., Molina, L.T., Worsnop, D.R., Molina, M.J., 2006. Secondary organic aerosol formation from anthropogenic air pollution: rapid and higher than expected. *Geophysical Research Letters* 33, L17811.
- Volkamer, R., Uecker, J., Wirtz, K., Platt, U., 2002a. OH-radical initiated oxidation of BTXM: formation and atmospheric fate of phenol-type compounds in the presence of NO_x. In: Midgley, P.M., Reuther, M. (Eds.), Proceedings of the EUROTRAC-2 Symposium 2002. Margraf Verlag, Weikersheim, pp. 1–5.
- Volkamer, R., Klotz, B., Barnes, I., Imamura, T., Wirtz, K., Washida, N., Becker, K.H., Platt, U., 2002b. OH-initiated oxidation of benzene; Part I. Phenol formation under atmospheric conditions. *Physical Chemistry Chemical Physics* 4, 1598–1610.
- Weikamp, E.A., Sage, A.M., Pierce, J.R., Donahue, N.M., Robinson, A.L., 2007. Organic aerosol formation from photochemical oxidation of diesel exhaust in a smog chamber. *Environmental Science and Technology* 41, 6969–6975.

Conclusion et perspectives

Mes travaux de recherche s'inscrivent dans le cadre général de la compréhension des phénomènes de pollution atmosphérique par les composés organiques volatils au travers d'expériences réalisées en laboratoire. Ils comportent deux volets : le premier volet porte sur l'étude de la réactivité en phase gazeuse de composés organiques volatils oxygénés ; le second porte sur l'étude de la formation d'aérosols organiques secondaires (AOS) à partir de l'ozonolyse de composés aromatiques oxygénés. Au cours de ces travaux, de nouveaux outils expérimentaux originaux ont été développés afin d'étudier ces phénomènes sous des angles différents et novateurs, notamment :

- (i) une chambre de simulation atmosphérique rigide couplée à un spectromètre de type cw-CRDS pour la détection au sein du réacteur même d'espèces atmosphériques clés (HO_2^\bullet). Ce type de réacteur est le premier, à notre connaissance, à être équipé d'une voie d'analyse par cw-CRDS ;
- (ii) un réacteur à écoulement laminaire avec injecteur mobile pour l'étude des premières étapes de formation des AOS, couplé, entre autres, à un spectromètre de masse à aérosol haute résolution et, très prochainement, à un spectromètre de masse haute résolution à transfert de protons. Ce type de réacteur est assez peu répandu et la qualité des outils d'analyse qui lui sont associés n'est souvent pas aussi intéressante.

Les premières études cinétiques et mécanistiques ont contribué à expliciter le mécanisme réactionnel d'oxydation par OH^\bullet de deux espèces oxygénées majeures de l'atmosphère : l'acétone et l'acide acétique, en particulier en déterminant les sites d'attaque du radical OH^\bullet sur la molécule oxygénée. L'étude de la réaction acétone + OH^\bullet a montré que la voie d'addition du radical sur la fonction carbonyle était négligeable et que cette réaction ne constitue pas une source d'acide acétique dans l'atmosphère. L'étude des cinétiques de réactions du radical OH^\bullet avec l'acide acétique et ses isotopes deutérés a permis de déterminer les rapports de branchement en fonction du site d'attaque du radical. Au travers d'études cinétiques de dégradation de composés aromatiques, nous avons ensuite montré que, contrairement à ce qui était habituellement observé, l'ozonolyse des

composés aromatiques oxygénés de type catéchols était importante d'un point de vue atmosphérique. La formation d'aérosols organiques secondaires dans ces réactions a été mise en évidence et quantifiée dans une série d'expériences réalisées dans des laboratoires français et européens.

Les dernières études réalisées sont liées au développement des dispositifs expérimentaux déjà mentionnés. La nouvelle chambre de simulation atmosphérique a permis l'étude du mécanisme de la réaction d'oxydation par OH^\bullet du méthyle nitrite, ce dernier étant couramment utilisé comme précurseur de radicaux OH^\bullet dans les chambres de simulation. La formation d'acide nitreux a ainsi été mise en évidence pour la première fois. Le radical HO_2^\bullet a également été détecté et quantifié pour la première fois de façon directe dans une chambre de simulation. En mesurant les cinétiques de recombinaison du radical à différentes pressions, nous avons mis en évidence une perte de HO_2^\bullet aux parois du réacteur par diffusion, perte qui peut s'avérer significative en particulier à des pressions de l'ordre du torr. Ces derniers travaux (les plus récents) seront poursuivis en y ajoutant une mesure des espèces stables par cw-CRDS et/ou par prélèvement et analyse par chromatographie en phase gazeuse, ou encore par analyse directe par spectrométrie de masse, et en comparant ces mesures aux sorties d'un modèle de simulation des mécanismes réactionnels. Il est également envisagé de développer une nouvelle cellule avec une voie de mesure par spectroscopie IRTF à long trajet optique (type cellule de White), afin de s'affranchir du prélèvement d'échantillons à basse pression, toujours délicat à réaliser. Plusieurs revues récentes ont souligné la nécessité d'approfondir notre connaissance des mécanismes d'oxydation des COV de deuxième, troisième, etc. génération (266, 300). Compte tenu du nombre très important de composés d'oxydation secondaires possibles, des études expérimentales exhaustives ne sont pas satisfaisantes, ni pour l'expérimentateur, ni pour le modélisateur, ce dernier utilisant systématiquement des méthodes de réduction de mécanismes réactionnels pour diminuer le temps de calcul. Il est donc envisagé de poursuivre l'étude de la réactivité de COVO multifonctionnels du type α -dicarbonylés suivie des α - et β -hydroxycarbonylés, en particulier les réactions avec le radical OH^\bullet et les processus de photolyse. Comme les α -dicarbonylés, les composés α - et β -hydroxycarbonylés possèdent des sources secondaires importantes (301, 302) et leur réactivité atmosphérique est très peu connue.

Enfin, le développement du réacteur à écoulement laminaire a été validé par l'étude des cinétiques d'ozonolyse de pentènes ; l'étude des produits issus de ces mêmes réactions est actuellement en cours (thèse de M. Duncianu et visite de deux professeurs invités en juillet – août 2011). Les composés précurseurs d'AOS visés dans les prochaines années sont des terpènes d'intérêt en air intérieur, cet environnement étant particulièrement important d'un point de vue santé

publique et des évènements de nucléation y étant fréquemment observés ((279) et références incluses). Les terpènes (en particulier l' α -pinène et le limonène) sont souvent observés en air intérieur : ils sont notamment utilisés pour parfumer les produits ménagers (ils constituent parfois le solvant même !) et sont émis par les objets en bois (303). Les concentrations mesurées dans des bâtiments non industriels sont de l'ordre de quelques dizaines de $\mu\text{g m}^{-3}$ (303) et les rapports concentrations intérieures / concentrations extérieures varient en moyenne d'un facteur 1 à 10, et jusqu'à 100 pour certains composés comme le limonène (304). Quant à l'ozone présent en air intérieur, il provient en bonne partie de l'extérieur via les dispositifs de renouvellement d'air des bâtiments, avec un rapport $[\text{O}_3]_{\text{intérieur}} / [\text{O}_3]_{\text{extérieur}}$ variant de 0,2 à 0,7 en moyenne (128). Les produits des réactions d'ozonolyse des terpènes – radicaux libres, COVO, particules – sont potentiellement plus dangereux pour la santé que les réactifs eux-mêmes (128, 303, 305). Dans le cas de l' α -pinène et du β -pinène, il a été observé un potentiel de formation d'AOS par nucléation considérablement plus important dans le cas de l'ozonolyse que dans le cas des réactions avec les radicaux OH^\bullet et NO_3^\bullet (105). Il est envisagé d'étudier la nature des composés présents dans les premières particules nucléées et de proposer des mécanismes de formation de ces espèces. Récemment, une étude de l'oxydation de l'isoprène par le radical NO_3^\bullet a suggéré que les réactions mutuelles et croisées $\text{RO}_2^\bullet + \text{RO}_2^\bullet \rightarrow \text{ROOR}$ représentaient un chemin dominant pour la formation des AOS, bien que cette voie réactionnelle soit minoritaire par rapport aux voies classiques $\text{RO}_2^\bullet + \text{RO}_2^\bullet \rightarrow 2 \text{RO}^\bullet + \text{O}_2$ et $\text{RO}_2^\bullet + \text{RO}_2^\bullet \rightarrow \text{ROH} + \text{R}_\text{H}\text{O} + \text{O}_2$ (306). Au travers de cet exemple, on constate que les mécanismes réactionnels derrière la nucléation nécessitent un effort particulier de recherche. Parallèlement et en complément à l'étude de ces mécanismes, on analysera l'influence des conditions expérimentales (humidité relative, présence initiale de particules, présence d'amines etc.) sur la formation des AOS et sur la composition chimique de la phase condensée.

La thématique des aérosols organiques secondaires sera aussi poursuivie dans les années à venir en y ajoutant un aspect vieillissement des AOS. Cette direction de recherche a été identifiée parmi les principales questions ouvertes à renseigner dans les prochaines années dans la revue de *Fuzzi et al.* (307). En effet, les expériences de laboratoire de simulation de la formation des AOS ne parviennent pas à reproduire correctement la composition de l'aérosol organique atmosphérique observé, ce qui témoigne de sa modification au cours du temps. Cette dynamique des AOS recouvre les interactions avec la lumière (308), avec la vapeur d'eau omniprésente (298, 309), avec des oxydants de l'atmosphère comme les oxydes d'azote et le radical OH^\bullet (310), ainsi qu'une réactivité en phase condensée comme la formation d'oligomères déjà observée en laboratoire (311, 312) et sur le terrain (313). Par ailleurs, lors du transport des particules, le phénomène de dilution et l'augmentation de la température peut entraîner une volatilisation de certains composés organiques

présents dans les particules (268, 314). Ces diverses transformations vont affecter les propriétés physiques, optiques et chimiques des particules et par conséquent l'impact de ces dernières sur l'environnement (climat, santé, ...). Nous utiliserons le réacteur à écoulement comme une source continue d'un aérosol organique 'frais' modèle qui sera introduit dans une chambre de simulation servant de chambre de vieillissement. Les aérosols seront caractérisés physiquement et chimiquement avant et pendant la phase de vieillissement au moyen des outils disponibles (SMPS, AMS, UPLC-MS et IC-MS). La ligne d'échantillonnage du PTR-MS (acquisition 2011) pourrait être adaptée en installant un dispositif de type denuder – thermodésorbeur afin de permettre l'analyse chimique de l'AOS (315).

Références bibliographiques

- (1) Ravishankara, A. R., Chemistry-climate coupling: the importance of chemistry in climate issues. *Faraday Discussions* 2005, 130, 9-26.
- (2) Vlachokostas, C.; Nastis, S. A.; Achillasa, C.; Kalogeropoulou, K.; Karmirisc, I.; Moussiopoulou, N.; Chourdakisa, E.; Baniasa, G.; Limperi, N., Economic damages of ozone air pollution to crops using combined air quality and GIS modelling. *Atmos. Environ.* 2010, 44, 3352-3361.
- (3) Guo, X. R.; Cheng, S. Y.; Chen, D. S.; Zhou, Y.; Wang, H. Y., Estimation of economic costs of particulate air pollution from road transport in China. *Atmos. Environ.* 2010, 44 (28), 3369-3377.
- (4) Bernstein, J. A.; Alexis, N.; Barnes, C.; Bernstein, I. L.; Nel, A.; Peden, D.; Diaz-Sanchez, D.; Tarlo, S. M.; Williams, P. B., Health effects of air pollution. *Journal of Allergy and Clinical Immunology* 2004, 114, 1116-1123.
- (5) Peel, J. L.; Tolbert, P. E.; Klein, M.; Metzger, K. B.; Flanders, W. D.; Todd, K.; Mulholland, J. A.; Ryan, P. B.; Frumkin, H., Ambient air pollution and respiratory emergency department visits. *Epidemiology* 2005, 16 (2), 164-174.
- (6) Brunekreef, B.; Holgate, S. T., Air pollution and health. *The Lancet* 2002, 360 (October 19), 1233-1242.
- (7) Halonen, J. I.; Lanki, T.; Tiittanen, P.; Niemi, J. V.; Loh, M.; Pekkanen, J., Ozone and cause-specific cardiorespiratory morbidity and mortality. *Journal of Epidemiology and Community Health* 2010, 64, 814-820.
- (8) Henrotin, J. B.; Zeller, M.; Lorgis, L.; Cottin, Y.; Giroud, M.; Béjot, Y., Evidence of the role of short-term exposure to ozone on ischaemic cerebral and cardiac events: the Dijon Vascular Project (DIVA). *Heart* 2010.
- (9) Chuang, G. C.; Yang, Z.; Westbrook, D. G.; Pompilius, M.; Ballinger, C. A.; White, C. R.; Krzywanski, D. M.; Postlethwait, E. M.; Ballinger, S. W., Pulmonary ozone exposure induces vascular dysfunction, mitochondrial damage, and atherogenesis. *American Journal of Physiology - Lung Cellular and Molecular Physiology* 2009, 297, L209-L216.
- (10) Vingarzan, R., A review of surface ozone background levels and trends. *Atmos. Environ.* 2004, 38, 3431-3442.
- (11) Solberg, S.; Derwent, R. G.; Hov, O.; Langner, J.; Lindskog, A., European abatement of surface ozone in a global perspective. *Ambio* 2005, 34 (1), 47-53.
- (12) Parrish, D. D.; Millet, D. B.; Goldstein, A. H., Increasing ozone in marine boundary layer inflow at the west coasts of North America and Europe. *Atm. Chem. Phys.* 2009, 9, 1303-1323.
- (13) Naess, O.; Nafstad, P.; Aamodt, G.; Claussen, B.; Rosland, P., Relation between concentration of air pollution and cause-specific mortality: four-year exposures to nitrogen dioxide and particulate matter pollutants in 470 neighborhoods in Oslo, Norway. *American Journal of Epidemiology* 2007, 165, 435-443.

- (14) Grineski, S. E.; Staniswalis, J. G.; Peng, Y.; Atkinson-Palombo, C., Children's asthma hospitalizations and relative risk due to nitrogen dioxide (NO₂): Effect modification by race, ethnicity, and insurance status. *Environmental Research* 2010, 110, 178-188.
- (15) Llop, S.; Ballester, F.; Estarlich, M.; Esplugues, A.; Rebagliato, M.; Iniguez, C., Preterm birth and exposure to air pollutants during pregnancy. *Environmental Research* 2010, 110, 778-785.
- (16) Peters, A.; Wichmann, H. E.; Tuch, T.; Heinrich, J.; Heyder, J., Respiratory effects are associated with the number of ultrafine particles. *American Journal of Respiratory and Critical Care Medicine* 1997, 155 (4), 1376-1383.
- (17) Pope, C. A., III; Burnett, R. T.; Thun, M. J.; Calle, E. E.; Krewski, D.; Ito, K.; Thurston, G. D., Lung cancer, cardiopulmonary mortality, and long-term exposure to fine particulate air pollution. *Journal of the American Medical Association* 2002, 287 (9), 1132-1141.
- (18) WHO, *The World Health Report 2002. Reducing Risks, Promoting Healthy Life*. World Health Organization: Geneva, 2002; Vol. Available at http://www.who.int/whr/2002/en/whr02_en.pdf.
- (19) Maitre, A.; Bonneterre, V.; Huillard, L.; Sabatier, P.; de Gaudemaris, R., Impact of urban atmospheric pollution on coronary disease. *European Heart Journal* 2006, 27 (19), 2275-2284.
- (20) Amann, M.; Derwent, R. G.; Forsberg, B.; Hänninen, O.; Hurley, F.; Krzyzanowski, M.; de Leeuw, F.; Liu, S. J., *Health Risks of Ozone from Long-range Transboundary Air Pollution*. WHO: 2008.
- (21) Ahmad, K., Pollution cloud over south Asia is increasing ill health. *The Lancet* 2002, 360 (9332), 549.
- (22) Citepa Emissions dans l'air - Composés Organiques Volatils Non Méthaniques. www.citepa.org.
- (23) Seinfeld, J. H.; Pandis, S. N., *Atmospheric Chemistry and Physics*. John Wiley & Sons: 1998.
- (24) Shao, M.; Lu, S.; Liu, Y.; Xie, X.; Chang, C.; Huang, S.; Chen, Z., Volatile organic compounds measured in summer in Beijing and their role in ground-level ozone formation. *J. Geophys. Res.* 2009, 114, D00G06.
- (25) Mason, S. A.; Field, R. J.; Yokelson, R. J.; Kochivar, M. A.; Tinsley, M. R.; Ward, D. E.; Hao, W. M., Complex effects arising in smoke plume simulations due to inclusion of direct emissions of oxygenated organic species from biomass combustio. *J. Geophys. Res.* 2001, 106 (D12), 12527-12539.
- (26) Apel, E. C.; Emmons, L. K.; Karl, T.; Flocke, F.; Hills, A. J.; Madronich, S.; Lee-Taylor, J.; Fried, A.; Weibring, P.; Walega, J.; Richter, D.; Tie, X.; Mauldin, L.; Campos, T.; Weinheimer, A.; Knapp, D.; Sive, B.; Kleinman, L.; Springston, S.; Zaveri, R.; Ortega, J.; Voss, P.; Blake, D.; Baker, A.; Warneke, C.; Welsh-Bon, D.; de Gouw, J.; Zheng, J.; Zhang, R.; Rudolph, J.; Junkermann, W.; Riemer, D. D., Chemical evolution of volatile organic compounds in the outflow of the Mexico City Metropolitan area. *Atmos. Chem. Phys.* 2010, 10, 2353-2375.
- (27) Jimenez, J. L.; Canagaratna, M. R.; Donahue, N. M.; Prévot, A. S. H.; Zhang, Q.; Kroll, J. H.; DeCarlo, P. F.; Allan, J. D.; Coe, H.; Ng, N. L.; Aiken, A. C.; Docherty, K. S.; Ulbrich, I. M.; Grieshop, A. P.; Robinson, A. L.; Duplissy, J.; Smith, J. D.; Wilson, K. R.; Lanz, V. A.; Hueglin,

C.; Sun, Y. L.; Tian, J.; Laaksonen, A.; Raatikainen, T.; Rautiainen, J.; Vaattovaara, P.; Ehn, M.; Kulmala, M.; Tomlinson, J. M.; Collins, D. R.; Cubison, M. J.; Dunlea, E. J.; Huffman, J. A.; Onasch, T. B.; Alfarra, M. R.; Williams, P. I.; Bower, K.; Kondo, Y.; Schneider, J.; Drewnick, F.; Borrmann, S.; Weimer, S.; Demerjian, K. L.; Salcedo, D.; Cottrell, L.; Griffin, R. J.; Takami, A.; Miyoshi, T.; Hatakeyama, S.; Shimono, A.; Sun, J. Y.; Zhang, Y. M.; Dzepina, K.; Kimmel, J. R.; Sueper, D.; Jayne, J. T.; Herndon, S. C.; Trimborn, A. M.; Williams, L. R.; Wood, E. C.; Middlebrook, A. M.; Kolb, C. E.; Baltensperger, U.; Worsnop, D. R., Evolution of Organic Aerosols in the Atmosphere. *Science* 2009, 326 (5959), 1525-1529.

(28) Hamilton, J. F.; Webb, P. J.; Lewis, A. C.; Hopkins, J. R.; Smith, S.; Davy, P., Partially oxidised organic components in urban aerosol using GCXGC-TOF/MS. *Atm. Chem. Phys.* 2004, 4, 1279-1290.

(29) Dimitriadis, B., Methodology in air pollution studies using irradiation chambers. *J. Air Poll. Control Assoc.* 1967, 17 (7), 460-466.

(30) Finlayson-Pitts, B. J.; Pitts, J. N., Jr., *Atmospheric Chemistry: Fundamentals and Experimental Techniques*. John Wiley & Sons: New York, 1986.

(31) Kamens, R. M.; Jeffries, H. E.; Fox, D. L.; Alexander, L., A smog chamber study of the potential effects of hydrocarbon reductions on nighttime NO₂ concentrations. *Atmos. Environ.* 1977, 11, 225-229.

(32) Carter, W. P. L.; Winer, A. M.; Darnall, K. R.; Pitts, J. N., Jr., Smog chamber studies of temperature effects in photochemical smog. *Environ. Sci. Technol.* 1979, 13 (9), 1094-1100.

(33) Howard, C. J., Kinetic measurements using flow tubes. *J. Phys. Chem.* 1979, 83 (1), 3-9.

(34) Poulet, G.; Laverdet, G.; Le Bras, G., Rate constant and branching ratio for the reaction of hydroxyl with chloride oxide (ClO). *J. Phys. Chem.* 1986, 90 (1), 159-165.

(35) Lightfoot, P. D.; Lesclaux, R.; Veyret, B., Flash photolysis study of the methylperoxy + methylperoxy reaction: rate constants and branching ratios from 248 to 573 K. *J. Phys. Chem.* 1990, 90 (2), 700-707.

(36) Foster, P.; Dehaut, P.; Besson, J., Construction d'une enceinte de simulation pour l'étude de la réactivité chimique de polluants gazeux en présence de poussières. *Pollution Atmosphérique* 1984, Octobre-Décembre 1984, 245-253.

(37) Doussin, J.-F.; Ritz, D.; Durand-Jolibois, R.; Monod, A.; Carlier, P., Design of an environmental chamber for the study of atmospheric chemistry: new developments in the analytical device. *Analisis (Paris)* 1997, 25, 236-242.

(38) Jeffries, H. E.; Fox, D.; Kamens, R. M., Outdoor smog chamber studies: light effects relative to indoor chambers. *Environ. Sci. Technol.* 1976, 10 (10), 1006-1011.

(39) Winer, A. M.; Graham, R. A.; Doyle, G. J.; Bekowies, P. J.; McAfee, J. M.; Pitts, J. N., Jr., An evacuable environmental chamber and solar simulator facility for the study of atmospheric photochemistry. *Adv. Environ. Sci. Technol.* 1980, 10, 461-511.

- (40) Akimoto, H.; Hoshino, M.; Inoue, G.; Sakamaki, F.; Washida, N.; Okuda, M., Design and characterization of the evacuable and bakable photochemical chamber. *Environ. Sci. Technol.* 1979, 13 (4), 471-475.
- (41) Cocker, D. R., III; Flagan, R. C.; Seinfeld, J. H., State-of-the-art chamber facility for studying atmospheric aerosol chemistry. *Environ. Sci. Technol.* 2001, 35, 2594-2601.
- (42) Carter, W. P. L.; Cocker, D. R., III; Fitz, D. R.; Malkina, I. L.; Bumiller, K.; Sauer, C.; Pisano, J. T.; Bufalino, C.; Song, C., A new environmental chamber for evaluation of gas-phase chemical mechanisms and secondary aerosol formation. *Atmos. Environ.* 2005, 39, 7768-7788.
- (43) Brauers, T.; Bohn, B.; Johnen, F.-J.; Rohrer, R.; Rodriguez Bares, S.; Tillmann, R.; Wahner, A. *The atmosphere simulation chamber SAPHIR: a tool for the investigation of photochemistry*, EGS - AGU - EUG Joint Assembly, Nice, 6 - 11 April, 2003, p 4449.
- (44) Becker, K. H., *The European Photoreactor EUPHORE*. BUGH Wuppertal (Germany): Wuppertal, 1996.
- (45) Glowacki, D. R.; Goddard, A.; Hemavibool, K.; Malkin, T. L.; Commane, R.; Anderson, F.; Bloss, W. J.; Heard, D. E.; Ingham, T.; Pilling, M. J.; Seakins, P. W., Design of and initial results from a Highly Instrumented Reactor for Atmospheric Chemistry (HIRAC). *Atmos. Chem. Phys.* 2007, 7, 5371-5390.
- (46) Crunaire, S. *Instrumentation et validation d'une chambre de simulation des réactions chimiques de la troposphère*; DEA, Université Lille 1: Douai, 2002.
- (47) Turpin, E. Cinétique et mécanisme de dégradation atmosphérique de trois composés organiques volatils : l'acétone, le phénol et le catéchol. Thèse, Université Lille 1, Villeneuve d'Ascq, 2004.
- (48) Romanini, D.; Kachanov, A. A.; Sadeghi, N.; Stoeckel, F., CW cavity ring down spectroscopy. *Chem. Phys. Lett.* 1997, 264, 316-322.
- (49) Crunaire, S. Développement d'un spectromètre cw-CRDS et son application à l'étude de mécanismes de réaction en chambre de simulation atmosphérique. Thèse, Université Lille 1, Villeneuve d'Ascq, 2005.
- (50) Djehiche, M. Développement d'un couplage cw-CRDS – chambre de simulation pour la mesure in situ du radical HO₂ et d'espèces d'intérêt atmosphérique. Thèse, Université Lille 1, Douai, 2011.
- (51) Djehiche, M.; Tomas, A.; Fittschen, C.; Coddeville, P., First direct detection of HONO in the reaction of methylnitrite (CH₃ONO) with OH radicals. *Environ. Sci. Technol.* 2011, 45 (2), 608-614.
- (52) Djehiche, M.; Tomas, A.; Fittschen, C.; Coddeville, P., First cavity ring-down spectroscopy HO₂ measurements in a large photoreactor. *Z. Phys. Chem.* 2011, 225, 983 – 992.
- (53) Duncianu, M. Réacteur à écoulement pour l'étude de la formation des aérosols organiques secondaires par ozonolyse de composés organiques volatils : développement analytique, validation cinétique et ozonolyse de composés biogéniques. Thèse, Université Lille 1, Villeneuve d'Ascq, 2011.

- (54) Duncianu, M.; Olariu, R. I.; Visez, N.; Riffault, V.; Tomas, A.; Coddeville, P., Development of a new flow-reactor for kinetic studies. Application to the ozonolysis of a series of alkenes. *J. Phys. Chem. A* 2011, Submitted.
- (55) Turpin, E.; Fittschen, C.; Tomas, A.; Devolder, P., Reaction of OH radicals with acetone: Determination of the branching ratio for the abstraction pathway at 298 K and 1 Torr. *J. Atmos. Chem.* 2003, 46, 1-13.
- (56) Caralp, F.; Forst, W.; Hénon, E.; Bergeat, A.; Bohr, F., Tunneling in the reaction of acetone with OH. *Phys. Chem. Chem. Phys.* 2006, 8, 1072-1078.
- (57) Turpin, E.; Tomas, A.; Fittschen, C.; Devolder, P.; Galloo, J.-C., Acetone-h₆ or -d₆ + OH reaction products: Evidence for heterogeneous formation of acetic acid in a simulation chamber. *Environ. Sci. Technol.* 2006, 40 (19), 5956-5961.
- (58) Crunaire, S.; Tarmoul, J.; Fittschen, C.; Tomas, A.; Lemoine, B.; Coddeville, P., Use of cw-CRDS for studying the atmospheric oxidation of acetic acid in a simulation chamber. *Appl. Phys. B* 2006, 85, 467-476.
- (59) Szabo, E.; Tarmoul, J.; Tomas, A.; Fittschen, C.; Dobe, S.; Coddeville, P., Kinetics of the OH-radical initiated reactions of acetic acid and its deuterated isotopes. *React. Kinet. Catal. Lett.* 2009, 96 (2), 299-309.
- (60) Rosado-Reyes, C. M.; Francisco, J. S., Atmospheric oxidation pathways of acetic acid. *J. Phys. Chem. A* 2006, 110 (13), 4419-4433.
- (61) Hamilton, J. F.; Webb, P. J.; Lewis, A. C.; Reviejo, M. M., Quantifying small molecules in secondary organic aerosol formed during the photo-oxidation of toluene with hydroxyl radicals. *Atmos. Environ.* 2005, 39, 7263-7275.
- (62) Grosjean, E.; Grosjean, D., The gas-phase reaction of alkenes with ozone: formation yields of carbonyls from biradicals in ozone-alkene-cyclohexane experiments. *Atmos. Environ.* 1998, 32 (20), 3393-3402.
- (63) Szabo, E.; Djehiche, M.; Riva, M.; Fittschen, C.; Coddeville, P.; Sarzynski, D.; Tomas, A.; Dobé, S., Atmospheric chemistry of 2,3-pentanedione: Photolysis and reaction with OH radicals. *J. Phys. Chem. A* 2011, 115, 9160-9168.
- (64) Tomas, A.; Olariu, R. I.; Barnes, I.; Becker, K. H., Kinetics of the reaction of O₃ with selected benzenediols. *Int. J. Chem. Kin.* 2003, 35, 223-230.
- (65) Olariu, R. I.; Tomas, A.; Barnes, I.; Wirtz, K. *Atmospheric ozone degradation reaction of 1,2-dihydroxybenzene: Aerosol formation study. The European Photoreactor EUPHORE, 4th report 2001*; Institute of Physical Chemistry, Bergische Universität Wuppertal: Wuppertal, 2003; pp 47-63.
- (66) Coeur-Tourneur, C.; Tomas, A.; Guilloteau, A.; Henry, F.; Ledoux, F.; Visez, N.; Riffault, V.; Wenger, J.; Bedjanian, Y., Aerosol formation yields from the reaction of 1,2-dihydroxybenzene with ozone. *Atmos. Environ.* 2009, 43 (14), 2360-2365.

- (67) Taylor, W. D.; Allston, T. D.; Moscato, M. J.; Fazekas, G. B.; Kozlowski, R.; Takacs, G. A., Atmospheric photodissociation lifetimes for nitromethane, methyl nitrite, and methyl nitrate. *Int. J. Chem. Kin.* 1980, 12, 231-240.
- (68) Calvert, J. G.; Atkinson, R.; Becker, K. H.; Kamens, R. M.; Seinfeld, J. H.; Wallington, T. J.; Yarwood, G., *The mechanisms of atmospheric oxidation of aromatic hydrocarbons*. Oxford University Press: New York, 2002.
- (69) Crosley, D. R., The measurement of OH and HO₂ in the atmosphere. *J. Atmos. Sci.* 1995, 52 (19), 3299-3314.
- (70) Heard, D.; Pilling, M. J., Measurement of OH and HO₂ in the troposphere. *Chem. Rev.* 2003, 103, 5163-5198.
- (71) Hornbrook, R. S.; Crawford, J. H.; Edwards, G. D.; Goyea, O.; Mauldin, R. L.; Olson, J. S.; Cantrell, C. A., Measurements of tropospheric HO₂ and RO₂ by oxygen dilution modulation and chemical ionization mass spectrometry. *Atmos. Chem. Phys. Discuss.* 2010, 10, 22219-22277.
- (72) Berden, G.; Peeters, R.; Meijer, G., Cavity ring-down spectroscopy: experimental schemes and applications. *Int. Rev. Phys. Chem.* 2000, 19 (4), 565-607.
- (73) Berden, G.; Engeln, R., *Cavity Ring-Down Spectroscopy*. Wiley: 2009.
- (74) Romanini, D.; Lehmann, K. K., Ring-down cavity absorption spectroscopy of the very weak HCN overtone bands with six, seven, and eight stretching quanta. *J. Chem. Phys.* 1993, 99 (9), 6287-6301.
- (75) Mazurenka, M.; Orr-Ewing, A. J.; Peverall, R.; Ritchie, G. A. D., Cavity ring-down and cavity enhanced spectroscopy using diode lasers. *Annu. Rep. Prog. Chem., Sect. C* 2005, 101, 100-142.
- (76) Wheeler, M. D.; Newman, S. M.; Orr-Ewing, A. J.; Ashfold, M. N. R., Cavity ring-down spectroscopy. *J. Chem. Soc., Faraday Trans.* 1998, 94 (3), 337-351.
- (77) Hollas, J. M., *Spectroscopie*. Dunod: 1998.
- (78) Pilling, M. J.; Seakins, P. W., *Reaction Kinetics*. Oxford University Press: 1995.
- (79) Atkinson, R.; Carter, W. P. L.; Winer, A. M.; Pitts, J. N., Jr., An experimental protocol for the determination of OH radical rate constants with organics using methyl nitrite photolysis as an OH radical source. *J. Air Poll. Control Assoc.* 1981, 31, 1090-1092.
- (80) Atkinson, R.; Arey, J., Atmospheric degradation of volatile organic compounds. *Chem. Rev.* 2003, 103 (12), 4605-4638.
- (81) Mellouki, A.; Le Bras, G.; Sidebottom, H., Kinetics and mechanisms of the oxidation of oxygenated organic compounds in the gas phase. *Chem. Rev.* 2003, 103 (12), 5077-5096.
- (82) Wiebe, H. A.; Villa, A.; Hellmann, T. M.; Heicklen, J., Photolysis of methyl nitrite in the presence of nitrogen oxide, nitrogen dioxide, and oxygen. *J. Am. Chem. Soc.* 1973, 95 (1), 7-13.
- (83) Cox, R. A.; Derwent, R. G.; Kearsley, S. V.; Batt, L.; Patrick, K. G., Photolysis of methyl nitrite: Kinetics of the reaction of the methoxy radical with O₂. *J. Photochem.* 1980, 13, 149-163.

- (84) Raff, J. D.; Finlayson-Pitts, B. J., Hydroxyl radical quantum yields from isopropyl nitrite photolysis in air. *Environ. Sci. Technol.* 2010, 44 (21), 8150-8155.
- (85) Atkinson, R.; Baulch, D. L.; Cox, R. A.; Crowley, J. N.; Hampson, R. F.; Hynes, R. G.; Jenkin, M. E.; Rossi, M. J.; Troe, J., Evaluated kinetic and photochemical data for atmospheric chemistry: Volume II. Gas phase reactions of organic species. *Atmos. Chem. Phys.* 2006, 6, 3625-4055.
- (86) Atkinson, R.; Baulch, D. L.; Cox, R. A.; Crowley, J. N.; Hampson, R. F.; Hynes, R. G.; Jenkin, M. E.; Rossi, M. J.; Troe, J., Evaluated kinetic and photochemical data for atmospheric chemistry: Volume I - gas phase reactions of O_x, HO_x, NO_x and SO_x species. *Atmos. Chem. Phys.* 2004, 4, 1461-1738.
- (87) Nielsen, O. J.; Sidebottom, H.; Donlon, M.; Treacy, J., Rate constants for the gas-phase reactions of OH radicals and Cl atoms with n-alkyl nitrites at atmospheric pressure and 298 K. *Int. J. Chem. Kin.* 1991, 23, 1095-1109.
- (88) Guilmot, J.-M.; Mélen, F.; Herman, M., Rovibrational parameters for cis-nitrous acid. *J. Mol. Spectrosc.* 1993, 160, 401-410.
- (89) Zhao, W.; Gao, X.; Hao, L.; Huang, M.; Huang, T.; Wu, T.; Zhang, W.; Chen, W., Use of integrated cavity output spectroscopy for studying gas phase chemistry in a smog chamber: Characterizing the photolysis of methyl nitrite (CH₃ONO). *Vib. Spectrosc.* 2007, 44, 388-393.
- (90) Jain, C.; Morajkar, P.; Schoemaeker, C.; Viskolcz, B.; Fittschen, F., Measurement of absolute absorption cross sections for HONO in the near infrared region by cw-CRDS technique coupled to laser photolysis. *J. Phys. Chem.* 2011, 115 (39), 10720-10728.
- (91) Atkinson, R.; Baulch, D. L.; Cox, R. A.; Crowley, J. N.; Hampson, R. F.; Hynes, R. G.; Jenkin, M. E.; Rossi, M. J.; Troe, J., Evaluated kinetic and photochemical data for atmospheric chemistry: Volume III - gas phase reactions of inorganic halogens. *Atmos. Chem. Phys.* 2007, 7, 981-1191.
- (92) Fall, R., Abundant oxygenates in the atmosphere: a biochemical perspective. *Chem. Rev.* 2003.
- (93) Chang, C.-T.; Liu, T.-H.; Jeng, F.-T., Atmospheric concentrations of the Cl atom, ClO radical, and HO radical in the coastal marine boundary layer. *Environmental Research* 2004, 94, 67-74.
- (94) Chang, S.; Allen, D. T., Atmospheric chlorine chemistry in southeast Texas: Impacts on ozone formation and control. *Environ. Sci. Technol.* 2006, 40 (1), 251-262.
- (95) Thiébaud, J.; Crunaire, S.; Fittschen, C., Measurements of line strengths in the 2ν₁ band of the HO₂ radical using laser photolysis/continuous wave cavity ring-down spectroscopy (cw-CRDS). *J. Phys. Chem. A* 2007, 111, 6959-6966.
- (96) Henry, K. M.; Donahue, N. M., Effect of the OH radical scavenger hydrogen peroxide on secondary organic aerosol formation from α-pinene ozonolysis. *Aeros. Sci. Technol.* 2011, 45 (6), 686-690.

- (97) Sander, S. P.; Finlayson-Pitts, B. J.; Friedl, R. R.; Golden, D. M.; Huie, R. E.; Keller-Rudek, H.; Kolb, C. E.; Kurylo, M. J.; Molina, M. J.; Moortgat, G. K.; Orkin, V. L.; Ravishankara, A. R.; Wine, P. H., *Chemical kinetics and photochemical data for use in atmospheric studies, Evaluation number 15*. Jet Propulsion Laboratory: Pasadena, 2006.
- (98) Marrero, T. R.; Mason, E. A., Gaseous diffusion coefficients. *J. Phys. Chem. Ref. Data* 1972, 1, 3.
- (99) Lesclaux, R., Combination of peroxy radicals in the gas phase. In *Peroxy radicals*, Alfassi, Z. B., Ed. John Wiley & Sons Ltd.: New York, 1997; pp 81-112.
- (100) Ezell, M. J.; Johnson, S. N.; Yu, Y.; Perraud, V.; Bruns, E. A.; Alexander, M. L.; Zelenyuk, A.; Dabdub, D.; Finlayson-Pitts, B. J., A new aerosol flow system for photochemical and thermal studies of tropospheric aerosols. *Aeros. Sci. Technol.* 2010, 44, 329-338.
- (101) Ripperton, L. A.; Jeffries, H. E.; White, O., Formation of Aerosols by Reaction of Ozone with Selected Hydrocarbons. In *Photochemical Smog and Ozone Reactions*, SOCIETY, A. C., Ed. 1972; pp pp 219-231.
- (102) Iinuma, Y.; Böge, O.; Miao, Y.; Sierau, B.; Gnauk, T.; Herrmann, H., Laboratory studies on secondary organic aerosol formation from terpenes. *Faraday Discussions* 2005, 130 (15), 1-16.
- (103) Lee, A.; Goldstein, A. H.; Keywood, M. D.; Gao, S.; Varutbangkul, V.; Bahreini, R.; Ng, N. L.; Flagan, R. C.; Seinfeld, J. H., Gas-phase products and secondary aerosol yields from the ozonolysis of ten different terpenes. *J. Geophys. Res.* 2006, 111, D07302.
- (104) Lee, A.; Goldstein, A. H.; Kroll, J. H.; Ng, N. L.; Varutbangkul, V.; Flagan, R. C.; Seinfeld, J. H., Gas-phase products and secondary aerosol yields from the photooxidation of 16 different terpenes. *J. Geophys. Res.* 2006, 111 (D17305).
- (105) Bonn, B.; Moortgat, G. K., New particle formation during α - and β -pinene oxidation by O_3 , OH and NO_3 , and the influence of water vapour: particle size distribution studies. *Atmos. Chem. Phys.* 2002, 2, 183-196.
- (106) Emmerson, K. M.; Carslaw, N.; Pilling, M. J., Urban atmospheric chemistry during the PUMA campaign 2: Radical budgets for OH, HO_2 and RO_2 . *J. Atmos. Chem.* 2005, 52 (2), 165-183.
- (107) Lee, J. D.; Lewis, A. C.; Monks, P. S.; Jacob, M.; Hamilton, J. F.; Hopkins, J. R.; Watson, N. M.; Saxton, J. E.; Ennis, C.; Carpenter, L. J.; Carslaw, N.; Fleming, Z.; Bandy, B. J.; Oram, D. E.; Penkett, S. A.; Slemr, J.; Norton, E.; Rickard, A. R.; Whalley, L. K.; Heard, D. E.; Bloss, W. J.; Gravestock, T.; Smith, S. C.; Stanton, J.; Pilling, M. J.; Jenkin, M. E., Ozone photochemistry and elevated isoprene during the UK heatwave of August 2003. *Atmos. Environ.* 2006, 40, 7598-7613.
- (108) McGillen, M. R.; Carey, T. J.; Archibald, A. T.; Wenger, J. C.; Shallcross, D. E.; Percival, C. J., Structure-activity relationship (SAR) for the gas-phase ozonolysis of aliphatic alkenes and dialkenes. *Phys. Chem. Chem. Phys.* 2008, 10, 1757-1768.
- (109) Singh, H. B.; Chen, Y.; Staudt, A.; Jacob, D. J.; Blake, D. R.; Heikes, B.; Snow, J., Evidence from the Pacific troposphere for large global sources of oxygenated organic compounds. *Nature* 2001, 410 (26 April), 1078-1081.

- (110) Singh, H. B.; Salas, L. J.; Chatfield, R. B.; Czech, E.; Fried, A.; Walega, J.; Evans, M. J.; Field, B. D.; Jacob, D. J.; Blake, D. R.; Heikes, B.; Talbot, R. W.; Sachse, G.; Crawford, J. H.; Avery, M. A.; Sandholm, S.; Fuelberg, H., Analysis of the atmospheric distribution, sources, and sinks of oxygenated volatile organic chemicals based on measurements over the Pacific during TRACE-P. *J. Geophys. Res.* 2004, 109 (D15S07).
- (111) Spaulding, R. S.; Schade, G. W.; Goldstein, A. H.; Charles, M. J., Characterization of secondary atmospheric photooxidation products: Evidence for biogenic and anthropogenic sources. *J. Geophys. Res.* 2003, 108, 4247.
- (112) Kesselmeier, J.; Staudt, M., Biogenic volatile organic compounds (VOC): An overview on emission, physiology and ecology. *J. Atmos. Chem.* 1999, 33 (1), 23-88.
- (113) Shim, C.; Wang, Y.; Singh, H. B.; Blake, D. R.; Guenther, A. B., Source characteristics of oxygenated volatile organic compounds and hydrogen cyanide. *J. Geophys. Res.* 2007, 112 (D10305).
- (114) Schade, G.; Goldstein, A. H., Fluxes of oxygenated volatile organic compounds from a ponderosa pine plantation. *J. Geophys. Res.* 2001, 106 (D3), 3111-3123.
- (115) Grosjean, D.; Grosjean, E.; Gertler, A. W., On-road emissions of carbonyls from light-duty and heavy-duty vehicles. *Environ. Sci. Technol.* 2001, 35, 45-53.
- (116) Fontaras, G.; Karavalakis, G.; Kousoulidou, M.; Ntziachristos, L.; Bakeas, E.; Stournas, S.; Samaras, Z., Effects of low concentration biodiesel blends application on modern passenger cars. Part 2: Impact on carbonyl compound emissions. *Environmental Pollution* 2010, 158, 2496-2503.
- (117) He, C.; Ge, Y.; Tan, J.; You, K.; Han, X.; Wang, J.; You, Q.; Shah, A. N., Comparison of carbonyl compounds emissions from diesel engine fueled with biodiesel and diesel. *Atmos. Environ.* 2009, 43, 3657-3661.
- (118) *EMEP / CORINAIR Emission Inventory Guidebook*; European Environment Agency: 2006.
- (119) Lewis, A. C.; Carslaw, N.; Marriott, P. J.; Kinghorn, R. M.; Morrison, P.; Lee, A. L.; Bartle, K. D.; Pilling, M. J., A larger pool of ozone-forming carbon compounds in urban atmospheres. *Nature* 2000, 405 (15 June), 778-781.
- (120) Grosjean, D., Formaldehyde and other carbonyls in Los Angeles ambient air. *Environ. Sci. Technol.* 1982, 16 (5), 254-262.
- (121) Ehhalt, D. H., On the photochemical oxidation of natural trace gases and man-made pollutants in the troposphere. *The Science of the Total Environment* 1994, 143, 1-15.
- (122) de Gouw, J.; Middlebrook, A. M.; Warneke, C.; Goldan, P. D.; Kuster, W. C.; Roberts, J. M.; Fehsenfeld, F. C.; Worsnop, D. R.; Canagaratna, M. R.; Pszenny, A. A. P.; Keene, W. C.; Marchewski, M.; Bertman, S. B.; Bates, T. S., Budget of organic carbon in a polluted atmosphere: Results from the New England Air Quality Study in 2002. *J. Geophys. Res.* 2005, 110 (D16305).
- (123) Yu, J.; Flagan, R. C.; Seinfeld, J. H., Identification of products containing -COOH, -OH, and -C=O in atmospheric oxidation of hydrocarbons. *Environ. Sci. Technol.* 1998, 32 (16), 2357-2370.

- (124) Jenkin, M. E.; Clemitshaw, K. C., Ozone and other secondary photochemical pollutants: chemical processes governing their formation in the planetary boundary layer. *Atmos. Environ.* 2000, 34, 2499-2527.
- (125) Kwan, A. J.; Crouse, J. D.; Clarke, A. D.; Shinozuka, Y.; Anderson, B.; Crawford, J. H.; Avery, M. A.; McNaughton, C. S.; Brune, W. H.; Singh, H. W.; Wennberg, P. O., On the flux of oxygenated volatile organic compounds from organic aerosol oxidation. *Geophysical Research Letters* 2006, 33 (L15815).
- (126) Pope, F. D.; Gallimore, P. J.; Fuller, S. J.; Cox, R. A.; Kalberer, M., Ozonolysis of maleic acid aerosols: Effect upon aerosol hygroscopicity, phase and mass. *Environ. Sci. Technol.* 2010, 44, 6656-6660.
- (127) Monks, P.; Granier, C.; Fuzzi, S.; Stohl, A.; Williams, M. L.; Akimoto, H.; Amann, M.; Baklanov, A.; Baltensperger, U.; Bey, I.; Blake, N.; Blake, R. S.; Carslaw, N.; Cooper, O. R.; Dentener, F. J.; Fowler, D.; Fragkou, E.; Frost, G. J.; Generoso, S.; Ginoux, P.; Grewe, V.; Guenther, A. B.; Hansson, H. C.; Henne, S.; Hjorth, J.; Hofzumahaus, A.; Huntrieser, H.; Isaksen, I. S. A.; Jenkin, M. E.; Kaiser, J.; Kanakidou, M.; Klimont, Z.; Kulmala, M.; Laj, P.; Lawrence, M. G.; Lee, J. D.; Liousse, C.; Maione, M.; McFiggans, G.; Metzger, A.; Mieville, A.; Moussiopoulos, N.; Orlando, J. J.; O'Dowd, C. D.; Palmer, P. I.; Parrish, D. D.; Petzold, A.; Platt, U.; Pöschl, U.; Prévot, A. S. H.; Reeves, C. E.; Reimann, S.; Rudich, Y.; Sellegri, K.; Steinbrecher, R.; Simpson, D.; ten Brink, H. M.; Theloke, J.; van der Werf, G. R.; Vautard, R.; Vestreng, V.; Vlachokostas, C.; von Glasow, R., Atmospheric composition change - global and regional air quality. *Atmos. Environ.* 2009, 43, 5268-5350.
- (128) Weschler, C. J., Ozone in indoor environments: Concentration and chemistry. *Indoor Air* 2000, 10 (4), 269-288.
- (129) Weschler, C. J.; Hodgson, A. T.; Wooley, J. D., Indoor chemistry: Ozone, volatile organic compounds, and carpets. *Environ. Sci. Technol.* 1992, 26 (12), 2371-2377.
- (130) Derwent, R. G.; Jenkin, M. E.; Saunders, S. M.; Pilling, M. J., Photochemical ozone creation potentials for organic compounds in northwest Europe calculated with a master chemical mechanism. *Atm. Env.* 1998, 32 (14/15), 2429-2441.
- (131) Derwent, R. G.; Jenkin, M. E.; Saunders, S. M., Photochemical ozone creation potentials for a large number of reactive hydrocarbons under European conditions. *Atmos. Environ.* 1996, 30 (2), 181-199.
- (132) Derwent, R. G.; Jenkin, M. E.; Saunders, S. M.; Pilling, M. J.; Simmonds, P. G.; Passant, N. R.; Dollard, G. J.; Dumitrescu, P.; Kent, A., Photochemical ozone formation in north west Europe and its control. *Atm. Env.* 2003, 37, 1983-1991.
- (133) Bowman, F.; Pilinis, C.; Seinfeld, J. H., Ozone and aerosol productivity of reactive organics. *Atmos. Environ.* 1995, 29 (5), 579-589.
- (134) Carter, W. P. L., Development of ozone reactivity scales for volatile organic compounds. *Journal of the Air and Waste Management Association* 1994, 44, 881-899.
- (135) Yokelson, R. J.; Goode, J. G.; Ward, E. E.; Susott, R. A.; Babbitt, R. E.; Wade, D. D.; Bertschi, I.; Griffith, D. W. T.; Hao, W. M., Emissions of formaldehyde, acetic acid, methanol, and

other trace gases from biomass fires in North Carolina measured by airborne Fourier transform infrared spectroscopy. *J. Geophys. Res.* 1999, 104 (D23), 30109-30125.

(136) Xiao, H.; Zhu, B., Modelling study of photochemical ozone creation potential of non-methane hydrocarbon. *Water, Air, and Soil Pollution* 2003, 145, 3-16.

(137) Volkamer, R.; Sheehy, P.; Molina, L. T.; Molina, M. J., Oxidative capacity of the Mexico City atmosphere - Part 1: A radical source perspective. *Atmos. Chem. Phys.* 2010, 10, 6969-6991.

(138) Monod, A.; Poulain, L.; Grubert, S.; Voisin, D.; Wortham, H., Kinetics of OH-initiated oxidation of oxygenated organic compounds in the aqueous phase: new rate constants, structure-activity relationships and atmospheric implications. *Atmos. Environ.* 2005, 39 (40), 7667-7688.

(139) Singh, H. W.; Kanakidou, M.; Crutzen, P. J.; Jacob, D. J., High concentrations and photochemical fate of oxygenated hydrocarbons in the global troposphere. *Nature* 1995, 378 (2 Novembre), 50-53.

(140) Ito, A.; Sillman, S.; Penner, J. E., Effects of additional nonmethane volatile organic compounds, organic nitrates, and direct emissions of oxygenated organic species on global tropospheric chemistry. *J. Geophys. Res.* 2007, 112 (D06309).

(141) Moortgat, G. K., *Evaluation of radical sources in atmospheric chemistry through chamber and laboratory studies, RADICAL final report.* JRC Ispra (It): 2002.

(142) Madronich, S., Chemical evolution of gaseous air pollutants down-wind of tropical megacities: Mexico City case study. *Atmos. Environ.* 2006, 40 (31), 6012-6018.

(143) Zhang, Q.; Jimenez, J. L.; Canagaratna, M. R.; Allan, J. D.; Coe, H.; Ulbrich, I.; Alfarra, M. R.; Takami, A.; Middlebrook, A. M.; Sun, Y. L.; Dzepina, K.; Dunlea, E.; Docherty, K.; DeCarlo, P. F.; Salcedo, D.; Onasch, T.; Jayne, J. T.; Miyoshi, T.; Shimojo, A.; Hatakeyama, S.; Takegawa, N.; Kondo, Y.; Schneider, J.; Drewnick, F.; Borrmann, S.; Weimer, S.; Demerjian, K. L.; Williams, P.; Bower, K.; Bahreini, R.; Cottrell, L.; Griffin, R. J.; Rautiainen, J.; Sun, J. Y.; Zhang, Y. M.; Worsnop, D. R., Ubiquity and dominance of oxygenated species in organic aerosols in anthropogenically-influenced Northern Hemisphere midlatitudes. *Geophysical Research Letters* 2007, 34 (L13801), 1-6.

(144) Kawamura, K., Identification of C₂-C₁₀ α-oxocarboxylic acids, pyruvic acid, and C₂-C₃ α-dicarbonyls in wet precipitation and aerosol samples by capillary GC and GC-MS. *Anal. Chem.* 1993, 65, 3505-3511.

(145) Li, Y.-C.; Yu, J. Z., Composition profile of oxygenated organic compounds and inorganic ions in PM_{2.5} in Hong Kong. *Environ. Chem.* 2010, 7 (4), 338-349.

(146) Johnson, D.; Utembe, S. R.; Jenkin, M. E.; Derwent, R. G.; Hayman, G. D.; Alfarra, M. R.; Coe, H.; McFiggans, G., Simulating regional scale secondary organic aerosol formation during the TORCH 2003 campaign in the southern UK. *Atmos. Chem. Phys.* 2006, 6, 403-418.

(147) Simoneit, B. R. T.; Kobayashi, M.; Mochida, M.; Kawamura, K.; Lee, M.; Lim, H.-J.; Turpin, B. J.; Komazaki, Y., Composition and major sources of organic compounds of aerosol particulate matter sampled during the ACE-Asia campaign. *J. Geophys. Res.* 2004, 109 (D19S10).

- (148) Leikauf, G. D., Hazardous air pollutants and asthma. *Environmental Health Perspectives* 2002, 110 (4), 505–526.
- (149) Jacob, D. J.; Field, B. D.; Jin, E. M.; Bey, I.; Li, Q.; Logan, J. A.; Yantosca, R. M.; Singh, H. B., Atmospheric budget of acetone. *J. Geophys. Res.* 2002, 107 (D10).
- (150) Moore, D. P.; Remedios, J. J.; Waterfall, A. M., Global distributions of acetone in the upper troposphere from MIPAS–E spectra. *Atmospheric Chemistry and Physics Discussions* 2010, 10, 23539–23557.
- (151) Holzinger, R.; Carsten, W.; Hansel, A.; Jordan, A.; Lindinger, W.; Scharffe, D. H.; Schade, G.; Crutzen, P. J., Biomass burning as a source of formaldehyde, acetaldehyde, methanol, acetone, acetonitrile, and hydrogen cyanide. *Geophysical Research Letters* 1999, 26, 1161–1164.
- (152) Janson, R.; de Serves, C., Acetone and monoterpene emissions from the boreal forest in northern Europe. *Atmos. Environ.* 2001, 35, 4629–4635.
- (153) Zhou, X.; Mopper, K., Photochemical production of low-molecular-weight carbonyl compounds in seawater and surface microlayer and their air-sea exchange. *Marine Chemistry* 1997, 56, 201–213.
- (154) Rosado-Reyes, C. M.; Francisco, J. S., Atmospheric oxidation pathways of propane and its by-products: acetone, acetaldehyde, and propionaldehyde. *J. Geophys. Res.* 2007, 112 (D14310).
- (155) Carrasco, N.; Doussin, J.-F.; O'Connor, M. P.; Wenger, J. C.; Picquet-Varrault, B.; Durand-Jolibois, R.; Carlier, P., Simulation chamber studies of the atmospheric oxidation of 2-methyl-3-buten-2-ol: Reaction with hydroxyl radicals and ozone under a variety of conditions. *J. Atmos. Chem.* 2006, 56 (1), 33–55.
- (156) Goldstein, A. H.; Schade, G. W., Quantifying biogenic and anthropogenic contributions to acetone mixing ratios in a rural environment. *Atmos. Environ.* 2000, 36, 4997–5006.
- (157) Reissell, A.; Harry, C.; Aschmann, S. M.; Atkinson, R.; Arey, J., Formation of acetone from the OH radical- and O₃-initiated reactions of a series of monoterpenes. *J. Geophys. Res.* 1999, 104 (D11), 13868–13879.
- (158) Yu, Y.; Ezell, M. J.; Zelenyuk, A.; Imre, D.; Alexander, L.; Ortega, J.; D'Anna, B.; Harmon, C. W.; Johnson, S. N.; Finlayson-Pitts, B. J., Photooxidation of α -pinene at high relative humidity in the presence of increasing concentrations of NO_x. *Atmos. Environ.* 2008, 42, 5044–5060.
- (159) Wisthaler, A.; Jensen, N. R.; Winterhalter, R.; Lindinger, W.; Hjorth, J., Measurements of acetone and other gas phase product yields from the OH initiated oxidation of terpenes by proton-transfer-reaction mass spectrometry (PTR-MS). *Atmos. Environ.* 2001, 35, 6181–6191.
- (160) Hermans, I.; Nguyen, T. L.; Jacobs, P. A.; Peeters, J., Tropopause chemistry revisited: HO₂-initiated oxidation as an efficient acetone sink. *J. Am. Chem. Soc.* 2004, 126, 9908–9909.
- (161) Reiner, T.; Möhler, O.; Arnold, F., Measurements of acetone, acetic acid, and formic acid in the northern midlatitude upper troposphere and lower stratosphere. *J. Geophys. Res.* 1999, 104 (D11), 13943–13952.

- (162) Gierczak, T.; Gilles, M. K.; Bauerle, S.; Ravishankara, A. R., Reaction of hydroxyl radical with acetone. 1. Kinetics of the reactions of OH, OD, and ^{18}OH with acetone and acetone- d_6 . *J. Phys. Chem. A* 2003, 107 (25), 5014-5020.
- (163) Gierczak, T.; Burkholder, J. B.; Bauerle, S.; Ravishankara, A. R., Photochemistry of acetone under tropospheric conditions. *Chemical Physics* 1998, 231, 229-244.
- (164) Aloisio, S.; Francisco, J. S., The photochemistry of acetone in the presence of water. *Chem. Phys. Lett.* 2000, 329, 179-184.
- (165) Blitz, M. A.; Heard, D. E.; Pilling, M. J.; Arnold, S. R.; Chipperfield, M. P., Pressure and temperature-dependent quantum yields for the photodissociation of acetone between 279 and 327.5 nm. *Geophysical Research Letters* 2004, 31 (L06111), 1-5.
- (166) Nadasdi, R.; Kovacs, G.; Szilagyi, I.; Demeter, A.; Dobe, S.; Berces, T.; Marta, F., Exciplex laser photolysis study of acetone with relevance to tropospheric chemistry. *Chem. Phys. Lett.* 2007, 440, 31-35.
- (167) Khamaganov, V. G.; Karunanandan, R.; Horowitz, A.; Dillon, T. J.; Crowley, J. N., Photolysis of $\text{CH}_3\text{C}(\text{O})\text{CH}_3$ at 248 and 266 nm: pressure and temperature dependent overall quantum yields. *Phys. Chem. Chem. Phys.* 2009, 11, 6173-6181.
- (168) Somnitz, H.; Ufer, T.; Zellner, R., Acetone photolysis at 248 nm revisited: pressure dependence of the CO and CO_2 quantum yields. *Phys. Chem. Chem. Phys.* 2009, 11, 8522-8531.
- (169) McKeen, S. A.; Gierczak, T.; Burkholder, J. B.; Wennberg, P. O.; Hanisco, T. F.; Keim, E. R.; Gao, R. S.; Liu, S. C.; Ravishankara, A. R.; Fahey, D. W., The photochemistry of acetone in the upper troposphere: A source of odd-hydrogen radicals. *Geophysical Research Letters* 1997, 24 (24), 3177-3180.
- (170) Wennberg, P. O.; Hanisco, T. F.; Jaeglé, L.; Jacob, D. J.; Hintsä, E. J.; Lanzendorf, E. J.; Anderson, J. G.; Gao, R. S.; Keim, E. R.; Donnelly, S. G.; Del Negro, L. A.; Fahey, D. W.; McKeen, S. A.; Salawitch, R. J.; Webster, C. R.; May, R. D.; Herman, R. L.; Proffitt, M. H.; Margitan, J. J.; Atlas, E. L.; Schauffler, S. M.; Flocke, F.; McElroy, C. T.; Bui, T. P., Hydrogen radicals, nitrogen radicals, and the production of O_3 in the upper troposphere. *Science* 1998, 279 (5347), 49-53.
- (171) Singh, H. B.; O'Hara, D.; Herlth, D.; Sachse, W.; Blake, D. R.; Bradshaw, J. D.; Kanakidou, M.; Crutzen, P. J., Acetone in the atmosphere: Distribution, sources and sinks. *J. Geophys. Res.* 1994, 99 (D1), 1805-1819.
- (172) Crowley, J. N.; Ammann, M.; Cox, R. A.; Hynes, R. G.; Jenkin, M. E.; Mellouki, A.; Rossi, M. J.; Troe, J.; Wallington, T. J., Evaluated kinetic and photochemical data for atmospheric chemistry: Volume V - Heterogeneous reactions on solid substrates. *Atmos. Chem. Phys.* 2010, 10, 9059-9223.
- (173) Murphy, J. G.; Oram, D. E.; Reeves, C. E., Measurements of volatile organic compounds over West Africa. *Atm. Chem. Phys.* 2010, 10, 5281-5294.
- (174) Usher, C. R.; Michel, A. E.; Grassian, V. H., Reactions on mineral dust. *Chem. Rev.* 2003, 103, 4883-4939.

- (175) Wollenhaupt, M.; Crowley, J. N., Kinetics studies of the reactions $\text{CH}_3 + \text{NO}_2 = \text{products}$, $\text{CH}_3\text{O} + \text{NO}_2 = \text{products}$, and $\text{OH} + \text{CH}_3\text{C}(\text{O})\text{CH}_3 = \text{CH}_3\text{C}(\text{O})\text{OH} + \text{CH}_3$, over a range of temperature and pressure. *J. Phys. Chem. A* 2000, 104 (27), 6429-6438.
- (176) Vasvari, G.; Szilagyi, I.; Bencsura, A.; Dobé, S.; Berces, T.; Hénon, E.; Canneaux, S.; Bohr, F., Reaction and complex formation between OH radical and acetone. *Phys. Chem. Chem. Phys.* 2001, 3, 551-555.
- (177) Vandenberg, S.; Vereecken, L.; Peeters, J., The acetic acid forming channel in the acetone + OH reaction: a combined experimental and theoretical investigation. *Phys. Chem. Chem. Phys.* 2002, 4, 461-466.
- (178) Tyndall, G. S.; Orlando, J. J.; Wallington, T. J.; Hurley, M. D.; Goto, M.; Kawasaki, M., Mechanism of the reaction of OH radicals with acetone and acetaldehyde at 251 and 296K. *Phys. Chem. Chem. Phys.* 2002, 4, 2189-2193.
- (179) Masgrau, L.; Gonzales-Lafont, A.; Lluch, J. M., Variational transition-state theory rate constant calculations with multidimensional tunneling corrections of the reaction of acetone with OH. *J. Phys. Chem. A* 2002, 106 (48), 11760-11770.
- (180) Poulain, L.; Katrib, Y.; Isikli, E.; Liu, Y.; Wortham, H.; Mirabel, P.; Le Calvé, S.; Monod, A., In-cloud multiphase behaviour of acetone in the troposphere: Gas uptake, Henry's law equilibrium and aqueous phase photooxidation. *Chemosphere* 2010, 81, 312-320.
- (181) Xu, W.; Raftery, D., In situ solid-state nuclear magnetic resonance studies of acetone photocatalytic oxidation on titanium oxide surfaces. *Journal of Catalysis* 2001, 204 (1), 110-117.
- (182) Kagwade, S. V.; Clayton, C. R.; Chidambaram, D.; Halada, G. P., Photochemical breakdown of acetone on copper. *Electrochimica Acta* 2001, 46, 2337-2342.
- (183) Smith, I. W. M.; Ravishankara, A. R., Role of hydrogen-bonded intermediates in the bimolecular reactions of the hydroxyl radical. *J. Phys. Chem. A* 2002, 106 (19), 4798-4807.
- (184) Shannon, R. J.; Taylor, S.; Goddard, A.; Blitz, M. A.; Heard, D. E., Observation of a large negative temperature dependence for rate coefficients of reactions of OH with oxygenated volatile organic compounds studied at 86–112 K. *Phys. Chem. Chem. Phys.* 2010, 12, 13511-13514.
- (185) Talukdar, R.; Gierczak, T.; McCabe, D. C.; Ravishankara, A. R., Reaction of hydroxyl radical with acetone. 2. Products and reaction mechanism. *J. Phys. Chem. A* 2003, 107 (25), 5021-5032.
- (186) Pöschl, U., Atmospheric aerosols: Composition, transformation, climate and health effects. *Angewandte Chemistry International Edition* 2005, 44, 7520-7540.
- (187) Raff, J. D.; Stevens, P. S.; Hites, R. A., Relative rate and product studies of the OH-acetone reaction. *J. Phys. Chem. A* 2005.
- (188) Paulot, F.; Wunch, D.; Crouse, J. D.; Toon, G. C.; Millet, D. B.; DeCarlo, P. F.; Vigouroux, C.; Deutscher, N. M.; Gonzales Abad, G.; Notholt, J.; Warneke, T.; Hannigan, J. W.; Warneke, C.; de Gouw, J.; Dunlea, E. J.; De Mazière, M.; Griffith, D. W. T.; Bernath, P.; Jimenez, J. L.; Wennberg, P. O., Importance of secondary sources in the atmospheric budgets of formic and acetic acids. *Atmospheric Chemistry and Physics Discussions* 2010, 10, 24435-24496.

- (189) Khare, P.; Kumar, N.; Kumari, K. M.; Srivastava, S. S., Atmospheric formic and acetic acids: An overview. *Reviews of Geophysics* 1999, 37 (2), 227-248.
- (190) Preunkert, S.; Legrand, M.; Jourdain, B.; Dombrowski-Etchevers, I., Acidic gases (HCOOH, CH₃COOH, HNO₃, HCl, and SO₂) and related aerosol species at a high mountain Alpine site (4360 m elevation) in Europe. *J. Geophys. Res.* 2007, 112 (D23S12), 1-7.
- (191) de Gouw, J.; Warneke, C.; Stohl, A.; Wollny, A. G.; Brock, C. A.; Cooper, O. R.; Holloway, J. S.; Trainer, M.; Fehsenfeld, F. C.; Atlas, E. L.; Donnelly, S. G.; Stroud, V.; Lueb, A., Volatile organic compounds composition of merged and aged forest fire plumes from Alaska and western Canada. *J. Geophys. Res.* 2006, 111 (D10303).
- (192) Kesselmeier, J., Exchange of short-chain oxygenated volatile organic compounds (VOCs) between plants and the atmosphere: A compilation of field and laboratory studies. *J. Atmos. Chem.* 2001, 39 (3), 219-233.
- (193) Keene, W. C.; Galloway, J. N., The biogeochemical cycling of formic and acetic acids through the troposphere: an overview of current understanding. *Tellus* 1988, 40B, 322-334.
- (194) Keene, W. C.; Galloway, J. N., Considerations regarding sources for formic and acetic acids in the troposphere. *J. Geophys. Res.* 1986, 91, 14466-14474.
- (195) Shaw, S.; Mitloehner, F.; Jackson, W.; Depeters, E.; Fadel, J.; Robinson, P.; Holzinger, R.; Goldstein, A., Volatile organic compound emissions from dairy cows and their waste as measured by proton-transfer-reaction mass spectrometry. *Environ. Sci. Technol.* 2007, 41, 1310-1316.
- (196) Xu, G.; Lee, X.; Lv, Y., Urban and rural observations of carboxylic acids in rainwater in Southwest of China: the impact of urbanization. *J. Atmos. Chem.* 2009, 62 (3), 249-260.
- (197) Arlander, D. W.; Cronn, D. R.; Farmer, J. C.; Menzia, F. A.; Westberg, H. H., Gaseous oxygenated hydrocarbons in the remote marine troposphere. *J. Geophys. Res.* 1990, 95 (D10), 16391-16403.
- (198) Khwaja, H. A., Atmospheric concentrations of carboxylic acids and related compounds at a semiurban site. *Atmos. Environ.* 1995, 29 (1), 127-139.
- (199) von Kuhlmann, R.; Lawrence, M. G.; Crutzen, P. J.; Rasch, P. J., A model for studies of tropospheric ozone and nonmethane hydrocarbons: Model evaluation of ozone-related species. *J. Geophys. Res.* 2003, 108 (D23), 4729.
- (200) Sommariva, R.; de Gouw, J. A.; Trainer, M.; Atlas, E.; Goldan, P. D.; Kuster, W. C.; Warneke, C.; Fehsenfeld, F. C., Emissions and photochemistry of oxygenated VOCs in urban plumes in the Northeastern United States. *Atmos. Chem. Phys.* 2011, 11, 7081-7096.
- (201) Chebbi, A.; Carlier, P., Carboxylic acids in the troposphere, occurrence, sources, and sinks: a review. *Atmos. Environ.* 1996, 30 (24), 4233-4249.
- (202) Xu, G.; Lee, X.; Lü, Y.; Chen, Y.; Huang, D., Seasonal variations of carboxylic acids and their contributions to the rainwater acidity: A case study of Guiyang and Shangzhong, China *Chinese Science Bulletin* 2010, 55 (16), 1667-1673.

- (203) Tong, S. R.; Wu, L. Y.; Ge, M. F.; Wang, W. G.; Pu, Z. F., Heterogeneous chemistry of monocarboxylic acids on α -Al₂O₃ at different relative humidities. *Atmos. Chem. Phys.* 2010, 10, 7561-7574.
- (204) Vañtilingom, M.; Charbouillot, T.; Deguillaume, L.; Maisonobe, R.; Parazols, M.; Amato, P.; Sancelme, M.; Delort, A.-M., Atmospheric chemistry of carboxylic acids: microbial implication versus photochemistry. *Atmospheric Chemistry and Physics Discussions* 2011, 11, 4881-4911.
- (205) Carl, S. A.; Vereecken, L.; Peeters, J., Kinetic parameters for gas-phase reactions: Experimental and theoretical challenges. *Phys. Chem. Chem. Phys.* 2007, 9, 4071-4084.
- (206) Dagaut, P.; Wallington, T. J.; Liu, R.; Kurylo, M. J., The gas phase reactions of hydroxyl radicals with a series of carboxylic acids over the temperature range 240-440K. *Int. J. Chem. Kin.* 1988, 20, 331-338.
- (207) Singleton, D. L.; Paraskevopoulos, G.; Irwin, R. S., Rates and mechanism of the reactions of hydroxyl radicals with acetic, deuterated acetic, and propionic acids in the gas phase. *J. Am. Chem. Soc.* 1989, 111 (14), 5248-5251.
- (208) Butkovskaya, N. I.; Kukui, A.; Pouvesle, N.; Le Bras, G., Rate constant and mechanism of the reaction of OH radicals with acetic acid in the temperature range 229-300 K. *J. Phys. Chem. A* 2004, 108 (34), 7021-7026.
- (209) Crunaire, S.; Fittschen, C.; Lemoine, B.; Tomas, A.; Coddeville, P., *Environmental Simulation Chambers – Application to Atmospheric Chemical Processes*. Kluwer Academic Publishers: Dordrecht, 2006.
- (210) Huang, Y.; Dransfield, T. J.; Miller, J. D.; Rojas, R. D.; Castillo, X. G.; Anderson, J. G., Experimental study of the kinetics of the reaction of acetic acid with hydroxyl radicals from 255 to 355 K. *J. Phys. Chem. A* 2009, 113 (2), 423-430.
- (211) Huang, Y.; Dransfield, T. J.; Anderson, J. G., Experimental evidence for the pressure dependence of the reaction rate constant between acetic acid and hydroxyl radicals. *J. Phys. Chem. A* 2010, 114, 11538-11544.
- (212) Khamaganov, V. G.; Bui, X. V.; Carl, S. A.; Peeters, J., Absolute rate coefficient of the OH + CH₃C(O)OH reaction at T = 287 - 802 K. The two faces of pre-reactive H-bonding. *J. Phys. Chem. A* 2006, 110, 12852-12859.
- (213) Vimal, D.; Stevens, P. S., Experimental and theoretical studies of the kinetics of the reactions of OH radicals with acetic acid, acetic acid-d₃, and acetic acid-d₄ at low pressure. *J. Phys. Chem. A* 2006, 110 (40), 11509-115516.
- (214) De Smedt, F.; Bui, X. V.; Nguyen, T. L.; Peeters, J.; Vereecken, L., Theoretical and experimental study of the product branching in the reaction of acetic acid with OH radicals. *J. Phys. Chem. A* 2005, 109 (10), 2401-2409.
- (215) Sun, W.; Saeys, M., First principles study of the reaction of formic and acetic acids with hydroxyl radicals. *J. Phys. Chem. A* 2008, 112 (30), 6918-6928.
- (216) Szabo, E. Atmospheric kinetics and photochemistry of oxygenated volatile organic compounds. Thèse, Université Lille 1 et Université de Szeged (H), Szeged, 2011.

- (217) Aumont, B.; Szopa, S.; Madronich, S., Modelling the evolution of organic carbon during its gas-phase tropospheric oxidation: development of an explicit model based on a self generating approach. *Atmos. Chem. Phys.* 2005, 5, 2497-2517.
- (218) Weitkamp, E. A.; Sage, A. M.; Pierce, J. R.; Donahue, N. M.; Robinson, A. L., Organic aerosol formation from photochemical oxidation of diesel exhaust in a smog chamber. *Environ. Sci. Technol.* 2007, 41, 6969-6975.
- (219) Moortgat, G. K., Important photochemical processes in the atmosphere. *Pure Appl. Chem.* 2001, 73 (3), 487-490.
- (220) Lu, K. D.; Rohrer, F.; Holland, F.; Fuchs, H.; Bohn, B.; Brauers, T.; Chang, C.-C.; Häsel, R.; Hu, M.; Kita, K.; Kondo, Y.; Li, X.; Lou, S. R.; Nehr, S.; Shao, M.; Zeng, L. M.; Wahner, A.; Zhang, Y. H.; Hofzumahaus, A., Observation and modelling of OH and HO₂ concentrations in the Pearl River Delta 2006: a missing OH source in a VOC rich atmosphere. *Atmos. Chem. Phys. Discuss.* 2011, 11, 11311-11378.
- (221) Peeters, J.; Nguyen, T. L.; Vereecken, L., HO_x radical regeneration in the oxidation of isoprene. *Phys. Chem. Chem. Phys.* 2009, 11 (28), 5935-5939.
- (222) Sinha, V.; Williams, J.; Lelieveld, J.; Ruuskanen, T. M.; Kajos, M. K.; Patokoski, J.; Hellen, H.; Hakola, H.; Mogensen, D.; Boy, M.; Rinne, J.; Kulmala, M., OH reactivity measurements within a boreal forest: Evidence for unknown reactive emissions. *Environ. Sci. Technol.* 2010, 44 (17), 6614-6620.
- (223) Choi, W.; Faloon, I. C.; Bouvier-Brown, N. C.; McKay, M.; Goldstein, A. H.; Mao, J.; Brune, W. H.; LaFranchi, B. W.; Cohen, R. C.; Wolfe, G. M.; Thornton, J. A.; Sonnenfroh, D. M.; Millet, D. B., Observations of elevated formaldehyde over a forest canopy suggest missing sources from rapid oxidation of arboreal hydrocarbons. *Atmos. Chem. Phys.* 2010, 10, 8761-8781.
- (224) Kundu, S.; Kawamura, K.; Andreae, T. W.; Hoffer, A.; Andreae, M. O., Molecular distributions of dicarboxylic acids, ketocarboxylic acids and α -dicarbonyls in biomass burning aerosols: implications for photochemical production and degradation in smoke layers. *Atm. Chem. Phys.* 2010, 10, 2209-2225.
- (225) Burdock, G. A., *Fenaroli's Handbook of Flavor Ingredients*, 5th ed. CRC Press: Boca Raton, FL, 2005.
- (226) Fu, T.-M.; Jacob, D. J.; Wittrock, F.; Burrows, J. P.; Vrekoussis, M.; Henze, D. K., Global budgets of atmospheric glyoxal and methylglyoxal, and implications for formation of secondary organic aerosols. *J. Geophys. Res.* 2008, 113 (D15303).
- (227) Yu, J.; Jeffries, H. E.; Sexton, K. G., Atmospheric photooxidation of alkylbenzenes - I. Carbonyl product analyses. *Atmos. Environ.* 1997, 31 (15), 2261-2280.
- (228) Smith, D.; Kleindienst, T. E.; McIver, C. D., Primary product distributions from the reaction of OH with m-, p-xylene, 1,2,4- and 1,3,5-trimethylbenzene. *J. Atmos. Chem.* 1999, 34, 339-364.
- (229) Obermeyer, G.; Aschmann, S. M.; Atkinson, R.; Arey, J., Carbonyl atmospheric reaction products of aromatic hydrocarbons in ambient air. *Atmos. Environ.* 2009, 43, 3736-3744.

- (230) Arey, J.; Obermeyer, G.; Aschmann, S. M.; Chattopadhyay, S.; Cusick, R. D.; Atkinson, R., Dicarbonyl products of the OH radical-initiated reaction of a series of aromatic hydrocarbons. *Environ. Sci. Technol.* 2009, 43 (3), 683-689.
- (231) Healy, R. M.; Temime, B.; Kuprovskite, K.; Wenger, J. C., Effect of relative humidity on gas/particle partitioning and aerosol mass yield in the photooxidation of p-xylene. *Environ. Sci. Technol.* 2009, 43 (6), 1884-1889.
- (232) Plum, C. N.; Sanhueza, E.; Atkinson, R.; Carter, W. P. L.; Pitts, J. N., OH radical rate constants and photolysis rates of α -dicarbonyls. *Environ. Sci. Technol.* 1983, 17 (8), 479-484.
- (233) Klotz, B.; Graedler, F.; Sorensen, S.; Barnes, I.; Becker, K. H., A kinetic study of the atmospheric photolysis of α -dicarbonyls. *Int. J. Chem. Kin.* 2001, 33, 9-20.
- (234) Mukhopadhyay, A.; Mukherjee, M.; Ghosh, A. K.; Chakraborty, T., UV photolysis of α -cyclohexanedione in the gas phase. *J. Phys. Chem. A* 2011, 115, 7494-7502.
- (235) Horowitz, A.; Meller, R.; Moortgat, G. K., The UV-VIS absorption cross sections of the α -dicarbonyl compounds: pyruvic acid, biacetyl and glyoxal. *Journal of Photochemistry and Photobiology A* 2001, 146, 19-27.
- (236) Dagaut, P.; Wallington, T. J.; Liu, R.; Kurylo, M. J., A kinetic investigation of the gas-phase reactions of OH radicals with cyclic ketones and diones: mechanistic insights. *J. Phys. Chem.* 1988, 92 (15), 4375.
- (237) Matsunaga, S. N.; Kawamura, K., Determination of a- and b-hydroxycarbonyls and dicarbonyls in snow and rain samples by GC-FID and GC-MS employing benzyl hydroxyl oxime derivatization. *Anal. Chem.* 2000, 72, 4742-4746.
- (238) Strekowski, R. S.; George, C., Measurement of Henry's law constants for acetone, 2-butanone, 2,3-butanedione, and isobutyraldehyde using a horizontal flow reactor. *J. Chem. Eng. Data* 2005, 50 (3), 804-810.
- (239) Faust, B. C.; Powell, K.; Rao, C. J.; Anastasio, C., Aqueous-phase photolysis of biacetyl (an α -dicarbonyl compound): a sink for biacetyl and a source of acetic acid, peroxyacetic acid, hydrogen peroxide, and the highly oxidizing acetylperoxyl radical in aqueous aerosols, fogs, and clouds. *Atmos. Environ.* 1997, 31 (3), 497-510.
- (240) Sareen, N.; Schwier, A. N.; Shapiro, E. L.; Mitroo, D.; McNeill, V. F., Secondary organic material formed by methylglyoxal in aqueous aerosol mimics. *Atmos. Chem. Phys.* 2010, 10, 997-1016.
- (241) Atkinson, R.; Arey, J.; Aschmann, S. M., Atmospheric chemistry of alkanes: Review and recent developments. *Atmos. Environ.* 2008, 42 (23), 5859-5871.
- (242) Atkinson, R.; Tuazon, E. C.; Aschmann, S. M., Atmospheric chemistry of 2-pentanone and 2-heptanone. *Environ. Sci. Technol.* 2000, 34 (4), 623-631.
- (243) Ma, S.; Barnes, I.; Becker, K. H., Atmospheric degradation of glycidaldehyde: Photolysis and reaction with OH radicals. *Environ. Sci. Technol.* 1998, 32 (22), 3515-3521.

- (244) Seaton, A.; Godden, D.; MacNee, W.; Donaldson, K., Particulate air pollution and acute health effects. *The Lancet* 1995, 345 (8943), 176-178.
- (245) Zmirou, D.; Barumandzadeh, T.; Balducci, F.; Ritter, P.; Laham, G.; Ghilardi, J. P., Short term effects of air pollution on mortality in the city of Lyon, France, 1985-90. *Journal of Epidemiology and Community Health* 1996, 50 (April), S30-S35.
- (246) Pope, C. A., III; Ezzati, M.; Dockery, D. W., Fine-particulate air pollution and life expectancy in the United States. *New England Journal of Medicine* 2009, 360 (4), 376-386.
- (247) Pope, C. A., III, Epidemiology of fine particulate air pollution and human health: Biologic mechanisms and who's at risk? *Environmental Health Perspectives Supplements* 2000, 108 (S4), 713-723.
- (248) Peled, R., Air pollution exposure: Who is at high risk? *Atmos. Environ.* 2011, 45 (10), 1781-1785.
- (249) Fonken, L. K.; Xu, X.; Weil, Z. M.; Chen, G.; Sun, Q.; Rajagopalan, S.; Nelson, R. J., Air pollution impairs cognition, provokes depressive-like behaviors and alters hippocampal cytokine expression and morphology. *Molecular Psychiatry* 2011, 16, 987-995.
- (250) Solomon, S.; Qin, D.; Manning, M.; Chen, Z.; Marquis, M.; Averyt, K. B.; Tignor, M.; Miller, H. L. *Climate change 2007: The physical science basis*; IPCC: Cambridge, UK, 2007.
- (251) Löndahl, J.; Swietlicki, E.; Lindgren, E.; Loft, S., Aerosol exposure versus aerosol cooling of climate: what is the optimal emission reduction strategy for human health? *Atm. Chem. Phys.* 2010, 10, 9441-9449.
- (252) Fenger, J., Urban air quality. *Atmos. Environ.* 1999, 33, 4877-4900.
- (253) Kanakidou, M.; Seinfeld, J. H.; Pandis, S. N.; Barnes, I.; Dentener, F. J.; Facchini, M. C.; Van Dingenen, R.; Ervens, B.; Nenes, A.; Nielsen, C. J.; Swietlicki, E.; Putaud, J. P.; Balkanski, Y.; Fuzzi, S.; Hjorth, J.; Moortgat, G. K.; Winterhalter, R.; Myhre, C. E. L.; Tsigaridis, K.; Vignati, E.; Stephanou, E. G.; Wilson, J., Organic aerosol and global climate modelling: A review. *Atmos. Chem. Phys.* 2005, 5, 1053-1123.
- (254) Lim, H.-J.; Turpin, B. J., Origins of primary and secondary organic aerosol in Atlanta: Results of time-resolved measurements during the Atlanta supersite experiment. *Environ. Sci. Technol.* 2002, 36 (21), 4489-4496.
- (255) Hoyle, C. R.; Myhre, G.; Berntsen, T. K.; Isaksen, I. S. A., Anthropogenic influence on SOA and the resulting radiative forcing. *Atm. Chem. Phys.* 2009, 9, 2715-2728.
- (256) Millet, D. B.; Donahue, N. M.; Pandis, S. N.; Polidori, A.; Stanier, C. O.; Turpin, B. J.; Goldstein, A. H., Atmospheric volatile organic compound measurements during the Pittsburgh Air Quality Study: Results, interpretation, and quantification of primary and secondary contributions. *J. Geophys. Res.* 2005, 110 (D07S07), 1-17.
- (257) Kreyling, W. G.; Semmler, M.; Möller, W., Health effects of ultrafine particles. In *European Aerosol Conference*, Elsevier, Journal of Aerosol Science: 2004.

- (258) Oberdörster, G.; Celein, R. M.; Ferin, J.; Weiss, B., Association of particulate air pollution and acute mortality: Involvement of ultrafine particles? *Inhalation Toxicology* 1995, 7 (1), 111-124.
- (259) Ibaldo-Mulli, A.; Wichmann, H. E.; Kreyling, W. G.; Peters, A., Epidemiological evidence on health effects of ultrafine particles. *Journal of Aerosol Medicine* 2004, 15 (2), 189-201.
- (260) Maynard, A. D.; Maynard, R. L., A derived association between ambient aerosol surface area and excess mortality using historic time series data. *Atmos. Environ.* 2002, 36, 5561-5567.
- (261) Schlessinger, R. B.; Kunzli, N.; Hidy, G. M.; Gotschi, T.; Jerrett, M., The health relevance of ambient particulate matter characteristics: Coherence of toxicological and epidemiological inferences. *Inhalation Toxicology* 2006, 18, 95-125.
- (262) Atkinson, R. W.; Fuller, G. W.; Anderson, H. R.; Harrison, R. M.; Armstrong, B., Urban ambient particle metrics and health: A time series analysis. *Epidemiology* 2010, 21 (4), 501-511.
- (263) Shiraiwa, M.; Kondo, Y.; Iwamoto, T.; Kita, K., Amplification of light absorption of black carbon by organic coating. *Aerosol Science and Technology* 2010, 44, 46-54.
- (264) Dusek, U.; Frank, G. P.; Curtius, J.; Drewnick, F.; Schneider, J.; Kürten, A.; Rose, D.; Andreae, M. O.; Borrmann, S.; Pöschl, U., Enhanced organic mass fraction and decreased hygroscopicity of cloud condensation nuclei (CCN) during new particle formation events. *Geophysical Research Letters* 2010, 37 (L03804).
- (265) Kulmala, M.; Laakso, L.; Lehtinen, K. E. J.; Riipinen, I.; Dal Maso, M.; Anttila, T.; Kerminen, V.-M.; Hörrak, U.; Vana, M.; Tammet, H., Initial steps of aerosol growth. *Atm. Chem. Phys.* 2004, 4, 2553-2560.
- (266) Kroll, J. H.; Seinfeld, J. H., Chemistry of secondary organic aerosol: Formation and evolution of low-volatility organics in the atmosphere. *Atmos. Environ.* 2008, 42, 3593-3624.
- (267) George, I. J.; Vlasenko, A.; Slowik, J. G.; Broekhuizen, K.; Abbatt, J. P. D., Heterogeneous oxidation of saturated organic aerosols by hydroxyl radicals: uptake kinetics, condensed-phase products, and particle size range. *Atmos. Chem. Phys.* 2007, 7, 4187-4201.
- (268) Dall'Osto, M.; Thorpe, A.; Beddows, D. C. S.; Harrison, R. M.; Barlow, J. F.; Dunbar, T.; Williams, P. I.; Coe, H., Remarkable dynamics of nanoparticles in the urban atmosphere. *Atmos. Chem. Phys.* 2011, 11, 6623-6637.
- (269) Shrivastava, M.; Zelenyuk, A.; Imre, D.; Beranek, J.; Easter, R.; Zaveri, R. A.; Fast, J., Reformulating the atmospheric lifecycle of SOA based on new field and laboratory data. *Atmos. Chem. Phys. Discuss.* 2011, 11, 20107-20139.
- (270) Anttila, T.; Kerminen, V.-M., Condensational growth of atmospheric nuclei by organic vapours. *Journal of Aerosol Science* 2003, 34 (1), 41-61.
- (271) Kerminen, V.-M.; Petäjä, T.; Manninen, H. E.; Paasonen, P.; Nieminen, T.; Sipilä, M.; Junninen, H.; Ehn, M.; Gagné, S.; Laakso, L.; Riipinen, I.; Vehkamäki, H.; Kurten, T.; Ortega, I. K.; Dal Maso, M.; Brus, D.; Hyvärinen, A.; Lihavainen, H.; Leppä, J.; Lehtinen, K. E. J.; Mirme, A.; Mirme, S.; Hörrak, U.; Berndt, T.; Stratmann, F.; Birmili, W.; Wiedensohler, A.; Metzger, A.; Dommen, J.; Baltensperger, U.; Kiendler-Scharr, A.; Mentel, T. F.; Wildt, J.; Winkler, P. M.;

Wagner, P. E.; Petzold, A.; Minikin, A.; Plass-Dülmer, C.; Pöschl, U.; Laaksonen, A.; Kulmala, M., Atmospheric nucleation: highlights of the EUCAARI project and future directions. *Atmos. Chem. Phys.* 2010, 10, 10829-10848.

(272) de Gouw, J.; Jimenez, J. L., Organic aerosols in the Earth's atmosphere. *Environ. Sci. Technol.* 2009, 43 (20), 7614-7618.

(273) Volkamer, R.; Jimenez, J. L.; San Martini, F.; Dzepina, K.; Zhang, Q.; Salcedo, D.; Molina, L. T.; Worsnop, D. R.; Molina, M. J., Secondary organic aerosol formation from anthropogenic air pollution: Rapid and higher than expected. *Geophysical Research Letters* 2006, 33 (L17811), 1-4.

(274) Holmes, N. S., A review of particle formation events and growth in the atmosphere in the various environments and discussion of mechanistic implications. *Atmos. Environ.* 2007, 41, 2183-2201.

(275) Kulmala, M.; Vehkamäki, H.; Petaja, T.; Dal Maso, M.; Lauri, A.; Kerminen, V. M.; Birmili, W.; McMurry, P. H., Formation and growth rates of ultrafine atmospheric particles: a review of observations. *Journal of Aerosol Science* 2004, 35, 143-176.

(276) Lee, S.-H.; Young, L. H.; Benson, D. R.; Suni, T.; Kulmala, M.; Junninen, H.; Campos, T. L.; Rogers, D. C.; Jensen, J., Observations of nighttime new particle formation in the troposphere. *J. Geophys. Res.* 2008, 113 (D10210), 1-7.

(277) Wiedensohler, A.; Cheng, Y. F.; Nowak, A.; Wehner, B.; Achtert, P.; Berghof, M.; Birmili, W.; Wu, Z. J.; Hu, M.; Zhu, T.; Takegawa, N.; Kita, K.; Kondo, Y.; Lou, S. R.; Hofzumahaus, A.; Holland, F.; Wahner, A.; Gunthe, S. S.; Rose, D.; Su, H.; Pöschl, U., Rapid aerosol particle growth and increase of cloud condensation nucleus activity by secondary aerosol formation and condensation: A case study for regional air pollution in northeastern China. *J. Geophys. Res.* 2009, 114 (D00G08).

(278) Laaksonen, A.; Hamed, A.; Joutsensaari, J.; Hiltunen, L.; Cavalli, F.; Junkermann, W.; Asmi, A.; Fuzzi, S.; Facchini, M. C., Cloud condensation nucleus production from nucleation events at a highly polluted region. *Geophysical Research Letters* 2005, 32 (L06812).

(279) Hovorka, J.; Branis, M., New particle formation and condensational growth in a large indoor space. *Atmos. Environ.* 2011, 45, 2736-2749.

(280) Boy, M.; Kulmala, M., The part of the solar spectrum with the highest influence on the formation of SOA in the continental boundary layer. *Atmos. Chem. Phys.* 2002, 2, 375-386.

(281) Yue, D. L.; Hu, M.; Zhang, R. Y.; Wang, Z. B.; Zheng, J.; Wu, Z. J.; Wiedensohler, A.; He, L. Y.; Huang, X. F.; Zhu, T., The roles of sulfuric acid in new particle formation and growth in the mega-city of Beijing. *Atm. Chem. Phys.* 2010, 10, 4953-4960.

(282) Smith, J. N.; Dunn, M. J.; VanReken, T. M.; Iida, K.; Stolzenburg, M. R.; McMurry, P. H.; Huey, L. G., Chemical composition of atmospheric nanoparticles formed from nucleation in Tecamac, Mexico: Evidence for an important role for organic species in nanoparticle growth. *Geophysical Research Letters* 2008, 35, L04808.

(283) Odum, J. R.; Hoffmann, T.; Bowman, F.; Collins, D.; Flagan, R. C.; Seinfeld, J. H., Gas/particle partitioning and secondary organic aerosol yields. *Environ. Sci. Technol.* 1996, 30 (8), 2580-2585.

- (284) Fiegel, H.; Voges, H.-W.; Hamamoto, T.; Umemura, S.; Iwata, T.; Miki, H.; Fujita, Y.; Buysch, H.-J.; Garbe, D.; Paulus, W., *Phenol Derivatives*. Wiley-VCH: Weinheim, 2002.
- (285) Fine, P. M.; Cass, G. R.; Simoneit, B. R. T., Chemical characterization of fine particle emissions from the fireplace combustion of woods grown in the Southern United States. *Environ. Sci. Technol.* 2002, 36 (7), 1442–1451.
- (286) Hays, M. D.; Fine, P. M.; Geron, C. D.; Kleeman, M. J.; Gullett, B. K., Open burning of agricultural biomass: Physical and chemical properties of particle-phase emissions. *Atmos. Environ.* 2005, 39 (36), 6747-6764
- (287) Derwent, R. G.; Jenkin, M. E.; Saunders, S. M.; Pilling, M. J., Photochemical ozone creation potentials for organic compounds in northwest Europe calculated with a master chemical mechanism. *Atmos. Environ.* 1998, 32 (14/15), 2429-2441.
- (288) Henry, F.; Coeur-Tourneur, C.; Ledoux, F.; Tomas, A.; Menu, D., Secondary organic aerosol formation from the gas phase reaction of hydroxyl radicals with m-, o- and p-cresol. *Atmos. Environ.* 2008, 42, 3035-3045.
- (289) Volkamer, R.; Klotz, B.; Barnes, I.; Imamura, T.; Wirtz, K.; Washida, N.; Becker, K. H.; Platt, U., OH-initiated oxidation of benzene. Part I. Phenol formation under atmospheric conditions. *Phys. Chem. Chem. Phys.* 2002, 4, 1598-1610.
- (290) Klotz, B.; Volkamer, R.; Hurley, M. D.; Sulbaeck Andersen, M. P.; Nielsen, O. J.; Barnes, I.; Imamura, T.; Wirtz, K.; Becker, K. H.; Platt, U.; Wallington, T. J.; Washida, N., OH-initiated oxidation of benzene. Part II. Influence of elevated NO_x concentrations. *Phys. Chem. Chem. Phys.* 2002, 4, 4399-4411.
- (291) Henze, D. K.; Seinfeld, J. H.; Ng, N. L.; Kroll, J. H.; Fu, T.-M.; Jacob, D. J.; Heald, C. L., Global modeling of secondary organic aerosol formation from aromatic hydrocarbons: high- vs. low-yield pathways. *Atmos. Chem. Phys.* 2008, 8, 2405-2420.
- (292) Olariu, R. I.; Klotz, B.; Barnes, I.; Becker, K. H.; Mocanu, R., FT-IR study of the ring-retaining products from the reaction of OH radicals with phenol, o-, m-, and p-cresol. *Atmos. Environ.* 2002, 36, 3685-3697.
- (293) Berndt, T.; Böge, O., Gas-phase reaction of OH radicals with phenol. *Phys. Chem. Chem. Phys.* 2003, 5, 342-350.
- (294) Olariu, R. I.; Barnes, I.; Becker, K. H.; Klotz, B., Rate coefficients for the gas-phase reaction of OH radicals with selected dihydroxybenzenes and benzoquinones. *Int. J. Chem. Kin.* 2000, 32, 696-702.
- (295) Yamamoto, Y.; Niki, E.; Shiokawa, H.; Kamiya, Y., Ozonation of organic compounds. 2. Ozonation of phenol in water. *J. Org. Chem.* 1979, 44 (13), 2137-2142.
- (296) Guilloteau, A. Etude multiphasique de polluants organiques aromatiques : répartition des Hydrocarbures Aromatiques Polycycliques dans les suies et formation d'aérosols dans l'ozonolyse du catéchol. Thèse, Université d'Orléans, Orléans, 2007.

- (297) Coeur-Tourneur, C.; Foulon, V.; Laréal, M., Determination of aerosol yields from 3-methylcatechol and 4-methylcatechol ozonolysis in a simulation chamber. *Atmos. Environ.* 2010, 44, 852-857.
- (298) Ofner, J.; Krüger, H.-U.; Grothe, H.; Schmitt-Kopplin, P.; Whitmore, K.; Zetzsch, C., Physico-chemical characterization of SOA derived from catechol and guaiacol – a model substance for the aromatic fraction of atmospheric HULIS. *Atmos. Chem. Phys.* 2011, 11, 1-15.
- (299) Ofner, J.; Krüger, H.-U.; Zetzsch, C., Time resolved infrared spectroscopy of formation and processing of secondary organic aerosol. *Z. Phys. Chem.* 2010, 224, 1171-1183.
- (300) Hallquist, M.; Wenger, J.; Baltensperger, U.; Rudich, Y.; Simpson, D.; Claeys, M.; Dommen, J.; Donahue, N. M.; George, C.; Goldstein, A. H.; Hamilton, J. F.; Herrmann, H.; Hoffmann, T.; Iinuma, Y.; Jang, M.; Jenkin, M. E.; Jimenez, J. L.; Kiendler-Scharr, A.; Maenhaut, W.; McFiggans, G.; Mentel, T. F.; Monod, A.; Prévot, A. S. H.; Seinfeld, J. H.; Surratt, J. D.; Szmigielski, R.; Wildt, J., The formation, properties and impact of secondary organic aerosol: current and emerging issues. *Atmos. Chem. Phys.* 2009, 9, 5155-5236.
- (301) Bethel, H. L.; Atkinson, R.; Arey, J., Kinetics and products of the reactions of selected diols with the OH radical. *Int. J. Chem. Kin.* 2001, 33, 310-316.
- (302) Bethel, H. L.; Atkinson, R.; Arey, J., Hydroxycarbonyl products of the reactions of selected diols with the OH radical. *J. Phys. Chem. A* 2003, 107 (32), 6200-6205.
- (303) Wolkoff, P.; Clausen, P. A.; Wilkins, C. K.; Nielsen, G. D., Formation of strong airway irritants in terpene/ozone mixtures. *Indoor Air* 2000, 10 (2), 82-91.
- (304) Jia, C.; Batterman, S.; Godwin, C., VOCs in industrial, urban and suburban neighborhoods, Part 1: Indoor and outdoor concentrations, variation, and risk drivers. *Atmos. Environ.* 2008, 42, 2083-2100.
- (305) Weschler, C. J., Ozone's impact on public health: Contributions from indoor exposures to ozone and products of ozone-initiated chemistry. *Environmental Health Perspectives* 2006, 114 (10), 1489-1496.
- (306) Ng, N. L.; Kwan, A. J.; Surratt, J. D.; Chan, A. W. H.; Chhabra, P. S.; Sorooshian, A.; Pye, H. O. T.; Crouse, J. D.; Wennberg, P. O.; Flagan, R. C.; Seinfeld, J. H., Secondary organic aerosol (SOA) formation from reaction of isoprene with nitrate radicals (NO₃). *Atmos. Chem. Phys.* 2008, 8 (14), 4117-4140.
- (307) Fuzzi, S.; Andreae, M. O.; Huebert, B. J.; Kulmala, M.; Bond, T. C.; Boy, M.; Doherty, S. J.; Guenther, A. B.; Kanakidou, M.; Kawamura, K.; Kerminen, V.-M.; Lohmann, U.; Russel, L. M.; Pöschl, U., Critical assessment of the current state of scientific knowledge, terminology, and research needs concerning the role of organic aerosols in the atmosphere, climate, and global change. *Atm. Chem. Phys.* 2006, 6, 2017-2038.
- (308) Bateman, A. P.; Nizkorodov, S. A.; Laskin, J.; Laskin, A., Photolytic processing of secondary organic aerosols dissolved in cloud droplets. *Phys. Chem. Chem. Phys.* 2011, 13, 12199-12212.

- (309) Koehler, C. A.; Fillo, J. D.; Ries, K. A.; Sanchez, J. T.; De Haan, D. O., Formation of secondary organic aerosol by reactive condensation of furandiones, aldehydes, and water vapor onto inorganic aerosol seed particles. *Environ. Sci. Technol.* 2004, 38 (19), 5064-5072.
- (310) Bertram, A. K.; Ivanov, A. V.; Hunter, M.; Molina, L. T.; Molina, M. J., The reaction probability of OH on organic surfaces of tropospheric interest. *J. Phys. Chem. A* 2001, 105, 9415-9421.
- (311) Gross, D. S.; Gälli, M. E.; Kalberer, M.; Prévot, A. S. H.; Dommen, J.; Alfarra, M. R.; Duplissy, J.; Gaeggeler, K.; Gascho, A.; Metzger, A.; Baltensperger, U., Real-time measurement of oligomeric species in secondary organic aerosol with the aerosol time-of-flight mass spectrometer. *Anal. Chem.* 2006, 78 (7), 2130-2137.
- (312) Sadezky, A.; Winterhalter, R.; Kanawati, B.; Römpf, A.; Spengler, B.; Mellouki, A.; Le Bras, G.; Chaimbault, P.; Moortgat, G. K., Oligomer formation during gas-phase ozonolysis of small alkenes and enol ethers: new evidence for the central role of the Criegee Intermediate as oligomer chain unit. *Atmos. Chem. Phys.* 2008, 8, 2667-2699.
- (313) Denkenberger, K. A.; Moffet, R. C.; Holecek, J. C.; Rebotier, T. P.; Prather, K. A., Real-time, single-particle measurements of oligomers in aged ambient aerosol particles. *Environ. Sci. Technol.* 2007, 41 (15), 5439-5446.
- (314) Grieshop, A. P.; Donahue, N. M.; Robinson, A. L., Is the gas-particle partitioning in alpha-pinene secondary organic aerosol reversible? *Geophysical Research Letters* 2007, 34 (L14810), 1-5.
- (315) Hellen, H.; Dommen, J.; Metzger, A.; Gascho, A.; Duplissy, J.; Tritscher, T.; Prévot, A. S. H.; Baltensperger, U., Using proton transfer reaction mass spectrometry for online analysis of secondary organic aerosols. *Environ. Sci. Technol.* 2008, 42 (19), 7347-7353.

RESUME

Mes travaux de recherche s'inscrivent dans le cadre général de la compréhension des phénomènes de pollution atmosphérique au travers d'expériences réalisées en laboratoire. Ils comportent deux volets : le premier porte sur l'étude de la réactivité en phase gazeuse de composés organiques volatils oxygénés ; le second porte sur l'étude de la formation d'aérosols organiques secondaires (AOS) à partir de l'ozonolyse de composés aromatiques oxygénés. Au cours de ces travaux, de nouveaux outils expérimentaux originaux ont été développés afin d'étudier ces phénomènes sous des angles différents et novateurs, notamment (i) une chambre de simulation atmosphérique rigide couplée à un spectromètre de type cw-CRDS (Cavity Ring-Down Spectroscopy) pour la détection au sein du réacteur même d'espèces atmosphériques clés (HO_2) et (ii) un réacteur à écoulement laminaire avec injecteur mobile pour l'étude des premières étapes de formation des AOS, couplé, entre autres, à un spectromètre de masse à aérosol haute résolution.

Les études cinétiques et mécanistiques en phase gazeuse ont contribué à expliciter le mécanisme réactionnel d'oxydation par OH de deux espèces oxygénées majeures de l'atmosphère : l'acétone et l'acide acétique, en particulier en déterminant les sites d'attaque du radical OH sur la molécule oxygénée. Au travers d'études cinétiques de dégradation de composés aromatiques, nous avons ensuite montré que, contrairement à ce qui était habituellement observé, l'ozonolyse des composés aromatiques oxygénés de type catéchols était importante d'un point de vue atmosphérique. La formation d'aérosols organiques secondaires dans ces réactions a été mise en évidence et quantifiée dans une série d'expériences réalisées dans des laboratoires français et européens.

Les derniers travaux sont liés au développement des dispositifs expérimentaux déjà mentionnés. La nouvelle chambre de simulation atmosphérique a permis l'étude du mécanisme de la réaction d'oxydation par OH du méthyle nitrite, ce dernier étant couramment utilisé comme précurseur de radicaux OH dans les chambres de simulation. La formation d'acide nitreux a ainsi été mise en évidence pour la première fois. Dans une deuxième étude, les cinétiques de disparition du radical HO_2 ont été observées pour la première fois, à notre connaissance, dans un réacteur de ce type et nous avons montré que la diffusion aux parois pouvait être significative dans des expériences en chambre de simulation à basse pression et ainsi modifier les mécanismes réactionnels étudiés. Enfin, le développement du réacteur à écoulement laminaire a été validé par l'étude des cinétiques et des produits d'ozonolyse de pentènes, étude dans laquelle un produit de réaction non oxydé a été observé pour la première fois. Cette validation permet d'envisager l'étude de réactions plus complexes produisant des AOS.

ABSTRACT

My research activities lie within the framework of the understanding of atmospheric pollution events through laboratory experiments. These activities are divided in two parts: the first part deals with the study of the reactivity of oxygenated volatile organic compounds; the second deals with the study of secondary organic aerosol (SOA) formation from the ozonolysis of oxygenated aromatic compounds. At the same time, original experimental tools have been developed to study these processes under various and innovative points of view, particularly (i) an atmospheric simulation chamber coupled to a cw-CRDS (continuous-wave Cavity Ring-Down Spectroscopy) spectrometer for the *in situ* detection of key atmospheric species (HO_2) and (ii) a laminar flow reactor with a mobile injection head for the study of the first steps in the SOA formation coupled to a high resolution aerosol mass spectrometer, among other instruments.

Kinetic and mechanistic studies on the OH-initiated oxidation of two major oxygenated compounds in the atmosphere – acetone and acetic acid – have taken part in the understanding of the gaseous reaction mechanisms. Especially, the branching ratios of the initiating reactions have been determined. Then, through kinetic studies on the degradation of aromatic compounds, we have shown that the ozonolysis of catechol-type oxygenated aromatic compounds is significant in the atmosphere, which was not expected for aromatic compounds. In addition, the formation of secondary organic aerosols in these ozonolysis reactions has been demonstrated for the first time and quantified through experiments in French and European facilities.

The most recent research works are in line with the development of the above-mentioned experimental tools. The new atmospheric simulation chamber has allowed the mechanistic study of the OH-initiated methyl nitrite reaction, this organic compound being largely used as OH radical source in atmospheric simulation chamber experiments. The formation of nitrous acid has been observed and quantified for the first time. In a second study, the HO_2 radical kinetics have been recorded for the first time in such a reactor (to the best of our knowledge) and it has been shown that HO_2 radical diffusion to the reactor walls could be significant in low pressure experiments performed in such photoreactors and thus, could modified chemical reaction mechanisms. Finally, the development of the laminar flow reactor has been validated by determining the kinetics and products of pentene ozonolysis; in this study, a non oxidized product has been observed for the first time. This validation enables to consider the study of more complex reactions producing SOA.